Poznan University of Technology

Faculty of Chemical Technology

Institute of Chemistry and Technical Electrochemistry

Division of Applied Electrochemistry

Sylwia Ślesińska

Research on the electrode charging and carbon degradation in electrochemical capacitors

PhD Thesis

Scientific Supervisors:

Dr. Krzysztof Fic

Dr. Jakub Menzel

Poznań, 2025

Acknowledgements

I would like to thank my supervisor **Dr. Krzysztof Fic** and my co-supervisor **Dr. Jakub Menzel**; for their supervisory role, constant support, many lengthy and interesting scientific discussions, generous guidance and valuable time during the duration of my PhD studies.

I am also indebted to **Professor Elżbieta Frąckowiak** and **Professor François Béguin** for their kind suggestions and guidance during my time in the Power Sources Group.

Special thanks to **Dr. Camelia Matei Ghimbeu** for the warm welcome, kind help and opportunity to work with the *Carbon and Hybrid Materials* group from the Institute of Materials Science of Mulhouse (IS2M), Mixed research Unit, CNRS-University of Haute Alsace.

I would also like to acknowledge all present and past **Power Sources Group** members, as well as my co-authors: special thanks to Anetta, Przemysław, Adam Ś. and Maciej.

Lastly, my biggest appreciation goes to my husband **Adam**, my **parents**, my **family**, as well as all my lovely **friends** for the continuous love and support throughout this challenging yet exciting time.

Abstract

This doctoral thesis is devoted to elucidation of processes taking place at the electrode/electrolyte interface in electrochemical capacitors (ECs) with an emphasis on both aqueous and organic media, as well as in Li-ion capacitors (LICs). To improve the performance of the devices mentioned, it is crucial to understand and properly describe their mechanism of charge storage. For this, the use of advanced techniques and new approaches should be proposed concerning fundamental research. In the context of developing more stable and durable energy storage systems with longer lifespans, especially for industrial applications, elaboration of the specific causes of accelerated degradation of the carbon electrodes was also investigated.

This work was therefore divided into four thematic sections: The first section (**Chapter I**) entails general preface to the energy market, followed by introduction to energy storage devices, with a strong focus on electrochemical capacitors and lithium-ion capacitors: their principle of operation, construction and commonly used materials and electrolytes. The chapter follows up with a current literature review on fundamental studies and ageing studies in electrochemical capacitors, closing on a subsection where electrochemical techniques used throughout the work are discussed.

Chapter II – opens the second section of the thesis, with a summary of papers **P1** and **P2** that deal with investigation of molecular level charging mechanisms in electrochemical capacitors based on activated carbon (AC) paired with aqueous electrolytes. This fundamental research deals with various aspects: the first is based on *operando* monitoring of pH value changes during the charging and discharging of an electrochemical capacitor in an aqueous neutral salt solution. The change of pH values at the vicinity of the capacitor electrode was found to be dynamic: strongly potential-dependent and different for individual electrodes.

The other work establishes ionic fluxes in AC materials paired with various electrolyte compositions and concentrations using electrochemical quartz crystal microbalance (EQCM), as well as new approaches towards more efficient applications. The point of zero charge (PZC) meaning for the charging mechanism description was also demonstrated, using various electrochemical techniques, with an improved method for its determination based on step potential electrochemical spectroscopy (SPECS). Also, a concept of range of zero charge (RZC) for AC operating in aqueous electrolytes was

introduced for the first time, which implies that PZC should not be considered as an absolute one-point potential value.

The third section (**Chapter III**) is dedicated to the ageing mechanisms of AC electrodes in organic media, for both ECs and LICs – most commonly used devices for industrial applications. Contributing factors based on increasing voltage and the role of oxygen functionalities on ageing of the systems were determined. It presents a summary based on paper P3 and article A1. In both works, electrochemical techniques were coupled with physicochemical analyses. The former focuses on ageing mechanisms of the AC electrode and determines both the structural and chemical changes leading to energy fading in LICs. The use of half-cell configuration allowed to isolate the fundamental processes occurring at a single electrode only, without the complexities introduced by a full cell. The most important finding evidenced that an increase in applied voltage not only results in in faster system degradation but governs the ageing chemistry.

Article A1 focuses on the assessment of EC performance at high voltage in industrial electrolyte, 1 mol L^{-1} TEABF$_4$ (tetraethylammonium tetrafluoroborate) in AN (acetonitrile). Specifically, a role of AC oxygenated functionalities on accelerated ageing is presented. These findings unravel complex degradation pathways, where unlike previous assumptions, the type rather than the total amount of oxygenated functionalities on the AC electrode were established to influence the degradation pathways.

The final section contains abstracts of articles that are not directly linked to the thesis, nevertheless, demonstrate scientific output gained during the PhD studies. Additionally, the list of figures and tables included in the thesis, scientific accomplishments and literature are presented.

Streszczenie

Niniejsza praca doktorska poświęcona jest wyjaśnieniu procesów zachodzących na granicy faz elektroda/elektrolit w kondensatorach elektrochemicznych, ze szczególnym uwzględnieniem elektrolitów wodnych i organicznych, a także w kondensatorach litowo-jonowych. Aby poprawić wydajność wspomnianych urządzeń, ważne jest zrozumienie i właściwe opisanie ich mechanizmu magazynowania ładunku. W tym celu należy zaproponować zastosowanie zaawansowanych technik i nowych podejść w zakresie badań podstawowych. W kontekście opracowania bardziej stabilnych i trwałych systemów magazynowania energii o dłuższej żywotności, zwłaszcza do zastosowań przemysłowych, zbadano również szczegółowe przyczyny przyspieszonej degradacji elektrod węglowych.

Dlatego też niniejszą pracę podzielono na cztery sekcje tematyczne: Część pierwsza (**Rozdział I**) zawiera ogólne wprowadzenie do rynku energii, po którym następuje wprowadzenie do urządzeń magazynujących energię, ze szczególnym uwzględnieniem kondensatorów elektrochemicznych oraz kondensatorów litowo-jonowych: ich zasady działania, budowy i powszechnie stosowanych materiałów i elektrolitów. Rozdział kończy się przeglądem aktualnej literatury na temat badań podstawowych i badań starzeniowych kondensatorów elektrochemicznych, zamykając się podrozdziałem, w którym omawiane są techniki elektrochemiczne stosowane w pracy.

Rozdział II – otwiera drugą część pracy, zawierającą podsumowanie publikacji P1 i P2, które dotyczą badania mechanizmów ładowania na poziomie molekularnym w kondensatorach elektrochemicznych opartych na węglu aktywowanym w połączeniu z elektrolitami wodnymi. Te podstawowe badania dotyczą różnych aspektów: pierwsze opiera się na monitorowaniu pH w trybie *operando* podczas ładowania i wyładowania kondensatora elektrochemicznego w wodnym neutralnym roztworze soli. Stwierdzono, że zmiana pH pobliżu elektrod kondensatora jest dynamiczna: silnie zależy od potencjału i jest różna dla poszczególnych elektrod.

W drugiej publikacji opisano strumienie jonowe w materiałach węglowych w połączeniu z różnymi składami i stężeniami elektrolitów przy użyciu elektrochemicznej mikrowagi kwarcowej (EQCM), a także nowe podejścia do bardziej wydajnych zastosowań z nią związanych. Wykazano znaczenie punktu zerowego ładunku (PZC) dla opisu mechanizmu ładowania, wykorzystując różne techniki elektrochemiczne, z

udoskonaloną metodą jego wyznaczania opartą na spektroskopii elektrochemicznej z krokowo zmiennym potencjałem ang. *step potential electrochemical spectroscopy* (SPECS). Po raz pierwszy wprowadzono także koncepcję zakresu ładunku zerowego, ang. *region of zero charge* (RZC) dla węgla aktywowanego pracującego w elektrolitach wodnych, co oznacza, że PZC nie należy traktować jako bezwzględnej jednopunktowej wartości potencjału.

Część trzecia (**Rozdział III**) poświęcona jest mechanizmom starzenia elektrod węglowych w środowisku organicznym, zarówno dla kondensatorów elektrochemicznych jak i kondensatorów litowo-jonowych – najczęściej stosowanych urządzeń w zastosowaniach przemysłowych. Określono czynniki takie jak wzrost napięcia oraz rola tlenowych grup funkcyjnych na starzenie się układów. Zawiera ona podsumowanie na podstawie publikacji P3 oraz artykułu A1. W obu pracach techniki elektrochemiczne połączono z analizami fizykochemicznymi. Pierwsza skupia się na mechanizmach starzenia elektrody węglowej i określa zarówno zmiany strukturalne, jak i chemiczne prowadzące do zaniku zdolności do magazynowania energii w kondensatorze litowo-jonowym. Zastosowanie konfiguracji pół-ogniwa pozwoliło na wyizolowanie podstawowych procesów zachodzących tylko na pojedynczej elektrodzie, bez komplikacji wprowadzanych przez pełne ogniwo. Najważniejsze odkrycie wykazało, że wzrost napięcia nie tylko powoduje szybszą degradację systemu, ale także kieruje procesami starzenia.

Artykuł A1 koncentruje się na ocenie działania kondensatora elektrochemicznego przy wysokim napięciu w elektrolicie komercyjnym, tj. 1 mol L^{-1} tetrafluoroboranie tetraetyloamonu (TEABF$_4$) w acetonitrylu (AN). W szczególności przedstawiono rolę tlenowych grup funkcyjnych w przyspieszonym starzeniu. Odkrycia te opisują złożone ścieżki degradacji, w przypadku których w przeciwieństwie do poprzednich założeń ustalono, że na ścieżki degradacji bardziej wpływa rodzaj niż całkowita ilość utlenionych grup funkcyjnych elektrody węglowej.

Abbreviations

AC   – activated carbon

ACF   – activated carbon fibre

ADN   –adiponitrile

AN   - acetonitrile

CB   – carbon black

CDC   – carbide-derived carbon

CE   – counter electrode

CI   – current interrupt

CNH   – carbon nanohorn

CNTs   – carbon nanotubes

CV   – cyclic voltammetry

CVD   – chemical vapor deposition

DFT   – Density Functional Theory

DEC   – diethyl carbonate

DEMS   – differential electrochemical mass spectroscopy

DMC   – dimethyl carbonate

DMF   – N,N-dimethyl formamide

EC   – electrochemical capacitor

ECD   – electrochemical dilatometry

EC/DM   – ethylene carbonate/dimethylcarbonate

EDL   – electrical double-layer

EDLC   – electrical double-layer capacitor

EIS   – electrochemical impedance spectroscopy

ESR   – equivalent series resistance

EV   – electric vehicle

EQCM   – electrochemical quartz crystal microbalance

$[FSI]^-$ - bis(fluoromethane sulfonyl imide)

GCD   – galvanostatic charge-discharge

GCMS   – gas chromatography mass spectrometry

GCS   – Gouy-Chapman-Stern

GITT – Galvanostatic Intermittent Titration Technique

GO – graphene oxide

HEP – hydrogen evolution potential

HER – hydrogen evolution reaction

HIP – hybrid ion capacitor

IL – ionic liquid

IR - infrared spectroscopy

LIB – lithium-ion battery

LIC – lithium-ion capacitor

$LiClO_4$ – lithium perchlorate

$LiPF_6$ – lithium hexafluorophosphate

LMO – lithium metal oxide

LTO – lithium titanate

LVO – lithium vanadate

MD – molecular dynamics

MS –mass spectrometry

$NaPF_6$ –sodium hexafluorophosphate

NMP – N-Methyl-2-pyrrolidone

NMR – nuclear magnetic resonance

OCV – open circuit voltage

OEP – oxygen evolution potential

OER – oxygen evolution reaction

PANI – polyaniline

PC – propylene carbonate

PEEK – poly(ether ether ketone)

PPy – polypyrrole

PSD – pore size distribution

PTFE – poly(tetrafluoroethylene)

PVDF – poly(vinylidene fluoride)

PZC - point of zero charge

R&D - research and development

RE – reference electrode

rGO   – reduced graphene oxide

RZC   - region of zero charge

SCE   - saturated calomel electrode

SEI   - solid electrolyte interphase

SEM   - scanning electron microscopy

SHE   - standard hydrogen electrode

SPECS   - step potential electrochemical spectroscopy

SPEIS   - staircase potential electrochemical impedance spectroscopy

SSA   - specific surface area

TEABF$_4$ - tetraethylammonium tetrafluoroborate

[TFSI]$^-$ - bis(trifluoromethane sulfonyl imide)

WE   – working electrode

XPS   – x-ray photoelectron spectroscopy

XRD   – x-ray diffraction

List of Contents

Chapter I:

Literature review

1. Introduction

The end of year 2023 marked an important steppingstone for climate action in the form of the 28th United Nations Climate Change conference (COP28). Under the Paris Agreement, which legally binds international treaty on climate change, [1] a decision was reached between respective governments to speed transition away from fossil fuels. In such light, notable improvements on energy capacity and efficiency are set to be established by 2030. [2, 3] This move will most definitely prove to be a driving force for regained interest and consequently, a notable boost in both economic and research and development (R&D) sectors in the energy storage systems industry. The current global energy storage systems market, including thermal, electrochemical and mechanical energy storage, was valued at 246.54 billion (USD) in 2023 and is expected to increase steadily between 2024 and 2031 to almost double in value, as illustrated in Figure 1. [4, 5]
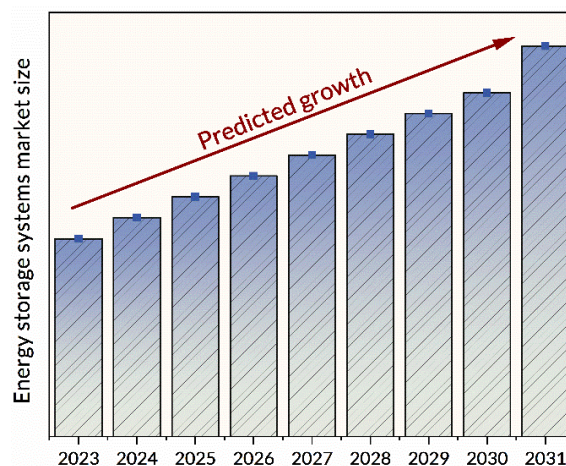

Figure 1. Energy storage systems market size forecast between 2023-2031 based on [4, 5].

Apart from that, the growth of energy consumption all over the globe has been already noted over the past decade or so. Thus collectively, together with predicted future demand, it raises the need for more efficient, altogether better suited and reliable solutions to meet the needs of the ever-changing and fast-paced modern world. One must also keep in mind the environmental aspects, where preferably clean energy technologies based on e.g. renewable sources such as wind, water or sun can be employed. One cannot, however, solely rely on these sources based on intermittency

alone; their availability will depend on location, season, weather conditions, to name a few. This is where energy storage technologies such as secondary batteries and electrochemical capacitors (ECs) can play a crucial role, by not only storing the excess energy, but also by balancing supply and demand and providing the energy itself when required. [6, 7] ECs especially, are noteworthy in this context due to their remarkable characteristics, such as long cyclability and high power density. [8, 9] They however suffer from notable self-discharge and have rather restricted charge storage capacity. [10, 11] Therefore, they require further improvements and research. This would allow them to compete with the state-of-the-art technologies, such as lithium ion batteries (LIBs), which have been the 'go-to' choice when it comes to portable electronic devices for years and are currently gaining popularity in both aerospace and electric vehicle (EV) sectors. [12]

2. Electrochemical Capacitors

2.1 Basics to capacitors

A capacitor has the ability to store and release energy, with many different types available on the market. It consists of two electrodes in parallel, separated by a dielectric as represented in Figure 2. When connected to an external power supply, charge carriers collect on the surface of the electrodes. This causes them to have negative and positive charges respectively. As the two electrodes maintain equal charge of the opposite sign, electric field is created, and this allows for an electric energy to be stored as a result. [13-15]
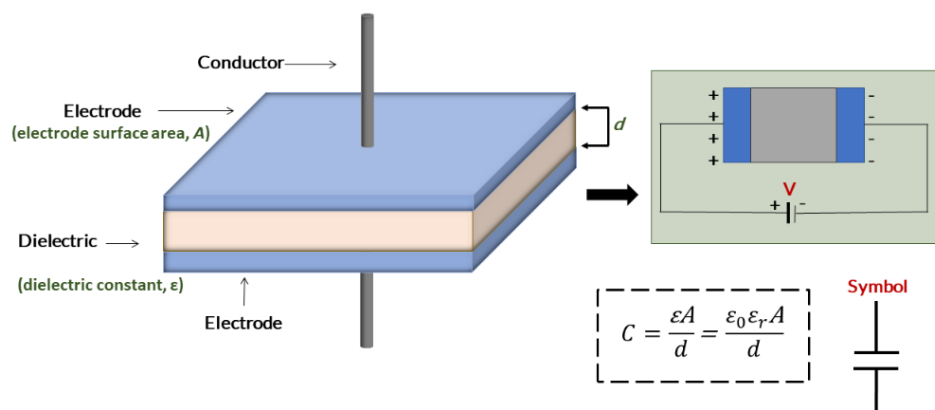

Figure 2. Schematic diagram of a basic capacitor and equation for capacitance (C), based on [14, 16, 17]

$$C = \frac{\varepsilon A}{d} = \frac{\varepsilon_0 \varepsilon_r A}{d}$$

As represented by the equation, the capacitance (C) is proportional to the surface area of the electrode (A) and is also inversely proportional to distance between the electrodes (*d*). [14, 18] Thus, an important relationship is established, where, the higher the surface area of the electrode, the higher the capacitance. Capacitance, measured in Farads (F) can be also expressed in terms of charge (Q) and voltage (V):

$$C = Q/V$$

eq.1

Whereas, energy, (E) can be represented as follows:

$$E = Q.V$$

eq.2

Based on these representations, energy can be ultimately expressed as:

eq.3

$$U = \frac{1}{2}(Q^2/C) = \frac{1}{2}Q.V = \frac{1}{2}C.V^2$$

The dielectric constant (ε) represents the ratio of the permittivity of the vacuum (ε_0) to the permittivity of the dielectric (ε_{0r}). Thus, it can be established that material's dielectric constant increases with the amount of polarization it develops in an applied field of a certain strength. [19]

As aforementioned, different types of capacitors can be considered. The most popular include electrolytic, silver mica, ceramic, tantalum, electrochemical and foil, with some presented in Figure 3. The choice of the correct capacitor that meets the user's needs will naturally depend on the intended application. However, several other criteria need to be also considered such as size, temperature, capacitance, voltage rating and cost. [20]
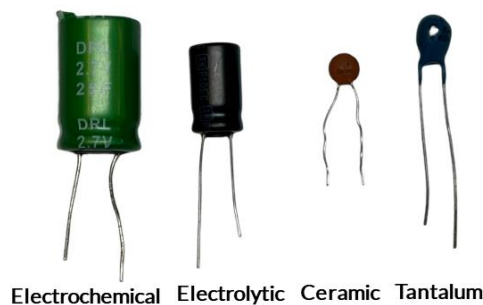

Electrochemical Electrolytic Ceramic Tantalum

Figure 3. Different types of capacitors

ECs in particular, can reach very high volumetric and specific capacitances, thus high energy density amongst all other capacitors. Typically, one would expect values of capacitance to be within the range of pF and μF in a typical capacitor, [13] therefore ECs have much more to offer in this context. This is achieved by incorporation of high surface area carbon electrodes together with thinner dielectrics directed by the double layer thickness. [14, 15, 21, 22] Moreover, they offer high cyclability (>10^6 charge–discharge cycles), which makes them the perfect devices for use in transportation, industrial and everyday applications. [9, 23-28] The general strategy to improve their energy output is based on eq.2, where both the enhancement of the capacitance and increasing of the operating voltage of the device are considered.

2.2   *ECs: construction and principle of operation*

ECs are also referred to as 'ultracapacitors', 'supercapacitors' or 'electrochemical double-layer capacitors' (EDLCs). The name of the latter, however, stems from the devices fundamental charge storage principle. Therefore, it's rather imperative to highlight that when referring to ECs, one must remember that they could also include other charge storage mechanisms, e.g. those based on redox processes. [29, 30]

ECs consist of two high surface area porous electrodes (most often activated carbon (AC)), where upon polarization one becomes positively charged while the other negatively charged) placed directly onto metal current collectors (such as stainless steel, gold, aluminum) separated by a membrane and immersed in an electrolytic solution. The electrodes can be identical (symmetrical cell) or different from one another (asymmetrical). The membrane prevents direct contact between the electrodes, thus avoiding possible short circuits which would immediately discharge the capacitor. It must, however, allow for the ions from the electrolyte to move freely as to facilitate charge and discharge processes. The electrolyte itself not only provides ions but acts as their carrier. The solvent is either water or an organic molecule. [31-33] For reference, Figure 4 represents a schematic diagram of a typical laboratory scale EC.
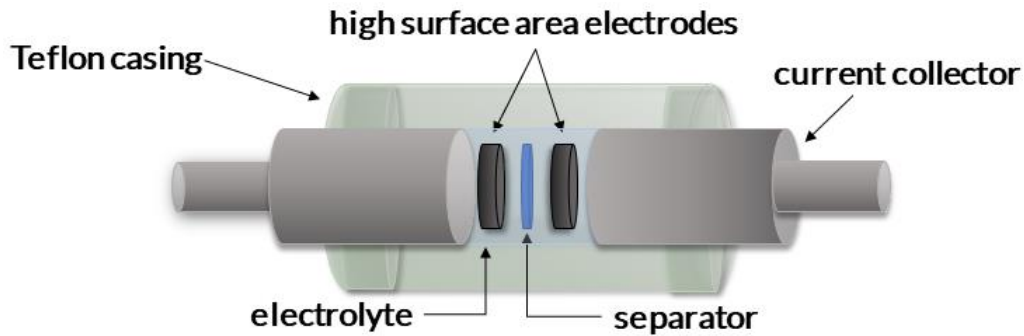
Figure 4. Laboratory scale EC

Upon charging; that is, when potential difference is applied between the electrodes; [34] the cations from the electrolytic solution adsorb onto the surface of the negative electrode, whereas the anions onto the positive electrode, forming an electrical double-layer (EDL) at each electrode/electrolyte interface. The opposite takes place upon discharge, i.e. counter-ions desorb from the electrode surface (Figure 5). Both the size and charge of the ions present as well as concentration of the electrolyte will determine the double layer thickness, which in turn influences the capacitance of the device. [13, 35] Moreover, the electrode itself will also determine the number of charge stored; for smooth and flat planar electrodes it will be directly associated with its geometrical surface, whereas for porous electrodes it can be enhanced.
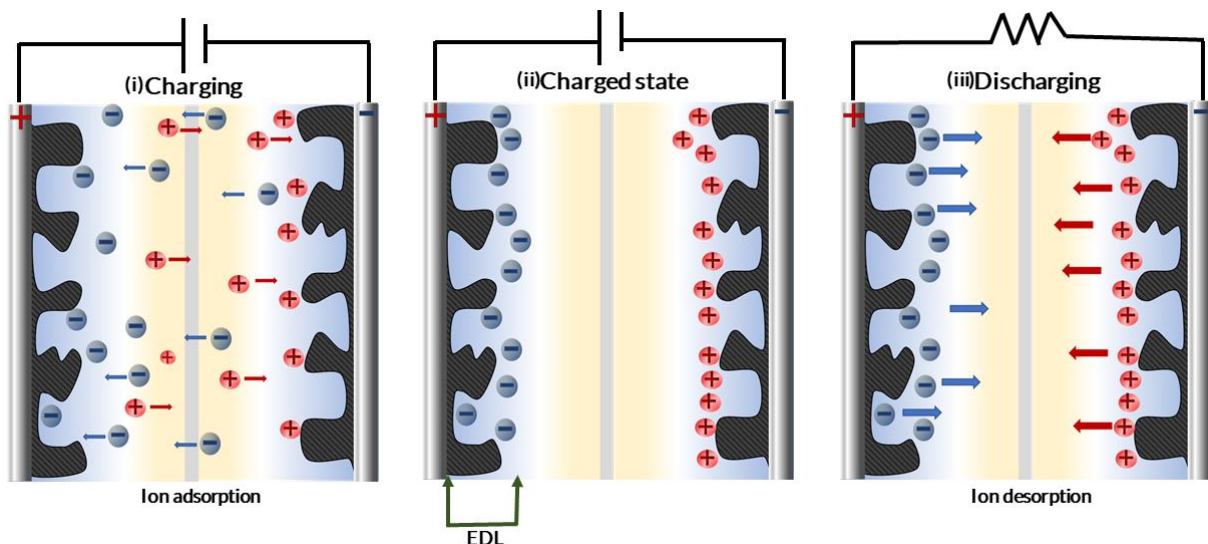

Figure 5. Simplified working principle of EDLC: during (i) charging, (ii) when charged and (iii) discharging, based on [36]

When considering the charged state, the complete cell comprises of two capacitors which are connected in series. [37] Therefore, for a symmetrical capacitor the capacitance of the cell (C_{cell}) in Farads (F) [14, 21] can be considered as:

$$C_{cell} = \frac{1}{C_+} + \frac{1}{C_-}$$
eq.4

Where C_+ and C_- represent capacitances of positive and negative electrodes respectively. [38] In theory, the capacitances of both electrodes in such case will be the same. Thus, the equation can be simplified to:

$$C_{cell} = \frac{C_e}{2}$$
eq.5

Where,

$$C_e = C_+ = C_-$$
eq.6

Therefore, the capacitance of a device will be twice as small as the capacitance calculated per electrode. In reality, however, these electrodes might vary; their thickness, size or even type of material used will give rise to different capacitance values. Hence, recalculation per active surface area (areal capacitance in F/cm^2), mass (gravimetric capacitance in F/g) or volume (volumetric capacitance in F/cm^3) is needed. One would most often find gravimetric capacitance of an electrode (C_E) reported in scientific works, where an active mass of a single electrode (m_{act}) in grams is considered:

$$C_E = \frac{2 . C_{cell}}{m_{act}}$$
eq.7

The gravimetric capacitance of a whole cell can be obtained through division of C_E by 4, thus it will be 4 times smaller than the gravimetric capacitance of an electrode. Once again, all of this becomes significant when comparing or reporting research results; often, such information is omitted, which can cause further confusion within the scientific community. Moreover, it must be noted that high capacitance values alone do not strictly indicate material's ability to be employed as *high* performance electrodes for ECs and will be affected by other factors such as electrical conductivity. [39]

The power (P) of the device is another important parameter which is the energy it produces or uses per unit of time. It is dependent on voltage and internal resistance (ESR):

$$P = \frac{U^2}{4 \cdot ESR}$$
<div align="right">eq.8</div>

Where the ESR is the main limiting factor. It includes all the internal resistances that impede the flow of current inside an EC.

2.3 EDL Theory

As beforementioned, EDL is a structure that forms at the interface of an electrolyte and a charged surface of the electrode. [23] Originally, it was Helmholtz who proposed the concept of double layer on a charged electrode surface in 1853. [40, 41] The model assumes adsorption of a layer consisting of a single ion on polarized electrode surface. However, it lacks information about electrode-electrolyte interface. Thus, this model was later improved by Gouy- Chapman, where the diffuse layer was considered, using the Poisson-Boltznann theory. [42, 43] Ultimately, capacitance can then be regarded as a non-constant value because it is affected by the applied voltage and the concentration of ions. Later, Stern introduced the concept of dividing the electrolyte region into two distinct layers: Stern and diffuse layers. The former constitutes of an inner layer that is inaccessible to ionic species, whereas the latter describes the ion distribution that is inhomogeneous. [44] Based on this model, (Gouy-Chapman-Stern (GSC)) one can therefore assume the EDL capacitance to consist of compact double-layer capacitance (C_{inner}) and diffuse region capacitance ($C_{diffuse}$) [14]

$$\frac{1}{C_{dl}} = \frac{1}{C_{inner}} + \frac{1}{C_{diffuse}}$$
<div align="right">eq.9</div>

This concept was then extended by Grahame to include the inner Helmholtz plane (IHP) which encompasses the Stern layer (closest to the electrode surface) and the outer Helmholtz plane (OHP) which is placed at the closest distance of hydrated ions to the electrode surface (further from IHP). [45] The IHP was considered to be consisting of specifically adsorbed ions (that is, those that are strongly bound to the electrode surface) and solvent molecules, where the mentioned ions are completely dehydrated or only

partially dehydrated. [46] The OHP will therefore include non-specifically adsorbed hydrated ions.

Although these classical models (GCS) help to present simplified approach to the ion behavior and the resulting EDL structure, (which can then help in understanding of various electrochemical processes), one must remember that they may not always be applicable alone for porous electrodes. In such case, modifications must be considered to include e.g. pore size effects, pore size distribution (PSD), and pore shape. [47, 48] These models also do not consider molecular nature of the ions and solvent [49, 50] which is why more advanced modelling techniques, such as molecular dynamics (MD) simulations and Density Functional Theory (DFT) can prove advantageous in gaining a more comprehensive understanding of EDL for porous electrode materials.

2.4   Electrode Materials for ECs

Based on the type of charge accumulation mechanism, the electrode materials employed in ECs can be broadly divided into porous carbons and pseudocapacitive materials. Of course, various composites that possess characteristics of both also exist. More distinctive categorization is included in Figure 6:
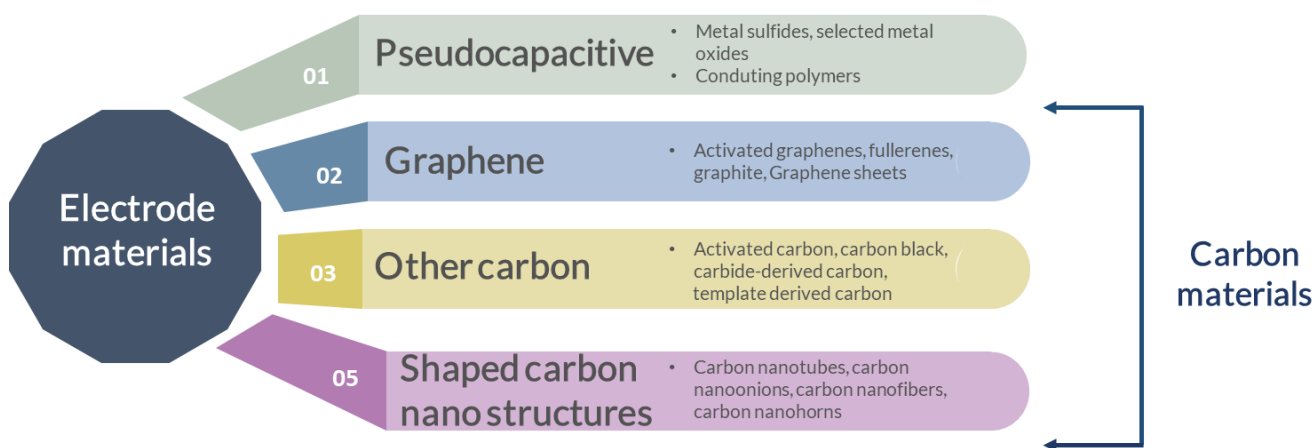

Electrode materials

- **01 Pseudocapacitive**
  - Metal sulfides, selected metal oxides
  - Conduting polymers
- **02 Graphene**
  - Activated graphenes, fullerenes, graphite, Graphene sheets
- **03 Other carbon**
  - Activated carbon, carbon black, carbide-derived carbon, template derived carbon
- **05 Shaped carbon nano structures**
  - Carbon nanotubes, carbon nanoonions, carbon nanofibers, carbon nanohorns

Carbon materials

Figure 6. Electrode materials used for ECs

Carbon materials

Amongst carbon materials, typically, AC is the electrode material of choice for ECs applications. It is a form of carbon that is produced by various carbonaceous raw materials, some of natural origin, such as rice husk, wood, coconut shells and bamboo.

[51-56] Through activation processes, its' surface area, pore size distribution (PSD) as well as pore size can be altered to fit specific needs. [57] The activation process can be either physical or chemical and is governed by activating agents. In physical activation of the carbon precursor, oxidation takes place at high temperatures, where CO_2 and H_2O steam are most often used. In the chemical activation procedure, KOH, $ZnCl_2$, NaOH and H_3PO_4 are most representative chemical agents that are employed. [58] Moreover, the AC materials that are obtained through chemical activation process give in general, higher mass yields and are more porous compared to those acquired by physical methods. [59-61] After activation, porous network is produced in the bulk; in the grains, micropores (<2nm), mesopores (2-50nm) and macropores (>50nm) can be obtained. [30] Through activation process also, carbon can become rich in oxygen atoms (from few % - 30 wt%) in the form of surface oxygen functionalities such as carboxyl, lactone, phenol, ether etc, which can effectively enhance capacitance of the ECs. [62-64] ACs are also characterized by large specific surface area (SSA) (>1000 m^2 g^{-1}), good electrical conductivity, resistance to corrosion, and tunable properties; such as surface chemistry, morphology, and texture. [65, 66] These properties can be altered by chosen synthesis, type of precursor or application of post-treatment methods. Moreover, they are readily available, can be synthesized in various forms (powder, clothes, fibers) and are low-cost materials making them perfect for research and industrial applications. Synthetic ACs can also be attained when produced from polymer gels at high temperatures and inert environment. They are characterized by improved control over the porosity which is attained during the synthesis and activation processes. Additionally, the gel that is used as a precursor has an adjustable cross-linked structure, which results in an AC with a 3D structure and high conductivity.[57] Regarding SSA, it's worth noting that theoretically, it is assumed that the larger the SSA the larger the specific capacitance. However, pore shape and size may result in similar values of SSA, making this statement somehow restricted. The accessibility of pores to the ions from the electrolyte is another important issue that needs to be addressed in this matter, since it will directly impact the effective surface area available for charge storage. [67] ACs can also come in form of fibres, that includes highly porous activated carbon fibres (ACFs) which are acquired via electro-spinning methods. [68, 69] Essentially, they can be categorized as a combination of activated carbons and carbon fibers. Other carbon materials include carbide-derived

carbons (CDCs), [70] carbon aerogels, [71] carbon blacks (CBs) [72] and template derived carbons (TDCs). [73] Carbon materials used as electrodes can be also subdivided into two other groups, mainly graphene materials and shaped carbon nano structures which will be discussed in more detail.

(i)   Graphene materials

Because of their exceptional electrical conductivity and very large surface area, graphene-based materials have the potential to be used as components in electrodes in ECs. They include fullerenes, graphene sheets, graphite and activated graphenes. Graphene is 2D sheet containing sp^2 carbon atoms arranged in a honeycomb network of six-member rings. [74, 75] It can therefore be considered as a 'building block' for all the other graphitic materials unit for building all graphitic materials with different dimensionalities (0D, 1D, 3D). [76] Theoretically, a single-layer graphene's surface area would result in high EDL capacitance and energy density. However, this surface area is much reduced, as for charge transfer to occur, a dense cross-linked network must be formed. [77, 78] To effectively improve SSA without compromising the electrical properties, methods such as chemical activation, light treatment an self-assembly can be considered. [79] Graphene can be produced by several methods: reduction of graphene oxides (GO), epitaxial growth, chemical vapor deposition (CVD) and liquid phase exfoliation.

(ii)   Shaped carbon nano structures

This class of carbon materials are known to possess very specific and controlled shapes/morphologies that are obtained through various engineering and synthesis methods. [80] This allows them to be specifically 'tailored' to specific needs, whether it be for catalysis, energy storage, electronics or biomedicine. These shaped carbon nano structures include materials such as carbon nanotubes (CNTs), [81] carbon nanofibers, [82] carbon nanoonions [83] and carbon nanohorns. [84] CNTs are particularly interesting for EC applications due to their electrical, chemical stability and mechanical characteristics. They are basically cylinders of rolled up sheets of graphene, that can be classified into three types: single walled CNTs (SWCNTs), double-walled CNTs (DWCNTs) and multi-walled CNTs (MWCNTs), the difference being in number of sheets of graphene it comprises of. They can be produced by a number of methods, including arc

discharge, laser ablation, and CVD. [85] To effectively boost up the ECs performance, CNTs are usually used as part of a composite electrode, such as with AC and graphene, [86, 87] for synergistic effects and cost management.

Pseudocapacitive materials

Amongst the pseudocapacitive materials, metal oxides (MnO_2, , RuO_2), conducting polymers (PPy,PANI) , metal sulfides (MoS_2, ReS_2) and their corresponding composites have been studied and used as electrode materials for ECs. [88-92] Although these materials can provide higher energy densities than traditional carbon materials (as they involve fast and reversible redox reactions that take place at the electrode surface), they tend to suffer from kinetic limitations and rather poor capacitance retention upon cycling, [93, 94] hence, the use of composite materials which combines synergetic effects. In general, however, the field of pseudocapacitive materials is constantly developing- where novel materials, their enhanced functionality, and a better comprehension of their underlying mechanisms are developed.
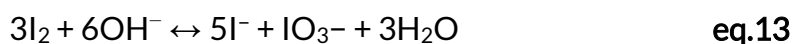
2.5   Electrolytes for ECs

The performance of the EC is greatly influenced by the choice of the electrolyte, particularly, their voltage window and cycle stability. [95] Thus, to effectively increase the device's energy density, electrolyte approach is plausible and can be implemented, as it depends on charge stored and operating voltage window. Moreover, matching the electrolyte and electrode material with optimized pore size is vital, as it will influence the capacitance of the device. [95] The electrolytes for ECs can be classified into liquid, solid-state and quasi-solid state, where liquid electrolytes are the most popular choice. [21, 96-100] This is because ECs are high power devices, thus liquid electrolytes are capable to deliver high ionic mobility. These liquid electrolytes can be further divided into: aqueous (e.g. Li_2SO_4, KOH, H_2SO_4), organic (e.g. $TEABF_4$/AN, $LiPF_6$/EC:DMC) and ionic liquids (e.g. [EMIM][BF_4], [BMIM][BF_4]) where as far as commercial systems are concerned, organic based electrolytes are preferred due to wide potential window (~2.5-2.8 V). [101] In general, regarding the criteria for EC applications, the following should always be considered: viscosity, ionic conductivity, price, accessibility, environmental impact and potential window. Nevertheless, a fair trade-off between those properties must be reached, as no 'perfect' electrolyte has been discovered yet.

Aqueous electrolytes

Aqueous based electrolytes are characterized by low cost, high conductivity (temperature and concentration dependent) and are environmentally safe. Additionally, they can incorporate redox reactions which boost specific capacitance stored. Their use commercially, however, is limited due to a narrow voltage window governed by thermodynamic stability of water (1.23 V), which in contrast to aprotic medium, is not a matter of concern. Nonetheless, they remain quite well studied systems to date, with a strong focus being recently shifted towards fundamental studies that can explain their limitations. [98, 102-117] Amongst aqueous electrolytes, alkaline and acidic electrolytes are widely selected for EC applications, due to high ionic conductivities i.e. for. 6M KOH it is 0.6 S cm^{-1} at 25 °C. [118] This allows for rapid charge transfer and contributes to device's high power density. However, their corrosive nature and safety concerns limit their use for certain applications. Corrosion of current collectors is particularly problematic and so the use of expensive metals is necessary, such as gold, which is highly impractical for commercial use. In such light, aqueous electrolytes based on inorganic salts are promising candidates for ECs and are often employed in such systems. They are characterized by better electrochemical stability, are non-corrosive and have a wide potential window up to 1.6 V (for neutral alkali metal sulphate and nitrate based electrolytes) compared to the reported values of 0.8 V or 1.0 V for 1 mol L^{-1} H_2SO_4 and 6M KOH electrolytes. [32, 96, 107, 119-122] The extended operating voltage window is owning to overpotentials for oxygen and hydrogen evolution reactions (OER) and (HER) exhibited by such pH neutral electrolytes. In fact, it was demonstrated that 1 mol L^{-1} Li_2SO_4 coupled with microporous AC was able to operate up to 2.2 V for ~ 15,000 charging/discharging cycles at 1 A g^{-1}. [96] However, associated aging related contributors such as corrosion were diminished through the use of gold current collectors. Thus when stainless steel current collectors were used the same system, it was shown that the EC can safely operate up to 1.5 V. [123] Above this value, generation of gases and electrode oxidation is initiated. Still, this value is quite impressive and much higher than those reached by acidic and alkaline electrolytes, yet not high enough to compete with organic based electrolytes. Another approach is based on Faradaic contribution from redox species, which provides an increase in specific capacitance and thus allows to reach much higher energy density values. In that manner, redox active

electrolytes prove to be an attractive alternative. They are characterized by an adjustable redox potential that can be controlled through concentration and pH, as well as improved diffusion in the liquid state. [106, 124, 125] The main disadvantage of such solutions include self-discharge through redox species shuttling, unpredictable and variable cyclability and losses related to diffusion overvoltage. [126, 127] Amongst the redox active electrolytes, those based on iodides were shown to be an attractive choice, such as those based on KI and CsI. [128] The redox potential of iodide allows for wider operating voltage window to be reached compared to other redox electrolytes. Moreover, higher power density and theoretical capacity can be obtained. Unfortunately, ECs incorporating iodide-based electrolytes still face their challenges. Although redox reactions are reversible, changes in pressure, concentration and pH can inevitably shift the equilibrium potential. According to the Pourbaix diagram, [129] the redox activity of the iodide based species can generate its' different forms, depending on the pH of the electrolytic solution:

$$2I^- \leftrightarrow I_2 + 2e^- \qquad\qquad \text{eq.10}$$

$$3I^- \leftrightarrow I_3^- + 2e^- \qquad\qquad \text{eq.11}$$

$$5I^- \leftrightarrow I_5^- + 4e^- \qquad\qquad \text{eq.12}$$

$$3I_2 + 6OH^- \leftrightarrow 5I^- + IO_3{-} + 3H_2O \qquad\qquad \text{eq.13}$$

Particularly, formation of polyiodides (I_3^- and I_5^-) and iodate (IO_3^-) can be unfavorable for ECs long term performance, leading to reduced concentration of redox-active species and pore clogging [104, 130, 131]. Although numerous studies have been proposed as to gain deeper insights into performance of neutral aqueous electrolytes from fundamental point of view (especially those based on iodides and sulphates are prominent [102, 121, 128, 132]) advancements in the field for nitrate-based electrolytes is regrettably lacking.

Organic electrolytes

Organic electrolytes for ECs consist of a conducting salt, for example: tetraethylammonium tetrafluoroborate (TEABF$_4$), lithium hexafluorophosphate (LiPF$_6$), sodium hexafluorophosphate (NaPF$_6$) and lithium perchlorate (LiClO$_4$); dissolved in an organic solvent, such as, acetonitrile (AN), propylene carbonate (PC), adiponitrile (ADN), ethylene carbonate (EC) diethyl carbonate (DEC), N,N-dimethyl formamide (DMF) and

dimethyl carbonate (DMC). As beforementioned, they are widely used in commercial markets due to the wide and nondisruptive operating voltage window. As a matter of fact, due to the highest conductivity in given solvents; i.e. AN, PC, and DMF; electrolytes based on TEABF$_4$ are most often chosen on a commercial scale. [133] Organic electrolytes in general are however, characterized by high flammability, cost, toxicity, non-eco-friendly nature and rather problematic preparation and handling that requires oxygen and water free environments. On top of that, they have higher resistivity compared to aqueous electrolytes, where ionic conductivities of 1 M TEABF$_4$/AN *vs.* 30 wt% H$_2$SO$_4$ are 0.06 S cm^{-1} and 0.8 S cm^{-1} at 25 °C respectively. In fact, it was demonstrated that the ESR of EC based on AC and 0.5 M TBAPF$_6$/AN was within the range of 7 - 12 Ω cm^{-2} and 0.75 Ω cm^{-2} for system containing 0.5 M H$_2$SO$_4$. [134] Presence of impurities or water trace should also be accounted for, as they will inevitably limit the electrochemical performance of the EC through unwanted side reactions and water decomposition reactions, i.e. electrochemical stability is affected. Such is the case for TEABF$_4$/AN electrolyte, in which hydrolysis of BF$_4$ can yield detrimental and corrosive HF that leads to a much more pronounced degradation of the EC. [135] Moreover, water traces were also found to affect the self-discharge process. [136] Even though organic electrolytes have many cons, their advantages still outweigh the disadvantages – commercial ECs **must** have long, and stable cycle life paired with higher energy densities for practical applications. Therefore, active research is carried out in order to address and improve those disadvantages, whether it be by exploring various additives or development of safer electrolytes for improved thermal stability or flammability issues. [137-140] In this sense, solid-state electrolytes have been also considered as an alternative due to their non-flammable nature. [141] Regarding specific capacitance values, they are lower for organic electrolytes compared to aqueous ones in carbon based ECs. [142] This could be somehow linked to larger size of solvated ions in organic electrolytes that would then have difficulty penetrating the carbon porosity, and thus, affecting the EDL capacitance. Additionally, it was shown that the capacitance is indeed affected by ion/pore size match; Koh *et al.* have proved such claim when studying quaternary ammonium BF$_4$ salts in microporous carbon electrodes, where the capacitance was found to be proportional to the reciprocal of the radii of bare cations. [143] Therefore, the relationship between pore size of carbon electrodes and the ion size

from the electrolyte becomes important when capacitance values of an organic based EC are to be effectively boosted. Besides, other factors must also be considered, including degree of solvation/de-solvation and even carbon pore morphologies on EDL structure, for which theoretical (such as modelling) or *in-situ* studies (i.e. electrochemical quartz crystal microbalance (EQCM), can be employed. [144] [145, 146]

Ionic Liquids

The mentioned drawbacks exhibited by traditional aqueous and/or organic electrolytes, such as limited potential windows, conductivity or thermal stability can be tackled with the use of ionic liquids (ILs). That's why they can be considered as an 'alternative' choice in that matter. They comprise of organic cations and inorganic/organic anions that have tunable chemical and physical properties (hence coined as 'designer solvents') and melting points below 100°C. [147] Based on the composition, they can be classified as: zwitter ionic, aprotic or protic, with the latter (e.g. pyrrolidinium bis(trifluoromethanesulfonyl)imide ([Pyrr][TFSI]), pyrrolidinium nitrate (PyNO$_3$)), having limited interest in the EC field due to lower operating voltage (1.2–2.5 V) than aprotic IL electrolytes. [148-151] Essentially, the most often used anions for EC applications are: hexafluorophosphate [PF$_6$]$^-$, bis(trifluoromethane sulfonyl imide) [TFSI]$^-$, bis(fluorosulfonyl imide) [FSI]$^-$ and tetrafluoroborate [BF$_4$]$^-$, and cations: phosphonium, sulfonium, imidazolium, pyrrolidinium and ammonium. However, ILs have three major disadvantages which deem them unsuitable in commercial setting: high viscosity, price (constituting of synthesis, purification, overall cost) and rather poor conductivity. Amongst ILs, those based on imidazolium are characterized by higher conductivity compared to other ILs, hence why they are extensively studied for use in both ECs and hybrid ECs. [101] Moreover, it's worth noting that incorporation with organic solvents can aid in improvement of their properties, such as simultaneous increase in capacitance and decreased internal resistance., as shown when DMF was introduced to [BMIM][PF$_6$] in an asymmetric AC//MnO$_2$ EC. [152] For pyrrolidinium-based ILs such approach allows for increase in conductivity and decrease in viscosity, considering the solvation effect. [101] In such light, when both price and physical properties are considered, incorporation of ILs as an electrolyte component rather than in a pure form seems more advantageous for future prospects in energy storage field.

2.6 Comparison to other energy storage devices

To effectively compare ECs with other energy storage devices, it is necessary to express them in terms of power and energy densities. Thus, representation on the *Ragone Plot* is advised, as illustrated in Figure 6. It's imperative to note that none of the mentioned devices are discredited; each has its' own use and its specific set of characteristics that determines its intended application.
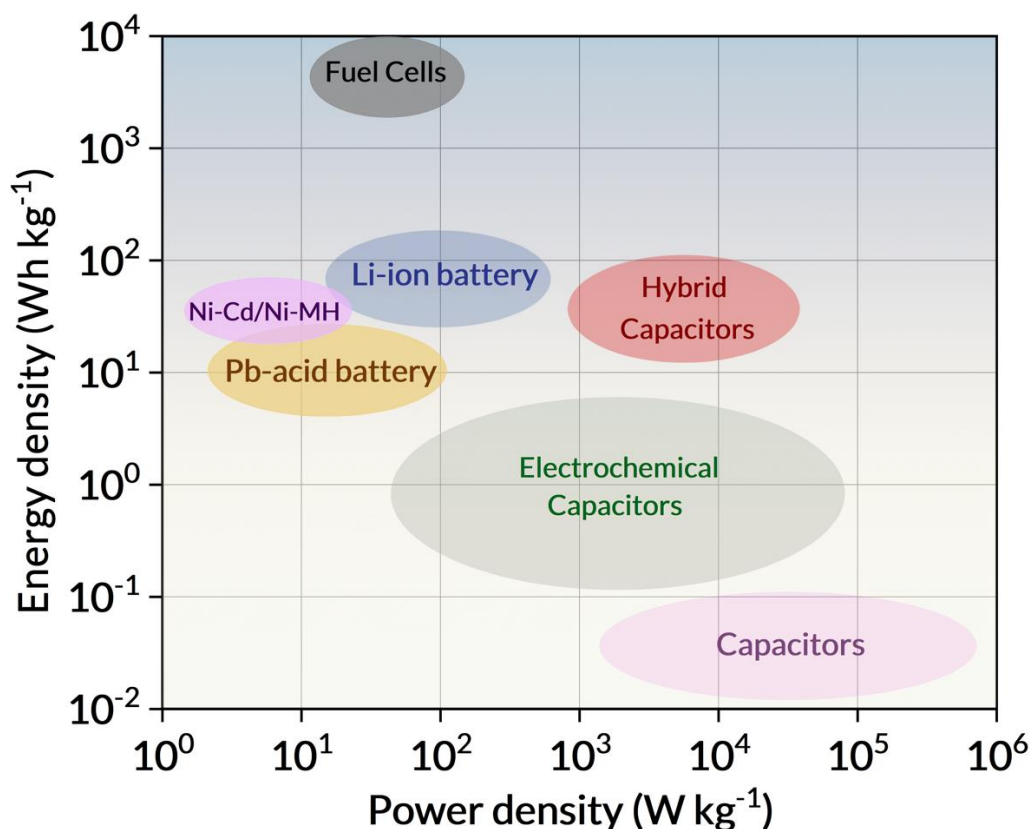

Figure 7. Ragone Plot, based on [153]

Given that, ECs offer a "bridge" between these two parameters compared to e.g. a conventional capacitor which possesses very high-power density but rather poor energy density which ultimately restricts its usage. However, in contrast to batteries such as LIBs, ECs offer limited energy density but superior power density and much extended cyclability due to its charge storage mechanism that doesn't include irreversible chemical reactions. LIBs can supply a minimum specific energy of 200 Wh kg^{-1} and specific power <350 W kg^{-1}, whereas for commercial ECs those values can reach on average 5 Wh kg^{-1} and ~11 kW kg^{-1} respectively. [154] Moreover, high power performance of ECs can be attainable at temperatures down to - 40 °C, which is not the

case for batteries. [13] More comprehensive comparison between batteries, ECs and capacitors is given in Table 1, where the most vital parameters are included.

Table 1 Comparison of various characteristics between given energy storage devices, adapted from [23]

Parameters	Battery	ECs	Capacitor
Specific power (W kg^{-1})	<1000	500-10,000	>10,000
Specific energy (W h kg^{-1})	10-100	1-10	< 0.1
Coulombic efficiency (%)	70-85	85-98	~100
Cycle-life	~1000	>500,000	Almost infinite
Charge time	1-5 h	s to min	10^{-6}- 10^{-3}
Discharge time	0.3- 3 h	s to min	10^{-6}- 10^{-3}

Thus, on a comparative note, when pros and cons of both technologies (that is batteries and ECs) are considered, one could argue that they aren't 'perfect' and could potentially benefit from one another to deliver superior high energy-high power devices with extended cycle life. This is where the concept of a hybrid ion capacitor (HIC) comes into play, which combines the positive EDL electrode and battery-like negative electrode. [155-160] Such device has the ability to deliver 4 or 5 times higher energy values compared to traditional ECs through incorporation of intercalation mechanism in one of the electrodes, and the use of carbonate based electrolyte which yields higher operating voltage of ~4.2 V, [161, 162] compared to a commercial symmetric organic electrolyte based EC, where this value is limited to only ~2.7 V.

Among the most prominent in the category of HICs is the lithium-ion capacitor (LIC), which will be further discussed and studied.

3. Lithium-ion capacitor

3.1 Construction and principle of operation

One of the first LIC based on nanostructured $Li_4Ti_5O_{12}$ (LTO) and AC was constructed and evaluated by Amatucci *et al.* in 2001. [163] However, it was only when graphite was introduced as the negative electrode material when the device began to be commercialized. [164] Since then, significant advancements in performance, materials and cell design have been made in the field. [165-169] This is largely due to the much improved understanding of these devices and their operation on a fundamental level. Such approach specifically allows for targeting specific problems linked to decline in cycle life and degradation of the device.

With regards to the construction, LIC merges two electrodes with different mechanisms: lithium-ion battery type negative electrode which uses intercalation mechanism and an EDL positive electrode. This approach allows for the device to combine dual benefits of both devices: ECs (extended cycle life of up to 100 000 cycles and high specific power ~10 kW kg^{-1}) and LIBs (high specific energy of ~14 Wh kg^{-1}). [170-172] Moreover, it suffers from much less self-discharge compared to ECs and has wide operating temperature range (-40- 70 °C). [173]

Like in other energy storage devices, the electrolyte's role is to transfer charge, and the separator is a porous thin material that ensures the electrodes do not come into direct contact, thus avoiding short circuits. The separator can be polymer, paper, glass fibre or ceramic, largely depending on the electrolyte used. With regards to the electrolyte, most commonly 1 mol L^{-1} LiPF$_6$ in EC:DMC (lithium hexafluorophosphate solution in ethylene carbonate and dimethyl carbonate) is used in both research and industry. To improve solid electrolyte interphase (SEI) formation, ionic conductivity, electrolyte stability, wettability or thermal behavior, various electrolyte additives might be considered. [174, 175]The addition of conductive additives such as carbon black or carbon nanotubes to the active material of the electrode ensures improved electrical conductivity. It must be, however, well dispersed within the material and its' amount optimized to ensure efficient ion transport. [176, 177] Moreover, unlike LIBs, LICs require an additional step in the form of pre-lithiation of the negative electrode that takes place during the first

charging cycle. [178] Although this is a vital step that compensates for irreversible lithium loss and improves Coulombic efficiency of the device, [179-181] it introduces significantly higher costs and potential problems related to manufacturing on a commercial scale.

The operation principle of LICs constructed in this doctoral work, is based on lithium ion intercalation at the negative electrode and anion adsorption into the porosity of the positive electrode during charging, with the opposite taking place upon discharging process (represented in Figure 7). [182-184] The power of the LIC device is thus limited by the negative electrode; this is because the intercalation process is much slower than the adsorption process taking place at the positive electrode. Conversely, the specific energy is limited by the positive electrode, due to its' non-faradaic nature. [171]
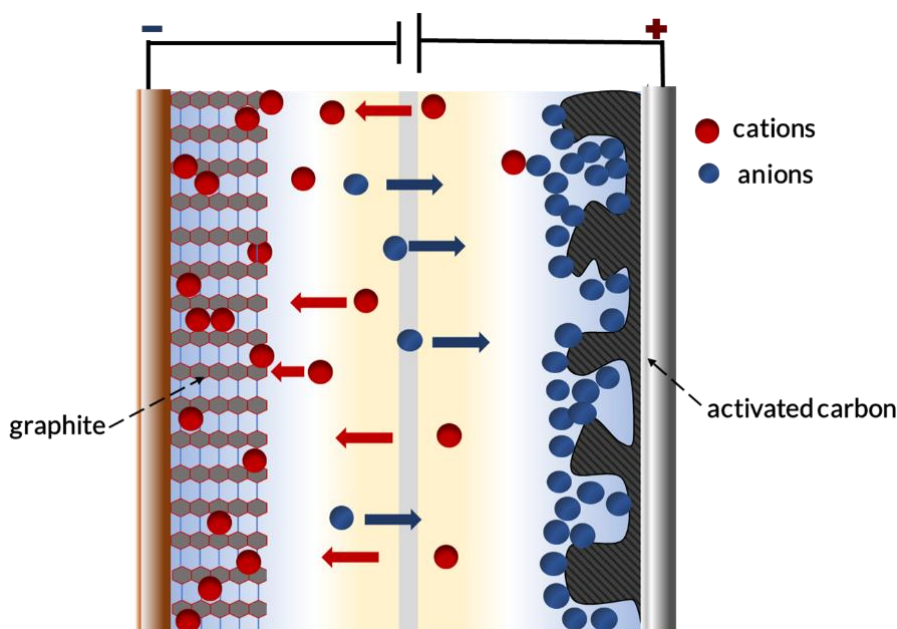

Figure 8. Simplified working principle of the LIC during charging process

3.2   Electrode materials for LICs

Electrode materials are a crucial part of LICs and have a significant impact on their performance. [173, 185, 186] Cathodes for LICs can be categorized into those based on carbon materials (AC, graphene, templated mesoporous carbon, aerogels, CNTs), [183, 187-190] composite materials (carbonous or Li-metal oxide (LMO) based) [191] or intercalation materials (lithium metal oxides). [192, 193] In terms of commercial

feasibility, AC prevails as the chosen cathode material, due to beforementioned properties such as its availability, high surface area, tunable properties, good electrical conductivity, and relative low cost in. [194] In addition, various different precursors based on biomass waste can be used, which have gained vast popularity due to their abundant and renewable nature. [195] These range from lignin, [196] algae, [197] tobacco leaves, [198] sawdust, petroleum coke and coconut shells. Some of those have not gone as far as beyond lab-scale use, whilst the last three are commonly used commercially. On the other hand, LMO based materials can achieve higher capacity but have limited power output due to poor electrical conductivity and diffusion coefficient. [187] Regarding anode materials, they can be neatly divided into three main groups: (i) insertion type materials; including carbonaceous, lithium containing oxides such as lithium titanate (LTO), [199] lithium vanadate (LVO) [200] or their composites, [201] (ii) conversion type materials such as chalcogenides and transition metal oxides, [202, 203] and alloy type materials. [204] LTO is particularly advantageous due to its' 'zero strain' attributes, which implies that during charge/discharge cycles it experiences minimal dimensional changes. [205] Another currently studied anode material for LICs showcasing promising prospects is the two-dimensional MXenes, such as those based on $Ti_3C_2T_x$. However, $Ti_3C_2T_x$ nanosheets in particular, tend to 'restack', thus various composites with carbon materials e.g. reduced graphene oxide (rGO), AC and CNTs are often incorporated to overcome this problem. [206-208]

3.3   Electrolytes for LICs

As mentioned, the electrolyte plays an important part in LIC operation. Apart from the obvious role of providing ions and their transport, it serves an additional purpose of participating in SEI formation. The most common electrolytes in the LIC field are based on several organic solvents (such as EC, DMC, EMC (ethyl methyl carbonate), PC, DEC) and lithium salts. Fluorinated salts such as industry's golden standard $LiPF_6$, possess high ionic conductivity, form passivation layer on aluminum current collector on the positive electrode and have good charge-discharge kinetics. [209] However, they can release toxic hydrogen fluoride when exposed to water traces or during improper handling, raising rather serious concerns in terms of safety, health and environment. Another common practice involves preparation of electrolytes based on two or more solvents, i.e.

EC/DMC, EC/DEC/DMC etc. for enhanced performance. One would almost always find EC to be the solvent of choice or at least one of the contributors, due to its' ability to form stable SEI on the surface of the negative electrode. [173] This is not always the case for other solvents, especially to achieve on their own, PC being a good example in such case. [210-214] PC can however improve low temperature performance of the LIC when used as an additive, as shown by Wang *et al.* [214] Addition of other low viscosity solvents such as DMC, DEC, and EMC to EC can also be advantageous as it will increase Li^+ migration rate. [173] Therefore, it's safe to say that through electrolyte additive incorporation, even in low concentrations, performance of the LIC device can be vastly improved; whether it be in the realm of boosted cyclability, safety of interphase stability.
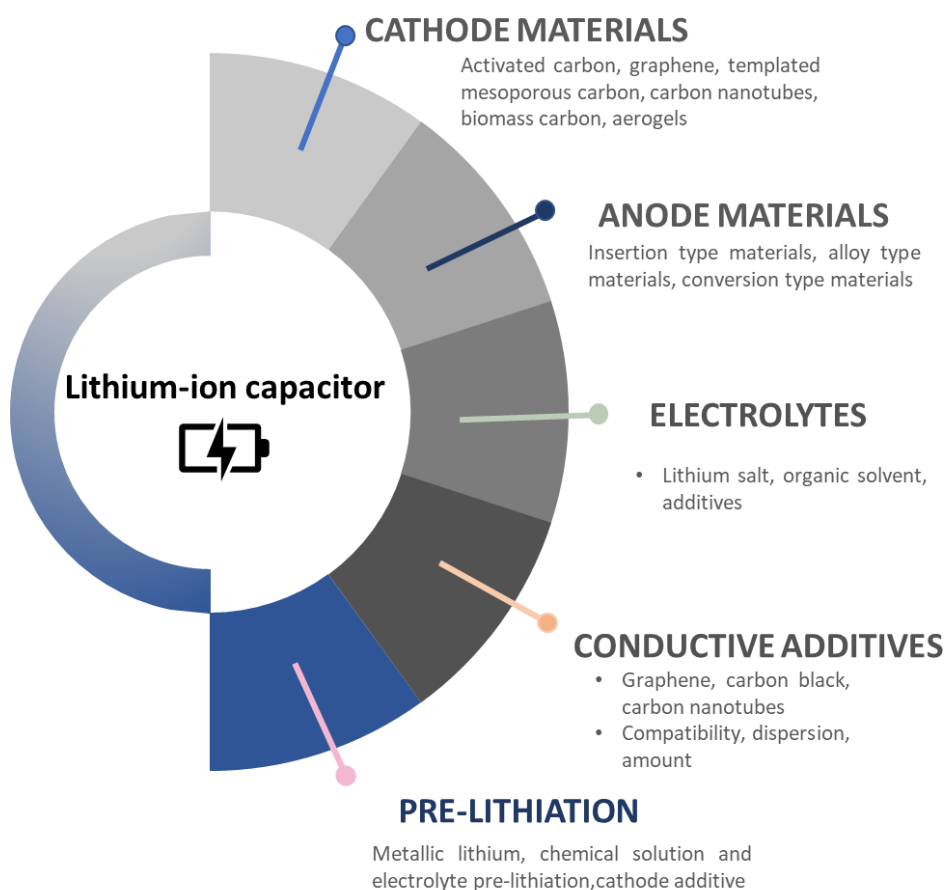

CATHODE MATERIALS
Activated carbon, graphene, templated mesoporous carbon, carbon nanotubes, biomass carbon, aerogels

ANODE MATERIALS
Insertion type materials, alloy type materials, conversion type materials

ELECTROLYTES
• Lithium salt, organic solvent, additives

CONDUCTIVE ADDITIVES
• Graphene, carbon black, carbon nanotubes
• Compatibility, dispersion, amount

PRE-LITHIATION
Metallic lithium, chemical solution and electrolyte pre-lithiation, cathode additive

Lithium-ion capacitor

Figure 9. Summary of LIC components and important features, based on [171, 173]

4. Fundamental studies of ECs

To improve ECs' performance, it is crucial to understand and properly describe the mechanism of charge storage within these devices. For this, the use of advanced techniques and new approaches should be proposed concerning fundamental studies. The concept of research on electrode charging in ECs revolves around understanding the intricate relationship between the electrode materials and the electrolyte during the charging and discharging processes. Especially, when activated carbon and aqueous electrolytes are paired, the processes taking place during EC charging/discharging are not as straightforward due to the complex structure and surface chemistry of activated carbon electrodes. As far as techniques which can be applied to study charge storage mechanisms in ECs, they can be categorized into: (i) *in-situ* and (ii) *operando* techniques. From the fundamental approach, they are incredibly valuable as they bridge the gap between theoretical understanding and practical performance. As opposed to modelling and simulations, they allow for **real-time** observation of the dynamic processes happening at the electrode/electrolyte interface, thus an experimental validation is reached for the studied systems. [215] Of course, the two can be used alongside each other for even better outcome; Venâncio *et al.* investigated the stability of electrodes and organic electrolytes in ECs based on *operando* Raman and FT-IR together with atomistic molecular dynamics (MD) simulations and electrochemical techniques. [216] Another work used MD simulations coupled with *operando* ECD to investigate the pore-ion population changes in an AC-based electrode of LICs. [217] However, it is not always plausible to use such approach and those studies are limited in the existing literature. Combination of one or two *in-situ* and/or *operando* techniques is far more common, and allows for gaining a comprehensive understanding of phenomena in question at the nanoscale, especially since the adsorption/desorption process in systems with AC is affected by the **ion-pore size mismatch, ion-exchange mechanism** and the **ion solvation effect**. [218] Amongst those techniques, the most established ones include: (i) *in-situ* spectroscopic techniques (nuclear magnetic resonance (NMR) spectroscopy, electrochemical impedance spectroscopy (EIS)), (ii) X-ray based techniques (X-ray diffraction (XRD) and X-ray photoelectron spectroscopy (XPS)), gravimetric techniques (*in-situ* electrochemical quartz crystal microbalance (EQCM), differential

electrochemical mass spectroscopy (DEMS)), *in-situ/operando* optical based techniques (Raman spectroscopy, FTIR) and <u>mechanical</u> techniques such as *operando* ECD. EQCM stands out as a valuable technique for studying the electrode/electrolyte interface and has gained growing interest in the electrochemistry community over the last decade or so. It provides high level sensitivity to mass changes at the electrode surface; thus, one can detect adsorption/desorption of ions during operation. The principle of operation is based on the application of a thin piezoelectric quartz crystal that is placed in between two metal electrodes. This is then used to apply an alternating electric field across the crystal, which causes a vibrational motion of the crystal at its resonance frequency. [219, 220] Recorded frequency changes are then converted to respective mass changes, as per Saurbrey's equation (eq.14), which is valid for rigid films. Therefore, one needs to also consider resistance changes ($\triangle R$) which are recorded simultaneously to the frequency changes. There aren't any definitive guidelines for EQCM users regarding the exact value of $\triangle R$. However, it has been accepted that resistance changes smaller than ±2% should be considered for further mass recalculation (to be considered as sufficiently rigid for gravimetric calculations), which is regarded as an acceptable range in the electrochemical society. [144, 221, 222]

$$\Delta m = - \frac{\Delta f \cdot A \cdot \sqrt{\rho \cdot \mu}}{2f_o^2}$$ eq.14

In the Saurbrey's equation above: A = surface area of quartz crystal [m^2], ρ= density of quartz (2.648 g cm^{-3}), μ= shear modulus of quartz (2.947 10^{11} g cm^{-1} s^{-2}), $\triangle f$= change in frequency [Hz], and f_0= fundamental resonance frequency of the crystal [Hz]. [223] Essentially, a change in the mass of the WE (which would be the electrode material coated onto the resonator) causes frequency changes. During ion adsorption, the mass of the WE increases, therefore, decreasing the registered frequency of the piezoelectric crystal. The opposite happens during ion desorption. As a subsequent step, Faraday equation is implemented (eq.15) which ultimately allows to compare the experimental and theoretical mass changes in the s called mass *vs.* charge ratio plot:

$$\Delta m = - \frac{\Delta Q \cdot M}{F \cdot z}$$ eq.14

Where Δm= mass change [g], ΔQ= charge exchanged [C], M= molar mass of ion adsorbed/desorbed [g mol^{-1}], F = Faraday's constant [96 485 C mol^{-1}], and z is the

number of exchanged electrons (i.e., the valence number of adsorbed/desorbed ion). The use and applicability of dilute solutions with highly porous carbons in EQCM studies needs to be mentioned as well, where due to its highly sensitive nature, concentrated electrolytic solution cannot be well implemented due to much larger mass. In terms of ECs, EQCM has been widely applied for investigation in various porous carbon materials (e.g. TiC-CDC, carbon blacks, RGO). [66, 221, 224-228] However, studies focused on ECs with ACs in aqueous electrolytes are very limited, where mostly organic medium and ILs predominate. [102, 226, 229] As mentioned, this arises from the intricate charging behavior of the interface (based on co-ion adsorption, counter-ion adsorption and ion reorganization, often involving a 'multi-step' approach- yet adding more scientific involution!) and, specifically, from the complex structure and surface chemistry of AC electrodes. . One could therefore say that there is a rather large gap between the theoretical description of an ideal interface of an EC and the experimental behavior of a 'real' electrode (such AC) in water-based systems, which emphasizes the need for further scientific advancements in this area. Additionally, the charge storage mechanism will depend on the properties of the carbon material (surface functionalities, pore size, topology) and the nature of the ions (such as size and charge number). Such studies have been reported in the literature, with **ion transport** and **ion desolvation** being the main processes discussed. The degree of desolvation specifically, has been shown to be is directly linked to the ion size/charge number as well as pore size for alkali metal cations and halide anions with microporous/mesoporous porous carbons (BP-880, BP2000 and YP-17). [225] Similar findings were concluded with CDC-1 nm and CDC-0.65 nm in 2 mol L^{-1} EMIm$^+$TFSI$^-$/AN electrolyte [221] and in another study that looked at a direct assessment of the behavior of electroadsorbed ions and solvent molecules confined in micropores of AC electrodes in contact with aprotic electrolytes (based on PC solutions of quaternary (tetraalkyl) ammonium salts). [226] Furthermore, those studies emphasize the intricate nature of ion dynamics at the electrode/electrolyte interface: the interplay of electrode material properties, electrolyte characteristics, electrochemical parameters, and the inherent sensitivity of EQCM to interfacial changes needs to be considered. In such light, each system under investigation requires individual study and tailored analysis. Generalizations are inherently limited by the unique combination of these factors, emphasizing that a thorough understanding of charge storage

mechanisms in ECs requires a meticulous individual approach when it comes to EQCM investigations.

5. Ageing studies

Initial electrochemical performance of proposed systems alone does not deliver adequate information when their applicability is concerned. Ageing studies in energy storage devices are thus crucial to ensure their safety, improved performance and predictability, as well as to enhance cost-effectiveness which is imperative especially from industrial point of view. However, the associated degradation mechanisms are rather complex and will strongly depend on many factors: electrolyte, electrode material, binder type, purity of materials, current collectors, possible contamination such as water trace (in organic electrolytes) and operating conditions (voltage, temperature). [230] Temperature and voltage in particular, will have similar effects on the pace of the ageing process, that is, an increase in either would induce faster decomposition, which wouldn't normally occur at such speed if the voltage or temperature applied was lower. Subsequently, as soon as the energy needed for the decomposition process is obtained, electrochemical decomposition is initiated. [231] However, ECs can also degrade below their maximum operating voltage. [232] Additionally, for LICs which combine electrode materials of both LIB and EC, both aging characteristics need to be anticipated. Hence, it becomes imperative to isolate and study the effect of each factor to 'unlock' their impact on devices' degradation from a fundamental point of view. Additionally, conclusions drawn from studies done on laboratory and industrial scales will inherently differ and cannot be always compared; as in each case, different ageing protocols are implemented. Big companies also tend to keep their internal information private- ensuring secrecy against potential rivals on the market. However, a universal guidance regarding ECs ageing can be found (International standard IEC 62391-1) [233] which specifies the end of life criterion to be defined by 20% capacitance loss and/or 200% increase in internal resistance (ESR) measured. Therefore, such an approach was used for the ageing studies in the doctoral work. Moreover, when discussing ageing studies, one must compare and contrast differences and similarities between *cycling* and *floating* protocols. The former involves recording

several thousands of galvanostatic charge–discharge cycles within a specified voltage range, thus can be quite time consuming, especially for organic based ECs and LICs which are characterized by longer cycle lives compared to water-based systems. *Floating* on the other hand, is based on a potentiostatic hold at elevated voltage and is also referred to as 'accelerated ageing'. Compared to *cycling*, it has extended exposure time at harsh conditions, thus experimentally, will last a shorter amount of time which can be beneficial when time restrictions are concerned. The choice between the two ageing protocols depends on the intended use of the device. *Floating* would be more suited for 'simulating' applications where ECs are used as backup power or for energy storage, since a constant voltage is maintained, whereas *cycling* would depict typical operational conditions of ECs for use in applications like regenerative braking. Furthermore, it was proved that in water based electrolytes, they have different influence on electrode's structure, time of operation and resistance. [234] Therefore, one cannot argue about one being more 'realistic' than the other; it simply takes acknowledging the differences and gathering information one would obtain from either. Keeping all of that in mind, it's safe to say that it would be almost impossible to assign one universal ageing process to each device, whether it be ECs or LICs, as it will heavily depend on the mentioned conditions. Hence, only very general observations can be made. While the knowledge about these general processes of degradation are understood and have been widely studied in different electrolyte environments, [107, 115, 135, 234-241] more extensive studies are sought after, especially when based on combined physicochemical and electrochemical approaches. The incorporation of *operando* or *in-situ* studies can be especially helpful for a more 'in depth' approach, such as *operando* GC-MS, temperature dynamic investigations, *in-situ* Raman Spectroscopy or simulations. [242-245] This can allow to identify new or less understood mechanisms that need further elucidation. Regarding ageing mechanisms in ECs, general conclusions that focus on (i) electrode degradation: loss of SSA, pore blockage, carbon functionalization due to oxidation/reduction and material corrosion as well as (ii) electrolyte decomposition and subsequent side reactions with the electrode and/or binder as well as formation of insoluble species that impede electrochemical performance, can be made. In organic media, presence of a binder will additionally impose different parasitic reactions at high voltage altogether, as the amount and types of surface active sites is varied. [237] In such

light, the effect of carbon functionalization on ageing is another aspect worth exploring. As briefly described in section *2.4. Electrode Materials*, carbon materials for use in energy storage devices, can contain various oxygen or nitrogen containing surface functionalities. The former can be divided into acidic (e.g. acid anhydride, carboxyl, phenol) and basic (e.g. carbonyl, quinone). Additionally, impurities left over from their synthesis in the form of metal oxides, sulfides and halides can be present. [231] While some functionalities aid in improving ECs performance initially (mainly due to enhanced wettability in selected electrolytes, increased active sites and possible pseudocapacitive response by reversible redox reactions by certain groups like quinone) [246-248], they can also have detrimental influence on their long term performance. [249] Generally, it was shown that surface functionalities on the AC electrode oxidize and form new functionalities. [135, 236] He *et al.* reported that system with high surface area AC electrodes in aqueous medium can oxidize even at relatively low voltages, leading to gas evolution and performance degradation; more specifically, due to the presence of lactone, anhydride, phenol, quinone and carbonyl carbon functionalities. [250] Other study in aqueous electrolytic solutions, based on Li_2SO_4 and $LiNO_3$ salts concluded similar findings. [111] Moreover, similar relationship was established for some ageing studies in organic electrolytes: that is, that functional groups have a negative impact on cyclic stability of ECs (although such studies are limited compared to those performed in aqueous media). [251] Work by Azaïs *et al.* highlighted the importance of surface functionalities and their concentration on the performance fade in ECs, suggesting, amongst other factors; such as microporosity and absence of moisture; limited functionality of carbon to be beneficial in that matter. [235] Yang *et al.* performed ageing studies at 2.5 V, 70 °C in 1 M TEABF$_4$/PC and reported formation of a reaction product layer linked to a higher functional group populations in AC which directly deteriorated the capacitive performance of the device. [252] However, such claims are not definite, as concluded by Liu *et al.* that found the presence of acidic functionalities to be favorable in protection of carbon surface and further structural changes by formation of a polymer layer on both positive and negative electrodes. [241] As evidenced, the subject matter is rather ambiguous, and no general conclusion can be made regarding carbon oxygen surface functionalities and their effect on ageing. Once again, it seems to be highly dependent on: selected experimental conditions (voltage, temperature), materials used

and electrolytic solution studied (aqueous *vs.* organic). Therefore, one cannot deny that more extensive research on this topic is also required. In conclusion, elucidating on the ageing phenomena in energy storage devices is still valid. Consequently, the two proposed approaches for the doctoral study, focusing on effects of 1) varied voltage and 2) oxygen surface functionalities on ageing have been proposed and implemented to contribute to the existing knowledge in the field. The study of LICs and organic based ECs allowed for a strategic and broader exploration of the two most advanced and auspicious technologies to date.

6. Electrochemical research techniques

Electrochemical techniques are indispensable for assessing electrochemical cells; they essentially provide crucial insights about their behavior and performance. The electrochemical cells mentioned can be tested according to two configuration: in either two or three-electrode set-ups. In the former, counter and reference electrodes (CE and RE) are shorted, thus the voltage measured is the cell voltage. In the latter, RE is added which has a stable and known potential (such as saturated calomel electrode (SCE) with measured potential of 0.241 V *vs.* standard hydrogen electrode (SHE)) and allows the potential of the working electrode (WE) to be measured. Alternatively, a two-electrode configuration with a RE is plausible, in which the RE allows for simultaneous monitoring of the potential distribution between the WE and CE. Hence why three and two electrode with RE configurations are widely used for fundamental studies, as it allows for information to be gathered on behavior of both: individual electrodes and of the overall system studied. Two electrode configuration is also perfectly acceptable- where it can be used to assess the overall device performance, which is more relevant for practical performance applications, for example in commercial capacitors. Thus, the choice of a selected configuration will depend on what one wants to observe/study. The proposed work (which comprises of three scientific articles and one manuscript) utilizes all three approaches, which are described in more detail in the experimental sections of each. The use of two-electrode configuration was solely used for the ageing studies in the organic medium, while the other fundamental studies in the aqueous medium include all three set-ups. With regards to the electrochemical techniques, cyclic voltammetry, galvanostatic charge/discharge (GCD), current interrupt (CI), staircase potentio

electrochemical impedance spectroscopy (SPEIS) and step potential electrochemical spectroscopy (SPECS) were used and are described in more detail within this section.

6.1 Cycling voltammetry

CV is an extensively used technique within the electrochemistry community due to its versatile nature. It can be used for accurate determination of quantitative and qualitative responses and for mechanistic studies, particularly on a laboratory scale. [14] It is based on recording of a current response during a potential scan at a given scan rate, the potential is then swept back linearly in a reverse direction i.e. the resulting current is measured as a function of the applied potential. For EC studies, CV is mainly used for qualitative studies, although one can calculate capacitance values from the collected data. However, more accurate quantitative information can be acquired by the GCD technique. The resulting voltammogram's shape gives crucial information about the device's performance and energy storage mechanism. [253] For ECs, a rectangular shape denotes an 'ideal' capacitive behavior, related to the formation of an EDL at the electrode-electrolyte interface, which is a reversible and fast process. The current response is relatively constant in the given potential range. In such way, it is also possible to determine the optimal working potential window and the onset of decomposition reactions, where the current measured would start to increase towards the maximum applied potential point. Moreover, any deviations from the rectangular shape can suggest internal resistance issues (in the form of a sloping current response) and presence of a redox reaction (also its reversibility and kinetics). Another important aspect is related to applied scan rate, usually expressed in mV s^{-1}. The chosen scan rate will depend on the aim of the experiment; in lower scan rates (e.g. in the range of 1-10 mV s^{-1}) sufficient time is allocated for ion diffusion, and thus, performance of EC can be more effectively determined. When fast scan rates are applied (50-100 mV s^{-1}), the current response is higher, but the measured capacitance is lower. Essentially, they are used to explore the behavior of ECs at high charge-discharge rates.

6.2 Galvanostatic charge/discharge

In contrast to CV, GCD technique involves charging and discharging of the EC at a constant current where voltage response is measured. As mentioned, it is used to accurately assess its' capacitance, energy, power, resistance and cyclability. [254] The

capacitance can be calculated either from the discharge curve integration or directly from the slope of the curve. Since the curve profile is hardly ever perfectly linear, it is advised to use the former approach. A sudden decrease in voltage that is observed at the beginning of the discharge cycle is called a voltage drop, primarily caused by device's ESR that comprises the total resistance within the device. [127] Therefore for ECs, a more pronounced voltage drop would indicate its' poorer performance and can thus be helpful in assessing the state of health changes during degradation or ageing studies.

6.3   Current interrupt

The CI technique measures the ohmic resistance (R_Ω) by rapidly interrupting the current flowing through the device and the resulting change in voltage is then observed. Simply,

$$R = \frac{\Delta V}{I}$$ eq.15

where R is the resistance of the cell, ΔV is the difference between the voltage of the cell before and after CI, and I is the current. This technique is particularly suitable for ageing studies (and others), as it is a non-destructive and rapid technique, which allows for resistance changes to be monitored efficiently. Moreover in the CI technique, voltage drop caused by the ESR needs to be accounted for and 'corrected', thus a process called iR compensation is used. [255] The level of compensation (in terms of percentage) needs to be adjusted individually according to the studied system. Generally, one would consider partial compensation (within the range of 80-95%) to abstain from possible overcorrection that would intrinsically give inaccurate results. Ideally however, one would determine the right percentage through observation or experimentally for most suitable settings. [256]

6.4   Staircase potentio electrochemical impedance spectroscopy

SPEIS technique combines elements of EIS and potential step techniques thus, it can be considered as a variation of EIS. The data obtained from EIS measurements can be represented in various forms but Nyquist (plot of an imaginary part against real part of impedance data) and Bode (plot of phase angle and modulus as a function of frequency) are the most popular in EC studies (Figure 10), and they are obtained over a wide range of frequencies. In fact, it is a preferred technique for studies based on porous electrodes,

as it allows for the pore size to be evaluated. [257-259]Thus, this technique can give insights into the dynamic behavior of the studied system, where charge transfer resistance, time constants associated with processes such as diffusion, charge transfer and EDL formation, ESR, degradation over time and capacitance can be obtained for EC characterization. [260, 261] In SPEIS, the impedance measurement is not performed at one potential but rather at different potentials throughout the chosen potential window, thus providing additional information on potential-dependent relationships of the electrochemical system (such as resistance and capacitance).
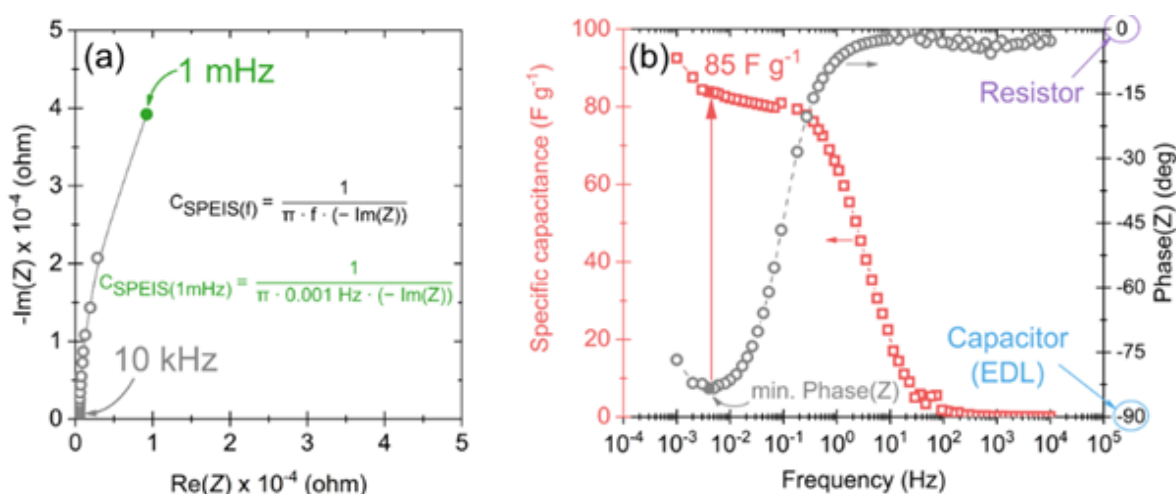
Figure 10. Representation of the: (a) Nyquist and (b) Bode plots. Extracted from [223]

6.5   Step potential electrochemical spectroscopy

SPECS technique was first developed in 2015 by M. F. Dupont and S. W. Donne to characterize the behavior of EC electrodes. [262] It involves an application of a sequence of small potential steps (ΔE) across the potential window in both directions (anodic and cathodic). Greater accuracy can be achieved through application of smaller potential steps. A rest period (t) between each potential step is applied and it is where the electrode can achieve quasi-equilibrium before the next step. As a result of each potential step, a current-time (i-t) transient is produced. This in turn can be modelled according to the expected behavior of various charge storage processes. The total current (I_T) is calculated accordingly:

$$I_T = \frac{\Delta E}{R_{s,P}} \exp\left(-\frac{t}{R_{s,P} C_P}\right) + \frac{\Delta E}{R_{s,P}} \exp\left(-\frac{t}{R_{s,G} C_G}\right) + \frac{B}{t^{0,5}} + I_E \qquad \text{eq.16}$$

Where ΔE = potential step, $R_{s,P}/R_{s,G}$ = series resistance of porous and geometric components, t = time of each registered step, B = diffusion parameter and I_E = equilibrium/residual current. [263, 264] The I_T can then be separated into its individual components:

$$I_T = I_P + I_G + I_D + I_E \qquad \text{eq.17}$$

Were I_P and I_G correspond to currents of EDL formation: in the porosity of the electrode and on easily accessible electrode surface of the electrolyte, whereas I_D is the current related to ion diffusion and I_E is the residual/equilibrium current. By division of the current curve area by the active mass of the electrode and ΔE (equation 17), one can obtain the corresponding capacitance (equation 18):

$$C = \frac{A}{M \cdot \Delta E} \qquad \text{eq.18}$$

$$C_T = C_P + C_G + C_D + C_E \qquad \text{eq.19}$$

Thus, SPECS is a useful and effective method that can provide deeper insights into the electrochemical system operation, compared to other electrochemical techniques alone e.g. CV or SPEIS. It is particularly useful for ECs, where contribution of each parameter can be thoroughly assessed, especially when investigating new electrode materials and/or electrolytic solutions. It can also complement other electrochemical techniques, such as *operando* electrochemical dilatometer (ECD). Galek *et al.* studied two ACs coupled with an ionic liquid EMIm$^+$TFSI$^-$ electrolyte and were able to extract the quantity of the current responsible for charge transfer in the micropores of the carbon material using SPECS and ECD. [109] Moreover, another study investigated lithium intercalation into graphite using the SPECS and galvanostatic intermittent titration technique (GITT), displaying its versatile nature. [265]

7. Summary

We continue to see, year by year, the need for more sustainable energy solutions. ECs play a crucial role in enabling these advancements, as they "bridge the gap" between traditional capacitors and batteries. They are characterized by high power density and rapid charge/discharge abilities, offering a compelling solution for a wide range of applications that require quick bursts of energy and reliable, long-term performance. ECs can also be used as a complementary technology to batteries in a so-called 'hybrid system', where a synergistic energy storage system that overcomes the limitations of each individual technology is created. In such a way, the overall performance can be successfully optimized. However, in order to use the full potential of ECs and complimentary hybrid systems, in-depth research focused on **fundamental** and **aging** studies seems to be vital. This dual approach allows for future development of better electrochemical systems, defined by more efficient and durable nature. Moreover, they are indispensable for translating new electrode material and electrolyte innovations into practical technologies. As outlined in this chapter, theoretical assumptions cannot be always implemented in relation to the interactions at the electrode/electrolyte interface. The idea of research on electrode charging in ECs revolves around understanding the intricate relationship between the electrode materials and the electrolyte during the charging and discharging processes. It is indeed a rather complex matter influenced by a multitude of factors, such as material properties, electrolyte properties and operational conditions. Additionally, the study of both organic and aqueous media can allow for a more comprehensive understanding and opens up a wider range of possibilities for optimizing performance. It does so by highlighting their different strengths and limitations, which ultimately can complement each other's improvements. Even though the research on ECs is extensive and continues to expand as of now, further investigation is required to address the remaining conundrums related to charge storage mechanisms and ion fluxes in certain electrolytes as well as factors influencing their long-term performance.

The goal of the presented thesis is to thus expand on the current knowledge on these processes with the use of advanced *operando* and analytical techniques as well as elaboration on the specific causes of accelerated degradation of the carbon electrodes.

Chapter II:

Fundamental studies on electrode charging in aqueous media

P1 and P2

P1. Operando Monitoring of Local pH Value Changes at the Carbon Electrode Surface in Neutral Sulfate-Based Aqueous Electrochemical Capacitors

Authors: Adam Ślesiński, **Sylwia Sroka**, Krzysztof Fic, Elżbieta Frąckowiak, Jakub Menzel
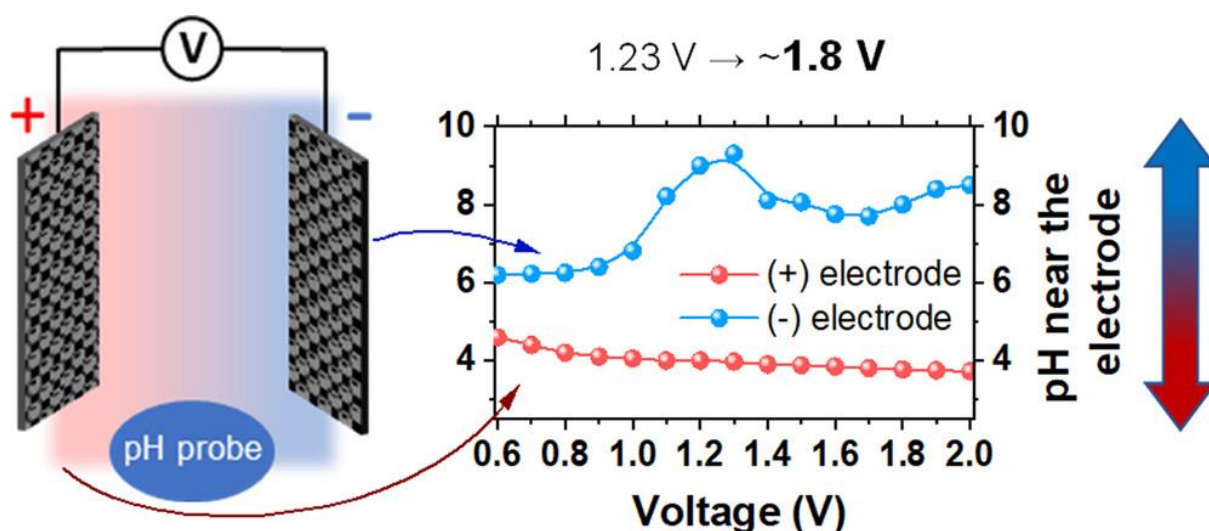
Contribution: Investigation: operando pH measurements, floating measurements, EQCM measurements and data curation, writing—original draft and formal analysis.

Graphical abstract:

Motivation and Summary

Current literature mainly reports on the pH of the bulk electrolytic solution after cycling, which changes from neutral to alkaline. [102, 113, 234] However, the pH of the bulk solution can differ greatly from the pH at the surface of the electrode. Based on this information, one cannot verify whether: specific electrode undergoes radical pH changes, if those changes are continuous or sudden, the influence of different operating conditions and factors related to electrode and electrolyte composition, or how the pH values change during cycling (**dynamic** changes). Therefore, tracking pH changes at

individual electrodes during operation can reveal not only the extent and rate of pH shifts, but can be then correlated with capacitor performance and associated degradation mechanisms. Another related aspect is potential pressure changes that might arise as a consequence of the shift in pH or accelerated side reactions, caused by gas evolution. According to the Nerst equation, theoretical electrode potentials of HER and OER will change according to the pH of the solution. Therefore, the change in potential ranges of individual electrodes will be induced, which affects the operating voltage window of the system in question. Higher operating voltages also accelerate corrosion processes. This is because high voltage can be the driving force for the onset of electrochemical reactions as well as water electrolysis. In the following article, an electronic circuit of the pH probe was constructed which worked independently of external capacitor polarization induced by the potentiostat. It allowed for the pH changes to be monitored at respective electrodes in neutral sulfate-based aqueous EC coupled with microporous AC electrodes in *operando* mode, with the results being further collaborated with *operando* GCMS and EQCM measurements for more in-depth outlook. The work showed that the pH changes within the EC are quite dynamic and different at each electrode; strongly governed by the potential applied, with the negative electrode displaying alkalization while progressive acidification was noted for the positive electrode. The onset of those changes was evident from initial cycles and at low voltages. Moreover, it allowed for OER and HER potentials to be recalculated, where the studied system exceeded an operating cell voltage of 1.23 V. The observed pH changes at respective electrodes were governed by the reactions that take place at the electrode/electrolyte interface. GCMS measurements were thus included to show not only the by-product formation related to such reactions (namely CO_2 and H_2O_2), but also to explain the observed pH changes. Similarly, EQCM allowed to track ion fluxes that would explain the acidification of the positive electrode, brought about by the adsorption of OH^- and its simultaneous consumption by the oxidation of the carbon electrode.

Operando Monitoring of Local pH Value Changes at the Carbon Electrode Surface in Neutral Sulfate-Based Aqueous Electrochemical Capacitors

Adam Slesinski,* Sylwia Sroka, Krzysztof Fic, Elzbieta Frackowiak, and Jakub Menzel*

ACCESS | Metrics & More | Article Recommendations

ABSTRACT: The operando monitoring of pH during the charging and discharging of an electrochemical capacitor in an aqueous neutral salt solution is presented. Proper knowledge of transient and limiting pH values allows for a better understanding of the phenomena that take place during capacitor operation. It also enables the proper assignment of the reaction potentials responsible for water decomposition. It is shown that the pH inside the capacitor is strongly potential-dependent and different for individual electrodes; therefore, the values of the evolution potentials of hydrogen and oxygen cannot be precisely calculated based only on the initial pH of the electrolyte. The operando measurements indicate that the pH at the positive electrode reaches 4, while at the negative electrode, it is 8.5, which in theory could shift the theoretical operating voltage well beyond 1.23 V. On the other hand, high voltage cannot be easily maintained since the electrolyte of both electrode vicinities is subjected to mixing. Operando gas monitoring measurements show that the evolution of electrolysis byproducts occurs even below the theoretical decomposition voltage. These reactions are important in maintaining a voltage-advantaged pH difference within the cell. At the same time, the electrochemical quartz crystal microbalance (EQCM) measurements indicated that the ions governing the pH (OH^-) that initially accumulated in the vicinity of the positive electrode enter the carbon porosity, losing their pH-governing abilities. pH fluctuations in the cell are important and play a vital role in the description of its performance during the cyclability at a given voltage. This is especially noticeable in cell floating at 1.3 V, where the pH difference between electrodes is the highest (6 units). The increase of the electrode separation distance acts similarly to the introduction of a semipermeable membrane toward the increase of the capacitor cycle life. During floating at 1.6 V, where the pH difference is not as high anymore (4 units), the influence of separation in terms of electrode stability, although present, is less notable.

KEYWORDS: *electrochemical capacitor, operando pH measurement, energy storage device, carbon electrode, neutral aqueous electrolyte, operando GC-MS measurement*
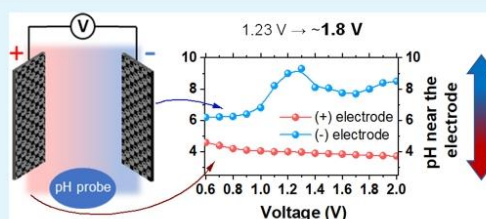
1. INTRODUCTION

The technological advancement and extensive production of electrically powered devices have led to the need to search for energy storage units produced on a large scale. Several widely used devices are powered by rechargeable units. Nowadays, electric vehicles (EVs), which are powered by lithium-ion batteries (LIBs), and related technologies in this field, have sparked a booming interest.[1−3] This kind of battery can thus be successfully applied, owing to its high energy density, ensuring efficient driving range per charge, as well as other parameters such as weight ratio of the battery system to the whole car, etc..[4−6] However, LIBs suffer from slow electrochemistry with strongly limited cyclability, which tremendously impacts their use in high-power applications, where fast acceleration or regenerative braking is of key importance.[7,8] Additionally, they require long charging times and have limited cycle life due to

volume changes in the material upon cycling operation, adding yet more drawbacks.[9−11] The already well-known energy storage system that overcomes those issues is built with the use of electrochemical capacitors (ECs). The principle of operation of the EC differs strongly from that of an electrochemical cell, as it relies primarily on physical phenomena rather than chemical. In this way, the processes that occur are faster and much more reversible, allowing these

devices to reach higher power density and superior cyclability ($>10^6$ charge–discharge cycles).[12–14] Owing to the charge storage mechanism, the voltage during capacitor charging and discharging ramps linearly with the state of charge, while for batteries it is almost constant, and its value depends on redox reactions. The major drawback of ECs is, without a doubt, their low specific energy storage capability. This problem can be tackled in two ways: by either increasing the operating cell voltage (U) and/or the specific capacitance (C), as these are the parameters that govern the energy stored in the device, as given by

$$E = \frac{CU^2}{2} \tag{1}$$

In electrochemical capacitors, the choice of a solvent is of utmost importance, as it governs the maximum voltage of the system. Currently, capacitors that operate in an organic medium as an electrolyte solution, mainly based on acetonitrile or propylene carbonate as solvents,[15,16] are the most widely used and commercialized, as the use of these media allows for a high, undisrupted voltage operation of up to 2.7 V.[17–20] However, these solvents pose several important drawbacks such as high toxicity, flammability, and price, which can greatly hinder further implementations in both industry and research settings.[21–24] The use of an aqueous medium proves to be a much better and greener alternative; however, it is characterized by a narrow voltage window of ~1.23 V[25,26] due to the decomposition of water, which, in turn, limits the energy stored by the device.[27–30] Although numerous studies have been done on the topic, progress related to research based on the enhancement of the operating voltage of aqueous electrolytes is undoubtedly lacking, and much of the focus is directed toward the development of high-capacitance electrode materials.[31] To increase operating voltage, potential ranges of both negative and positive electrodes must be considered, such as

$$U = \Delta E_+ + \Delta E_- \tag{2}$$

(where U is the operating voltage, ΔE_+ and ΔE_- being the potential ranges of positive and negative electrodes, respectively). However, these are strongly influenced by the oxygen evolution reaction (OER) and hydrogen evolution reaction (HER), respectively, which typically lead to a narrow stable thermodynamic potential window of aqueous electrolytes.[31] Thus, considering this, if the cutoff value of ΔE_+ is more positive and this of ΔE_- is more negative, a higher operating voltage could be achieved. From the practical point of view, to achieve high-voltage electrolyte, its pH must be considered, as shown in the Nernst equation

$$(\text{HER}) E_{(\text{H}^+/\text{H}_2)} = -0.059 \, \text{pH} \, [\text{V}] \tag{3}$$

$$(\text{OER}) \, E_{\text{H}_2\text{O}/\text{O}_2} = 1.23 - 0.059 \, \text{pH} \, [\text{V}] \tag{4}$$

where the theoretical electrode potentials of HER and OER can be calculated. Various approaches have been proposed to enhance this thermodynamically imposed limit. The most common is based on the differentiation of the pH of the solution in the vicinity of a single electrode. This is a vital concept, as the pH of the bulk solution can differ greatly from the pH at the surface of the electrode (as much as 4 pH units[32]) due to the consumption or production of H^+/OH^- during electrochemical operation.[33] Additionally, the differ-

entiation of pH values at individual electrodes can be used to establish the maximum safe voltage of the cell. It can be visualized on the Pourbaix diagram as in Figure 1. In a fixed pH
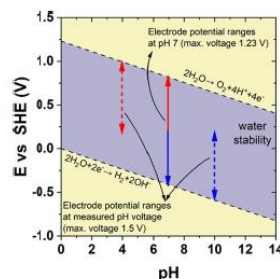

Figure 1. Pourbaix diagram for water.

electrolyte, the electrodes can only operate safely within a limit of 1.23 V, while when the pH is differentiated, this voltage can be successfully enlarged.[34] The effect of buffer agents on hydrogen adsorption and increase of pH at the interface were studied elsewhere; however, the pH was not measured in operando mode.[35]

So far, there have been numerous attempts to directly establish pH at the electrode surface from computational modeling and nonelectrochemical and electrochemical methods.[33,36–42] Some of these methods have proven to be more successful than others. For instance, Fuladpanjeh-Hojaghan et al. have used a pH mapping technique in which the pH distribution in electrochemical processes was successfully measured at each electrode using laser scanning confocal microscopy and various pH-sensitive fluorescent dyes.[33] It was shown that the pH at the positive electrode is lower (acidic) due to the presence of H^+ and higher (alkaline) at the negative electrode due to OH^- formation. Other techniques employed, such as optical or some electrochemical methods, can prove inaccurate and prone to a vast number of errors ranging from factors such as experimental difficulties, costly and complex equipment employed, to the problematic nature of transient pH values during data collection.[32]

The results of the works presented above were promising; however, no solid evidence was given with a thorough study on the pH difference during electrochemical operation in a capacitor cell. Here, for the first time, we propose a simple, cost-effective, and accurate (within the margin of error of approximately ±0.1 pH value) operando pH monitoring at the vicinities of the electrodes in a capacitor setting, where pH value changes can then be quantified as a function of the applied voltage. This approach not only allows for an accurate determination of transient pH value changes upon polarization at a given electrode surface but also offers a fast and direct response with an exact pH value reading. This information can help to further expand the current knowledge and elucidate the role of pH changes, so that optimization and improvement measures on EC's operation in aqueous media can be fulfilled.

2. EXPERIMENTAL SECTION

The electrochemical system consisted of binder-free carbon electrodes (Kynol ACC 507-20) of 10 mm diameter, anchored to the current collector using graphite conductive glue. The carbon electrode was of high purity, and additionally, temperature was treated at 120 °C for 2 h in a vacuum dryer to remove any physisorbed oxygen and water. Its

www.acsami.org

final oxygen content was determined by direct elemental analysis to be 1.5%. They were soaked in a 1 mol L^{-1} electrolyte (Li$_2$SO$_4$, Sigma-Aldrich, >98%) solution. The simultaneous electrochemical and pH measurements were carried out in a PTFE-body (1/2 inch straight tube fitting union) two-electrode cell with stainless steel 316 L current collectors (Figure 2). The upper wall of the fitting was adapted with a
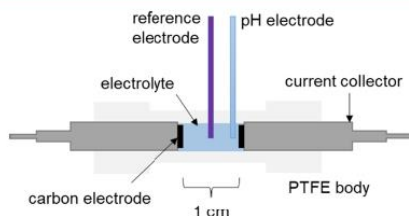

Figure 2. Scheme of the electrochemical setup and electrode positioning.

longitudinal hole, where a pH sensor microelectrode and a reference electrode were introduced. The exact positioning of the pH sensing electrode depended on the specific measurement target and is precisely stated in the consecutive sections of the article. However, to fit two sensing tips, carbon electrodes were initially fixed at a 1 cm distance from each other. Certainly, it introduced additional ohmic resistance to the capacitor cell; however, testing the capacitor at a slow 5 mV s^{-1} scan rate or keeping it at constant polarization (floating) at 1.6 V allowed undisturbed results to be obtained. The reference electrode (Hg/Hg$_2$SO$_4$) was added to monitor the responses of individual electrodes for direct comparison with the pH readings. The experiments were carried out using a BioLogic VMP3 potentiostat/galvanostat equipped with an analogue operating amplifier for the acquisition of parallel pH values.

The evolution of gases during capacitor operation was monitored in PAT-Cell-Gas (El-Cell) in an online mode using gas chromatography-coupled mass spectrometry (GC-MS, Bruker). The monitored masses were m/z = 44 and 34, assigned to carbon dioxide and hydrogen peroxide, respectively.

The electrochemical quartz crystal microbalance (EQCM) investigation was conducted using 1 mol L^{-1} Li$_2$SO$_4$ solution (pH = 7.9) as an electrolyte. The thickness of Kynol makes EQCM studies not feasible; therefore, activated carbon (AC) YP-50F (Kuraray, Japan) was selected, having textural properties (micro:mesoporosity ratio) similar to Kynol ACC 507-20. As the main goal of EQCM in this article was to deal solely with ion adsorption and not the chemical reactions, its surface chemistry was not considered in this experiment. The electrodes, which were coated on the quartz crystal resonator, were prepared in 80:20 (w/w) for an AC:binder mass ratio. The slurry consisted of AC powder mixed with a 5 wt % solution of poly(vinylidenedifluoride) (PVDF) binder (Sigma-Aldrich) in N-methyl-2-pyrrolidone (NMP) solvent (Sigma-Aldrich). The suspension was evenly drop-casted on a quartz crystal resonator (standard frequency 9 MHz, SEIKO EG&G, Japan) with a stainless steel current collector (SUS304) and dried at 60 °C for 12 h. The mass loading of the carbon coating was kept within the range of 30−60 μg ensuring a thin and even layer. Electrochemical measurements were performed in a poly(ether ether ketone) (PEEK) cell designed for EQCM measurements. The working electrode was the AC-coated resonator, placed at the bottom of the cell. Stainless steel foil was used as a counter electrode, and a saturated calomel electrode (SCE, +0.241 V vs standard hydrogen electrode (SHE)) was used as the reference electrode. An excess of the electrolyte (400 μL) was added, avoiding the presence of bubbles.

Point of zero charge (pzc) was determined in the EQCM cell via staircase potential electrochemical impedance spectroscopy (SPEIS) (10 kHz to 1 mHz), for which the specific capacitance values were calculated at 1 mHz and then plotted against the varied applied

potentials. This allowed the minimal value to be determined, representing pzc, that is, +0.2 V vs SHE.

Other electrochemical techniques included cyclic voltammetry (CV) at 50 mV s^{-1}, to kick-start the electrochemical response, followed by 5 mV s^{-1}, where the change in resonator frequency was simultaneously recorded by the EQCM and then recalculated into the change in mass with respect to the Sauerbrey equation

$$\Delta f = -f_0^2 \cdot \Delta m / N \cdot \rho \qquad (5)$$

where Δf is the change in frequency, f_0 is the fundamental resonance frequency of the crystal (Hz), Δm is the change in mass (g), N is the frequency constant for a quartz crystal resonator (Hz Å), and ρ is the quartz density (2.648 g cm^{-3}). Faraday's law (eq 6) was used to recalculate data from CV, allowing one to compare the experimental and theoretical mass changes in the mass vs charge ratio plot

$$\Delta m = \frac{\Delta Q \cdot M}{F \cdot z} \qquad (6)$$

where Δm is the change in mass, ΔQ is the charge exchanged (C), F is Faraday's constant (96 485 C mol^{-1}), M is the molar mass of ion adsorbed/desorbed (g mol^{-1}), and z is the number of exchanged electrons (i.e., the valence number of adsorbed/desorbed ions).

3. RESULTS AND DISCUSSION

Positioning the electrodes 1 cm apart was done not only to accommodate the sensing electrode tips but also to ensure that the electrolyte at the electrode vicinities was not under the mixing conditions, so that the experiment could be carried out in a controlled manner. Indeed, it might seem that such a configuration differs from the real capacitor cell, where the electrodes are tightly squeezed with the separator in between; however, for the demonstration, proof-of-concept, and further optimization purposes, this configuration was selected. Figure 3a shows cyclic voltammograms taken at 5 mV s^{-1} during the voltage window extension from 1.0 to 2.0 V, with a 0.2 V step. Even though a voltage of 2.0 is considerably high for the nonmodified system in the aqueous-based electrolyte, such a limit was selected to observe the effects within an extended range. Figure 3b contains the electrochemical response of the electrodes, which was recorded in the presence of a reference electrode. It is clear that after exceeding the thermodynamic stability of the solvent (water), the current leaps, related to its decomposition, appear. As the water ions take part in the reactions, the potentials at which the reactions take place are pH-dependent. The shaded regions indicate the limiting area where the H$_2$O decomposition starts within the entire pH range of 0−14.

It is possible to calculate the theoretical equilibrium potentials of the reactions of water reduction and oxidation at a given pH based on the formulae in eqs 3 and 4. The initial pH of the electrolyte is 7; however, after contact with carbon electrodes, it changes to 5.3. This immediate change occurs due to the presence of surface functional groups. Assuming that it remains unchanged during operation, the above potentials should be equal to E_{red} = −0.31 V and E_{ox} = 0.92 V, respectively (dotted lines). In contrast to the just-mentioned theoretical values, it is possible to read out the potential of the reactions of reduction and oxidation directly from the graph if it is assumed that the onsets of equilibrium reactions are exactly at the potentials where the faradic current starts to increase exponentially. Here, they are estimated to be −0.6 and 1.0 V, respectively (dashed lines). The discrepancy in the potential values emerges solely from the shift of equilibrium potentials, being dependent on the proton
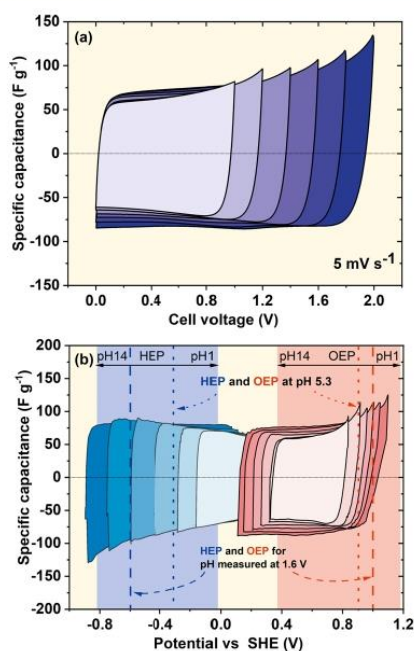
Figure 3. CV characteristics of ACC electrodes in the electrochemical cell (1 mol L^{-1} Li$_2$SO$_4$) during voltage extension from 1.0 to 2.0 V: (a) full cell and (b) individual electrodes. The shaded regions indicate the possible HER and OER regions in the full pH range; dotted lines indicate the theoretical solvent decomposition potential; dashed lines indicate the graph read potentials.

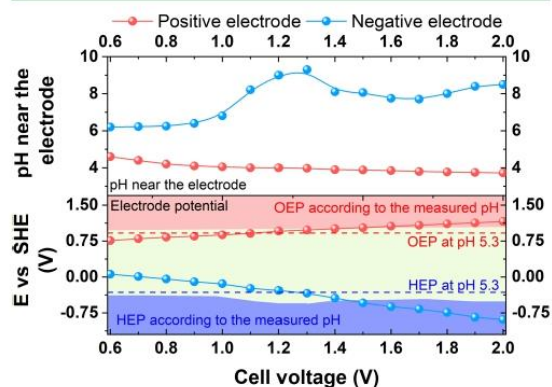readings during the potentiodynamic voltage extension of the capacitor from 0.6 to 2.0 V with a 0.1 V step.

Figure 4. Upper graph: electrolyte pH at the electrode surfaces of the capacitor charged to different voltages in 1 mol L^{-1} Li$_2$SO$_4$. Lower graph: measured electrode potential values and corresponding HEP and OEP at these pH values. The dashed lines indicate the theoretical OEP and HEP at a constant pH.

concentration polarization. If these potentials are recalculated into pH values using the rearranged version of eqs 3 and 4, they will correspond to pH values of 10 and 4.6, respectively. In the case of the negative electrode, the pH is higher by almost 5 units, while in the case of the positive electrode, the difference is not that significant. Furthermore, as might be observed in Figure 3a,b, the sharp increase in the current values recorded at the end of the charging sweeps becomes progressively postponed along with the extension of the voltage, suggesting that the pH values are constantly modified, thus dependent on voltage. Therefore, marking the vertical lines that indicate the onset of decomposition reactions as in Figure 3b (dotted, theoretical) makes sense only when the pH is known at a given point of potential. It is not enough to stipulate them only prior to the cell operation. Proper determination of the theoretical solvent decomposition line locations can be done only if the pH is known, that is, the solution is fully buffered or the pH is measured in parallel.

As the pH of the neutral salt solution is susceptible to changes, the introduction of a pH sensing probe into the capacitor cell was necessary to indicate the pH at a given time (potential). The measurement of pH is, of course, the same as the measurement of the concentration of H$^+$ ions; therefore, to ensure correct indications, the capacitor charging/discharging rates had to be slow enough to account for ion diffusion within the bulk of the electrolyte. This is because the ion adsorption/desorption phenomenon at the electrode/electrolyte interface is faster than the ion diffusion within the capacitor cell volume. Figure 4 shows the electrode potential extrema along with pH

It was noted that the pH at the positive electrode experienced progressive acidification. This effect was more evident at lower voltages, and then it decelerated when the voltages were above 1.0 V. It was probably balanced by the visible pH hump at the negative electrode, which started at that point of voltage, which is discussed below. The deceleration is therefore related to difficulties in maintaining the concentration polarization, as the pH was further from its initial value. Namely, once the cell voltage reached 1.0 V, the pH at the positive electrode dropped from the initial value of 5.3 down to 4, but further (from 1.0 to 2.0 V) only slightly to around 3.6. However, one should remember that the pH is a logarithmic unit and the real concentration changed significantly. The overall behavior of the pH at the negative electrode is more complex. First, the pH at 1.0 V was almost the same as the initial pH of the electrolyte. The total change did not follow a one-direction upward trend. Instead, the visible and significant change started at 1.0 V of cell voltage. It reached maximum alkalinity of 9.5 at around 1.3 V and then slightly declined to 8 at 1.7 V. Above 1.7 V, it increased back again to reach 8.5. Considering the pH balance within the system, the irrational change at the negative electrode can have its explanation in the analysis of accompanying electrode reactions. Second, it may be deduced that the pH at the negative electrode is strongly influenced by the concentration impact of the positive electrode or, in other words, the positive electrode domination. After a comparison of pH behavior at both electrodes, it can be seen that the maximum pH difference was 5 at a voltage of 1.3 V. Whenever there is a change in pH, the OER and HER potentials change. The pH measurements allowed for the actual HEP and OEP calculations to be performed (eqs 3 and 4). The calculated HEP and OEP are therefore corrected by the factor of variable pH (the results are shown as shaded regions in Figure 4). When the theoretical potentials of HEP and OEP are compared with the assumption of fixed pH (dashed lines) with the potentials of these reactions at instantaneous pH measured at a given cell voltage, the increasing discrepancy is noticed. Taking into account the

terminal electrode potentials and the electrode reaction potentials (HER and OER), the safe cell voltage limit appears to be 1.4 V. Although the probe tip was placed as close to the surface of the carbon electrode as possible, the distance was still higher than the diffusion layer thickness. Different scan rates of the experiment could result in different pH readings. For example, lower scan rates (which give more space for electrode kinetic-related effects to occur) would provide a situation that is closer to potentiostatic voltage hold conditions. Higher sweep rates would result in incorrect readings due to cell resistance overpotential. Therefore, to increase the data reliability, accounting for concentration polarization and slight variations of pH during alternate charging and discharging, it was decided to measure the pH under conditions resembling the stationary ones. Accordingly, it was done under potentiostatic conditions after the leakage current leveled out, therefore, when the concentration gradient reached equilibrium. Figure 5 shows pH readings during
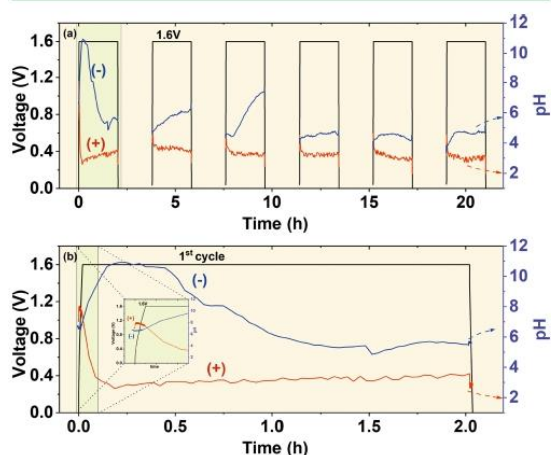
Figure 5. pH values monitored during potentiostatic floating at 1.6 V during (a) six potentiostatic cycles and (b) first cycle with the inset into the charging period. The pH values of both electrodes are represented on the secondary y-axis.

potentiostatic conditions at a cell voltage of 1.6 V. Again, looking at the overview (Figure 5a), the pH values are more stable at the positive electrode, exactly as it was observed during potentiodynamic experiments. Moreover, they are relatively stable within a single floating period of 2 h (excluding charging and discharging periods). On the contrary, the pH at the negative electrode exhibited more fluctuations with time and cycle number. Once the cell was charged to 1.6 V, the pH at the negative electrode immediately changed to the alkaline area (pH = 11), while that at the positive electrode was changed to the acidic one (pH = 3), as observed in Figure 5b. Such a pH difference was kept for a short time, and after less than half an hour, the pH difference diminished due to the loss of alkalinity at the negative electrode. At the same time, the pH of the positive electrode remained at the same value. This was yet another proof that the positive electrode imposed the negative one and finally governed the pH within the entire capacitor cell. It is easily seen in subsequent cycles that the pH of the negative electrode tends to increase; however, it is probably suppressed by the impact of the positive electrode.

The decrease in pH difference could probably be responsible for the reduction in future cell lifetime. The interesting pH fluctuation is observed within the first seconds of cell first charge, where the pH at the positive electrode increases, while the pH at the negative electrode decreases (Figure 5b, inset).

The detailed explanation of pH variation at the electrodes can be understood when considering the movement of ions and reactions taking place at the electrode/electrolyte interfaces. To provide a clear explanation, three scenarios should be considered: in no cell polarization ($U = 0$ V), in low-voltage polarization ($0 < U < 0.4$ V), and in high-voltage polarization ($U > 0.8$ V). These are shown schematically in Figure 6. Of course, when no polarization is applied, the ions are randomly distributed within the electrolyte solution (Figure 6a). When the voltage is progressively increased, the ions tend to move according to the action of the electric field, i.e., the positively charged cations move to the negative electrode, while the negatively charged ions move toward the positive one. Accordingly, the positive electrode compartment should undergo alkalization, while the negative one undergoes acidification. This statement finds confirmation, as observed previously in Figure 5b (inset), where it is indeed true initially during charging at low polarizations. The situation changes when the potential builds up further and dielectric breakdown of the electrode/electrolyte interface begins to occur. Electro-chemical reactions owing to the electron transfer impose the equilibria and, in turn, the pH at the electrodes. Again, it can be observed in Figure 5b (inset), where the direction of the pH changes immediately in the opposite direction.

The chemical reactions responsible for the government of pH are listed in Table 1. Contrary to planar and noble electrodes, the typical water decomposition electrode reactions are modified; here, porous carbon electrodes can be partly consumed. The general products are chemisorbed ($<C-H>_{ads}$) or gaseous hydrogen (H_2) at the negative electrode as well as CO_2 or modified surface functionalities at the positive one. As demonstrated, not only can the neutral form of water (H_2O) react as in reactions 9, 14, and 16 but also its charged and protonated form, H_3O^+ (reaction 10), and the deprotonated form, (OH^-) (reaction 15). The possible evolution of gaseous hydrogen (H_2) occurs at higher overvoltages at the negative electrode (reaction 11) or by the consumption of the oxygen groups from the carbon surface groups (reaction 12). The second case is confirmed by the reduced oxygen content in the negative electrode composition after the accelerated aging test at high voltage.[43,44] H_2O_2, on the other hand, a common byproduct of water electrolysis, which takes place at the positive electrode (reaction 17), can be further decomposed into water and oxygen. Oxygen will immediately react with carbon through two processes: in the first, CO_2 is produced (reaction 18); in the other, oxygen is chemisorbed. It has been suggested in the literature that H_2O_2 produced on the positive electrode might have a tendency to migrate toward the negative electrode through a separator, where it is consumed.[45] This would explain the evolution of CO_2 from reaction 13 at the negative electrode. Certainly, the same H_2O_2 decomposition reaction would take place as in reaction 18 at the positive electrode. Consumption of H_3O^+ and simultaneous production of OH^- intensify the alkalization rate at the negative electrode. This is why the hump at the negative electrode pH is observed in Figure 4. At sufficient overvoltage, reaction 12 takes place and further alkalization is suppressed. An important observation can be made by
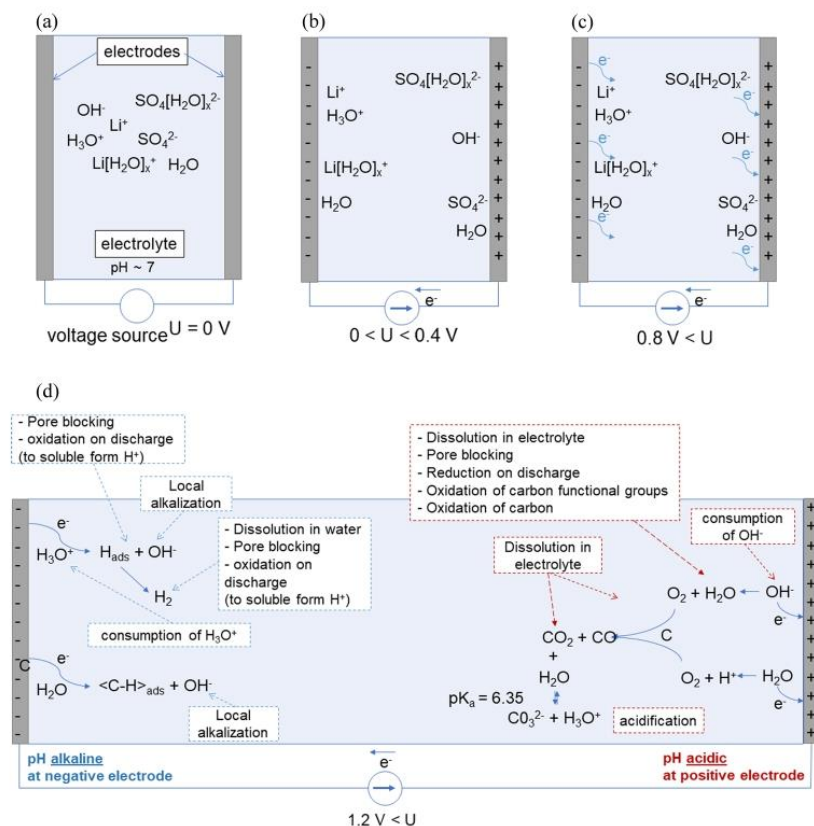
Figure 6. Schematic representations of electrode/electrolyte interfaces: (a) no polarization, (b) low voltage, (c) high voltage, and (d) selected chemical reactions taking place at high voltage.

Table 1. Electrode Reactions that Impose the pH at the Interfaces

negative electrode	positive electrode
$H_2O + C + e^- \rightarrow\ <C-H>_{ads} +OH^-$ (9)	$6\,H_2O + C \rightarrow 4\,H_3O^+ + CO_2 + 4\,e^-$ (14)
$H_3O^+ + 2\,C + 2\,e^- \rightarrow 2\,<C-H>_{ads} +OH^-$ (10)	$12\,OH^- + 3\,C \rightarrow 6\,H_2O + 3\,CO_2 + 12\,e^-$ (15)
$2\,<C-H_{ads}> \rightarrow\ 2\,C + H_2$ (11)	$CO_2 + 3\,H_2O \rightarrow CO_3^{2-} + 2\,H_3O^+$ (16)
$2\,<C-H_{ads}> + 4\,O(@carbon) \rightarrow 2\,CO_2 + H_2$ (12)	$4\,H_2O \rightarrow H_2O_2 + 2\,H_3O^+ + 2\,e-$ (17)
$2\,H_2O_2 + C \rightarrow 2\,H_2O + CO_2$ (13)	$2\,H_2O_2 + C \rightarrow 2\,H_2O + CO_2$ (18)

combining the substrates of reaction 15 with the products of reaction 16

$$9\,OH^- + 2\,C \rightarrow 2\,CO_3^{2-} + 3\,H_3O^+ + 8\,e^- \qquad (7)$$
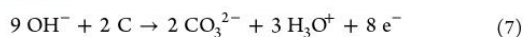
This reaction in eq 7 can explain two phenomena: the disappearance of the alkaline character at the positive electrode when increasing the voltage above 0.4 V (consumption of OH^- as high as 9 moles, therefore its strong acidification) and production of the solid-state deposit of lithium sulfate according to the reaction in eq 8[43]

$$2\,Li^+ + CO_3^{2-} \rightarrow Li_2CO_3 \qquad (8)$$

All of the electron-transfer reactions mentioned in Table 1 are not visible as typical peaks on voltammogram (Figure 3), but rather as current leaps because the substrates for these

reactions are different forms of a solvent, which are constantly available within the diffusion layer of the electrode/electrolyte interface.

It was experimentally proven using the GC-MS experiment that the chemical reactions listed in Table 1 take place under these conditions even below the theoretical limit of water decomposition (1.23 V). The evolution patterns of CO, CO_2, and O_2 gases were already presented elsewhere; however, they were not fully discussed.[46] This seems possible in the case where the internal pH difference within a capacitor cell is against the voltage-advantage direction; the positive electrode operates in the alkaline region, and the negative electrode operates in the acidic region (Pourbaix diagram), which is directly correlated with the ion separation pattern shown in Figure 6b. This is the reason why the evolution of CO_2 is

observed even at a voltage as low as 0.8 V (Figure 7). The delay in gas release at the negative electrode is observed due to
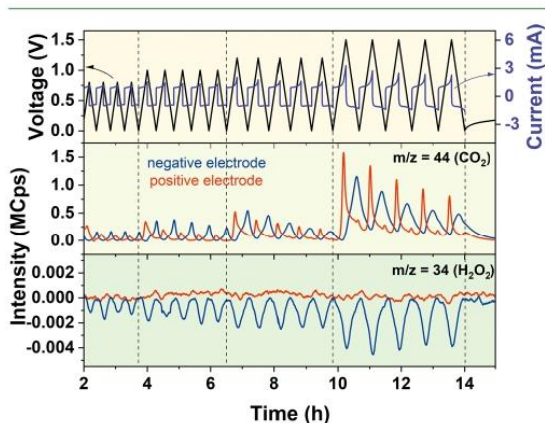

Figure 7. CO_2 evolution pattern is a fingerprint of the presence of the water decomposition reaction. The first row shows the electrochemical data, while the other row shows the evolution of carbon dioxide and hydrogen peroxide.

gas ejection during discharge at lower voltages. The evolution of CO_2 at the negative electrode can be found owing to reactions 12 and 13. The presence of CO_2 at the negative electrode may also be a consequence of gas diffusion in the capacitor cell during measurements. The signal of $m/z = 34$ (H_2O_2) was detected only at the negative electrode in the form of consumption peaks. This confirms that reaction 13 is valid, and, rather, all of the H_2O_2 produced on the positive electrode migrates from the positive electrode toward the negative one. The unfavorable conditions emerging only from the electrostatic attraction (low pH difference) are therefore counteracted by the chemical reactions of water decomposition. It means that the increase of capacitor voltage becomes a self-perpetuating phenomenon. This behavior suggests that the adverse pH difference formed beforehand at low voltages is responsible for the limitation of the stability window (<1.23 V), while it progressively broadens as the voltage increases.

To confirm the presence of the mentioned ions, EQCM measurements were conducted. This technique provides information about the ion and solvent molecule fluxes during the charging process of the porous AC electrode. The mass change profile and current response recorded for YP-50F operating in 1 M Li_2SO_4 electrolyte at 5 mV s^{-1} are presented in Figure 8a, where a similar trend in mass change and electrochemical response is observed for each cycle, proving its repeatability. Because of the low carbon loading on the resonator, the system is more sensitive to redox reactions and electrolyte decomposition. The sharp change in the current response observed at the terminal potentials is linked to electrolyte decomposition reactions associated with hydrogen storage and oxygen (carbon dioxide) evolution. Figure 8b shows the charge-to-mass ratio plot, with theoretical and experimental curves calculated from the Faraday law. The slopes fitted to the experimental curves were found to correspond to the adsorption of Li$^+$·1.5 H_2O and OH$^-$ for negative and positive polarizations, respectively. As it is not possible to adsorb 1.5 molecule of water, it is an average number of water molecules coadsorbed with the lithium ions.
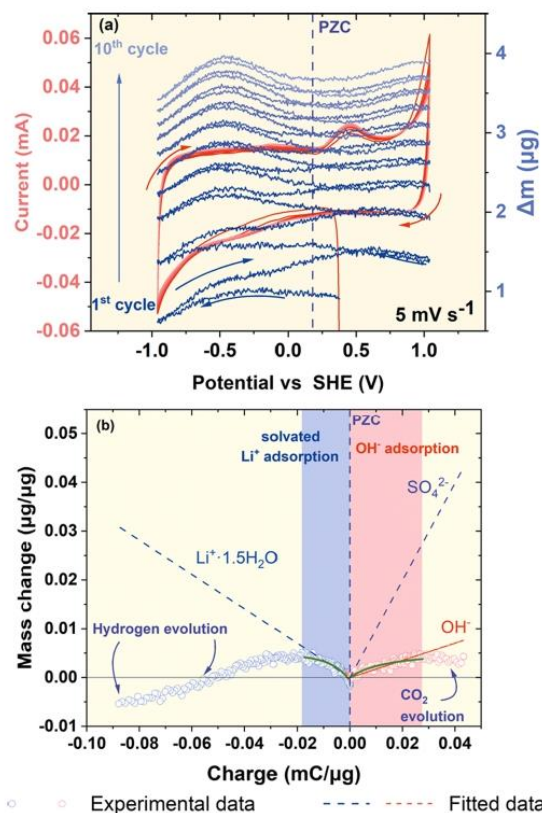

Figure 8. (a) CV and mass change response of YP-50F in a 1 mol L^{-1} Li_2SO_4 aqueous electrolyte at 5 mV s^{-1} and (b) electrode mass change vs charge during the polarization.

The exact regions for Li$^+$ and OH$^-$ adsorptions are denoted in the highlighted area on the graph. To eliminate the possibility of adsorption of other anions, a theoretical curve for bare $[SO_4]^{2-}$ was calculated, as seen in Figure 8b. The slope clearly does not correspond to the experimental one, debunking that possibility.

The EQCM results confirm the assumptions previously stated for the pH changes observed on the positive electrode in Figure 5. Initially, the pH value increases, as there are more OH$^-$ species available near the electrode surface. With an increase in potential, the adsorption of OH$^-$ takes place (some of which adsorb in the pores); thus, less OH$^-$ is present in the vicinity of the electrode. Simultaneously, the adsorbed OH$^-$ ions are consumed as in reaction 15 in Table 1. This brings about acidification, which lowers the pH at the positive electrode.

Upon negative polarization from pzc, an increase in the mass of the electrode can be observed, which denotes the adsorption of the cations, with insignificant change in the population of anions. A sharp decrease in mass can then be observed, which might be related to (1) the simultaneous adsorption of bare Li$^+$ and repulsion of OH$^-$ ($M = 6.941$ and $M = 17.008$ g mol^{-1} for Li$^+$ and OH$^-$, respectively), (2) repulsion of the water molecules from the bulk of pores and simultaneous adsorption of solvated ions, (3) desolvation of the Li$^+$ ion, or (4)

evolution of gas bubbles, which can negatively impact accuracy in the measured EQCM response.

For positive polarization, the electrode mass was found to increase slightly, which denotes the adsorption of bare OH^-. Then, a decrease in mass is observed (as for negative polarization), indicating similar behavior, where most likely (1) a large amount of water molecules are expelled from the pores while OH^- is adsorbed, (2) OH^- is adsorbed and solvated Li^+ gets expelled, or (3) the presence of carbon dioxide gas bubbles.

The pH fluctuations were also monitored for the capacitor in which the carbon electrodes were positioned as close as possible (4 mm from each other) and the pH sensing probe was at the same distance to both electrodes, thus exactly in the middle. Figure 9 shows the results of the pH monitoring
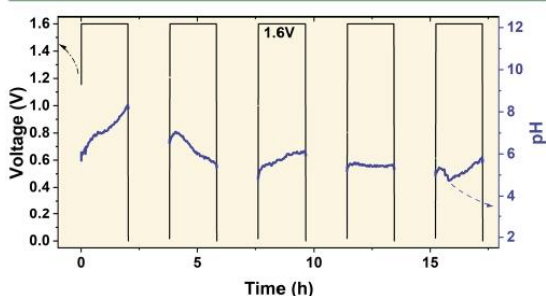
Figure 9. pH value monitored during potentiostatic floating at 1.6 V in 1 mol L^{-1} Li_2SO_4, with the electrode distance reduced to 4 mm in a pH cell.

during potentiostatic floating at 1.6 V. In this case, the pH varies strongly between 4.8 and 8.1. Initially, the electrolyte becomes alkaline, yet in the second cycle, it becomes acidic. This behavior is probably found in real electrochemical capacitors, where electrolytes from both adjacent carbon electrodes mix easily, which in fact overlap and are subject to mixing. Here, another proof of positive electrode acidic environment domination is found.

The measurement of pH values at the electrodes might be helpful for the determination of the maximum safe voltage of the cell at which the electrode potentials remain below the solvent decomposition onset potentials at given pH values. As the pH difference does not increase proportionally with voltage

(which can be deduced from Figure 4), there is an optimum voltage value, at which the pH difference is the highest. In the case of the investigated system, it is 1.3 V. This value is close to the theoretical value of water decomposition, with the additional contribution of hydrogen overpotential related to (owing to alkalization at the negative electrode) creating the optimum environment for the high cyclability of the cell. This may also contribute to the reduced gas production within the aqueous capacitor cell, which normally occurs at high voltages. The current methodology provides reliable verification of any pathway aimed at the introduction of the pH difference.

As the results of the investigations in the test cell indicate that the distance between the electrodes influences the pH gradients, it has been decided to verify the concept in the real electrochemical capacitor. For that purpose, the Swagelok cell was used and modulated electrode distances were applied. To be precise, it was done by employing one or multiple (three) separator layers. As the pH gradient was strongly influenced by the maximum cell voltage, the behavior was investigated at two voltages, that is, at 1.3 V (where pH difference is as high as 6 units) and 1.6 V (where pH difference is 4 units). Figure 10 shows the comparison of the cyclic voltammograms recorded before and after floating for 60 h at a voltage of 1.3 V using different separation distances of the electrodes. Both systems experienced aging after this floating experiment—the current humps suggesting a reversible reaction took place and the current leaps at the end of discharge were observed. The first case is always observed during floating at an elevated voltage and is related to oxidation of the positive electrode.[43,47−49] The latter case is related to the desorption of hydrogen at the negative electrode, which was produced during the high negative polarization of the electrode.[50,51] The aging phenomena are more evident in the cell where there was only one separator, that is, where the electrodes were closer to each other. It means that the electrodes positioned this way were aggravated by the mutual influence.

Visibly, the energy efficiency before and after the test dropped much more in the case of one separator system. All of these additional faradic processes contribute to the pseudocapacitance in the system. It is not desirable as it is related to the aging of the system. The drop in discharge capacitance at high voltages is equal in both cells, probably related to a phenomenon not related to pH fluctuations in the cell but rather due to pore clogging.[43,44,47]

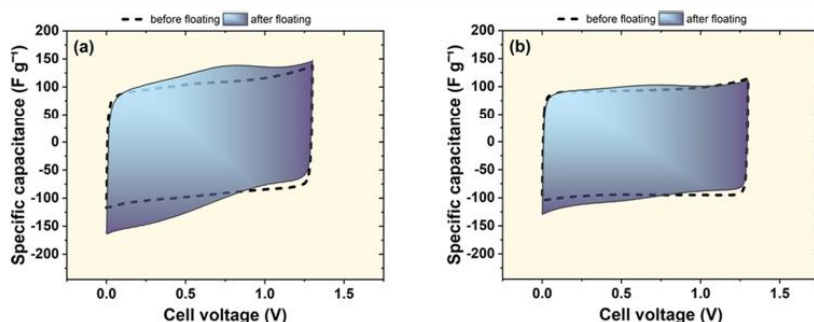A similar floating experiment was also conducted for a voltage of 1.6 V. In fact, the aging was more pronounced than

Figure 10. Cyclic voltammograms of the capacitors in 1 mol L^{-1} Li_2SO_4 recorded before and after the floating experiment at 1.3 V (5 mV s^{-1}). Capacitor containing (a) one separator and (b) three separator layers.
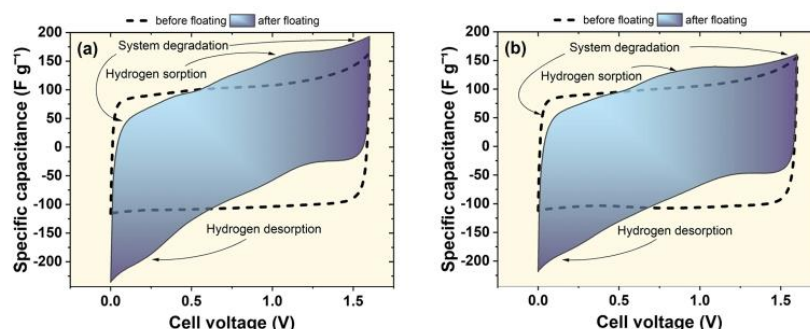
Figure 11. Cyclic voltammograms recorded for capacitors in 1 mol L^{-1} Li$_2$SO$_4$ recorded before and after the floating experiment at 1.6 V (5 mV s^{-1}). Capacitor containing (a) one separator and (b) three separator layers.

in the case of 1.3 V. Depending on the separation, differences might be noticed (Figure 11). This time, they are slightly less visible than in the case of 1.3 V; however, the tendency remained similar. Again, three separator systems retained better performance. After floating at 1.6 V, extensive deterioration is observed during discharge. Capacitance at high voltages is diminished, while additional capacitance appears at low voltages. This is caused by the fact that each polarized electrode cannot further retain its beneficial pH conditions due to the internal mixing of the electrolyte. Again at 1.6 V, the energy efficiency before and after the test dropped much more in the case of one separator system.

The process of water decomposition appears to be self-limiting in nature (acidification at the positive electrode and alkalization at the negative one); however, if these two processes are not exactly balanced, one may dominate and affect the other one. It seems to be extremely difficult to maintain the balance; therefore, a straightforward voltage increase above 1.3 V in aqueous-based capacitors having nonmodified electrodes is difficult. The adequate modification of electrodes, electrolytes, separators, or a combination of all of those seems to be necessary.

An important aspect inherent to the regulation of separation distance is, of course, the resistance of the electrolyte. As the electrolyte resistance contributes the most to the total series resistance of the cell, it might be anticipated that the higher the distance (thicker separator), the higher the series resistance. High-frequency impedance measurements indicated that the series resistance (equivalent series resistance (ESR)) of cells containing one and three separators increased twice from 0.45 to 0.92 Ω. Certainly, together with distance, the electrolyte reservoir volume is different. However, the total electrolyte volume between the electrodes does not play a crucial role at 1.6 V polarization. First, the electrolyte is subjected to a concentration gradient during polarization of the cell, and second, the electrolyte solvent progressively decomposes when it experiences excessive voltage. The former seems not to be an issue since the concentration of the electrolyte is usually high (at least 1 mol L^{-1}) and ion depletion would not occur. The latter can lead to electrolyte solvent depletion, an increase in the electrolyte salt concentration, and then its precipitation after the solubility limit is reached. The additional electrolyte solution reservoir in the carbon porosity might be an important property of the carbon, which can allow for a controlled environment in the system and thus becomes handy for the optimization of cell voltage abilities. The separation of

electrodes (and their surrounding electrolyte) can also be done using a membrane. It was shown that it can successfully extend the cycle life. For comparison, the electrolyte content in organic-based capacitors found in commercial units is extremely low (the separator can be as thin as 30 μm). At the same time, they do not require this kind of consideration, as the organic electrolyte ensures a satisfactory voltage to be reached, without exhibiting electrolyte decomposition redox reactions. It puts more effort on aqueous-based capacitors to be designed; however, by considering all of the above-mentioned aspects, it can be equally efficient. Together with its environmental and economic impact, it is certainly a noteworthy challenge. For the justification of carbon electrode role in the behavior of pH changes, a measurement with bare stainless steel current collectors was done. As a result, the pH at both stainless steel electrodes increased. The increase of pH at the positive electrode was a result of OH$^-$ ion attraction, while the alkalization at the negative electrode occurred due to discharging of the hydronium ions (H$_3$O$^+$) decreasing their concentration. As stainless steel is generally resistant to corrosion in these relatively short time measurements, its impact was not detected and studied. The long-term study of corrosion effects is interesting and important, which opens a new space for experiments.

4. CONCLUSIONS

The operando monitoring of local pH value changes at carbon electrode surfaces in aqueous electrochemical capacitors has been presented. The use of joint research techniques (pH operando monitoring, GC-MS, and EQCM measurements) allowed for a full description of the ion fluxes and electrolyte pH changes in an aqueous electrochemical capacitor.

In general, electrochemical capacitors with Li$_2$SO$_4$ solution used as an electrolyte are recognized as "neutral aqueous capacitors". Our research shows that the pH changes within the capacitor cell are dynamic and cannot be neglected. The onset of these changes begins even at low voltages and from the first cycle. Furthermore, they become especially important for a deep understanding of the maximum voltage abilities of the system. It provides insight into the aging process of electrochemical capacitors for voltage values above the theoretical water decomposition. The strict potential values at which solvent decomposition takes place cannot be calculated and defined beforehand on the basis of the initial electrolyte solution pH measurements. It can only be a primary approximation. The pH in the system is proton, thus,

potential-dependent; therefore, the value of this potential is changing depending on the voltage that is maintained by the system. Electrode separation has been shown to have a visible effect on the interpretation of the electrochemical results. Electrolyte decomposition traces can be found even at a voltage lower than the theoretical limit. The GC-MS experiment proved that the products (CO_2, H_2O_2) affect the surface chemistry of the carbon electrodes by inducting the pH changes, which are opposite to those expected from the electrostatic attraction of ions.

The pH at the positive electrode during charging, emerging from the accumulation of OH^-, initially alkalizes. After the critical potential has exceeded, the OH^- ions enter the porosity and the solution in the vicinity of the electrode becomes acidic. These findings were confirmed by the EQCM experiment, where the recorded mass change reflects the adsorption of OH^- instead of SO_4^{2-} ions.

To make aqueous-based capacitors reach high voltage and compete with organic-based capacitors, the consideration of pH maintenance seems to be vital. It is necessary to keep in mind that the trade-off between the energy, resistance, and cycle life is found. The higher the distance between the electrodes, the higher the energy, but also the resistance. As demonstrated, increasing the distance enhances the cycle life. If one wants to obtain a high-power cell, then instead of decreasing the electrode separation and thus resistance, it seems more convenient to use a high conductivity electrolyte. This will allow the same resistance to be maintained. Another issue emerges from system mass, which is highly dependent on the electrolyte amount and its concentration. Certainly, the less electrolyte, the higher gravimetric energy for the system can be obtained. The design of the perfect system should anticipate all of the parameters mentioned.

■ AUTHOR INFORMATION

Corresponding Authors

   Adam Slesinski − *Institute of Chemistry and Technical Electrochemistry, Poznan University of Technology, Poznan 60-965, Poland;* ● orcid.org/0000-0001-9074-9645; Email: adam.slesinski@put.poznan.pl

   Jakub Menzel − *Institute of Chemistry and Technical Electrochemistry, Poznan University of Technology, Poznan 60-965, Poland;* ● orcid.org/0000-0002-0431-159X; Email: jakub.menzel@put.poznan.pl

Authors

   Sylwia Sroka − *Institute of Chemistry and Technical Electrochemistry, Poznan University of Technology, Poznan 60-965, Poland;* ● orcid.org/0000-0002-9242-5561

   Krzysztof Fic − *Institute of Chemistry and Technical Electrochemistry, Poznan University of Technology, Poznan 60-965, Poland;* ● orcid.org/0000-0002-5870-7119

   Elzbieta Frackowiak − *Institute of Chemistry and Technical Electrochemistry, Poznan University of Technology, Poznan 60-965, Poland;* ● orcid.org/0000-0003-2518-3950

Complete contact information is available at:
https://pubs.acs.org/10.1021/acsami.2c09920

Author Contributions
A.S.: conceptualization, methodology, investigation, and writing—original draft; S.S.: investigation, writing—original draft, and formal analysis; J.M.: methodology, investigation, resources, funding acquisition, and writing—original draft; E.F.: supervision, resources, funding acquisition, and project administration; and K.F.: supervision, funding acquisition, project administration, and writing—review and editing.

Notes
The authors declare no competing financial interest.

■ ACKNOWLEDGMENTS

■ REFERENCES

(1) Wei, Q.; Xiong, F.; Tan, S.; Huang, L.; Lan, E. H.; Dunn, B.; Mai, L. Energy Storage: Porous One-Dimensional Nanomaterials: Design, Fabrication and Applications in Electrochemical Energy Storage (Adv. Mater. 20/2017). *Adv. Mater.* **2017**, *29*, No. 1602300.

(2) Or, T.; Gourley, S. W. D.; Kaliyappan, K.; Yu, A.; Chen, Z. Recycling of Mixed Cathode Lithium-Ion Batteries for Electric Vehicles: Current Status and Future Outlook. *Carbon Energy* **2020**, *2*, 6−43.

(3) Roy, K.; Li, T. Y.; Ogale, S.; Robertson, N. Hybrid Perovskite-Like Iodobismuthates as Low-cost and Stable Anode Materials for Lithium-Ion Battery Applications. *J. Mater. Chem. A* **2021**, *9*, 2689−2693.

(4) Duan, J.; Tang, X.; Dai, H. F.; Yang, Y.; Wu, W. Y.; Wei, X. Z.; Huang, Y. H. Building Safe Lithium-Ion Batteries for Electric Vehicles: A Review. *Electrochem. Energy Rev.* **2020**, *3*, 1−42.

(5) Li, W. D.; Erickson, E. M.; Manthiram, A. High-Nickel Layered Oxide Cathodes for Lithium-Based Automotive Batteries. *Nat. Energy* **2020**, *5*, 26−34.

(6) Marom, R.; Amalraj, S. F.; Leifer, N.; Jacob, D.; Aurbach, D. A Review of Advanced and Practical Lithium Battery Materials. *J. Mater. Chem.* **2011**, *21*, 9938−9954.

(7) Simon, P.; Gogotsi, Y. Materials for Electrochemical Capacitors. *Nat. Mater.* **2008**, *7*, 845−854.

(8) Yu, A.; Chabot, V.; Zhang, J. *Electrochemical Supercapacitors for Energy Storage and Delivery;* Taylor & Francis: Boca Raton, Florida, 2017.

(9) Simon, P.; Gogotsi, Y. Capacitive Energy Storage in Nano-structured Carbon-Electrolyte Systems. *Acc. Chem. Res.* **2013**, *46*, 1094−1103.

(10) Palacín, M. R.; de Guibert, A. Why Do Batteries Fail? *Science* **2016**, *351*, No. 1253292.

(11) Lin, Z.; Goikolea, E.; Balducci, A.; Naoi, K.; Taberna, P. L.; Salanne, M.; Yushin, G.; Simon, P. Materials for Supercapacitors: When Li-Ion Battery Power Is Not Enough. *Mater. Today* **2018**, *21*, 419−436.

(12) Lewandowski, A.; Galinski, M. Practical and Theoretical Limits for Electrochemical Double-Layer Capacitors. *J. Power Sources* **2007**, *173*, 822−828.

(13) González, A.; Goikolea, E.; Barrena, J. A.; Mysyk, R. Review on Supercapacitors: Technologies and Materials. *Renewable Sustainable Energy Rev.* **2016**, *58*, 1189−1206.

(14) Simon, P.; Gogotsi, Y. Perspectives for Electrochemical Capacitors and Related Devices. *Nat. Mater.* **2020**, *19*, 1151−1163.

(15) Béguin, F.; Presser, V.; Balducci, A.; Frackowiak, E. Super-capacitors: Carbons and Electrolytes for Advanced Supercapacitors (Adv. Mater. 14/2014). *Adv. Mater.* **2014**, *26*, 2283.

(16) *Supercapacitors Materials, Systems, and Applications*, Beguin, F.; Frackowiak, E., Eds.; Wiley-VCH: Weinheim, 2013.

(17) Kötz, R.; Carlen, M. Principles and Applications of Electro-chemical Capacitors. *Electrochim. Acta* **2000**, *45*, 2483−2498.

(18) Ruiz, V.; Santamaria, R.; Granda, M.; Blanco, C. Long-term Cycling of Carbon-Based Supercapacitors in Aqueous Media. *Electrochim. Acta* **2009**, *54*, 4481−4486.

(19) Na, R. Q.; Su, C. W.; Su, Y. H.; Chen, Y. C.; Chen, Y. M.; Wang, G. B.; Teng, H. S. Solvent-Free Synthesis of an Ionic Liquid Integrated Ether-Abundant Polymer as a Solid Electrolyte for Flexible Electric Double-Layer Capacitors. *J. Mater. Chem. A* **2017**, *5*, 19703−19713.

(20) Wang, X. H.; Li, Y. H.; Lou, F. L.; Buan, M. E. M.; Sheridan, E.; Chen, D. Enhancing Capacitance of Supercapacitor with Both Organic Electrolyte and Ionic Liquid Electrolyte on a Biomass-Derived Carbon. *RSC Adv.* **2017**, *7*, 23859−23865.

(21) Chaban, V. V.; Prezhdo, O. V. How Toxic Are Ionic Liquid/Acetonitrile Mixtures? *J. Phys. Chem. Lett.* **2011**, *2*, 2499−2503.

(22) Yang, Z.; Zhang, J.; Kintner-Meyer, M. C. W.; Lu, X.; Choi, D.; Lemmon, J. P.; Liu, J. Electrochemical Energy Storage for Green Grid. *Chem. Rev.* **2011**, *111*, 3577−3613.

(23) Song, Z.; Duan, H.; Zhu, D.; Lv, Y.; Xiong, W.; Cao, T.; Li, L.; Liu, M.; Gan, L. Ternary-Doped Carbon Electrodes for Advanced Aqueous Solid-State Supercapacitors Based on a "Water-in-Salt" Gel Electrolyte. *J. Mater. Chem. A* **2019**, *7*, 15801−15811.

(24) Nunes, W. G.; Pires, B. M.; De Oliveira, F. E. R.; de Marque, A. M. P.; Cremasco, L. F.; Vicentini, R.; Doubek, G.; Da Silva, L. M.; Zanin, H. Study of the Aging Process of Nanostructured Porous Carbon-Based Electrodes in electrochemical Capacitors Filled With Aqueous or Organic Electrolytes. *J. Energy Storage* **2020**, *28*, No. 101249.

(25) Abbas, Q.; Pajak, D.; Frackowiak, E.; Beguin, F. Effect of Binder on the Performance of Carbon/Carbon Symmetric Capacitors in Salt Aqueous Electrolyte. *Electrochim. Acta* **2014**, *140*, 132−138.

(26) You, B.; Tang, M. T.; Tsai, C.; Abild-Pedersen, F.; Zheng, X.; Li, H. Enhancing Electrocatalytic Water Splitting by Strain Engineering. *Adv. Mater.* **2019**, *31*, No. 1807001.

(27) Zhong, C.; Deng, Y.; Hu, W.; Qiao, J.; Zhang, L.; Zhang, J. A Review of electrolyte Materials and Compositions for Electrochemical Supercapacitors. *Chem. Soc. Rev.* **2015**, *44*, 7484−7539.

(28) Tobis, M.; Sroka, S.; Frackowiak, E. Supercapacitor with Carbon/MoS2 Composites. *Front. Energy Res.* **2021**, *9*, No. 209.

(29) Vindt, S. T.; Skou, E. M. The Buffer effect in Neutral Electrolyte Supercapacitors. *Appl. Phys. A* **2016**, *122*, No. 64.

(30) Ruiz, V.; Blanco, C.; Raymundo-Pinero, E.; Khomenko, V.; Beguin, F.; Santamaria, R. Effects of Thermal Treatment of Activated Carbon on the Electrochemical Behaviour in Supercapacitors. *Electrochim. Acta* **2007**, *52*, 4969−4973.

(31) Wan, F.; Zhu, J.; Huang, S.; Niu, Z. High-Voltage Electrolytes for Aqueous Energy Storage Devices. *Batteries Supercaps* **2020**, *3*, 323−330.

(32) Carneiro-Neto, E. B.; Lopes, M. C.; Pereira, E. C. Simulation of Interfacial pH Changes During Hydrogen Evolution Reaction. *J. Electroanal. Chem.* **2016**, *765*, 92−99.

(33) Fuladpanjeh-Hojaghan, B.; Elsutohy, M. M.; Kabanov, V.; Heyne, B.; Trifkovic, M.; Roberts, E. P. L. In-Operando Mapping of pH Distribution in Electrochemical Processes. *Angew. Chem., Int. Ed.* **2019**, *58*, 16815−16819.

(34) Slesinski, A.; Matei-Ghimbeu, C.; Fic, K.; Beguin, F.; Frackowiak, E. Self-Buffered pH at Carbon Surfaces in Aqueous Supercapacitors. *Carbon* **2018**, *129*, 758−765.

(35) Chien, H.-C.; Wu, T.-H.; Rajkumar, M.; Hu, C.-C. Effects of Buffer Agents on Hydrogen Adsorption and Desorption at/within Activated Carbon for the Negative Electrode of Aqueous Asymmetric Supercapacitors. *Electrochim. Acta* **2016**, *205*, 1−7.

(36) Cannan, S.; Macklam, I. D.; Unwin, P. R. Three-Dimensional Imaging of Proton Gradients at Microelectrode Surfaces Using Confocal Laser Scanning Microscopy. *Electrochem. Commun.* **2002**, *4*, 886−892.

(37) Rudd, N. C.; Cannan, S.; Bitziou, E.; Ciani, I.; Whitworth, A. L.; Unwin, P. R. Fluorescence Confocal Laser Scanning Microscopy as a Probe of pH Gradients in Electrode Reactions and Surface Activity. *Anal. Chem.* **2005**, *77*, 6205−6217.

(38) Engstrom, R. C.; Ghaffari, S.; Qu, H. W. Fluorescence Imaging of Electrode Solution Interfacial Processes. *Anal. Chem.* **1992**, *64*, 2525−2529.

(39) Leenheer, A. J.; Atwater, H. A. Imaging Water-Splitting Electrocatalysts with pH-Sensing Confocal Fluorescence Microscopy. *J. Electrochem. Soc.* **2012**, *159*, H752−H757.

(40) Fiedler, S.; Hagedom, R.; Schnelle, T.; Richter, E.; Wagner, B.; Fuhr, G. Diffusional Electrotitration - Generation of pH Gradients over Arrays of Ultramicroelectrodes Detected by Fluorescence. *Anal. Chem.* **1995**, *67*, 820−828.

(41) Galindo, F.; Burguete, M. I.; Vigara, L.; Luis, S. V.; Kabir, N.; Gavrilovic, J.; Russell, D. A. Synthetic Macrocyclic Peptidomimetics as Tunable pH Probes for the Fluorescence Imaging of Acidic Organelles in Live Cells. *Angew. Chem., Int. Ed.* **2005**, *44*, 6504−6508.

(42) Liu, X.; Euchner, H.; Zarrabeitia, M.; Gao, X.; Elia, G. A.; Groß, A.; Passerini, S. Operando pH Measurements Decipher H^+/Zn^{2+} Intercalation Chemistry in High-Performance Aqueous Zn/δ-V_2O_5 Batteries. *ACS Energy Lett.* **2020**, *5*, 2979−2986.

(43) Piwek, J.; Platek, A.; Frackowiak, E.; Fic, K. Mechanisms of the Performance Fading of Carbon-Based Electrochemical Capacitors Operating in a LiNO3 Electrolyte. *J. Power Sources* **2019**, *438*, No. 227029.

(44) Platek, A.; Piwek, J.; Fic, K.; Frackowiak, E. Ageing Mechanisms in Electrochemical Capacitors with Aqueous Redox-Active Electrolytes. *Electrochim. Acta* **2019**, *311*, 211−220.

(45) Przygocki, P.; Ratajczak, P.; Beguin, F. Quantification of the Charge Consuming Phenomena under High-Voltage Hold of Carbon/Carbon Supercapacitors by Coupling Operando and Post-Mortem Analyses. *Angew. Chem., Int. Ed.* **2019**, *58*, 17969−17977.

(46) He, M. L.; Fic, K.; Frackowiak, E.; Novak, P.; Berg, E. J. Ageing Phenomena in High-Voltage Aqueous Supercapacitors Investigated by In Situ Gas Analysis. *Energy Environ. Sci.* **2016**, *9*, 623−633.

(47) Fic, K.; Platek, A.; Piwek, J.; Menzel, J.; Slesinski, A.; Bujewska, P.; Galek, P.; Frackowiak, E. Revisited Insights into Charge Storage Mechanisms in Electrochemical Capacitors with Li_2SO_4-based Electrolyte. *Energy Storage Mater.* **2019**, *22*, 1−14.

(48) Liu, Y. H.; Soucaze-Guillous, B.; Taberna, P. L.; Simon, P. Understanding of Carbon-Based Supercapacitors Ageing Mechanisms by Electrochemical and Analytical Methods. *J. Power Sources* **2017**, *366*, 123−130.

(49) He, M.; Fic, K.; Frackowiak, E.; Novak, P.; Berg, E. J. Towards more Durable Electrochemical Capacitors by Elucidating the Ageing Mechanisms under Different Testing Procedures. *ChemElectroChem* **2019**, *6*, 566−573.

(50) Jurewicz, K.; Frackowiak, E.; Beguin, F. Towards the Mechanism of Electrochemical Hydrogen Storage in Nanostructured Carbon Materials. *Appl. Phys. A* **2004**, *78*, 981−987.

(51) Vix-Guterl, C.; Frackowiak, E.; Jurewicz, K.; Friebe, M.; Parmentier, J.; Beguin, F. Electrochemical Energy Storage in Ordered Porous Carbon Materials. *Carbon* **2005**, *43*, 1293−1302.

P2. *Fundamentals and Implication of Point of Zero Charge (PZC) Determination for Activated Carbons in Aqueous Electrolytes*

Authors: Sylwia Slesinska, Przemysław Galek, Jakub Menzel, Scott W. Donne, Krzysztof Fic, Anetta Płatek-Mielczarek
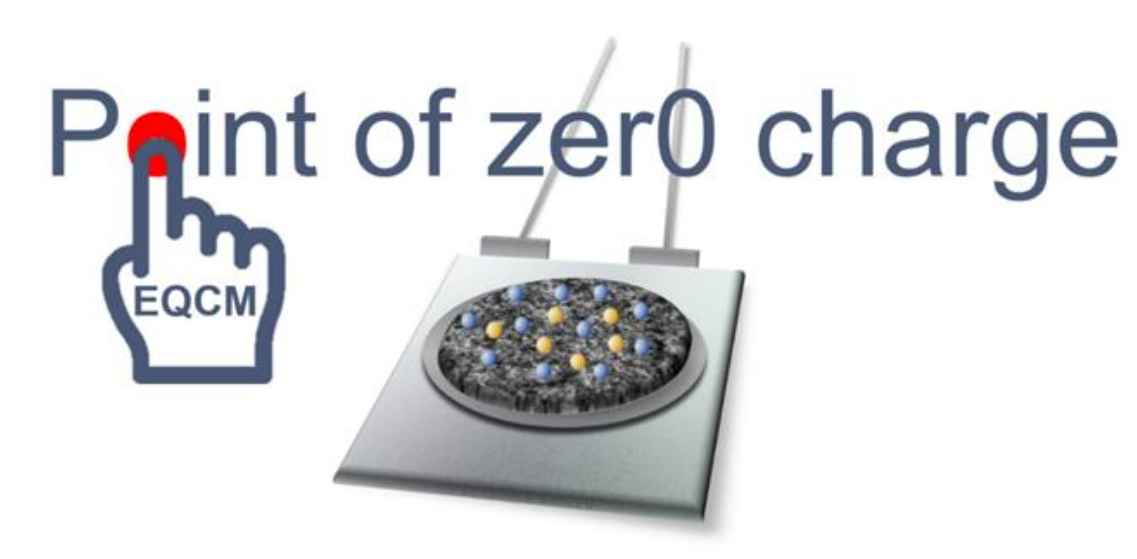
Contribution: Conceptualization, methodology, investigation: EQCM measurements, resonator and coating preparation, electrodes and electrolyte preparation, electrochemical measurements in Swagelok, EQCM and volume cells, elemental analysis, data collection, writing-original draft.

Graphical abstract:

Motivation and Summary

Understanding the complex relationship between ions and electrode surfaces in aqueous supercapacitors is imperative for optimizing their performance and longevity. While electrochemical techniques such as EIS and CV can give valuable insights into charge storage mechanisms, they fail to reveal the **mass-related** dynamics at the electrode-electrolyte interface on a molecular level. EQCM studies allow for direct monitoring of mass changes during charge/discharge processes in aqueous electrolytes, which can ultimately offer a unique perspective into the adsorption/desorption

phenomena, ion solvation effects, and structural rearrangements: all of which influence EC operation behavior. Current advancements in the "EQCM universe" are often limited to ideal materials, such as graphene, MXenes and CDC which have not yet found commercial applications. In such light, AC studies with the use of EQCM are limited, especially when coupled with aqueous electrolytes. These processes that are taking place during EC charging/discharging are not as straightforward: the complex structure and surface chemistry of activated carbon electrodes play an important role and make them more difficult to assess. Thus, the following work presents a study based on two porous activated carbons (highly microporous and micro/mesoporous) and planar resonators operating with aqueous electrolytes (based on neutral inorganic salts, such as lithium sulphate and nitrate as well as redox active electrolyte) to provide insights into PZC determination and ionic fluxes. In terms of EQCM, the correct determination of PZC is of key importance, as it determines the electrode potential value at which the formation of the EDL does not require any additional charge. It is considered as a starting point to all EQCM experiments where it 'separates' adsorption of cation and anions in a potential induced manner. So far, PZC has been evaluated using various techniques, with CV and EIS being the most common ones. However, such approaches are not always favorable and can pose a multitude of experimental difficulties and misleading information, all discussed at great length in the presented article. The motivation behind this work therefore resulted from a lack of comprehensive reports in the literature that would discuss such matters. Moreover, this work includes factors that were considered pivotal for PZC determination: *cell construction*, *reference electrode, electrolyte concentration, choice of an electrochemical technique, influence of the applied potential range and choice of an electrode material*. This allowed for a curated guideline to be designed, with the most favorable methodology for the determination of PZC. With regard to electrochemical techniques used, a universal method for PZC determination in the EQCM cell using SPECS technique was proposed, which was found to be the most efficient due to its' short implementation time and additional information regarding electrochemical processes it can provide. It was also demonstrated that for aqueous electrolytic solutions with AC electrodes the PZC should not be considered as one value, but rather a range, thus a new term 'range of zero charge' (RZC) introduced and discussed.

RESEARCH ARTICLE

Fundamentals and Implication of Point of Zero Charge (PZC) Determination for Activated Carbons in Aqueous Electrolytes

Sylwia Slesinska, Przemysław Galek, Jakub Menzel, Scott W. Donne, Krzysztof Fic,* and Anetta Płatek-Mielczarek*

The point of zero charge (PZC) is a crucial parameter for investigating the charge storage mechanisms in energy storage systems at the molecular level. This paper presents findings from three different electrochemical techniques, compared for the first time: cyclic voltammetry (CV), staircase potentio electrochemical impedance spectroscopy (SPEIS), and step potential electrochemical spectroscopy (SPECS), for two activated carbons (ACs) with 0.1 mol L^{-1} aqueous solution of LiNO$_3$, Li$_2$SO$_4$, and KI. The charging process of AC operating in aqueous electrolytes appears as a complex phenomenon – all ionic species take an active part in electric double-layer formation and the ion-mixing zone covers a wide potential region. Therefore, the so-called PZC should not be considered as an absolute one-point potential value, but rather as a range of zero charge (RZC). SPECS technique is found to be a universal and fast method for determining RZC, as applied here together with the EQCM. In most cases, the RZC covers a potential range from ≈100 to ≈200 mV and the correlation of the range with the carbon microtexture is clear, highlighting the role of the ion-sieving effect. It is postulated that PZC for porous materials in aqueous electrolytic solutions should be considered instead as RZC.

S. Slesinska, P. Galek, J. Menzel, K. Fic, A. Płatek-Mielczarek
Poznan University of Technology
Institute of Chemistry and Technical Electrochemistry
Berdychowo 4, Poznan 60965, Poland
E-mail: krzysztof.fic@put.poznan.pl; aplatek@ethz.ch
S. W. Donne
Discipline of Chemistry
University of Newcastle
Callaghan, New South Wales 2308, Australia
A. Płatek-Mielczarek
Laboratory for Multiphase Thermofluidics and Surface Nanoengineering
Department of Mechanical and Process Engineering
ETH Zurich
Sonneggstrasse 3, Zurich 8092, Switzerland
A. Płatek-Mielczarek
Unbound Potential GmbH
Bönirainstrasse 14, Thalwil 8800, Switzerland

1. Introduction

Research and development actions are needed to support the transition to green energy by proposing reliable energy storage systems. In an electrochemical society, there is a continuous discussion of the superiority of devices adapted to specific applications over universal ones. This has triggered the growing demand for more reliable and efficient energy storage devices, such as batteries or electrochemical capacitors (ECs). The latter offers much higher specific power (>10 kW kg^{-1}) and cyclability (>10^6) than current state-of-the-art batteries,[1–6] but ongoing research is still focused on increasing their energy density while retaining their particular charge/discharge properties. Since energy in ECs is stored mainly through the adsorption of ions at the electrode/electrolyte interface in the electric double-layer (EDL), ion dynamics investigations are in this context of essential importance. The process efficiency in ECs is largely affected by the electrode properties and ion behavior (both in the bulk of the electrolyte and within the electrode porosity).[7,8] However, it is difficult to distinguish these processes on the macroscale.

ECs use highly porous activated carbon (AC) materials,[9–13] which are characterized by a well-developed surface area (>1500 m^2 g^{-1}),[14] good electrical conductivity (50 S m^{-1}),[15] low cost,[16] and versatile porosity.[17] Although, recent studies have also found that the ion adsorption process in ACs is not straightforward. This process is affected by the ion-exchange mechanism, ion-pore size mismatch, and the ion solvation effect;[18] these all have an impact on the performance of the carbon electrode and need to be considered. For this purpose, a wide range of advanced in situ techniques have been recently explored, such as electrochemical quartz crystal microbalance (EQCM),[7,18–20] nuclear magnetic resonance spectroscopy,[21–24] infrared spectroscopy (IR),[5] and electrochemical dilatometry (ECD),[25,26] with the ability to elucidate the charge storage mechanisms directly at the nanoscale.

The selection of an electrolyte for ECs depends on the application and three main electrolyte groups can be distinguished: aqueous, organic, and ionic liquid.[27] H$_2$SO$_4$ or KOH are used in ECs due to their high ionic conductivity, as well as serving

as a good and well-understood environment for the fundamental characterization of new materials.[28,29] Inorganic salts have emerged as an alternative to highly corrosive alkaline and oxidative acidic electrolytes. Due to their nearly neutral pH in aqueous solutions, they exhibit overpotentials for oxygen (OER) and hydrogen (HER) evolution reactions, which extend the operational voltage window beyond thermodynamic stability.[30] Today, more insights into the performance of neutral aqueous electrolytes are provided to understand their limitations and push their operation. Molecular level dynamics of sulfate-based,[31,32] and iodide-based systems[8,33] have been successfully described. The description of the charging mechanism for nitrate-based or other neutral electrolytes is still sought, despite their common use in primary tests for new materials.[34,35]

EQCM enables the electrode/electrolyte interface to be monitored at the molecular level with advanced in situ tracking of viscoelastic property changes.[1,7,36–40] For EQCM measurements, the correct determination of the point of zero charge (PZC) is crucial because it determines the electrode potential value at which the formation of the EDL does not require any additional charge in a specific environment. Moreover, it influences all subsequent electrosorption processes at the electrode/electrolyte interface and describes the ion-sieving effect.[41,42] In this way, when the electrode is polarized outside the PZC, it will either attract cations or anions, or repel/reorganize specifically adsorbed ions from the electrode surface. EQCM enables the direct determination of the type of process (adsorption or desorption) and can help to provide a description of the kind of species adsorbed. However, detailed description and direct detection of ions concentration at the electrode/electrolyte interface can be done only using the NMR technique. For planar (formally non-porous) stainless steel electrodes, it has been recently shown that the hydration shell of the physiosorbed species in the EDL shifts the PZC.[43,44] In addition, the PZC of metal surfaces is a pH-independent variable, tested for dilute aqueous solutions; nevertheless, pH influences other reaction potentials, as they might be affected by solution species like H^+.[44] When porous carbon is applied as an electrode, the observed phenomenon cannot be simply discussed, and thus PZC is one of the key parameters to enable reliable data analysis.[39,45–47]

The PZC in electrochemical systems can be evaluated using various techniques. The most common are cyclic voltammetry (CV) and impedance spectroscopy (EIS). Minimum current response in CV tests using high scan rates for organic electrolytes, i.e., 10 mV s^{-1}[38,48] can be also verified with in situ measurement of minimal electronic conductivity versus applied potential.[49] For organic-based solution the minimum current versus applied potential is easily detectable. Interestingly, reported cyclic voltammetry for different ECs was not always conducted directly in 3-electrode EQCM cell, but often in 2-electrode with reference Swagelok cell.[36,50] EIS tests are performed at different potentials (PEIS), allowing one to present specific capacitance versus potential and to find its minimal value.[39,46,51] Recently, step potential electrochemical spectroscopy (SPECS) was first reported to be applied to determine PZC.[47] Each literature study applies one technique for the determination of PZC, and we find the description of the experimental conditions used very scarce. No clear evidence for a reason or purpose for application of one of these techniques can be found in the literature up to date.

Besides, SPECS and EQCM were already coupled to investigate the manganese dioxide electrodeposition process as a probe of capacitive behavior.[52] However, that study was not focused on PZC determination.

In our study, we explored various techniques that could enable an accurate and fast determination of PZC (with minimal over- or underestimation of the PZC value). A set of comparative PZC data was obtained on the basis of three techniques: staircase potentio electrochemical impedance spectroscopy (SPEIS), CV, and SPECS, all recorded directly in an EQCM setup, to create a rational comparison among the techniques described in the literature. The PZC value determined in the EQCM cell was compared with the value obtained in the 2-electrode with reference electrode Swagelok system and the 3-electrode cell, so-called volume cell, to show the influence of cell design on the PZC value. We also reported changes in EQCM responses for the microporous carbon electrode in three different aqueous electrolytes (sulphate, nitrate, and iodide based) to represent specific EDL formation at the porous carbon interface in the presence of water molecules despite the presence of polarized species. The water molecules, due to their concentration in the solution (0.1 mol L^{-1} inorganic salt electrolytic solutions were tested) extend PZC to a region of zero charge, further denoted as RZC. To confirm the observed phenomena, two microporous carbons and a planar stainless-steel surface were tested with three selected aqueous electrolytic solutions.

2. Results and Discussion

2.1. Point of Zero Charge Determination

To study porous activated carbons with a non-uniform and wide pore size distribution, dilute aqueous solutions (0.1 mol L^{-1}) were selected to keep the electroactive species concentration at a level that does not exceed the detection limits of the EQCM used (measurable frequency change). To ensure the high applicability of our study, the nonideal electrode material, with a significant micropore volume, $V_{micro} > 0.64$ cm^3 g^{-1}, was tested—representing activated carbons used in the full cell studies and possible commercial devices (Figures S1 and S2, Table S1, Supporting Information).

In **Figure 1**, the PZC values obtained by the CV, SPECS and SPEIS techniques in the EQCM cell are compared for 0.1 mol L^{-1} LiNO$_3$ (Figure 1a), Li$_2$SO$_4$ (Figure 1b) and KI (Figure 1c) with the YP-50F electrode material on the specific capacitance versus potential plot (for detailed CV – Figure S7, SPEIS – Figure S8, and SPECS methodology, see Supporting Information). Aqueous electrolytes were selected due to their satisfactory electrochemical performance at high voltages, >1.2 V, and satisfactory long-term stability.[8,31,34]

The experimental conditions for CV (for 5 and 50 mV s^{-1}, see Figure S7, Supporting Information) and SPECS were convergent, and the currents recorded from these techniques were converted to specific capacitance. For CV, 1 mV s^{-1} was applied and for SPECS, $E = 10$ mV with $t = 10$ s, providing an average scan rate of 1 mV s^{-1}. The PZC is determined as the lowest capacitance (current) value[53] in the intermediate potential range (directly correlated with the capacitance (C_{CV}) calculated from the CV technique based on Equation S2, Supporting Informa-
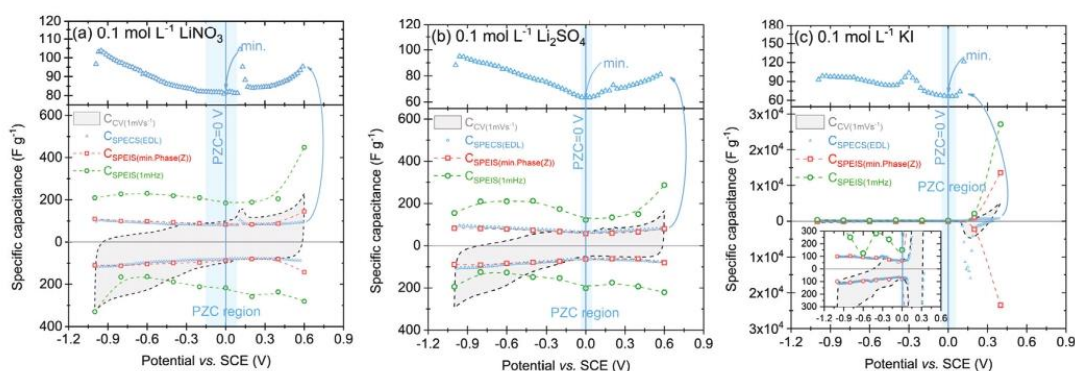
2409162 (2 of 10)

Figure 1. Specific capacitance versus potential calculated from three electrochemical techniques: CV (gray shade), SPECS (blue triangular scatter), and SPEIS (red square and green circular scatter) for YP-50F and 0.1 mol L^{-1} electrolytic solutions in EQCM cell a) LiNO$_3$, b) Li$_2$SO$_4$, and c) KI. The upper part of the plot represents the zoomed SPECS-specific capacitance versus potential in the E_{min} to E_{max} direction.

tion). However, this method might not be fully accurate since the voltammetry response is derived from the full current response, which is also related to diffusion-limited processes and EDL formation. The PZC corresponds to an electrostatic interaction between the electrode and the electrolyte (EDL formation only). This process might not be fast enough, particularly in a porous medium, such as activated carbons, being affected by transport-related phenomena. Diffusion-limited processes include those related to the oxidation/reduction of compounds and the intercalation/insertion and residual processes resulting from side reactions (such as electrolyte decomposition).[54] The Faradaic current could superimpose the EDL response, as shown in the CV profiles (dashed black lines in Figure 1a–c) near 0.15 V vs. SCE for LiNO$_3$, 0.15 and 0.2 V vs. SCE for Li$_2$SO$_4$ and −0.3 V vs. SCE for KI. This redox peak could be attributed to a redox response from quinone/hydroquinone-type functionalities, grafted onto carbon surface.[55] Further, as extreme potentials (E_{max} and E_{min}) were approached, the box-shaped CV profile was deformed by the increase in current related to the decomposition of the electrolyte.

$C_{SPEIS(1mHz)}$ curves for the LiNO$_3$-based system are not symmetric for both polarization directions (see Figure S8, Supporting Information). The same situation occurs for systems with Li$_2$SO$_4$ (Figure 1b) and KI (Figure 1c). Furthermore, for the KI redox system, the measurement toward E_{min} was impossible to perform correctly due to the high redox activity in the positive potential values (> 0 V vs SCE).

Unlike CV (Figure S7, Supporting Information) and SPEIS (Figure S8, Supporting Information), which are more prone to experimental limitations, SPECS is determined to be a promising technique for PZC identification, regardless of the experiment conditions (Figure 1; blue squares); thus, universal one for electrochemical capacitor testing. The advantage of this technique includes a short implementation step time (in this case, 1 mV s^{-1}). Moreover, the potential shift is quite gentle and enables detailed data to be recorded in the entire potential range, increasing the resolution and accuracy of the recorded data. These potential steps lead to a smooth behavior of (tentative) redox reactions and balanced ion redistribution in the pores. The advantage of SPECS over CV could be also seen in the ability to quantify the capacitive contribution of different charge-storing mechanisms, including those associated with EDL formation (see Supporting Information).[53,54]

The PZC in Figure 1 is not a specific potential value for the ACs, with a clear inflection point on the capacitance curve. Here, one can distinguish a wide potential range of RZC (blue region) from −0.15 to 0.09 V vs. SCE, with a comparable capacitance (82 F g^{-1}) for the LiNO$_3$-based system (with ±2% variation in the minimal specific capacitance value), providing a PZC range of 240 mV. For Li$_2$SO$_4$, this region is from −0.04 to 0.05 V (PZC range of 90 mV, data for two concentrations, 0.1 and 1 mol L^{-1}, can be found in Figure S9, Supporting Information) and for KI, this region is from −0.05 to 0.06 V (PZC range of 110 mV).

We propose to determine exact PZC values (if needed) in the middle (median) of this low capacitance region, here at 0 V versus SCE for three tested aqueous electrolytic solutions. Interestingly, an increase in $C_{SPECS(EDL)}$ and total capacitance can also be observed in the potential region where redox processes occur (for all tested electrolytes). Because redox processes induce charge transfer with the specific adsorbed ions, they affect the formation of the EDL itself. Furthermore, this response cannot be differentiated from C_{EDL}. An ambiguous increase in recorded current is observed due to quinone/hydroquinone redox activity of the electrode surface.

The SPECS technique provides insight into the charging mechanism of electrochemical capacitors by differentiating the capacitance contribution (see Supporting Information for detailed information about the technique and calculations), as shown in **Figure 2**.

The calculated total capacitance (C_T) of the system is identical to the C_{CV} (Figure 2) when identical measurement conditions are maintained (in this case, the average scanning rate of 1 mV s^{-1}). As expected for porous carbon materials, the main contribution to C_T is made by porous capacitance (C_P) due to the strongly developed specific surface area of the AC used (Figure S1, Supporting Information). The C_P curves show a butterfly shape that is usually visible for organic systems,[33,50] and fast repolarization processes are shown in the box-like shape. The share of geometric capacitance (C_G) is significantly lower for capacitive sys-
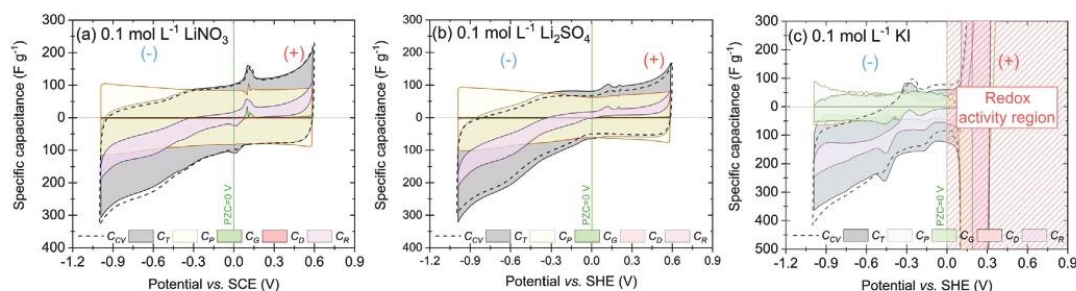
2409162 (3 of 10)

Figure 2. Capacitance components were calculated from the SPECS technique for 0.1 mol L^{-1} aqueous solution of a) LiNO$_3$, b) Li$_2$SO$_4$, and c) KI.

tems, that is, LiNO$_3$ (Figure 2a) and Li$_2$SO$_4$ (Figure 2b), resulting from the poorly developed electrode surface in direct contact with the electrolyte (low ratio of the geometric electrode interface to the electrolyte volume). Interestingly, for the redox-based system (Figure 2c), C_P and C_G are almost equal in the potential range lower than PZC, i.e., in the capacitive region, due to specific iodide adsorption onto the carbon surface. Unfortunately, the computational method does not allow to make such predictions (calculations of C_P and C_G) for the redox active region; thus, it was not applied. In the systems studied, the smallest capacitive contribution comes from ion diffusion (C_D), showing that the main charge storage mechanism is based on EDL formation. Moreover, residual capacitance (C_R) is responsible for any discrepancies from the ideal box-shaped shape characteristic for a capacitive response; the value of C_R increases in the potential regions where the electrolyte decomposition, specific ion adsorption, or redox processes occur. C_R is responsible for the overall C_T cyclic voltammogram shape deviating from the ideal C_P capacitive curve.

The influence of the potential range was also compared (1 vs. 1.6 V) on the PZC range for 0.1 mol L^{-1} LiNO$_3$. The same experimental conditions were applied in the narrow and wide potential tests using the SPECS technique. CV computed for both potential ranges do not differ qualitatively (Figure S9, Supporting Information). Both cyclic voltammograms represent capacitive behavior, visible in a rectangular-like shape. RZC differs here by 50 mV (Table S6, Supporting Information). This negligible difference results from using fresh experimental cells for this study. Thus, all components: carbon, electrode coating, electrolyte volume, inorganic salt impurities, etc. affect the result. Although, it was proved that the wide voltage window, i.e., 1.6 V, for selected experimental conditions (carbon and aqueous electrolyte) is still stable and reliable.

Our study also included the influence of cell construction on PZC values (see Figure S10, Supporting Information), as various experimental approaches are used in the literature. Unfortunately, a potential shift in electrochemical behavior was observed (Figure S10, Supporting Information) and resulted from different uncompensated resistance factors (Figure S11, Supporting Information). In addition, it seems that tested reference electrodes might influence the determination of the PZC value. It has been proven, that in contrast to overall cell construction (volume of electrolyte, working electrode loading, the distance between electrodes, etc.), reference electrode has a negligible influence

(Figure S13, Supporting Information); thus, for short-term experiments, no Cl$^-$ migration from the SCE electrode was tracked. The electrochemical tests of neutral-pH aqueous ECs were not susceptible to the RE type. However, cell construction had a large impact on individual electrode stability and should be considered while determining PZC.

In particular, all tested aqueous solutions are characterized by a wide PZC potential range (**Figure 3**) when determined using the SPECS method (min. capacitance value $\pm1\%$ or $\pm2\%$, please see Table S5, Supporting Information). The LiNO$_3$-based system shows mainly capacitive charge storage behavior[34,35] and also has the widest potential PZC range ($\approx$240 mV). Thus, the region of ion reorganization/mixing is not limited by the potential value itself, and both the Li$^+$ cations and the NO$_3^-$ anions have the same affinity for the electrode. On the contrary, KI is a pure redox system[56–60] characterized by a narrow PZC potential range (110 mV). Beyond this narrow potential range, other mechanisms occur, such as specific ion adsorption on the electrode surface.[8] Considering these facts and the ambiguous Li$_2$SO$_4$ charge storage mechanism,[31] it can be stated that it is a pseudocapacitive electrolyte. Its PZC range is rather narrow (90 mV), which can indicate SO$_4^{2-}$ specific adsorption on the electrode surface. Additionally, the SO$_4^{2-}$ ion flux during positive electrode charging has thus far been excluded.[31,32]

The parameter that should also be carefully considered when determining PZC is the mass loading of the electrode (Figure S4, Supporting Information). Higher mass loading increases capacitance by providing more active sites for charge storage. Lower mass loading reduces available ion interaction sites, impacting the clear observation of the RZC. In porous materials, mass loading influences ion penetration (diffusion) into the pores and EDL formation. Thicker electrodes may experience uneven charge distribution, poor conductivity, and potential gradients, complicating the determination of RZC. Additionally, higher mass loading can enhance Faradaic processes, further obscuring the identification of the zero potential range. It is also necessary to remember about the limitation in the EQCM system – the frequency range. Too large of an electrode mass or too large of the frequency changes during experiments (e.g., caused by a large mass of the ions considered or too high electrolyte concentration) may result in the output of the registered signal within the previously selected frequency region. Therefore, 2-electrode systems and 3-electrode system, as well as, full cell
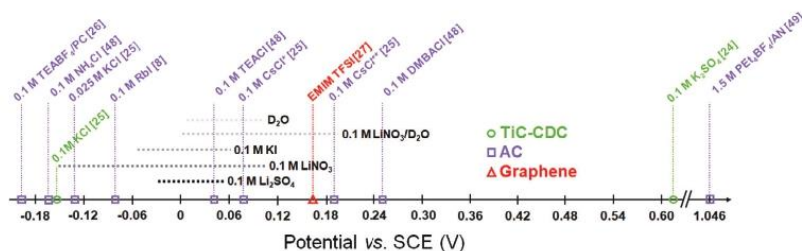
Figure 3. Summary of the PZC values reported in the literature and the RZC presented in our work for various aqueous and organic solutions; all recalculated versus SCE. Differentiation of the electrode material is as follows: Ti-CDC (circular scatter), AC (square scatter), and graphene (triangular scatter).[50,56]

studies and fundamental ones, should be characterized independently with great caution to the limiting factor for observed phenomena.

The determination of the RZC region in strong oxidation-reduction systems can become less straightforward than in pure EDL systems. In a simple electrochemical system without faradaic processes (no redox reactions), the RZC reflects the electrostatic balance between the electrode and the electrolyte. In a system with strong redox reactions, the RZC may shift depending on the redox couples present and the pH change. Redox-active species in the electrolyte might interact with the electrode in a way that alters the effective surface charge (via specific adsorption).[8] These redox reactions influence the electrode potential, and it might be more appropriate to consider the system's overall electrochemical behavior rather than isolating the RZC. The RZC still represents the minimal electrostatic interaction with the surrounding electrolytic solution, but the redox processes cause dynamic charging conditions. In systems where the material exhibits strong redox properties and has a well-developed specific surface area, determining the RZC is still feasible (example: KI as electrolytic solution Figure 1c). The highly developed surface of the material allows for a more precise determination of the RZC due to the distinct appearance of the minimum capacitance, which increases with either higher or lower applied potential (E_{max} and E_{min}). This is due to ion penetration into the pores and the expansion of the EDL. Conversely, for materials with less developed specific surfaces, determining the RZC may be more challenging (Figure S14, Supporting Information).

The width of RZC seems to also correlate to the size and charge of the ion present in the electrolytic solution. As shown in **Table 1** below, SO_4^{2-} has not only a larger ionic radius, but also a higher charge compared to I^- and NO_3^- anions. This favors stronger electrostatic attraction toward the oppositely charged surface of

the carbon electrode, resulting in increased specific adsorption, creating a net charge on the electrode surface. Consequently, only a small change in the electrode potential is necessary to affect this state and push it out of the equilibrium state, resulting in a narrower RZC.

We also believe that the effect of concentration on RZC needed to be verified for further clarification, that's why we have tested 1 and 0.1 mol L^{-1} Li_2SO_4 (Figure S9 and Tables S5 and S6, Supporting Information). Most of the low-concentration RZC overlap with the high concentration solution. However, the RZC region is highly extended due to a higher number of charges in the solution able to take part in EDL formation. Thus, the higher the concentration, the wider the RZC region. This also indicates that each system should be treated individually, and each studied concentration offers additional information for other researchers.

Studies on PZC determination methods are very limited in the literature; however, the authors usually refer to one specific measurement/technique; a minimum conductance value or a minimum capacitance value. At the PZC, the net charge on the electrode surface is zero, and the EDL capacitance reaches a minimum. Direct correlation lies in the fact that the minimum capacitance directly corresponds to the point where the net charge on the electrode surface is zero. Thus, the minimum capacitance is often used as a reliable indicator of the PZC, as it directly reflects the point of zero net charge on the electrode surface. Similarly, at the PZC, the electrode surface has no net charge, and the double layer is relatively symmetrical, which can reduce the ease of ion transport.

These values, Figure 3, were obtained by different techniques, varying in the experimental setups and experimental electrochemical conditions. For the ACs studied, YP-50F and DLC30 (Figure S15, Supporting Information), the wide PZC region is believed to result from the electrolyte/electrode interactions and a high share of solvent molecules during EDL formation.[64] AC has a wide variety of surface functional groups, high tortuosity, 3D porosity, and specific structure (Figures S1 and S4, Tables S1, S2, S3, Supporting Information). The planar metallic electrode (without defects and with a low specific surface area) correlates to a wide PZC region (Figure S14, Supporting Information), such as a wide potential window for ionic liquid on glassy carbon electrodes. For the two ACs studied, the PZC region is much narrower than that for the planar resonator (Figure S15, Supporting Information). However, for materials studied with D_2O, no difference in the RZC range is observed, confirming a particu-

Table 1. Ionic radius and RZC for anions in electrolytes used in this research.

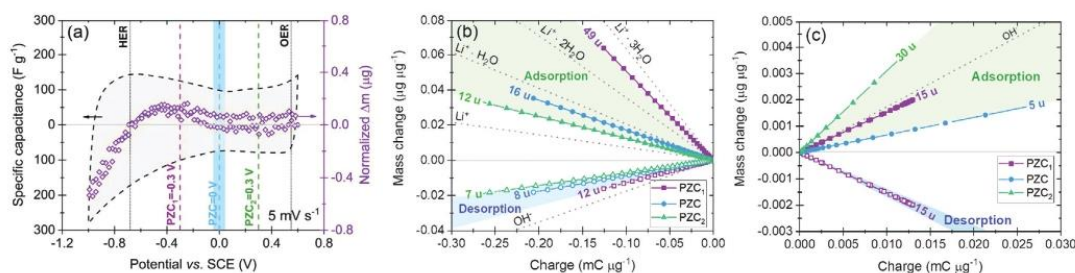| Electrolyte	Anion	Ionic radius[61,62]	RZC
0.1 M Li_2SO_4	SO_4^{2-}	0.242 nm	90 mV
0.1 M $LiNO_3$	NO_3^-	0.177 nm	240 mV
0.1 M KI	I^-	0.216 nm	110 mV

Figure 4. EQCM characterization of 0.1 mol L^{-1} Li$_2$SO$_4$ and YP-50F: a) specific capacitance versus potential at 5 mV s^{-1} with the assigned PZC; b) mass:charge plot for the assigned PZC in the polarization toward lower potential values from the PZC; c) mass:charge plot for the assigned PZC in the polarization toward higher potential values from the PZC.

lar electrolyte ion/electrode interaction when an inorganic salt is present.

2.2. EQCM Data Evaluation

The previous section addressed the proper and accurate determination of the PZC. However, in addition to the determination of PZC for 0.1 mol L^{-1} LiNO$_3$, Li$_2$SO$_4$, KI, and 0.1 mol L^{-1} LiNO$_3$ in D$_2$O (Figure 3), the significance of these data has not yet been quantified. Therefore, basic electrochemical tests (cyclic voltammetry at 5 mV s^{-1}) in combination with EQCM were performed to study the ion flux on the carbon electrode during the charging process (validation of the experimental setup is presented in Figure S16, Supporting Information). To interpret the influence of the PZC value on the evaluation of the data, a Li$_2$SO$_4$-based system was selected, and the data is presented in **Figure 4**. This system is: i) broadly described in the literature, ii) has a complex charging mechanism, and iii) has promising electrochemical performance (very long cyclability).[31]

After determining PZC using the techniques mentioned (average PZC = 0 V), mass change calculations were performed to establish PZC and two other artificially imposed values (PZC$_1$ and PZC$_2$). This results in a recalculation where the PZC is the following: 1) -300 mV from PZC (PZC$_1$) and resembles the PZC determined in the Swagelok cell (Figure S11, Supporting Information), 2) PZC = 0 V vs. SCE and is considered as the correct value determined for the studied system (Figure 1) and 3) +300 mV from PZC (PZC$_2$). In total, this provides a wide range of potential $\Delta E = 600$ mV in which PZC is considered, imposed, and discussed.

In Figure 4a, the hydrogen evolution potential (HER) is shown; the HER of this electrolyte equals −0.681 V vs. SCE, and the oxygen evolution potential (OER) of this electrolyte equals +0.549 V vs. SCE. According to Faraday's law (Equation 1), the change in mass (related to dissolution or deposition) is linearly correlated with the amount of charge that passes through the electrochemical setup. From the slopes of the mass:charge curves (Figure 4b,c), both adsorption and desorption data show multistep processes ongoing at the electrode/electrolyte interface (determination of ionic species is done based on Table S8, Supporting Information). According to the literature, one can assume the adsorption of Li$^+$ as well as its solvated forms, i.e., Li$^+ \bullet$ 2H$_2$O

(with $\Delta m = 42.97$ u) and OH$^-$ (with $\Delta m = 17.01$ u), during negative and positive polarizations, respectively (Table S8, Supporting Information).[31] This counter-ion adsorption/desorption process is considered as the amount of positively and negatively charged species in PZC can be equal resulting in a net zero charge value. In consequence, Figure 4b shows that the adsorption process is followed by the desorption process. In Figure 4c a two-step process is observed only for PZC$_1$, with an initial desorption and then adsorption of the mass difference (15 u). For negative polarization, the ionic species with a molecular weight between Li$^+$ and hydrated Li$^+ \bullet$ 3H$_2$O are responsible for the mass change. However, for positive polarization, where SO$_4$$^{2-}$ or OH$^-$ are anticipated, none of these were found. Therefore, the processes that occur at the positive electrode/electrolyte interface are not related to single ion adsorption. This is potentially related to: the carbon oxidation process that can continuously occur, specific SO$_4$$^{2-}$ ion adsorption on the YP-50F electrode, SO$_4$$^{2-}$ redox reactions (to S^{2+} and/or S^{4+} oxidation states[31]), or ion reorganization. Thus, the matching of ion flux for sulfate-based electrolytes is not that straightforward.

The electrolytic solution of 0.1 mol L^{-1} LiNO$_3$ was studied using EQCM for the first time (**Figure 5**). This electrolyte has been reported as a capacitive one (even at low concentrations);[35] therefore, ion fluxes based on Li$^+$ and NO$_3$$^-$ were anticipated.

Since the negative polarization range was largely extended from the PZC in all measurements, LiNO$_3$-based systems display adsorption followed by desorption while approaching increasingly lower potential values. When the 0.1 mol L^{-1} solution was prepared in DI water, no NO$_3$$^-$ anion flux was detected (Figure 5a), which led to the conclusion that the NO$_3$$^-$ anion, like SO$_4$$^{2-}$, was more prone to redox processes than EDL formation. It seems that NO$_3$$^-$ is likely to be reduced (to NO$_2$ and/or NO), due to the oxidation of carbon surface – leading to the redox balance and equilibrium at the interface. It is noteworthy that these gases have been found in another study with on-line mass spectrometry.[64] However, the same solution was prepared using D$_2$O (Figure 5b) – characterized by a higher molecular weight (see Supporting Information). In the second case, NO$_3$$^-$ adsorption and desorption were recorded, accompanied by an opposite sorption process of solvated cation (Li$^+ \bullet$ 2D$_2$O). RZC in this case shifts toward more positive potential values, slightly narrowing its potential range (Figure 3) related to a lower number of NO$_3$$^-$ ions specifically adsorbed on the electrode surface in the pres-
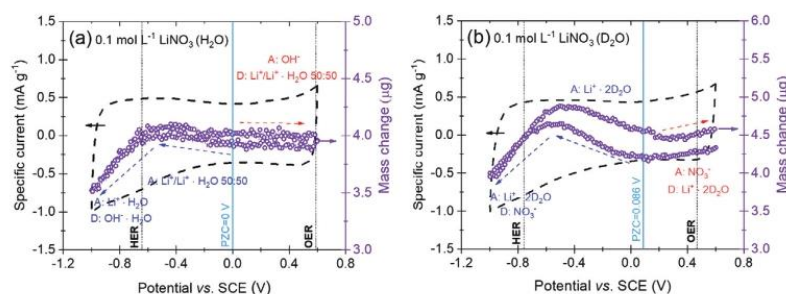
Figure 5. The charging mechanism for 0.1 mol L^{-1} LiNO$_3$ and YP-50F presented in specific capacitance versus potential at 5 mV s^{-1} in a) H$_2$O and b) D$_2$O.

ence of D$_2$O molecules instead of H$_2$O. The solvation shell of a lithium cation seems to be reasonable at this concentration, and interestingly, when D$_2$O is a solvent molecule—the solvated Li$^+$ ions detected by EQCM have a stable solvation shell. Moreover, a good correlation between the PZC values determined via SPECS and SPEIS and the mass change profile recorded by EQCM can be observed. This result further confirmed the need for accurate PZC determination and its insight into the charging mechanism; dividing the mass change curve correctly into different regimes where either cation or anion adsorption is the leading process in EDL formation. These experiments confirmed that the nitrate-based electrolyte is capacitive, NO$_3^-$ ions tend to be specifically adsorbed onto the AC surface, and that the flux of NO$_3^-$ ions can be detected for the case where specific adsorption of nitrate anion does not occur. When H$_2$O was used as a solvent, the OH$^-$ anion was more likely to form EDL than NO$_3^-$. These results also showed that pH, conductivity, ionic species (type and their activity), and solvent molecules influenced the charging mechanism in aqueous-based EC, emphasizing the importance of considering each system individually, quite often in not a straightforward way.

3. Conclusion

The PZC was determined using SPECS, SPEIS, and CV techniques for water-based solutions. Moreover, the PZC meaning for the description of the charging mechanism for aqueous electrochemical capacitors exploiting AC electrodes was discussed. We proposed a universal method for PZC determination in the EQCM cell using the SPECS technique, leading to the most accurate results, as demonstrated for sulfate- and nitrate-based systems. This revealed their charge mechanisms, which would not have been possible using other PZC determination techniques. We demonstrated that the PZC should be considered as an RZC rather than one value for aqueous electrolytic solutions with activated carbon electrodes, in contrast to organic-based ECs or ECs using well-organized electrode materials (homogenous in structure and texture).

We have proposed a guideline for future EQCM studies on charge storage mechanisms in energy storage systems. Regardless of the method selected, the RZC should be directly determined in the EQCM cell. The SPECS technique is reported to be an alternative and comprehensive method to determine the

RZC. In addition, this method provides important insights into the charging mechanism via deconvoluting the total specific capacitance into pore- and surface-related ones. The SPEIS experiment can also be useful for the determination of PZC, but the overall prolonged time needed to carry out this experiment can negatively impact the electrolyte stability, especially in the EQCM setup. It is crucial here to consider the specific capacitance calculated for the frequency determined from the Bode plot (close to phase angle −90°) to obtain the most reliable values. In our opinion, the most widely used CV technique cannot be recommended for the determination of RZC because porous activated carbons with a developed surface area (> 1500 m^2 g^{-1}) cause excessive formation of an electric double layer, which obscures the potential at which the minimum charge specifically accumulates at the electrode/electrolyte interface.

Studies of the electrolytic solution of LiNO$_3$ show that neutral, polar solvent molecules (H$_2$O vs. D$_2$O) do not significantly influence the PZC region but quantitatively influence the EDL at the electrode/electrolyte interface – affecting the charge storage mechanism. In aqueous solutions NO$_3^-$ anion is specifically adsorbed onto carbon surface, like SO$_4^{2-}$—proven in this study, and I$^-$. However, the number of species included in this phenomenon can be further analyzed via the application of a different solvent, which was successfully proven with D$_2$O solutions.

This systematic and rational study can serve as an indication of the correct determination of RZC and its key importance in energy storage devices. The most valuable take-home message from our study is to treat each system individually with respect to the selected method and technique used. The principles and limitations of all techniques selected must always be obeyed. Although aqueous-based systems reveal some similarities, their micro- and nanoscale observations show drastic differences in their charge storage mechanism, depending on the active material used, therefore, special attention should be paid to the interpretation of the data from this medium.

4. Experimental Section

Electrodes: Electrodes (coated on a quartz crystal resonator) were prepared based on two microporous ACs – Kuraray YP-50F (Japan) and Norit DLC Supra 30 (Cabot Carbone S.A.S.; France), denoted as YP-50F and DLC30, respectively. Their physicochemical characterization is shown in

the Supporting Information (Figures S1, S2, and Table S1, S2, Supporting Information). The texture data of the ACs are presented in Figure S1 and Table S1 (Supporting Information). The surface areas of both ACs are similar with values of 1702 and 1780 m^2 g^{-1} for YP-50F and DLC30, respectively. Although the microporosity volume (V_{micro}) is similar at 0.65 cm^3 g^{-1}, the mesopore volume (V_{meso}) is three times higher for DLC30 (0.25 cm^3 g^{-1}) than for YP-50F (0.08 cm^3 g^{-1}). Both materials consist mostly of micropores with an average diameter of 0.65 and 0.69 nm for YP-50F and DLC30, respectively. The powder of one of the ACs and a 5 wt.% solution of poly(vinylidenedifluoride) (PVDF) (Sigma–Aldrich; USA) in N-methyl-2-pyrrolidone (NMP) (Sigma–Aldrich; USA) were mixed – please refer to Supporting Information for a schematic of the resonator coating procedure, Figure S3 (Supporting Information). The AC:binder mass ratio in the final electrode material was 80:20. The electrode slurry was then mixed with a magnetic stirrer for 2 h. Stainless steel (SUS304) was used as the current collector of the quartz resonator with a standard finish (9 MHz; 21 mm^2; SEIKO EG & G; Japan). The collectors were lightly sanded with fine-grain sandpaper prior to drop casting of the electrode material. Mechanical treatment increases the adhesion of the conductive glue and electrode material to its surface and reduces resistance. After surface cleaning (with acetone), the collector was covered with a thin layer of conductive glue ≈60 µg (0.285 mg cm^{-2}; DAG; Henkel). The resonators were dried at 60 °C for 12 h to evaporate the solvent. The collectors with the conductive glue were then evenly coated with the electrode slurry using a drop-casting procedure with a wet drop mass of ≈230 µg. The resonators were subjected to the same drying procedure as described above. Ultimately, the mass loading of the dry carbon coating did not exceed 50 µg (0.285 mg cm^{-2}), ensuring a thin and rigid coating layer necessary for the EQCM application, Figure S4 and Table S3 (Supporting Information) (to consider Saurbrey equation, Equation S1, Supporting Information). The same electrode material was used to cover current collectors in the Swagelok-type cell (denoted as Swagelok) and volume cell. However, in this case, the active mass load was much higher (≈6.5 mg (5.75 mg cm^{-2})). All the specific capacitance values discussed were related to the active mass of the electrode material.

Elemental Analysis: The determination of the mass fractions of carbon, hydrogen, nitrogen, and oxygen was carried out with ThermoFisher Scientific FlashSmart (USA) equipment. The amount of oxygen was obtained through direct (separate) elemental analysis. The results are the average values of three separate analyses (Table S2, Supporting Information).

Electrolytes: The following compounds were used in the study: lithium nitrate (LiNO$_3$), lithium sulfate (Li$_2$SO$_4$), potassium iodide (KI), and solvents: DI water, and deuterium oxide (D$_2$O) with purity ≥99,5% (Sigma–Aldrich; USA). Electrolyte solutions (0.1 mol L^{-1} for LiNO$_3$, Li$_2$SO$_4$, and KI) were prepared in distilled water with an electrical conductivity <2 µS cm^{-1} (water purification system; Hydrolab; Poland). Furthermore, a 0.1 mol L^{-1} solution of LiNO$_3$ was prepared in D$_2$O (with conductivity ca. 20 µS cm^{-1}). The conductivity and pH of the given electrolytes are provided in Table S4 (Supporting Information).

Electrochemical Cells: The electrochemical cell consists of a polyetheretherketone (PEEK) body with a structure adapted to electrochemical measurements with the implementation of EQCM (Figure S5, Supporting Information). The resonator with an AC coating was placed at the bottom of the cell and served as the working electrode (WE). A stainless-steel foil was used as the counter electrode (CE) with a geometrical area that exceeded that of the WE (20 cm^2 of CE vs. 0.21 cm^2 of WE). A saturated calomel electrode (SCE; 0.241 V vs. SHE) was placed close to the resonator and acted as the reference electrode (RE). An excess of electrolyte (400 µL) was injected into the cell, ensuring that there were no trapped air bubbles. In a symmetric Swagelok cell consisting of a poly(tetrafluoroethylene) (PTFE) body, the WE and CE were separated by two GF/A porous membranes (Whatman; USA; d = 12 mm; thickness 260 µm). For this system, SCE and Hg/Hg$_2$SO$_4$/0.5 mol L^{-1} K$_2$SO$_4$ were used as reference electrodes. The same reference electrodes were used for the "in-house made" volume cell (also made out of PTFE). The volume cell provided construction conditions similar to those of the EQCM cell (excess of the electrolyte, oversized CE, and a large distance between WE and RE).

Electrochemical Investigation: All electrochemical measurements were performed on a multichannel potentiostat/galvanostat VMP3 (BioLogic; France). A QCA922 quartz analyzer (SEIKO EG & G; Japan) was connected to a potentiostat/galvanostat using an analog ±10 V BNC connection (for monitoring the frequency and resistance change). In this way, the QCM analyzer is controlled in the EQCM mode by the potentiostat/galvanostat during electrochemical measurements. The measurements (CV, SPECS controlled by chronoamperometry, and SPEIS) were conducted using EC-Lab software (BioLogic; France).

The electrochemical stability range was selected during preliminary experiments in a very broad potential range carried out in the EQCM cell (−1.3–1 V vs. SCE; Figure S6, Supporting Information). The scan rate (1 mV s^{-1}) was selected based on its sensitivity to all side reactions. The limiting potential values were selected to avoid the presence of water decomposition peaks. Registered preliminary data were not subjected to further interpretation. For LiNO$_3$ and Li$_2$SO$_4$ tests, the chosen potential window was equal to −1 to 0.6 V vs. SCE, and for KI, it was −1 to 0.4 V vs. SCE, which was consistent with other reported data.[8,31,35]

On the first assembly of the EQCM system, the experiments listed below were performed to determine the PZC:

1.1) 3 cycles of CV at 50 mV s^{-1} from open circuit voltage (OCV) and finished at OCV (system conditioning)
1.2) 1 cycle of CV at 1 mV s^{-1} from OCV and finished at minimum potential (E_{min})
1.3) 1 cycle of SPECS from E_{min} and finished at E_{min}
1.4) 1 cycle of SPEIS from E_{min} and finished at E_{min}

Data from experiment 1.2) were used for further comparison with SPECS and SPEIS data to specify the PZC. For further CV technique discussion, please see Figure S7 and Equation S2 (Supporting Information). SPECS is based on a series of equal-magnitude potential steps ($\triangle E = 10$ mV; controlled by chronoamperometry) with a rest time of 10 s. In the rest time, the current equilibrium (I–t transient) is established for each potential step. The selection of the potential step and the rest time during the SPECS experiment is related to the conductivity of the aqueous electrolyte. For further SPECS technique discussion, please see Equation S4 (Supporting Information). SPEIS begins with $E = 200$ mV in the frequency range from 10 kHz to 1 mHz (sinus amplitude $\nu_a = 5$ mV; points per decade $n_d = 10$; measures per frequency $n_a = 1$; with drift correction). For further SPEIS technique discussion, please see Figure S8 and Equation S3 (Supporting Information).

The second set of experiments aimed to investigate the EQCM changes, as is listed below.

2.1) 3 cycles of CV at 50 mV s^{-1} from OCV and finished at OCV (system conditioning)
2.2) 20 cycles of CV at 5 mV s^{-1} in the wide potential range (second system)

Only systems with stable performance, where the recorded resistance change was less than ±2% were considered for further mass recalculation ($\Delta R = \pm 2\%$). The mass change study using the determined PZC value combines electrochemical data (controlled by a potentiostat, I-E curves) and the simultaneously recorded change in the resonator frequency (measured by the EQCM, Δf). The change in resonator frequency could be directly recalculated into the mass change with respect to Equation S1 (Supporting Information).

Faraday's law (Equation 1) was used to recalculate the CV data, allowing a comparison of experimental and theoretical mass changes in the mass:charge ratio plot. In this equation, ΔQ is charge exchanged [C], F is Faraday's constant [96 485 C mol^{-1}], M is the molar mass of adsorbed/desorbed ionic species [g mol^{-1}], and z is the number of exchanged electrons (i.e., the valance number of adsorbed/desorbed ions) [-]).

$$\Delta m = \frac{\Delta Q \cdot M}{F \cdot z} \tag{1}$$

In the Swagelok cell, the potential range of both electrodes working with 0.1 mol L^{-1} LiNO$_3$ was determined in the 2-electrode system using CV at 1 mV s^{-1} (5 cycles from OCV to 1.6 V; considering voltage range from EQCM study, Figure S6, Supporting Information). The next procedure involved 3 CV cycles at 1 mV s^{-1} in a predetermined potential window (−0.86–0.74 V vs. SCE) in a 3-electrode system. The experiments were completed using 1 SPECS cycle (controlled by chronoamperometry) with the same conditions as in EQCM. The same testing protocol, with a 1.6 V operating voltage window, was applied to the volume cell.

Supporting Information

Supporting Information is available from the Wiley Online Library or from the author.

Conflict of Interest

The authors declare no conflict of interest.

Author Contributions

S.S. and P.G. are co-first authors and contributed equally to the article. S.S. performed methodology, investigation and conceptualized the project, and wrote the original draft. P.G. performed methodology, investigation, and data curation, conceptualized and visualized the project, and wrote the original draft. A.P.-M. conceptualized, supervised, and visualized the project, performed methodology, and data curation, and wrote the original draft. J.M. acquired funds, supervised the project, and wrote, reviewed & edited the final manuscript. S.W.D. performed validation, supervised the project, and wrote, reviewed & edited the final manuscript. K.F. acquired funds, supervised the project, and wrote, reviewed & edited the final manuscript.

Data Availability Statement

The data that support the findings of this study are available from the corresponding author upon reasonable request.

[1] W.-Y. Tsai, P.-L. Taberna, P. Simon, *J. Am. Chem. Soc.* **2014**, *136*, 8722.

[2] A. González, E. Goikolea, J. A. Barrena, R. Mysyk, *Renew. Sustain. Energy Rev.* **2016**, *58*, 1189.

[3] P. Simon, Y. Gogotsi, *Nat. Mater.* **2020**, *19*, 1151.

[4] A.-C. Forse, J.-M. Griffin, C. Merlet, J. Carretero-Gonzales, A-R.-O. Raji, N.-M. Trease, C.-P. Grey, *Nat. Energy* **2017**, *2*, 16216.

[5] F. W. Richey, B. Dyatkin, Y. Gogotsi, Y. A. Elabd, *J. Am. Chem. Soc.* **2013**, *135*, 12818.

[6] A. Ghosh, Y. H. Lee, *ChemSusChem* **2012**, *5*, 480.

[7] H. Shao, Y.-C. Wu, Z. Lin, P.-L. Taberna, P. Simon, *Chem. Soc. Rev.* **2020**, *49*, 3005.

[8] A. Platek-Mielczarek, E. Frackowiak, K. Fic, *Energy Environ. Sci.* **2021**, *14*, 2381.

[9] L. Borchardt, M. Oschatz, S. Kaskel, *Mater. Horiz.* **2014**, *1*, 157.

[10] H. Jiang, P.-S. Lee, C. Li, *Energy Environ. Sci.* **2012**, *6*, 41.

[11] G. Wang, L. Zhang, J. Zhang, *Chem. Soc. Rev.* **2012**, *41*, 797.

[12] Y. Zhai, Y. Duo, D. Zhao, P.-F. Fulvio, R.-T. Mayes, S. Dai, *Adv. Mater.* **2011**, *23*, 4828.

[13] L. L. Zhang, X. S. Zhao, *Chem. Soc. Rev.* **2009**, *38*, 2520.

[14] E. Frackowiak, *Carbon* **2001**, *39*, 937.

[15] A. Barroso-Bogeat, M. Alexandre-Franco, C. Fernández-González, A. Macías-García, V. Gómez-Serrano, *Phys. Chem. Chem. Phys.* **2014**, *16*, 25161.

[16] K. Fic, A. Platek, J. Piwek, E. Frackowiak, *Mater. Today* **2018**, *21*, 437.

[17] A. G. Pandolfo, A. F. Hollenkamp, *J. Power Sources* **2006**, *157*, 11.

[18] J. W. Gittins, K. Ge, Ch. J. Balhatchet, P.-L. Taberna, P. Simon, A. C. Forse, *J. Am. Chem. Soc.* **2024**, *146*, 12473.

[19] L. Wang, M. Peng, J. Chen, T. Hu, K. Yuan, Y. Chen, *Adv. Mater.* **2022**, *34*, 2203744.

[20] L. Wang, M. Peng, J. Chen, X. Tang, L. Li, T. Hu, K. Yuan, Y. Chen, *ACS Nano* **2022**, *16*, 2877.

[21] A.-C. Forse, C. Merlet, J. M. Griffin, C. P. Grey, *J. Am. Chem. Soc.* **2016**, *138*, 5731.

[22] A.-C. Forse, J.-M. Griffin, C. Merlet, P. Bayley, H. Wang, P. Simon, C.-P. Grey, *J. Am. Chem. Soc.* **2015**, *137*, 7231.

[23] H. Wang, A. C. Forse, J. M. Griffin, N. M. Trease, L. Trognko, P. L. Taberna, P. Simon, C. P. Grey, *J. Amer. Chem. Soc.* **2013**, *135*, 18968.

[24] J.-M. Griffin, A.-C. Forse, H. Wang, N.-M. Trease, P.-L. Taberna, P. Simon, C.-P. Grey, *Faraday Discuss.* **2014**, *176*, 49.

[25] P. Galek, P. Bujewska, S. Donne, K. Fic, J. Menzel, *Electrochim. Acta* **2021**, *377*, 138115.

[26] Y. Wang, D. Rochefort, *Meet. Abstr.* **2020**, *MA2020-01*, 6.

[27] F. Béguin, V. Presser, A. Balducci, E. Frackowiak, *Adv. Mater. (Weinheim)* **2014**, *26*, 2283.

[28] J. Yan, E.-Ch. Ren, K. Maleski, Ch.-B. Hatter, B. Anasori, P. Urbanowski, A. Sarycheva, Y. Gogotsi, *Adv. Funct. Mater.* **2017**, *27*, 1701264.

[29] Y. Wang, Z. Shi, Y. Huang, Y. Ma, Ch. Wang, M. Chen, Y. Chen, *J. Phys. Chem. C* **2009**, *113*, 13103.

[30] M. He, K. Fic, P. Novák, E.-J. Berg, E. Frackowiak, *ECS Meeting Abstr.* **2016**, *MA2016-02*, 1018.

[31] K. Fic, A. Platek, J. Piwek, J. Menzel, A. Slesinski, P. Bujewska, P. Galek, F. Frackowiak, *Energy Storage Mater.* **2019**, *22*, 1.

[32] A. Slesinski, S. Sroka, K. Fic, E. Frackowiak, J. Menzel, *ACS Appl. Mater. Interfaces* **2022**, *14*, 37782.

[33] G. Lota, K. Fic, E. Frackowiak, *Electrochem. Commun.* **2011**, *13*, 38.

[34] J. Piwek, A. Platek, E. Frackowiak, K. Fic, *J. Power Sources* **2019**, *438*, 227029.

[35] J. Piwek, A. Platek-Mielczarek, E. Frackowiak, K. Fic, *J. Power Sources* **2021**, *506*, 230131.

[36] Y.-C. Wu, P.-L. Taberna, P. Simon, *Electrochem. Commun.* **2018**, *93*, 119.

[37] M. D. Levi, S. Sigalov, D. Aurbach, L. In Daikhin, *J. Phys. Chem. C* **2013**, *117*, 14876.

[38] M. D. Levi, N. Levy, S. Sigalov, G. Salitra, D. Aurbach, J. Maier, *J. Am. Chem. Soc.* **2010**, *132*, 13220.

[39] J. Ye, Y.-C. Wu, K. Xu, K. Ni, N. Shu, P.-L. Taberna, Y. Zhu, P. Simon, *J. Am. Chem. Soc.* **2019**, *141*, 16559.

[40] R. Yan, M. Antonietti, M. Oschatz, *Adv. Energy Mater.* **2018**, *8*, 1800026.

[41] A. Auer, X. Ding, A. S. Bandarenka, J. Kunze-Liebhäuser, *J. Phys. Chem. C.* **2021**, *125*, 5020.

[42] S. Sigalov, M. D. Levi, L. Daikhin, G. Salitra, D. Aurbach, *J. Solid State Electrochem.* **2013**, *18*, 1335.

[43] P. Li, J. Huang, Y. Hu, S. Chen, *J. Phys. Chem. C.* **2021**, *125*, 3972.

[44] P. Xu, A. D. von Rueden, R. Schimmenti, M. Mavrikakis, J. Suntivich, *Nat. Mater.* **2023**, *22*, 503.

[45] I.-T. Kim, M. Egashira, N. Yoshimoto, M. Morita, *Electrochim. Acta.* **2011**, *56*, 7319.

[46] Y.-C. Wu, J. Ye, G. Jiang, K. Ni, N. Shu, P.-L. Taberna, Y. Zhu, P. Simon, *Angew. Chem.* **2021**, *133*, 13800.

[47] M. Bahdanchyk, Z. T. Sarı, A. Vicenzo, *ECS Meeting Abstracts* **2021**, *MA2021-02*, 1937.

[48] N. Shpigel, M.-D. Levi, S. Sigalow, D. Aurbach, L. Daikhin, V. Presser, *J. Phys. Cond. Matter.* **2016**, *28*, 114001.

[49] M. H B. Kastening, J. Kremeskotter, *J. Electroanal. Chem.* **1994**, *374*, 159.

[50] J. M. Griffin, A.-C. Forse, W.-Y. Tsai, P.-L. Taberna, P. Simon, C.-P. Grey, *Nat. Mater.* **2015**, *14*, 812.

[51] R. P. Janek, W. R. Fawcett, A. Ulman, *J. Phys. Chem.. B.* **1997**, *101*, 8550.

[52] A. J. Gibson, S. W. Donne, *J. Power Sources* **2017**, *359*, 520.

[53] H. Yin, H. Shao, B. Daffos, P.-L. Taberna, P. Simon, *Electrochem. Commun.* **2022**, *137*, 107258.

[54] M. F. Dupont, S. W. Donne, *Electrochim. Acta.* **2015**, *167*, 268.

[55] K. Fic, M. Meller, J. Menzel, E. Frackowiak, *Electrochim. Acta* **2016**, *206*, 496.

[56] M. D. Levi, S. Sigalov, G. Salitra, D. Aurbach, J. Maier, *Chem. Phys. Chem* **2011**, *12*, 854.

[57] A. Platek, J. Piwek, K. Fic, E. Frackowiak, *Electrochim. Acta* **2019**, *311*, 211.

[58] E. Frackowiak, M. Meller, J. Menzel, D. Gastol, K. Fic, *Faraday Discuss.* **2014**, *172*, 179.

[59] P. Przygocki, Q. Abbas, F. Béguin, *Electrochim. Acta* **2018**, *269*, 640.

[60] B. Akinwolemiwa, C. Peng, G. Z. Chen, *J. Electrochem. Soc.* **2015**, *162*, A5054.

[61] C. Kikuchi, H. Kurane, T. Watanabe, M. Demura, T. Kikukawa, T. Tsukamoto, *Sci. Rep.* **2021**, *11*, 7908.

[62] Y. Marcus, *Chem. Rev.* **1988**, *88*, 1475.

[63] A. Platek-Mielczarek, C. Nita, C. Matei Ghimbeu, E. Frackowiak, K. Fic, *ACS Appl. Mater. Interfaces* **2021**, *13*, 2584.

[64] K. Fic, M. He, E. J. Berg, P. Novak, E. Frackowiak, *Carbon* **2017**, *120*, 281.

Supplementary information

for

Fundamentals and implication of PZC determination for activated carbons in aqueous electrolytes

Sylwia Slesinska[1*], Przemysław Galek[1*], Jakub Menzel[1], Scott W. Donne[2], Krzysztof Fic[1**], Anetta Płatek-Mielczarek[1,3,4**]

[1]Poznan University of Technology, Institute of Chemistry and Technical Electrochemistry, Berdychowo 4, 60965, Poland

[2]Discipline of Chemistry, University of Newcastle, Callaghan, NSW, 2308 Australia

[3]Laboratory for Multiphase Thermofluidics and Surface Nanoengineering, Department of Mechanical and Process Engineering, ETH Zurich, Sonneggstrasse 3, 8092, Zurich, Switzerland

[4]Unbound Potential GmbH, Bönirainstrasse 14, 8800, Thalwil, Switzerland

*Authors with the equal contribution in article

**Corresponding authors: aplatek@ethz.ch, krzysztof.fic@put.poznan.pl

ORCID:

Slesinska S.: 0000-0002-9242-5561

Galek P.: 0000-0001-9841-9616

Menzel J.: 0000-0002-0431-159X

Donne S.W.: 0000-0001-9389-7870

Płatek-Mielczarek A.: 0000-0001-6231-3908

Fic K.: 0000-0002-5870-7119

Contents

EQCM theoretical introduction

EQCM consists of a thin piezoelectric quartz crystal placed between two metal electrodes used to apply an alternating electric field across the crystal. This causes a vibrational motion of the crystal at its resonance frequency.[1,2] The Saurbrey equation (**Eq. S1**) can then be applied to convert the frequency changes (Δf; Hz) to the mass changes (Δm; g). In this equation, A is surface area of quartz crystal [m^2], ρ is density of quartz (2.648 g cm^{-3}), μ is shear modulus of quartz (2.947 10^{11} g cm^{-1} s^{-2}), Δf is change in frequency [Hz], and f_0 is fundamental resonance frequency of the crystal [Hz].

$$\Delta m = -\frac{\Delta f \cdot A \cdot \sqrt{\rho \cdot \mu}}{2f_o^2} \tag{S1}$$

At PZC, EDL forms spontaneously because of the natural potential difference between the electrodes and unequilibrated surface charge at the maximum entropy state of the interface. At this point, the highest disorder of the interfacial water is observed.[3,4]

Thus, to quantitatively correlate the mass changes of the adsorbed ions and solvent molecules in EQCM, PZC should be assigned in a correct manner. The determination of adsorbed species is based on a mathematical model that results from Faraday's law and the mass change/charge relationship. In the case of one-element deposition or dissolution processes on the planar metallic surfaces, the mass change can be easily correlated with ongoing electrochemical processes.

Because PZC corresponds to an electrostatic electrode-electrolyte interaction (EDL formation only), diffusion-limited processes such as redox reactions should be excluded altogether. This is why the popular approach based on the determination of PZC through measured minimum capacitance from CV (related to the semiconducting behaviour of highly porous disordered carbons)[5] or SPEIS, as demonstrated in many works,[4,6-11] seems confusing for that reason. Also, when PZC is established, it is not always done in the same system as EQCM measurements.[12] It can lead to a different starting point in data evaluation, which can further cause an unrationed process description. Such a divergence can also result from cell construction limitations: size, distance between and type of electrodes, volume of electrolyte, and spatial organisation – what will be discussed within this manuscript.

AC characterization
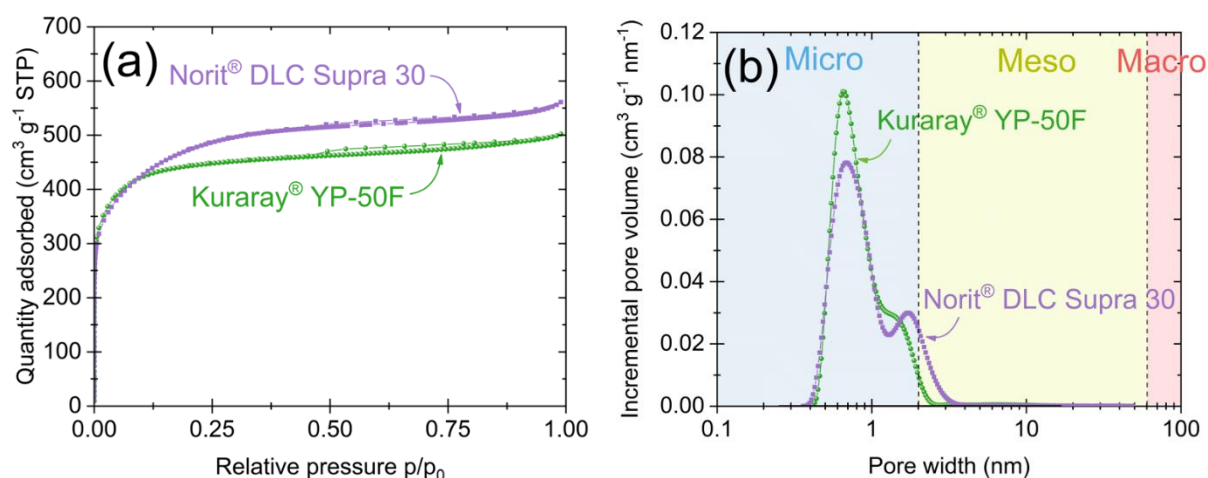
Fig. S1. Nitrogen adsorption at 77 K (**a**) isotherms and (**b**) pore size distributions of powder AC YP-50F and DLC30.

The textural properties of the YP-50F and DLC30 ACs are presented in **Fig. S1 and Tab. S1**. Nitrogen adsorption/desorption isotherm was recorded at 77 K (ASAP 2460; Micrometrics®, USA) to evaluate the porous texture. Prior to analysis, ACs were purged under helium flow for 12 h at 350°C and then placed under high vacuum for 5 h. The Brunauer–Emmett–Teller (SSA) equation was used to calculate the surface area at relative pressure range (0.01 – 0.05). Two-Dimensional Non-Local Density Functional Theory (2D-NLDFT) was applied to determine micro and mesopore volume values. The average pore diameter was obtained from the maximum peak value.

Tab. S1. Textural properties of AC YP-50F and DLC30 from nitrogen sorption/desorption tests at 77 K

	SSA, $m^2\ g^{-1}$	V_{micro}, $cm^3\ g^{-1}$	V_{meso}, $cm^3\ g^{-1}$
YP-50F	1702	0.64	0.08
DLC30	1780	0.66	0.25
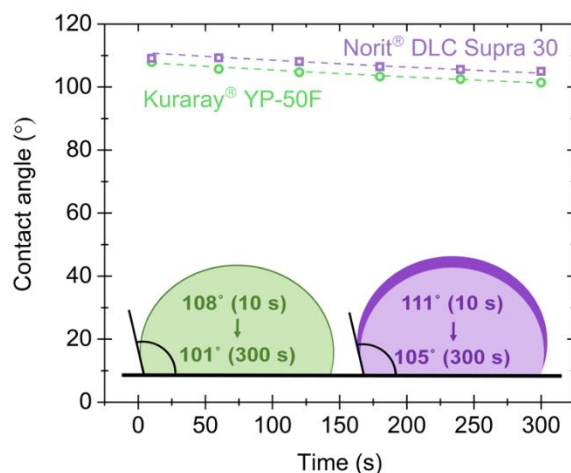
Fig. S2. Comparison of changes in dynamic contact angle during 300 s for H_2O on YP-50F and DLC30 based electrodes.

The contact angle measurements were performed with a computer-controlled goniometer (Dataphysics® OCA). The carbon samples in the form of coatings on steel foil (diameter 2 x 1 cm) were placed horizontally in front of the contact angle camera. The 2 μL volume drops of H_2O were injected with speed injection 0.5 μL s^{-1} on the surface of the electrode material.

Tab. S2. Elemental composition tested by elemental analysis for ACs: YP-50F and DLC30.

Activated carbon	C (%)	H (%)	N (%)	S (%)	O (%)	Total (%)
Kuraray® YP-50F	96.1	0.8	0	0	2.1	98
Norit® DLC Supra 30	95.2	0.5	0	0	2.2	98

Based on elemental analysis (EA) data, one can see that YP-50F and DLC30 carbons are almost identical in terms of elemental composition as presented in **Tab. S2.** They are equally oxidized in bulk (~2%). To test the wettability of both carbons, contact angle measurements with H_2O were performed, as described in **Fig. S2.** The results confirm that both carbons display hydrophobic characteristics with almost identical wettability $\Delta\theta = $ ~3°. That would explain why: DLC30 and YP-50F exhibit a similar PZC region in contact with the same aqueous liquid electrolyte; however, the value of specific capacitance can be correlated with their textural properties, and not with their surface chemistry. (**Fig. S1**).

Porous electrode coatings

The resonator preparation procedure is presented in **Fig. S3**.
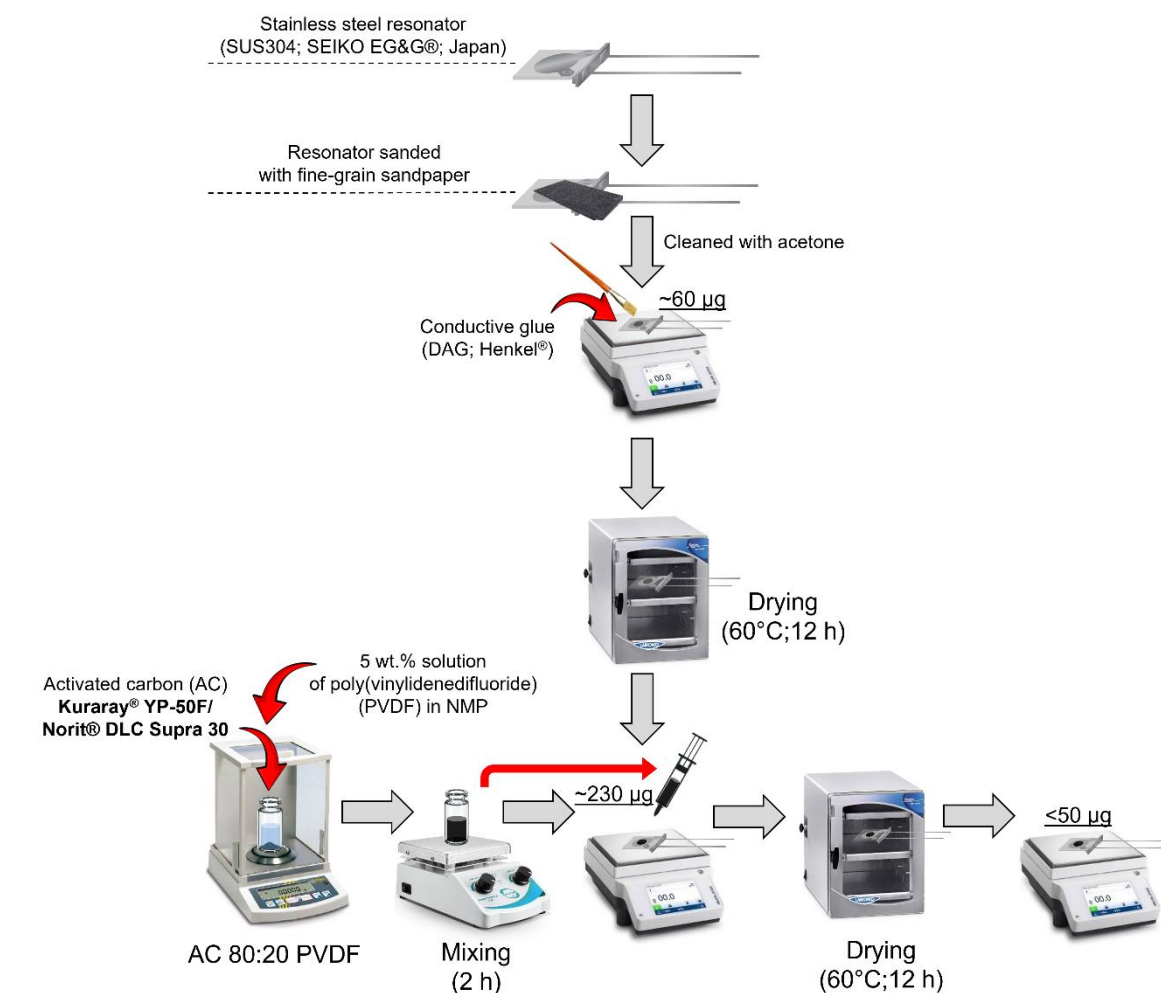
Fig. S3. The scheme of the coating preparation on the resonator surface.

SEM micrographs of prepared resonators are presented in **Fig. S4**.
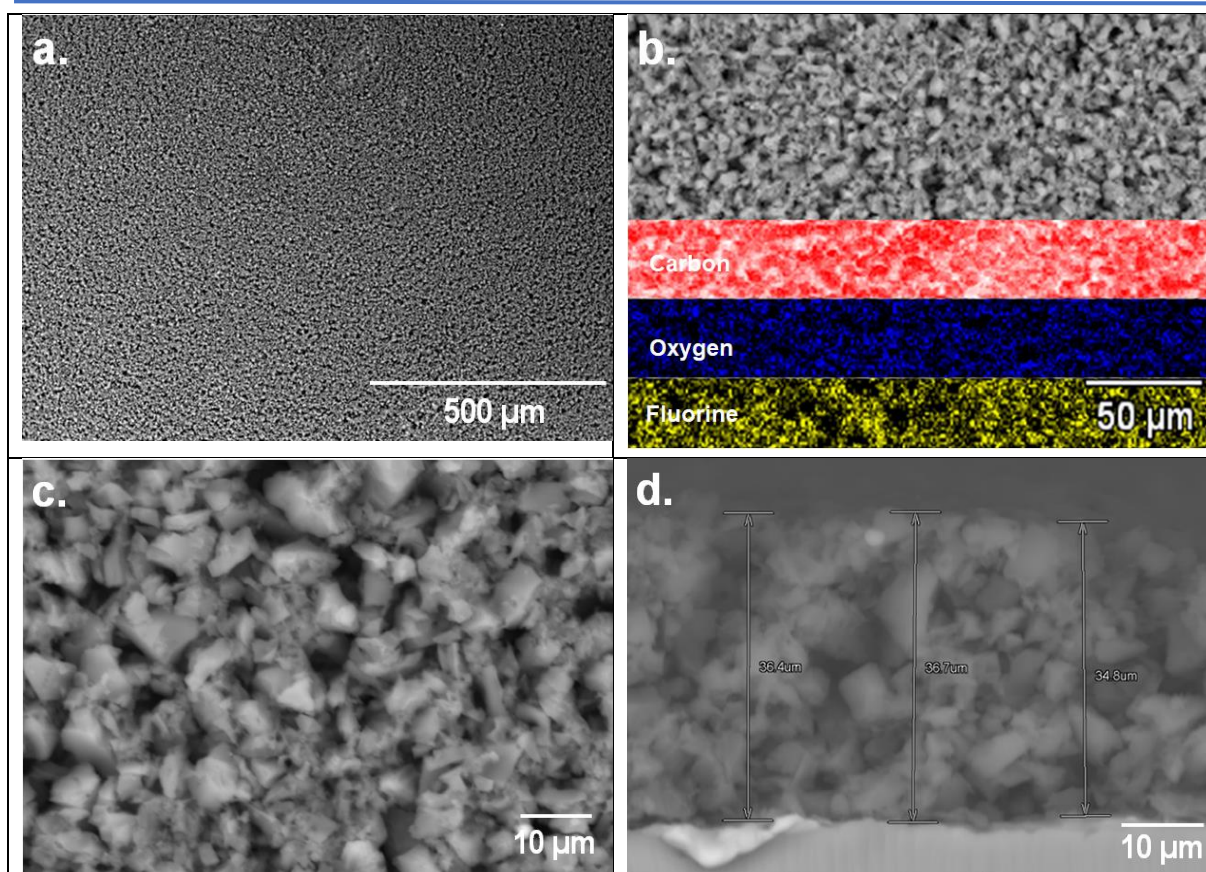
Fig. S4. SEM micrographs from top view a)-c) and cross-sectional d) for YP-50F coated resonator; b) EDX mapping of C, O, F chemical elements.

Resonators are homogenous and uniform (thickness ca ~35 µm). Carbon particles retain their shape and size comparing to the pristine one. Composition of YP-50F coating on resistor is presented in **Tab. S3** below:

Tab. S3. Weight % Elemental composition of the coating from the EDX analysis

C (%)	O (%)	F (%)	Total (%)
81.9	6.5	11.6	100

Electrolyte characterization

Tab. S4. Conductivity and pH of tested electrolytes with a concentration of 0.1 mol L^{-1}.

Solvent	Salt	Conductivity (mS cm^{-1})	pH
H_2O	$LiNO_3$	9.2	6.8
	Li_2SO_4	14.6	7.4
	KI	13.2	7.8
D_2O	$LiNO_3$	5.8	8.8

All studied electrolytes can be classified as aqueous neutral solutions (pH in the range of 6-8). This implies, that balance between alkaline and acidic ionic species is preserved. Low concentration solutions were selected based on EQCM sensitivity – therefore, conductivity values of such solutions are rather low. pH and conductivity were measured using Seven InLab Mettler Toledo® (USA) with appropriate sensor for aqueous solutions.

EQCM system
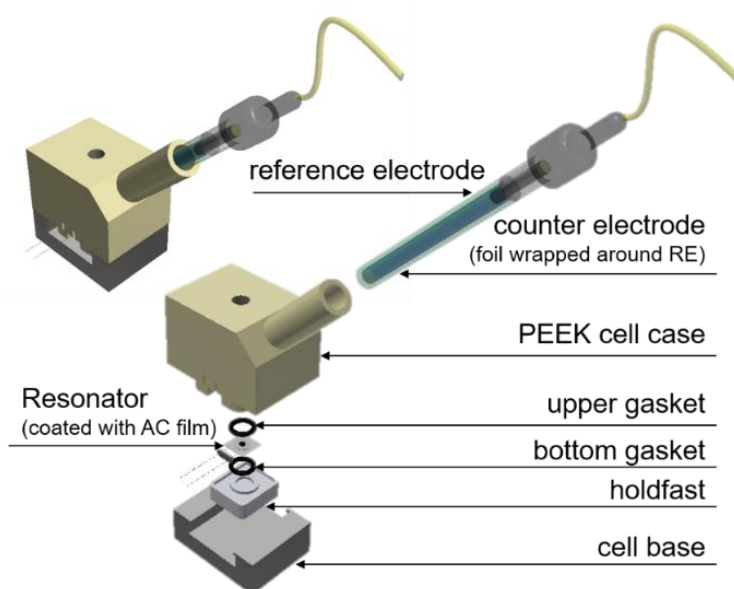
Fig. S5. EQCM cell scheme.

Wide potential range screening in EQCM system
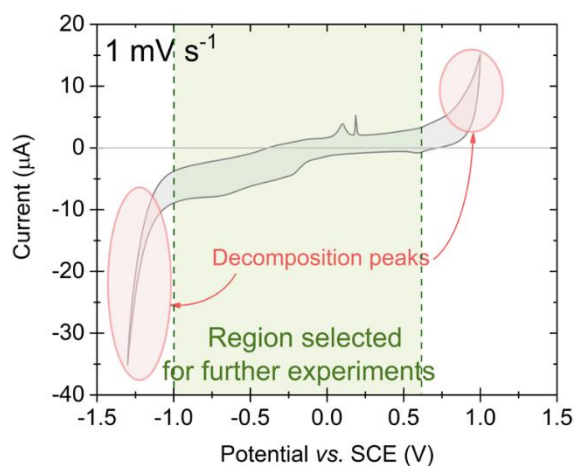
Fig. S6. Cyclic voltammogram for YP-50F and 0.1 mol L^{-1} LiNO$_3$ in EQCM system at 1 mV s^{-1}.

Discussion

CV technique for PZC determination

The CV technique allows to calculate the capacitance per electrode $C_{CV(v)}$ (according to the equation **Eq. S2**, where: I – current [A], v – scan rate [mV s^{-1}]).

$$C_{CV} = \frac{2 \cdot I}{v} \tag{S2}$$

For aqueous based electrolytes, especially with redox-active species present, one must thus consider applicable scan rate. **Fig. S7** presents cyclic voltammograms for the same system recorded using different scan rates, i.e., 1, 5, and 50 mV s^{-1}.
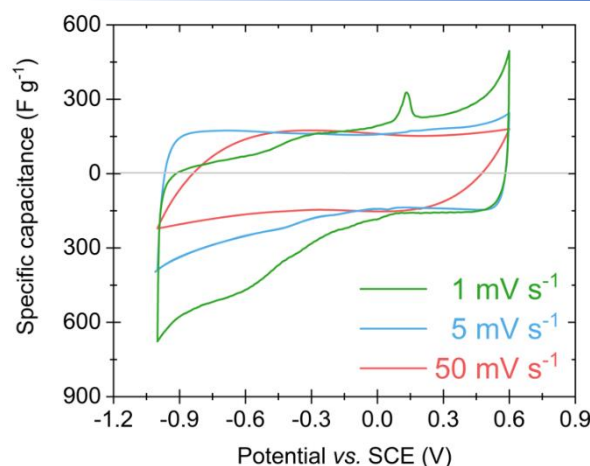
Fig. S7. Specific capacitance *vs.* potential based on cyclic voltammetry for 0.1 mol L^{-1} LiNO$_3$ and YP-50F at 1, 5, and 50 mV s^{-1} in the EQCM cell.

The CV profile recorded at slow scan rate (1 mV s^{-1}) represented the most detailed characterisation of the charging/discharging profile. The moderate scan rate, such as 5 mV s^{-1}, effectively depicts pure EDL behaviour – covering all current increase points, where certain redox/side reactions can occur. This is a satisfactory scan rate to characterise the performance of a device, considering that EC is supposed to operate at high power/current loads. The fast scan rate, like 50 mV s^{-1}, is, however, too fast to allow any ion flux to easily form EDL at the highly developed electrode surface area (**Fig. S1**) in aqueous solutions with moderate conductivity values (i.e., low concentrations). Thus, we begin to observe resistance components and delayed charge transfer at the electrode/electrolyte interface. One cannot withdraw any information on the charge storage mechanism while using fast scan rates. However, such a change in voltage/potential brings about other useful information – not considered for PZC determination. Therefore, for fundamental studies of aqueous electrolytes that focus on a molecular-level interaction between ionic species and electrode surface, slow scan rates (like 1 mV s^{-1}) and will be used in this study.

SPEIS technique for PZC determination

The SPEIS technique allows to calculate the capacitance $C_{SPEIS(f)}$ (according to the equation **Eq. S2,** where: f – frequency [Hz], $-Im(Z)$ – imaginary Z value [ohm]) (example given in **Fig. S8a**).

$$C_{SPEIS(f)} = \frac{1}{\pi \cdot f \cdot -Im(Z)} \tag{S3}$$

According to the given equation, $C_{SPEIS(f)}$ is variable and strongly depends on the chosen frequency value. Therefore, in addition to Nyquist plot (**Fig. S8a**), specific capacitance *vs.* frequency is generally reported for electrochemical capacitors (**Fig. S8b**).[13,14]
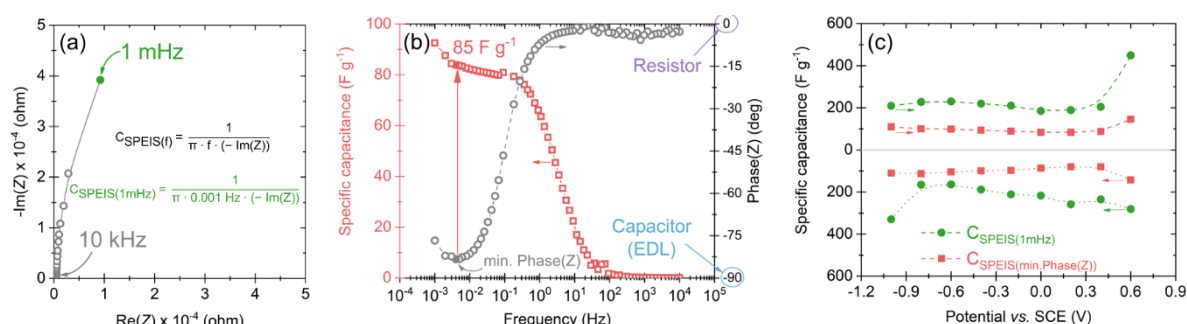
Fig. S8. Impedance study at 0 V *vs.* SCE for 0.1 mol L^{-1} LiNO$_3$ and YP-50F: (**a**) Nyquist and (**b**) Bode plot (**c**) Comparison of capacitance calculated for 1 mHz (green circles) and determined based on minimum *Phase(Z)* value (red squares).

Therefore, the selection of an adequate frequency for the specific capacitance calculation is crucial to obtain a representative curve that allows the determination of PZC. It should be remembered that choosing a specific frequency range does not necessarily result in an inflection (which corresponds to PZC) on the $C_{SPEIS(f)}$ curve on $C_{SPEIS(f)}$ *vs.* potential plot (see $C_{SPEIS(1mHz)}$ presented in **Fig. S8c**). Thus, with this technique, it is possible (with significant error) to determine the PZC – but only for some experimental conditions. For example,

finishing the experiment at a high frequency will only correspond to the data recording related to the system resistance (R) (resistive response with *Phase(Z) = 0°*), which would not allow for the full development of the EDL (capacitor response with *Phase(Z) = ˜ -90°*) (**Fig. S8b**). If, on the other hand, $C_{SPEIS(f)}$ is calculated on the basis of the low frequency, then apart from pure C_{EDL}, *the* capacitance related to side reactions is registered. It particularly concerns measurements in the extreme potentials, where the response resulting from electrolyte decomposition will be additionally registered. Faradaic charging becomes more predominant at low frequencies, whereas one must remember that the operating frequency cannot be excessively low for capacitive charging. The optimal frequency for capacitive charging is strongly dependent on electrode geometry and electrolyte conductivity.[15] Changing the direction of polarisation ($E_{max} \rightarrow E_{min}$) results in different $C_{SPEIS(1mHz)}$ than those calculated under $E_{min} \rightarrow E_{max}$ polarisation (**Fig. S8c**). The C_{EDL} response should be symmetric about the Y axis for capacitive systems. Surprisingly, upward capacitance, differences in values, and divergence in the capacitance trend in both polarisation directions are observed, probably because of irreversible oxidation processes that occur at the electrode/electrolyte interface at relatively high potentials (close to the oxygen evolution reaction – OER). Nevertheless, there is also another possibility to indicate PZC from SPEIS more accurately. C_{EDL} can be read from the Bode plot ($C_{SPEIS(min.Phase(Z))}$; **Fig. S8b**). As already mentioned, *Phase(Z)* = -90° and 0° correspond to an ideal capacitor and resistor response, respectively.[16,17] Under real conditions, the pure C_{EDL} can be read from the closest point to *Phase(Z)* = -90° (inflection point). By this method, it is possible to accurately determine C_{EDL} recorded for the minimum *Phase(Z)* value, but not without any problems. Firstly, it is necessary to prepare preliminary experiments (a trial setup), for which the frequency range will be selected with an inflection of *Phase(Z)* close to - 90°. A standard frequency range of 100 or 10 kHz to 1 mHz may not result in the Bode plot bending near *phase (Z)* = -90°. Furthermore, one needs to increase the number of points collected (by decreasing $\triangle E$) in the tested potential range to obtain representative results with a clear minimum C_{EDL} on the C_{EDL} *vs.* potential plot. Furthermore, the greater the accuracy of data collection (at a given potential step), the longer the total time of SPEIS experiment (for each potential step it can

last from a few minutes up to a few hours). For example, for the aqueous based systems presented in this study, single impedance (at given potential) was recorded for 34 min. Such a long holding time of a given potential step (especially in the extreme potentials) in the EQCM system, results in the electrolyte decomposition and its evaporation. At the same time, $\triangle E = 0.2$ V chosen here, for each PEIS measurement, leads to an incomplete spectrum in the investigated potential range; however, this is a compromise between the overall experimental time and the number of collected points. Another disadvantage of the step potential shift is the abrupt occurrence of potentially occurring reactions (e.g., redox) and the lack of time for the ion reorganisation participating in EDL formation. The gradual change of the potential has a better effect on the stabilised reorganisation of the charge on the surface of the electrode material. Such charging procedure differs from those in commercial systems, where the charging process is constant. However, apart from those disadvantages, it seems that the PZC value is more realistic when considering the minimum capacitance based on the minimum of Phase(Z) instead of the lowest frequency value. More observations have been discussed for $C_{SPEIS(min.Phase(Z))}$ and $C_{SPEIS(1mHz)}$ for different types of electrolytes in the subsequent part of the article.

SPECS technique for PZC determination

SPECS technique allows to separate the total system capacitance (C_T) calculated at a given potential step into individual capacitances corresponding to: EDL capacitance component $C_{EDL} = C_P + C_G$ (pure capacitor response) part of the porous (C_P) and geometrical (C_G) area of the electrode. Moreover, it is possible to separate capacitance resulting from ion diffusion (C_D) and residual capacitance (C_R) mainly related to redox and side reactions (e.g., electrolyte decomposition). In summary, C_T can be described as $C_T = C_P + C_G + C_D + C_R$. By dividing the area of individual current curves I_P, I_G, I_D, I_R [$\int A_t$, A s] registered at each potential step by $\triangle E$ and the mass of the electrode active material, it is possible to obtain individual values for the specific capacitance.[18] A detailed description of this technique can be found in the article presented by M. Dupont and S. Donne.

The specific capacitance of the individual components (C_T, C_P, C_G, C_D, C_R) obtained by the SPECS technique was calculated according to equation below.

$$C = \frac{A}{M \cdot \Delta E} \qquad\qquad \text{(S4)}$$

where:
C	– specific capacitance of given component		[F g^{-1}]
A	– surface area under given calculated current curve		[A s]
M	– mass of active mass		[g]
ΔE	– potential step (0.01 V)		[V]

Minimal specific capacitance variations

Tab. S5 PZC region for Li$_2$SO$_4$ depending on the concentration and minimal specific capacitance variations.

		E$_{min}$ *vs.* SCE, V	E$_{max}$ *vs.* SCE, V	ΔE, mV
±1%	0.1 mol L^{-1}	-0.02	+0.01	30
	1 mol L^{-1}	+0.05	+0.23	180
±2%	0.1 mol L^{-1}	-0.04	+0.05	90
	1 mol L^{-1}	+0.01	+0.32	310

In **Tab. S5** two different concentrations are compared 0.1 and 1 mol L^{-1} for Li$_2$SO$_4$ and in addition, two specific capacitance ranges for minimal value, ±1 or ±2%. One can observe that the higher the specific capacitance deviations, the wider the RZC. We opt that ±1% is not a sufficient range to consider for porous AC electrodes, especially for samples with quinone/hydroquinone redox pair activity. What is important to note is that the higher the electrolyte concentration, the wider the RZC. It is related to the number of charges accumulated at the electrode/electrolyte interface and in effect, wider potential zone of ion permselectivity failure of porous electrode. We assume that more porous electrode material could lead to the extension of RZC for specific concentration of aqueous solutions. Higher

aqueous solution concentration causes slight shift of RZC towards more positive potential values, what is caused by a higher quinone/hydroquinone redox peak activity at ca. 0.15 V *vs*. SCE in Li_2SO_4.

Considering all above-mentioned observations, we do postulate that capacitance variation ±2%, which corresponds to ˜1 F g^{-1} difference, is a reasonable potential range for a porous electrode material. Knowing experimental conditions and mathematical calculations, bigger accuracy of specific capacitance values is meaningless. Surface functionality redox reactions are very sensitive to aqueous environment, thus, selection of PZC instead of RZC can be fraught with more error and difficulty, which proves non-universality of this property for porous carbon materials. Additionally, porous electrode materials owing to their developed textural properties should be combined with diluted aqueous solutions to preserve required experimental conditions for Saurbrey equation application (ΔR < 2%) which can be observed in the literature data presented in **Fig. 3** (diluted solutions are mostly discussed).
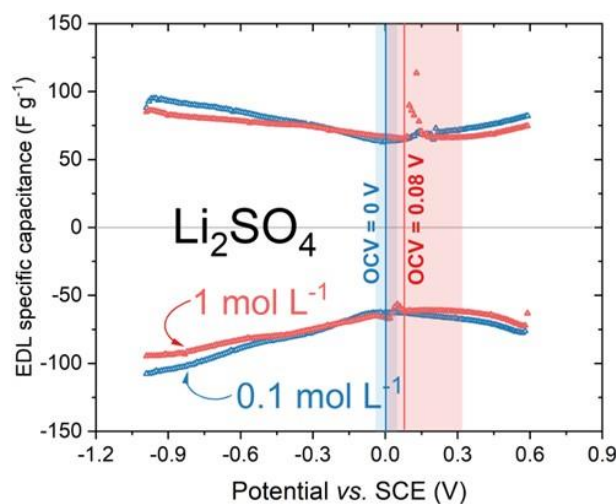
Fig. S9. PZC determination from specific capacitance vs. potential for Li_2SO_4 in two concentrations: 0.1 and 1 mol L^{-1}.

Tab. S6. Ionic radius and RZC for anions in electrolytes used in this research and RZC (taking into account minimum capacitance value ±2%).

Electrolyte	Anion	Ionic radius[12, 13]	RZC
0.1 M Li_2SO_4	SO_4^{2-}	0.242 nm	90 mV
1 M Li_2SO_4	SO_4^{2-}	0.242 nm	310 mV

Influence of the applied potential range on the position of PZC
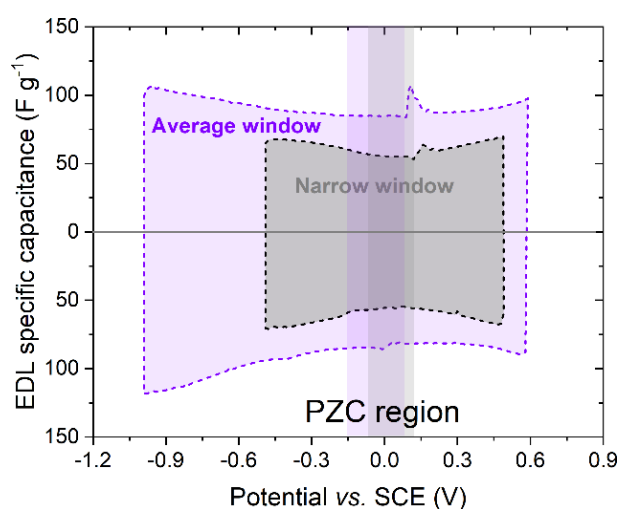
Fig S10. Influence of the applied potential range on the position of PZC in the 0.1 mol L^{-1} $LiNO_3$ electrolyte in the EQCM system.

Tab. S7. RZC for $LiNO_3$ studied in a narrow ($\Delta E = 1$ V) and a wide ($\Delta E = 1.6$ V) potential window.

	E_{min} *vs.* SCE, V	E_{max} *vs.* SCE, V	ΔE, mV
$\Delta E = 1.0$ V	-0.07	+0.12	190
$\Delta E = 1.6$ V	-0.15	+0.09	240

Cell construction for PZC determination

It is also vital to highlight the influence of the cell itself on the determination of PZC. We have demonstrated that if PZC is obtained in any other setup, i.e., such as Swagelok cell or volume cell, it will differ greatly from PZC in the EQCM cell (**Fig. S11**).
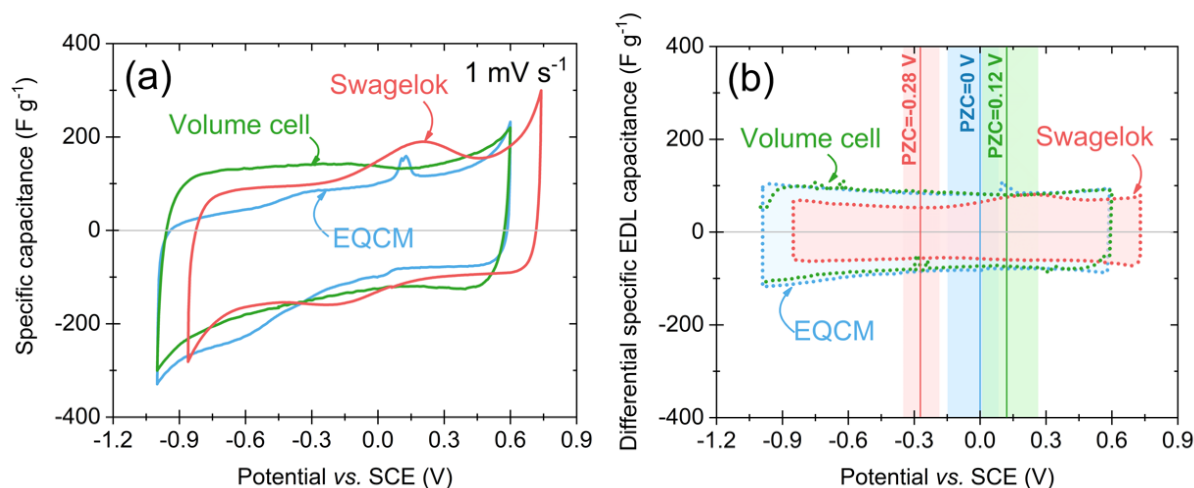
Fig. S11. Comparison for Swagelok (red line), EQCM (blue line), and volume cell (green line) (0.1 mol L^{-1} LiNO$_3$ electrolyte and YP-50F) of (**a**) specific capacitance *vs.* potential – CV experiment at 1 mV s^{-1} and (**b**) PZC and PZC region from SPECS experiment.

Electrochemical stability for the EQCM and the Swagelok cell differs by ca. 200 mV. This potential shift can be minimised using a similar component ratio as in the EQCM cell represented in the volume cell (WE to CE geometrical surface ratio, excess of electrolyte, CE electrode type). **Fig. S11a** presents the specific capacitance calculated from the cyclic voltammetry data for a scan rate of 1 mV s^{-1} in predetermined potential windows in the given systems. Measurements were made by repolarisation of one electrode in the wide potential range. CV plots for volume cell and EQCM overlap their potential range; however, the EQCM curve represents the highest extent of details (redox contribution). **Fig. S11b** presents the differential specific EDL capacitance ($C_{SPECS(EDL)} = C_P + C_G$) calculated based on the SPECS technique and is presented in the same graphical representation as in **Fig. S11a**. The Swagelok and EQCM/volume systems are incomparable because of the mutual shift of the electrochemical stability range, and consequently, the PZC. The ohmic drop associated with the varied distance between RE and WE was initially taken as the cause of the potential shift in Swagelok (**Fig. S12**). However, this does not seem to be an issue.
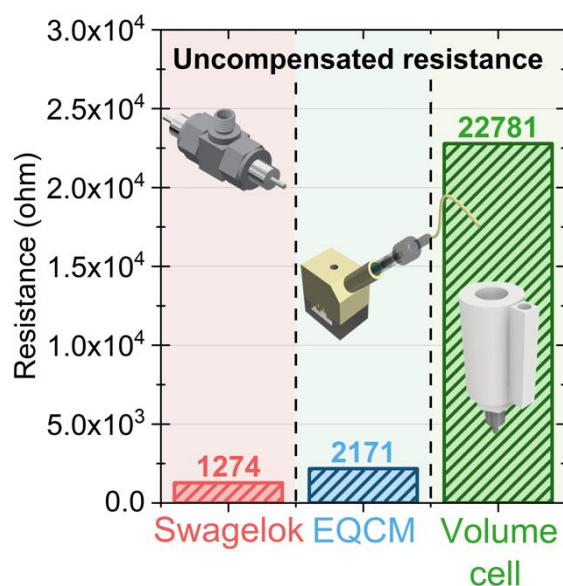
Fig. S12. Comparison of uncompensated (R_u) resistance between working and reference electrode for Swagelok, EQCM, and volume cell.

Measurement of uncompensated (R_u) resistances was conducted in 2-electrode configuration (in Swagelok, EQCM, and 'in-house made' volume cell) between working and reference electrode using current interrupt (CI) technique. Applied current density was 0.1 A g^{-1} with 80% compensation on R_u, where average values were determined on three cycles. R_u has values: 1274 ohm – Swagelok, 2171 ohm - EQCM and 22781 ohm – volume cell. It shows that the less confine system (large WE and CE distance, excess of electrolyte etc.) leads to higher uncompensated resistance value related with system design.

Although the volume cell has a much higher (several times) uncompensated resistance (R_u) value than the EQCM cell, the operating potential range of both systems is identical. For EQCM and Swagelok, the difference between $R_{u\text{-}EQCM}$ and $R_{u\text{-}Swagelok}$ is less than two times, yet there is a big difference in the electrochemical stability of both systems. It is well known that the potential range is dependent on the pH of the electrolyte. Therefore, the possible effect of pH changes resulting from migration of Cl$^-$ ions from SCE to Swagelok was considered and verified. However, this possibility was debunked (**Fig. S13**). In tight systems (without excess of electrolyte), such as Swagelok, the pH can change directly after immersion of the electrode in the electrolyte (without polarisation). This can acidify the

medium at the vicinity of the electrodes and is thus the only explanation for the observed shift. For systems with high CE/WE ratio and an excess of the electrolyte such as EQCM and volume cell, this phenomenon is limited. The pH adjustment in such systems is much more efficient because of the facilitated diffusion.

The difference in the value of PZC between Swagelok and other systems (EQCM and volume cell) with 0.1 mol L^{-1} $LiNO_3$ and YP-50F is significant (ΔE = 0.28 V) and can lead to misinterpretation of the data. The potential range for the EQCM (blue line) and volume cell (green line) is identical, which stems from a similar design in both systems (large electrolyte excess and asymmetry between WE/RE). In both cells, the PZC is shifted towards E_{max} and divided the entire potential window (1.6 V) into given potential ranges $\Delta E(+)$ = 0.6 V and $\Delta E(-)$ = 1 V in EQCM and $\Delta E(+)$ = 0.48 V and $\Delta E(-)$ = 1.12 V in volume cell. In the Swagelok cell, PZC is shifted towards E_{min} and the individual ranges are $\Delta E(+)$ = 1.02 V, and $\Delta E(-)$ = 0.58 V. Therefore, one can see that even for the capacitive symmetric system (Swagelok cell), the potentials are not divided equally for positive (WE) and negative (CE) electrodes. The construction of the system (size, volume, pressing, etc.) influences the operating potentials of the electrodes. The ohmic drop is a value that can explain this difference. The Ohmic drop is the amount of potential that is lost on the way from the reference electrode to the working electrode and results from the Ohmic resistance between the working electrode and the reference electrode – denoted as R_u. The distance between the electrodes and the conductivity of the solution can thus largely influence its value.

In addition, this non-uniform potential difference between two symmetrical electrodes informs about varied dominant processes during EC charging. Especially on the microscale at the electrode/electrolyte interface, where the equilibrium state cannot be taken for granted for the same system composition (YP-50F + 0.1 mol L^{-1} $LiNO_3$) but varies accordingly with the system construction and size. Similarly to the EQCM system, redox in Swagelok induces an increase in the EDL capacitance but in a much wider range of potential. What was noted was that the redox response is not visible in a volume system at

all as the probability of the gaseous side products to evolve is higher than their interaction within confined electrode porosity.

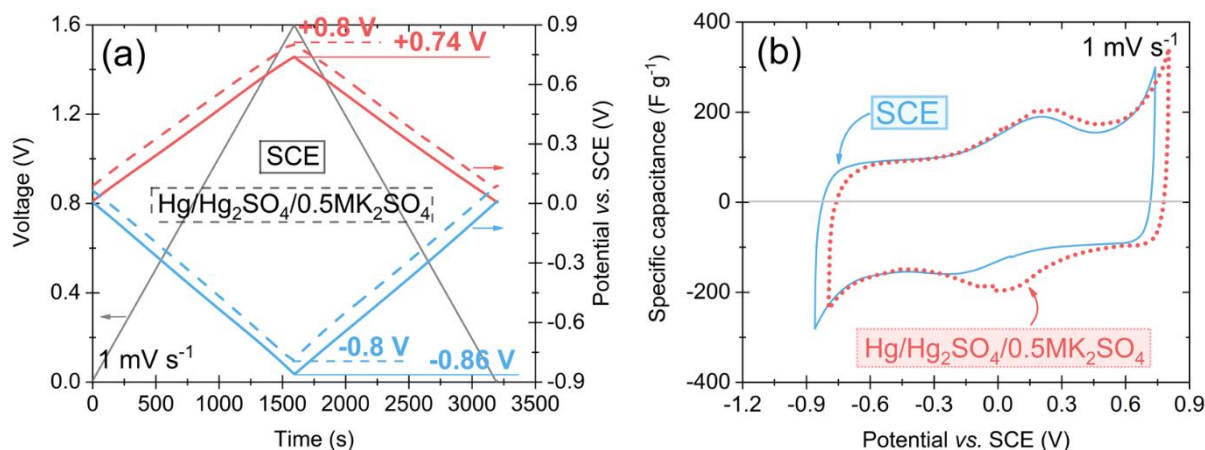**Reference influence on the electrochemical operation**

Fig. S13. (**a**) Difference in potential shift (for 1.6 V) in 3-electrod and (**b**) 2-electrode configuration using SCE and $Hg/Hg_2SO_4/0.5$ mol L^{-1} K_2SO_4 as a RE in 0.1 mol L^{-1} $LiNO_3$-based Swagelok system with YP-50F.

Comparison in **Fig. S13a** presents the shift in the potential of positive (red lines) and negative (blue lines) electrode for the Swagelok system with 0.1 mol L^{-1} $LiNO_3$, when SCE (solid line) or $Hg/Hg_2SO_4/0.5$ mol L^{-1} K_2SO_4 (dashed line) was used as the RE. The potential range was determined using CV with a scan rate 1 mV s^{-1} to 1.6 V (black line). **Fig. S13b** shows specific capacitance (calculated based on CV) for previously mentioned systems and previously determined potential ranges (with the repolarisation of one electrode).

The suspicion of a potential shift in the Swagelok relative to potentials of other systems (EQCM and volume cell) was the possible migration of Cl^- ions (as a result of a concentration gradient) from RE into the tested system. This migration of ions could induce a change in the electrolyte pH, and consequently, would lead to a change in the potential range of both electrodes. To eliminate this possibility, the SCE electrode was replaced with $Hg/Hg_2SO_4/0.5$

mol L^{-1} K_2SO_4. Salt bridge was used to avoid possible ion migration between the reference electrode and the electrolyte bulk.

The change of RE does not shift potential range towards negative values (comparable to EQCM and volume cell). It can be concluded that the type of RE does not affect such a significant shift of the potential observed in **Fig. S13** in Swagelok in comparison to the potential range of the rest systems. The use of $Hg/Hg_2SO_4/0.5$ mol L^{-1} K_2SO_4 shifts the potential even more towards positive values. The difference between the systems (with RE $Hg/Hg_2SO_4/0.5$ mol L^{-1} K_2SO_4 *vs.* SCE) is 60 mV. In this case, the potential shift in Swagelok in comparison to EQCM or volume cell results from the design of the cell, not from the pH changes caused from migration of ions from RE (even though Swagelok contains the lowest ratio of electrolyte volume to electrode mass). The close contact of both electrodes, their similar size and mass, and the much smaller volume of electrolyte than in EQCM/volume cell affect the susceptibility of the Swagelok to local pH changes, thus potential shift.

PZC determination for planar resonator and AC coatings

Another interesting aspect seems to be the determination of the PZC for the EQCM system with a resonator not covered with the carbon material (**Fig. S14**). It is challenging to determine PZC for D_2O, H_2O and 0.1 mol L^{-1} $LiNO_3$ based system with a planar resonator. For D_2O, a very wide range (~0.8 V) of minimum capacitance can be observed; for which it is impossible to determine one PZC value. However, for systems with H_2O and 0.1 mol L^{-1} $LiNO_3$, two local minima of the capacitance were registered. Most likely, a minimum close to 0 V *vs.* SCE is a region of the PZC, but it cannot be stated with certainty. These tests show that PZC is a unique property of the electrode material with a developed texture and a broad surface chemistry in contact with the liquid electrolyte.
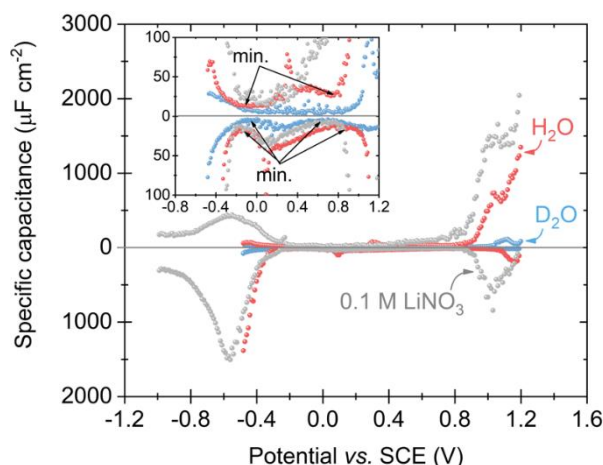
Fig. S14. Specific capacitance *vs.* potential for EQCM system with steel resonator (planar) and D_2O, H_2O, and 0.1 mol L^{-1} $LiNO_3$ as electrolyte.

In the second part of the study, the influence of AC used as electrode material was compared in the PZC region (in the EQCM system with D_2O as electrolyte) was compared (**Fig. S14**). The location and width of the PZC region (0.02 – 0.9 V *vs.* SCE) are identical, despite the different structural and textural characteristics of both materials. However, there is a difference in capacitance obtained with the SPECS technique; DLC30 based system has higher capacitance compared to YP-50F (**Fig. S15**). Interestingly, the biggest difference in capacitance is observed in the PZC region, while it decreases as extreme potentials are reached. This behaviour is due to the difference in the availability of the porous structure of both materials for any charges coming from the electrolyte. In the PZC region, the driving force (potential value) for ion adsorption is low. The surface, which is readily available for the electrolyte (including mesopores), is mostly charged with ions. The amount of charge adsorbed by DCL30 is greater due to the wider pore distribution range than YP-50F (**Fig. S1b**). In the E_{max} and E_{min} regions, the driving force of ion adsorption is large enough to draw the ions into the microporosity structure. The capacitance is equal in these regions for both materials. This proves that the same amount of charge is adsorbed in the microporous structure for both tested materials.
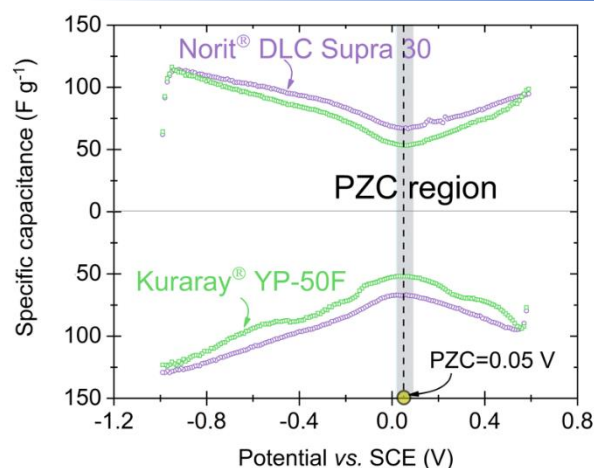
Fig. S15. Comparison of PZC region for EQCM system with YP-50F and DLC30 as electrode material (with D_2O as electrolyte).

EQCM system verification – comparison to literature data

First, in order to verify the operation of the EQCM system, redox electrolytes have been tested, namely: 0.1 mol L^{-1} KI and 0.1 mol L^{-1} RbI [8] – presented in **Fig. S16**. Cyclic voltammograms present typical iodide/iodine redox activity in the positive potential values. The system with KI electrolyte was tested in a narrower voltage window to resemble experimental conditions as for other capacitive electrolytic solutions tested (LiNO$_3$ and Li$_2$SO$_4$). 0.1 mol L^{-1} RbI is not a main electrolyte studied here, it was used for comparison and validation purpose, i.e., feasibility test to the reported literature data. [8] The mass change calculated for these two redox-based systems shows similar hysteresis loops in the range of the redox activity potential. Hysteresis loop, especially while ending at the higher mass change, informs about species trapped in the electrode pores. As gas formation in the I_2 form is assumed for such a concentration (0.1 mol L^{-1} MI, M = K^+, Rb^+), these small gas bubbles can be trapped in the narrow pores and the number of active species at the electrode/electrolyte interface will decrease with time. Moreover, the iodate-based precipitation can be observed over a limited lifetime of iodide-based EC.[19] The curves presented (specific capacitance and *m* as a function of potential) show that electrode coatings prepared on EQCM quartz crystal resonators work in a stable manner and can be further used for PZC discussion ($\Delta R_{RbI} = \Delta R_{KI} = \pm 1\%$).
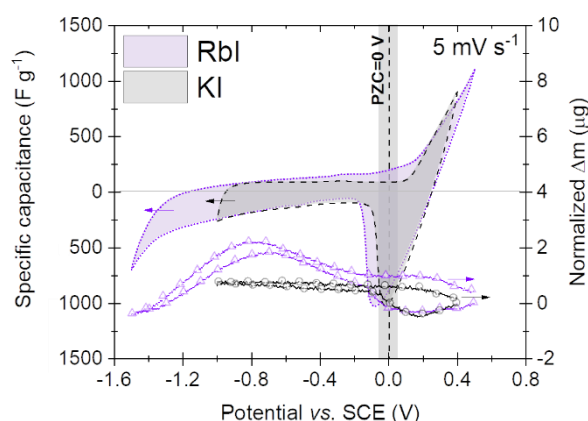
Fig. S16. Cyclic voltammetry 5 mV s^{-1} with normalized mass change for EQCM system with 0.1 mol L^{-1} electrolyte: RbI (violet) and KI (black) and YP-50F.

Tab. S8. Molar mass of ionic species and molecules possibly present in the 0.1 mol L^{-1} Li$_2$SO$_4$.

Molecule/ ionic species	Molar mass (g mol^{-1})	Positively charged species	Molar mass (g mol^{-1})	Negatively charged species	Molar mass (g mol^{-1})
H_2O	18.02	Li^+	6.94	O^-	16.00
CO	28.01	$Li^+ \cdot H_2O$	24.96	OH^-	17.01
O_2	32.00	$Li^+ \cdot 2H_2O$	42.97	$OH^- \cdot H_2O$	35.02
CO_2	44.01	$Li^+ \cdot 3H_2O$	60.99	$OH^- \cdot 2H_2O$	53.04
		$Li^+ \cdot 3.5H_2O$	69.99	$OH^- \cdot 2.5H_2O$	62.05
		$Li^+ \cdot 4H_2O$	79.00	$OH^- \cdot 3H_2O$	71.05
		$Li^+ \cdot 4.5H_2O$	88.01	$OH^- \cdot 4H_2O$	89.07
		$Li^+ \cdot 5H_2O$	97.02	$OH^- \cdot 5H_2O$	107.08
		H^+	1.01	$OH^- \cdot 6H_2O$	125.10
		$H^+ : H_3O^+$ (50 : 50)	10.02	$OH^- \cdot 6.5H_2O$	134.11
		H_3O^+	19.02	$OH^- \cdot 7H_2O$	143.11
				$OH^- \cdot 7.5H_2O$	152.12
				$OH^- \cdot 8H_2O$	161.13
				$SO_4^{2-} : OH^-$ (50 : 50)	56.53
				SO_4^{2-}	96.06
				SO_4^{2-}, OH^-	113.07
				$SO_4^{2-} \cdot H_2O$	114.08

D$_2$O as a solvent

Furthermore, D$_2$O solvent ($\varepsilon = 60$; 1.87 D) was used for LiNO$_3$ salt to see its influence on EDL formation compared to the water molecule ($\varepsilon = 80$; 1.84 D). D$_2$O molecule has lower hydration affinity (ε), as it does not create hydrogen bonds as easily as a H$_2$O molecule. Moreover, D$_2$O molecule is slightly more polar than H$_2$O and denser, therefore can affect EDL at the electrode/electrolyte interface, leading to a narrower PZC region. If min. specific

capacitance will be considered as one value, it divides PZC region in half. However, to the best of our knowledge, the PZC region discussed here informs about the perm-selectivity failure of electrode material in contact with a specific liquid electrolyte. Therefore, as discussed in the literature, this region should be excluded from ion flux divagation. In the further section, we will prove this and explain the implication of incorrectly assumed PZC value on the charge storage mechanism description.

References:

1   N. Shpigel, M.D. Levi, S. Sigalov, O. Girshevitz, D. Aurbach, L. Daikhin, P. Pikma, M. Marandi, A. Jänes, E. Lust, N. Jäckel, V. Presser, In situ hydrodynamic spectroscopy for structure characterization of porous energy storage electrodes, Nature materials 15(5) (2016) 570-575.

2   S. Boyd, K. Ganeshan, W.-Y. Tsai, T. Wu, S. Saeed, D.-e. Jiang, N. Balke, A.C.T. van Duin, V. Augustyn, Effects of interlayer confinement and hydration on capacitive charge storage in birnessite, Nature materials 20(12) (2021) 1689-1694.

3   P. Simon, Y. Gogotsi, Perspectives for electrochemical capacitors and related devices, Nature materials 19(11) (2020) 1151-1163.

4   Alexander C. Forse, John M. Griffin, C. Merlet, J. Carretero-Gonzalez, A.-Rahman O. Raji, Nicole M. Trease, Clare P. Grey, Direct observation of ion dynamics in supercapacitor electrodes using in situ diffusion NMR spectroscopy, Nature Energy 2(3) (2017).

5   F.W. Richey, B. Dyatkin, Y. Gogotsi, Y.A. Elabd, Ion Dynamics in Porous Carbon Electrodes in Supercapacitors Using in Situ Infrared Spectroelectrochemistry, Journal of the American Chemical Society 135(34) (2013) 12818-12826.

6   A. Ghosh, Y.H. Lee, Carbon-Based Electrochemical Capacitors, ChemSusChem 5(3) (2012) 480-499.

7   H. Shao, Y.-C. Wu, Z. Lin, P.-L. Taberna, P. Simon, Nanoporous carbon for electrochemical capacitive energy storage, Chemical Society reviews 49(1) (2020) 35-339.

8   A. Platek-Mielczarek, E. Frackowiak, K. Fic, Specific carbon/iodide interactions in electrochemical capacitors monitored by EQCM technique, Energy & environmental science 14(4) (2021) 2381-2393.

9   L. Borchardt, M. Oschatz, S. Kaskel, Tailoring porosity in carbon materials for supercapacitor applications, Materials horizons 1(2) (2014) 157-168.

10   H. Jiang, P.S. Lee, C. Li, 3D carbon based nanostructures for advanced supercapacitors, Energy & environmental science 6(1) (2012) 41-53.

11   G. Wang, L. Zhang, J. Zhang, A review of electrode materials for electrochemical supercapacitors, Chemical Society reviews 41(2) (2012) 797-828.

12   H. Yin, H. Shao, B. Daffos, P.-L. Taberna, P. Simon, The effects of local graphitization on the charging mechanisms of microporous carbon supercapacitor electrodes, Electrochemistry communications 137 (2022) 107258.

13   P. Bujewska, B. Gorska, K. Fic, Redox activity of selenocyanate anion in electrochemical capacitor application, Synthetic metals 253 (2019) 62-72.

14   D. Gastol, J. Walkowiak, K. Fic, E. Frackowiak, Enhancement of the carbon electrode capacitance by brominated hydroquinones, Journal of power sources 326 (2016) 587-594.

15   J. Wu, Y. Ben, D. Battigelli, H.-C. Chang, Long-Range AC Electroosmotic Trapping and Detection of Bioparticles, Industrial & engineering chemistry research 44(8) (2005) 2815-2822.

16   J.P. Guyer, An Introduction to Electrochemical Impedance Assessment of Coatings, The Clubhouse Press, El Macero, California, 2019.

17   B.E. Conway, Electrochemical Supercapacitors Scientific Fundamentals and Technological Applications / by B. E. Conway, 1st 1999. ed., Springer US, New York, NY, 1999.

18   M.F. Dupont, S.W. Donne, A Step Potential Electrochemical Spectroscopy Analysis of Electrochemical Capacitor Electrode Performance, Electrochimica acta 167 (2015) 268-277.

19   A. Platek, J. Piwek, K. Fic, E. Frackowiak, Ageing mechanisms in electrochemical capacitors with aqueous redox-active electrolytes, Electrochimica acta 311 (2019) 211-220.

Chapter III:

Carbon degradation in organic media

P3 and A1

P3. *Identifying the Activated Carbon Electrode Aging Pathways in Lithium-Ion Hybrid Capacitors*

Authors: Sylwia Slesinska, Bénédicte Réty, Camélia Matei-Ghimbeu, Krzysztof Fic, Jakub Menzel

Contribution: Methodology planning, investigation: electrochemical analysis, physicochemical analysis and corresponding data curation, visualization and writing of the original draft.

Graphical abstract:
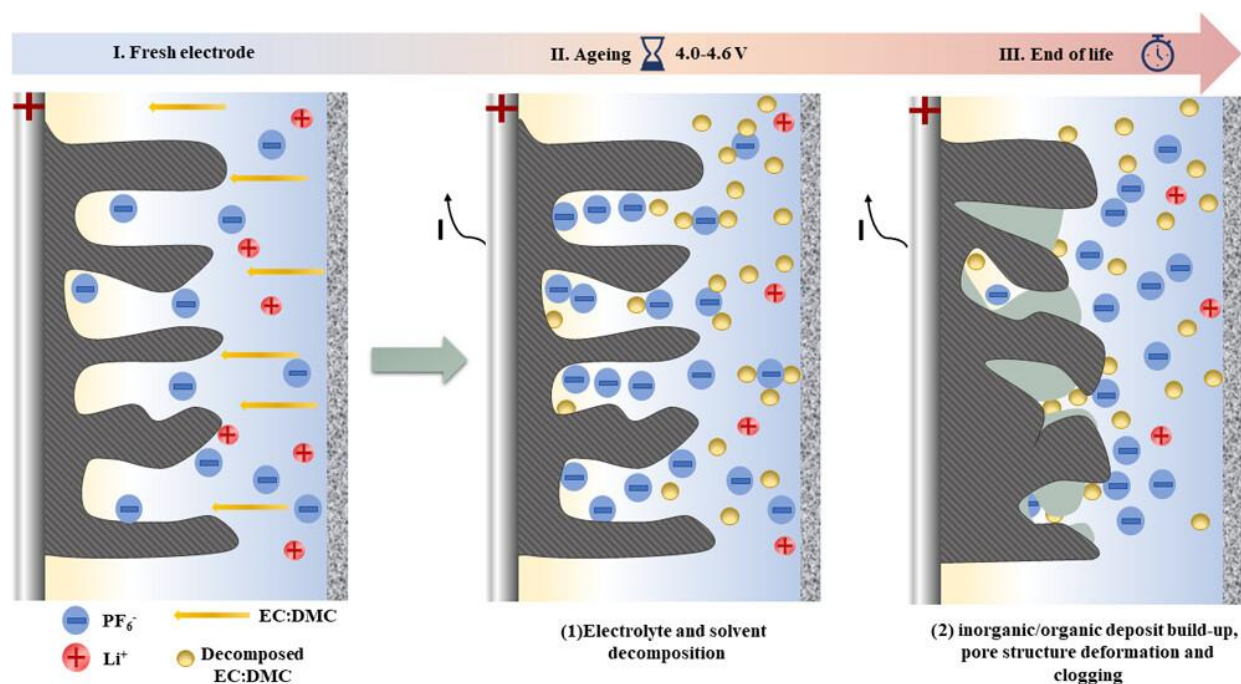
Motivation and Summary

The promise of LICs lies in their ability that combines both characteristics of high-power ECs and high-energy LIB. Therefore, understanding and mitigating the inevitable process of aging becomes necessary to ensure their long-term viability and reliable performance, especially if one considers their use in potential applications, such as electric vehicles (EVs (which are quite demanding). Carbon electrode is employed as a

capacitive charge storage component in LICs due to its characteristics such as high SSA and porous character. However, this also makes it susceptible to a variety of aging pathways related to electrolyte decomposition, surface oxidation and structural changes. More specifically, the high SA of carbon electrodes can promote electrolyte decomposition, leading to the formation of by-products that can then block its porosity and cause a loss of capacitive performance and increase in resistance. In such light, studies based on the ageing of porous carbon electrodes in LIC are an imperative component that can elucidate the mechanisms governing its performance decline. Such an approach can ultimately enable the development of tailored strategies that will enable more reliable and efficient device operation. The following article focuses on the degradation mechanisms of porous carbon electrodes in LICs performed during floating experiments and elucidates the related aging pathways at elevated voltages (4-4.6 V). The proposed approach utilized a half cell configuration, which was deliberately selected as to isolate the processes that take place at the electrode of interest (AC). Although full cells are more representative of 'real-world' applications, half-cells offer a valuable tool for understanding the fundamental processes. Additionally, the effect of a binder was removed through the use of the binder-less electrode (microporous carbon cloth). The application of various physicochemical *post-mortem* analyses (TPD-MS, Porosity measurements, EA, XPS, Raman Spectroscopy) allowed for a thorough investigation to explain the causes behind the performance fade in the studied systems, permitting various data to be acquired regarding changes that occur to the carbon electrodes. Ultimately, it was evidenced that (i) an increase in applied voltage results in faster degradation and that (ii) depending on the maximum voltage applied, the systems reached different end-of-life criteria. For systems floated at 4 V, simultaneous increase in resistance and decrease in capacitance was noted, whereas for ≥4.2, a more pronounced increase in resistance was evident. Moreover, when higher voltage is applied (≥4.2 V) it promotes oxidation and carbon functionalization, which explains the observed resistance decrease.

Article

Identifying the Activated Carbon Electrode Aging Pathways in Lithium-Ion Hybrid Capacitors

Sylwia Slesinska, Bénédicte Réty, Camélia Matei-Ghimbeu,* Krzysztof Fic, and Jakub Menzel*

Cite This: https://doi.org/10.1021/acsaem.4c01940

Read Online

ACCESS | Metrics & More | Article Recommendations | Supporting Information

ABSTRACT: This paper reports on several mechanisms of carbon aging in a hybrid lithium-ion capacitor operating with 1 mol L^{-1} $LiPF_6$ in an ethylene carbonate/dimethyl carbonate 1:1 vol/vol electrolyte. Carbon electrodes were subjected to a constant polarization protocol (i.e., floating) at various voltages and analyzed postmortem via several complementary techniques. The selected protocol was able to simulate the behavior of the real system. Due to the use of metallic lithium as the counter electrode, the influence of battery-like aging mechanisms was assumed to be limited. Our approach focused on the aging mechanisms related to the carbon electrode and determined the structural and chemical changes leading to energy fading in lithium-ion hybrid capacitors. It was shown that an increase in applied voltage not only results in faster

system degradation but directs the aging chemistry to different pathways: at moderate voltage values, both capacitance loss and simultaneous increase in resistance predominate. This could be associated with the decrease in carbon surface area and possible pore clogging with by-products of electrolyte degradation and carbon oxidation disrupting the C sp^2 network. When high voltage is applied, further oxidation of carbon occurs with an increase in measured resistance that leads to the relevant end-of-life criterion to be reached. Detailed postmortem analysis results attributed it to the formation of phenol and ether groups together with electrolyte decomposition products, higher oxidation levels, and structure degradation. It was evidenced that the decrease in the overall carbon conductivity and, in certain cases, modification of the textural properties ultimately aggravates the capacitor performance.

KEYWORDS: *Li-ion capacitor, carbon electrode, organic electrolyte, aging mechanism, floating aging*
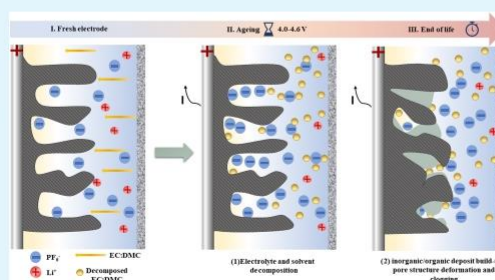
1. INTRODUCTION

From an industrial application point of view, porous carbon-based electrochemical capacitors (ECs) and Li-ion batteries (LiBs) are the most advanced technologies to date.[1-5] The principles of operation of ECs and LiBs significantly vary. ECs utilize physical charge storage processes rather than chemical processes (as in LiBs); thus, the processes occurring are much faster and reversible, providing higher power density and much-improved cyclability (>10^6 charge/discharge cycles).[6-8] However, the EC's energy density is much lower than that of LiBs. Therefore, the emergence of new technologies, such as hybrid capacitors (e.g., Li-ion capacitors (LiCs[9])), can benefit from both systems, where the specific and volumetric energy densities can be significantly increased (12−15 Wh kg^{-1})[10,11] while maintaining the high power and long-life characteristics of ECs.[12-14]

LiCs typically consist of one Li insertion material (e.g., $Li_3V_2(PO_4)_3$, $Li_4Ti_5O_{12}$) and high surface area materials (e.g., activated carbon) as electrodes.[12,13] To provide the long-term operation of these technologies, it is necessary to understand their degradation mechanisms. Although numerous studies have focused on the mechanisms of aging and proposed improve-

ments in LiBs and ECs,[15-22] limited work has been done in this area for LiCs, especially in terms of the aging of porous carbon electrodes. There is no doubt that the performance and longevity of LiCs are influenced by many factors: degree of prelithiation, operating temperature, applied electrode potential window, type of anode material, and instability of the lithiated anode, but their severity has been scarcely elaborated.[14,15,23-26] Most research to date reports the growth of the solid electrolyte interphase (SEI) as the main aging mechanism in LiBs and LiCs, which can be addressed via an oversized negative electrode; however, this does not completely suppress it.[11,16] Growth of the SEI on the surface of the negative electrode can increase its resistance, leading to a change in the potential of the positive electrode that can potentially generate LiF on the negative electrode above potentials of 4 V vs Li/Li^+.[17] Current aging

studies on LiCs, e.g., when high voltage was applied with liquid and gel polymer electrolytes, reported degradation related to mechanisms occurring at the electrodes rather than those of the electrolytes.[27] Other works report that the aging mechanisms strongly depend on the state of charge, especially concerning the negative electrode, where the growth of SEI was found to increase with the increase of the state of charge.[9]

Because LiCs combine LiB and EC electrode materials, aging can display similar characteristics to those found in electrochemical capacitors. In either an organic or an aqueous medium, this is related to the degradation of the positive electrode. In both cases, the measured Brunauer−Emmett−Teller (BET) specific surface area of the positive electrode after aging is significantly affected and reduced.[18−22,28−30] Ultimately, the aging mechanisms of both electrodes would be complementary, and depending on the selected conditions and materials used, the aging mechanisms could vary and prove to be rather complex in nature. In that light, exploration of various experimental "scenarios" could bring about new knowledge, which seems promising for future optimization of these devices.

Carbon electrode aging can be achieved by applying different aging protocols, such as galvanostatic cycling or voltage holding tests, i.e., floating; these protocols are already widely described in the literature.[29,31,32] Cycling stability tests are often evaluated by recording several thousands of galvanostatic charge−discharge cycles and are rather straightforward. Compared to floating tests (potentiostatic hold), they are, however, time-consuming. For example, in commercial electrochemical capacitors, 20% capacitance loss is observed after approximately 500 000−1 000 000 cycles.[33,34] In comparison, when tested in potentiostatic mode, a device based on organic electrolyte (TEABF$_4$/AN) suffered a 30% capacitance loss after 30 h and required 10 000 cycles during cycling tests to reach the same criterion.[32] Additionally, it was shown that cycling and floating have varied influences on the time of operation, structure of the electrode, and resistance of the total cell in aqueous media.[29] The former induces changes in the carbon structure with an insignificant influence on the measured resistance, whereas the former accelerates degradation. The latter is also termed "accelerated aging" due to the extended exposure time at high voltages in comparison to cycling; cycling is a reliable and time-efficient method of examining the state of health (SOH) of many energy storage devices, including LiC.[17−19] To effectively monitor the process, both the loss of capacitance and the increase in equivalent series resistance (ESR) need to be simultaneously monitored during operation. According to the international standard (IEC 62391-1),[20] a system failure is reported when the initial capacitance drops below 80% of its initial value or when the ESR has increased by 100%.

In this work, we report on the degradation mechanisms of porous carbon electrodes in LiCs at different elevated voltages: 4.0, 4.2, 4.4, and 4.6 V. The research was carried out with the application of a binder-free Kynol 507−20 activated carbon cloth as the working electrode and a typical LP-30 (1 mol L^{-1} LiPF$_6$ in an ethylene carbonate/dimethyl carbonate 1:1 vol/vol) electrolyte designed for Li-ion batteries. The proposed half-cell configuration allowed the isolation of the fundamental processes occurring at the carbon electrode only. This eliminated the complexities introduced by a full cell. Thus, a detailed study of the aging mechanisms associated with that specific electrode was achieved. The combined information gathered from post-mortem analyses, including elemental analysis, Raman spectroscopy, temperature-programmed desorption mass spectrom-

etry (TPD-MS), X-ray photoelectron spectroscopy (XPS), and porosimetry, elucidated the degradation paths and micro-structural changes of the electrodes.

2. EXPERIMENTAL SECTION

2.1. Electrodes and Electrochemical Cell Preparation. Circular self-standing electrodes (Ø = 16 mm, 18.6 mg) were cut from activated carbon fabric (Kynol ACC 507-20, Germany). Before electrochemical measurements, the carbon material was dried at 120 °C for 12 h under a vacuum to eliminate water and avoid potential oxidation. After electrochemical aging, the electrodes were washed in water and ethanol to remove the soluble impurities and then dried at 120 °C for 12 h under vacuum.

A solution of LiPF$_6$ salt at a concentration of 1 mol L^{-1} dissolved in 1:1 vol EC/DMC was purchased from Merck, Germany. The water content in the electrolyte declared by the producer was less than 20 ppm.

Electrochemical measurements were made on two-electrode ECC-ref cells (El-Cell, Germany). Before measurement, the electrode was soaked in the electrolyte and separated by a GF-D porous membrane (Whatman, UK). Metallic lithium was used as the counter electrode.

2.2. Electrochemical Analysis. Electrochemical measurements were performed with a computer-controlled multichannel potentiostat/galvanostat (VMP3, Biologic, France). Experimental techniques included galvanostatic charge/discharge with a current load of 0.5 A g^{-1}, cyclic voltammetry at scan rates of 2 mV s^{-1}, and determination of the current-interrupted ohmic drop at a current load of 0.2 A g^{-1} for 0.05 s. The floating protocol consisted of a 2 h voltage hold at terminal voltages interrupted by capacitance and resistivity measurements. All current and capacitance values were expressed per mass of one electrode if not stated otherwise.

2.3. Porosity Analysis. The nitrogen adsorption/desorption isotherm of the activated carbon electrode before and after aging was recorded using an ASAP 2460 analyzer (Micromeritics, USA) at 77 K. Prior to analysis, the samples were purged under helium flow for 24 h at 120 °C and then placed under high vacuum for 5 h. The low temperature of degassing was selected in order to avoid surface modification of carbon while ensuring the physisorbed species.[35] The specific surface area was calculated using the BET equation and verified with the pore size distribution, calculated using the 2D Non-Local Density Functional Theory (2D NLDFT) method.[36,37]

2.4. Elemental Analysis. The determination of the mass fractions of carbon, hydrogen, nitrogen, and oxygen was carried out with an Thermo Scientific FlashSmart equipment. The amount of oxygen was obtained through a direct (separate) elemental analysis. Our results are the averages of three separate analyses.

2.5. XPS Analysis. X-ray photoelectron spectroscopy (XPS) was performed with a VG SCIENTA SES-2002 spectrometer equipped with a concentric hemispherical analyzer. The incident radiation was generated by a monochromatic Al Kα X-ray source (1486.6 eV) that operated at 420 W (14 kV; 30 mA). A wide scan (survey) spectrum was recorded with a pass energy of 500 eV, and for high-resolution spectra, the pass energy used was 100 eV. The spectra were subjected to a Shirley baseline, and peak fitting was performed with mixed Gaussian−Lorentzian components with equal full width at half-maximum (fwhm) using CASAXPS version 2.3.18 software. All binding energies (BEs) are referenced to the C 1s (graphite-like sp^2 carbon) peak at 284.5 eV and given with a precision of 0.1 eV.

2.6. TPD-MS Examination. Measurements were carried out using a home-built TPD-MS setup under a secondary vacuum (10^{-5} Pa).[21,38] This equipment included an Inficon Transpector 2 mass spectrometer and a Leybold ITR100 Bayard-Alpert ionization vacuum gauge, which recorded continuous measurements of the intensity of the masses (m/z) of the released gases and the total gas pressure while the material was heated at a constant temperature rate. Before material analysis, the TPD-MS system was calibrated by separately measuring the mass spectrometer intensity and pressure of each gas: CO_2 ($m/z = 44$), CO ($m/z = 28$), H_2O ($m/z = 18$), and H_2 ($m/z = 2$). When the mass intensities and pressure measured during material analysis were

B

correlated with the calibration results, the desorption rate (μmol s^{-1} g^{-1} of material) of each gas could be determined versus the temperature. Moreover, the time integration of the TPD-MS curves provided the total amount of each gas per gram of material. In this study, TPD-MS measurements were performed under the following experimental conditions. The sample was placed in a quartz tube and heated to 950 °C at 10 °C/min. The maximum temperature was then maintained for 30 min before cooling. From the measured mass intensities and the calibration data, the pressure was calculated based only on the calibrated gases. By comparison of this calculated pressure with the real pressure measured by the vacuum gauge, the presence of uncalibrated gases was determined.

2.7. Raman Spectroscopy. Raman spectroscopy was performed with a DXR-2 computer-controlled Raman microscope (ThermoFisher Scientific, USA). The electrode spectrum was collected with the application of a 532 nm laser with an adjusted power of 8 mW. Analysis of the data obtained was performed with the Origin2021 software application. The peak positions and integration of the D/G bands were determined by deconvolution of the experimental spectrum.

3. RESULTS AND DISCUSSION

Figure 1 shows a cyclic voltammetry (CV) profile with a gradual voltage increase cutoff point from 4.0 to 4.6 V.
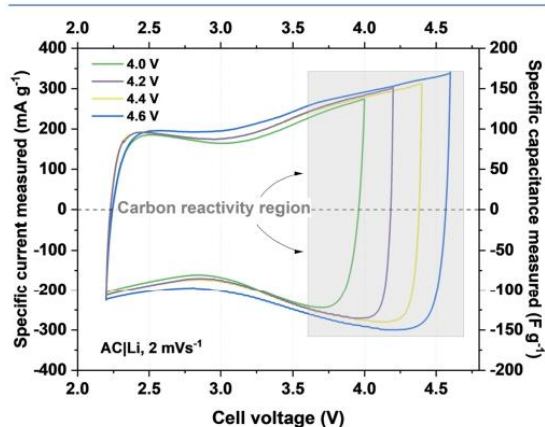
Figure 1. Cyclic voltammetry profiles (2 mV s^{-1}) of the Kynol ACC 507-20/metallic lithium system with 1 mol L^{-1} LiPF$_6$ in EC/DMC as the electrolyte; all scans start from 2.2 V, and terminal voltages were set to 4.0, 4.2, 4.4, and 4.6 V.

The voltammograms showed a characteristic "butterfly" shape, typical of LiC and organic-based EC, originating from different charge storage mechanisms and potential profiles for the electrodes. No sharp current increases, even at high voltage values, are considered as the lack of typical signs of system degradation; however, the interfacial activity of carbon should not be excluded. More detailed analysis indicates that the charge is symmetrically distributed with nearly 100% retention, also suggesting a lack of side reactions. It has been therefore assumed that 4.6 V is still the safe operating voltage, and the long-term performance was tested via potentiostatic hold, where the end-of-life criterion was defined as 20% of the initial capacitance loss or 100% resistance increase according to the international standard (IEC 62391-1).[20]

Figure 2 shows the changes in energy profiles with floating time and the corresponding increase in resistance with floating time at a given voltage. Additional charge/discharge curves before and after floating can be found in Figure S1.
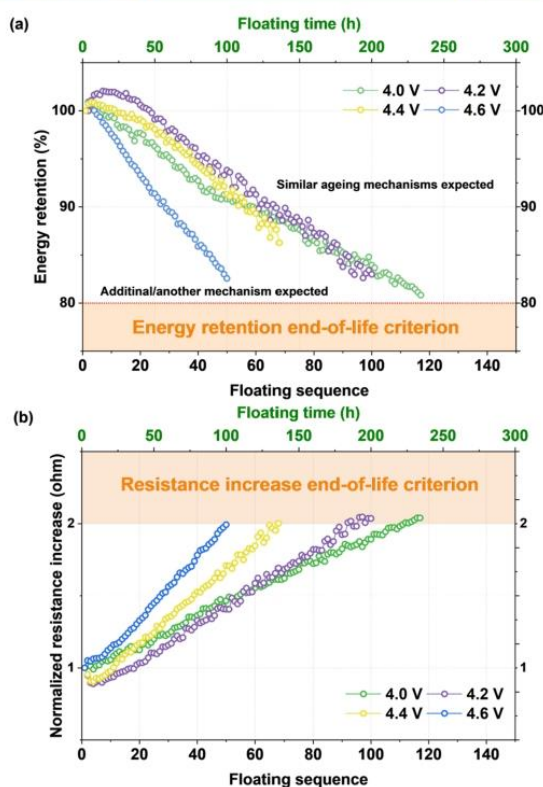

Figure 2. Results of the floating test for the LiCs with a 1 mol L^{-1} LiPF$_6$ electrolyte at various voltages (4.0–4.6 V). (a) Energy retention vs floating time and (b) relative resistance vs floating time.

From these data (Figure 2 and Table 1), two characteristic aging behaviors that significantly vary with the change in applied

Table 1. Comparison of Energy, Capacitance Retention, Resistance Increase, and End of Lifetime after Reaching the End-of-life Criterion

cell voltage (V)	4.0	4.2	4.4	4.6
energy retention (%)	83	84	84	83
capacitance retention (%)	80	82	86	86
resistance increase (%)	100	100	100	100
end-of-lifetime (h)	234	200	136	100

voltage are distinguished. At the voltage of 4.0 V, the loss of energy and the increase in resistance follow a similar linear trend, and the cell with the highest durability among all systems studied is achieved, where the resistance end-of-life criterion and capacitance loss are reached after ~240 h. Furthermore, there is a significant change when a higher voltage is applied. At 4.2 V and above, the resistance end-of-life criterium is reached while capacitance retention is above 80%. Moreover, with an increase in the voltage, the lifetime of the cells is limited from ~200 h for 4.2 V to ~100 h for 4.6 V voltage limitation. Additionally, the symptoms of electrolyte decomposition in initial cycles are observed in the form of decreased measured cell resistance, resulting from an increase in internal pressure, as evidenced by operando pressure measurements at 4 V (Figure S2).

Importantly, these results indicate that when considering accelerated aging experiments, it is crucial to monitor capacitance, energy retention, and resistance parameters since they do not necessarily change in an equal manner, especially when voltages close to or beyond the stability limit are concerned.

To further explain the aging and pore clogging phenomena, a series of postmortem analyses were completed to determine the electrochemical changes with any chemical or structural differences that occurred in the carbon electrodes and compared with the pristine Kynol 507-20 material, as the aging mechanism is not possible to deduce solely from the electrochemical data. Figure 3a shows N_2 adsorption/desorption isotherms measured
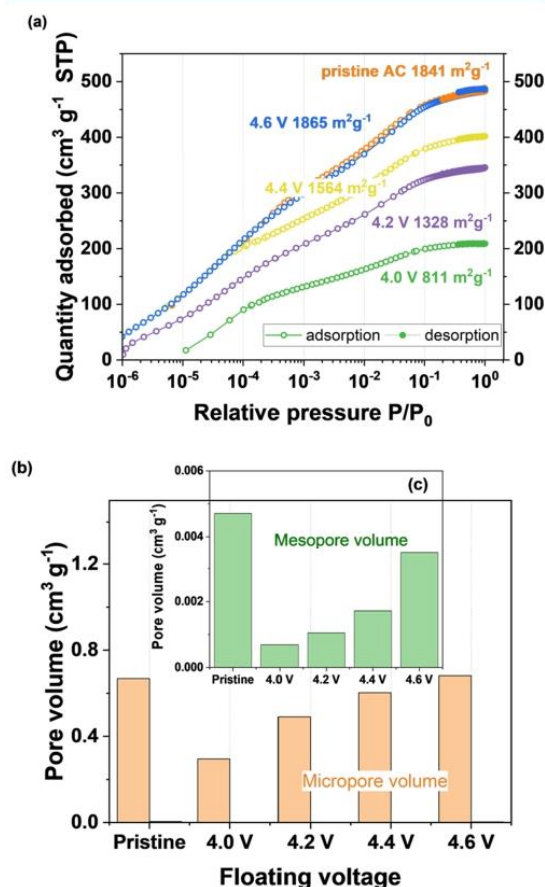
Figure 3. Porosity measurements for the pristine carbon cloth and the positive electrodes after the floating test at various voltages (4.0–4.6 V), (a) N_2 isotherms at 77 K, (b) comparison of V_{micro} and V_{meso} from 2D NLDFT, and (c) inset showing the V_{meso}.

at 77 K. To better demonstrate the changes in the micropore-related relative pressure regions, the x-axis is presented on a log scale. Pore size distribution is presented in Figure S3.

The material is characterized by a type I isotherm and a microporous texture with an additional mesopore contribution; the BET and 2D NLDFT surface area was ca. 1800 m^2 g^{-1}. The results showed a significant decrease in the specific surface area of the electrodes floated at 4.0 V, where the value changed from

1841 to 811 m^2 g^{-1}. Moreover, V_{micro} decreased from 0.67 cm^3 g^{-1} for pristine carbon to 0.29 cm^3 g^{-1} for the positive electrode aged at 4.0 V. In addition, V_{meso} decreased as well, approaching values close to zero. This followed the trend for water-based systems in which pore clogging by solid precipitates and residuals was observed.[28] It has to be mentioned that the profile of the isotherms suggests that the order of pore blocking is similar for both voltages; however, the severity (reflected by the quantity of adsorbed gas and relevant surface area decrease) changes with the voltage. This might also suggest that there is a significant role of the polarization protocol and pore accessibility. Additionally, the different nature of by-products of electrolyte decomposition being potential dependent might result in pore clogging at 4.0 V.[39] Noteworthy, for higher floating voltages (4.2 and 4.4 V), the change in S_{BET} was much less pronounced, with a decrease to 1328 and 1564 m^2 g^{-1}, respectively. The volume of pores appeared to be less affected as the time necessary to reach the end-of-life criterium decreased. At 4.6 V, S_{BET} and V_{micro} remained unchanged, where only a decrease in V_{meso} was observed. These results were strongly correlated with the electrochemical results, where the two aging pathways were considered. As aforementioned, the S_{BET} degradation might be connected with the time of the experiment where for the system aged at 4.0 V, more mechanical stress was applied than in the case of the system aged at >4.2 V. To better understand the involved processes, an elemental analysis of pristine and aged electrodes was performed (Figure S4a). This helped to quantify the elemental composition after floating at various voltages. Compared to the pristine electrode, a significant increase in oxygen content was found, i.e., from 1.5 to 5.0%, at 4.0 V. For higher voltages, a slight increase was further observed (7%), which remained rather constant for the electrodes cycled between 4.2 and 4.6 V. This implied the role of electrode oxidation on carbon conductivity decrease, which did not exponentially increase with a higher floating voltage but rather slightly changed by ~2% of oxygen. The same results were confirmed via XPS data analysis (Figure S4(b) and Table 2),

Table 2. XPS Chemical Composition of the Aged Electrodes at 4.0 and 4.6 V

element	C 1s	O 1s	N 1s	P 2p	F 1s	S 2p
pristine	92.01	5.53	0.00	0.16	0.00	0.00
4.0 V	81.12	17.54	0.00	0.23	0.00	0.00
4.6 V	78.64	19.92	0.54	0.34	0.26	0.26

where the surface composition of the electrodes was determined. In comparison to the pristine material, all electrodes displayed an increase in the oxygen content, with a simultaneous decrease in the carbon content. Traces of phosphorus were also present in all samples and increased by ~0.1% with higher voltages (Table 2).

At 4.6 V, 0.26% fluorine was found, indicating the decomposition of the LiPF$_6$ salt; this result is discussed in more detail in the context of TPD-MS analysis data. Therefore, the oxidation of carbon and formation of new, inorganic, and organic species with voltage was confirmed. A progressive decrease in the carbon content on the surface was also observed, but it is rather the result of increased content of other elements on the electrode surface due to electrolyte decomposition. However, the formation of gaseous products and degradation of the electrode cannot be excluded either. At initial cycles at high voltages, the oxygen functional groups found on the surface of
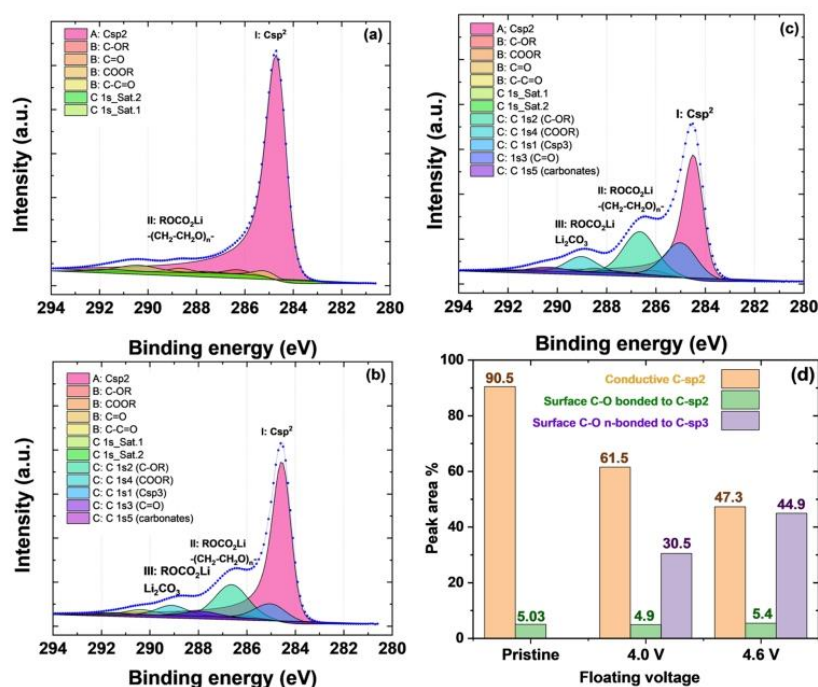
Figure 4. Deconvoluted XPS C 1s spectra for (a) pristine carbon; (b) carbon electrode after aging at 4.0 V; (c) carbon electrode after aging at 4.6 V; (d) surface compositions of the carbon electrodes prior to and after the floating test at different voltages. Color code: orange corresponds to C sp^2, green corresponds to C−OR, COOR, C=O, and C−C=O bonded to C sp^2, and violet corresponds to C−OR, COOR, C=O, C sp^3, and carbonate fractions.

the carbon cloth may be eventually oxidized to CO_2 and H_2O.[40] According to the literature, this could lead to the formation of Li_2O and H_2 on the negative electrode, which could deplete cyclable Li^+ ions and produce gas and HF.[41] However, as XPS is a surface technique, the exact state of the carbon electrode underneath the solvent/electrolyte degradation compounds cannot be assessed. Ar-etching experiments would be useful to gain insight into the chemical composition at different penetration depths of the electrode.

Moreover, the oxygen content obtained from XPS was higher than that from the elemental analysis, which further indicated that the aging process occurred mostly at the electrode/electrolyte interface. The fast oxidation of the carbon surface leading to a resistivity increase might explain the short lifespan and less affected S_{BET} as the terminal voltage increases. In addition, the detailed deconvolution of carbon XPS spectra is shown for the aged electrodes prior to and after the aging procedure at 4.0 and 4.6 V (Figures 4 and S5).

The fraction of conductive C sp^2 significantly declined with floating voltage, from 61.5 to 47.3%, and carbon oxidation led to a decrease in conductivity. The presence of C−O functional groups bonded to C sp^2 remained rather constant (∼5%), while those not bonded to C sp^2 significantly increased in comparison to the pristine carbon cloth. The lack of this component on the pristine carbon, its later appearance at 4.0 V, and its notable increase at 4.6 V indicated electrolyte/solvent decomposition.

The C component corresponded to species, such as lithium alkyl carbonate ($ROCO_2Li$), lithium carbonate (Li_2CO_3), and poly(ethylene oxide) polymer ($CH_2−CH_2−O$), formed on the electrode surface via the polymerization of EC already described

in the literature.[41,42] The presence of these species was observed on the C 1s peaks at 286.48 eV ($CH_2−CH_2−O$) and 288.95 eV ($LiCO_3$). $ROCO_2Li$ had a doublet at both indicated binding energies, corresponding to the CO-like (286.48 eV) and CO_3-like (288.95 eV) carbons. The solvent decomposition leads to lithium methyl carbonate ($LiOCO_2CH_3$) and lithium ethyl dicarbonate (($CH_2OCO_2Li)_2$).[43] These compounds were usually observed in the SEI formed on graphite materials cycled in the same electrolyte as used in the present study.[44] Their role is different, and the proportion of each species in the SEI layer impacts its properties. For example, Li_2CO_3 formed by the reaction of lithium with the electrolyte and/or solvent protects the carbon surface from further electrolyte decomposition. The organic alkyl carbonates derived from the solvent decomposition present an insulating nature, affecting the electrode conductivity. Nevertheless, the polymeric species (PEO) formed by carbon surface interaction with the electrolyte provide mechanical integrity to the SEI to withstand volume changes and stress occurring during cycling process.[45] However, the nature of these polymeric species can be different depending on the potential. It was demonstrated that at high voltages (>4.2 V vs Li^+/Li) the PEO might undergo oxidative polymerization via radicals (-O.), forming longer PEO chains and various gases.[46] Therefore, these longer-chain polymers formed at high voltage might rather block the mesopores, while the small-chain polymers formed at low voltage (4.0 V) are more susceptible to deposition in the micropore, blocking the entries and leading to a decrease of S_{BET} and micropore volume.
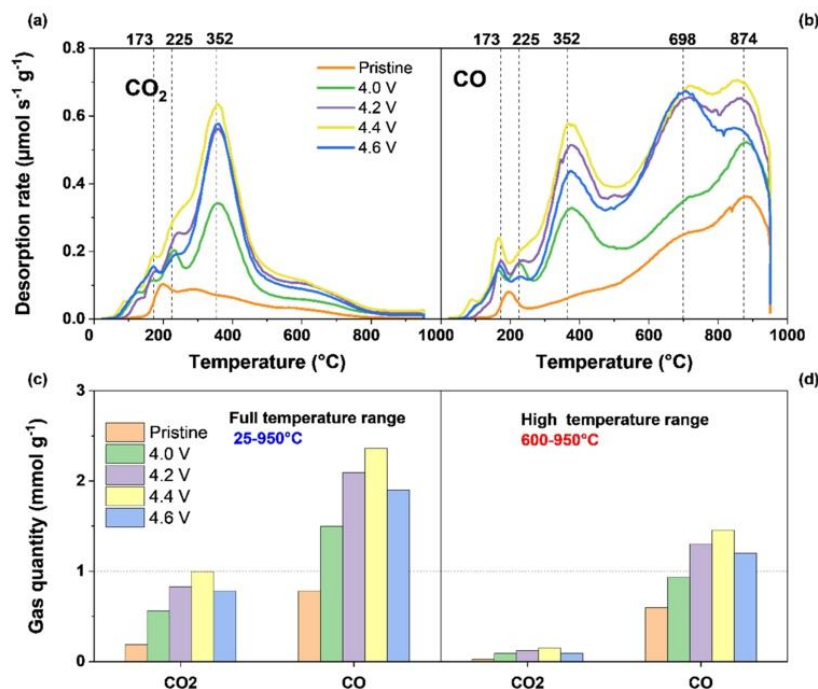
Figure 5. TPD-MS profiles of the pristine and cycled electrodes: desorption rates of (a) CO_2 and (b) CO and the total gas quantities (c) between 25 and 950 °C and (d) between 600 and 950 °C.

As both inorganic and organic species are found in the SEI, a compromise between electronic insulation and ion conductivity is ensured.

The formation of all of these species confirmed the presence of an insulating layer on the carbon surface. This layer impeded the observation of new oxygen-based functional groups formed on the carbon surface after cycling, considering the low penetration depth of the XPS technique (maximum 10 nm). However, the TPD-MS results, which enabled bulk analysis of electrodes (Figure 5c,d), showed both the formation of oxygen functional groups and electrolyte degradation products.

Temperature-programmed desorption coupled to mass spectrometry (TPD-MS) is a qualitative and quantitative measurement that is used to characterize the surface chemistry of carbon materials. This method enables the quantification of surface-oxygenated functional groups. Calculated (based on calibrated gases) and measured TPD-MS pressure profiles are shown in Figure S6 (Supporting Information) for the pristine and 4.6 V samples. The pressure profiles for samples at 4.0, 4.2, and 4.4 V are similar to those for 4.6 V. The temperatures at which the two curves do not overlap show the presence of uncalibrated gases. These uncalibrated gases prevent accurate quantification of the calibrated gases at the temperature at which they have evolved due to the contribution of additional m/z to the total intensity of the m/z of the calibrated gases. From Figure S6, an uncalibrated peak at approximately 200 °C is present in both pristine and cycled electrodes, potentially due to the physisorbed contamination. Two additional uncalibrated peaks are observed at 230 and 360 °C for all cycled materials but are absent in the pristine material. In particular, the peak at 360 °C is very intense, indicating the presence of uncalibrated gases. To obtain more insight into the nature of the gases that are evolved

in these regions, Figure 6 shows the MS profiles. Graphs a−e show the uncalibrated m/z species.

Several masses, which can be related to fluorinated functional groups or decomposition of the $LiPF_6$ electrolyte, are recorded, such as those of COF, COF_2, and CF_2. The release of HF can also be observed, which is potentially responsible for the fluorination of the carbon structure and the release of fluorinated groups. HF can also lead to fluorination of the silica crucible, as indicated by the presence of mass $m/z = 85$; this is possibly the result of the decomposition of silica-fluorinated groups created during heat treatment with TPD-MS.[42] Mass $m/z = 85$ can also be associated with a fragment peak of POF_3, which produces a $m/z = 104$ (Figure S7). POF_3 can be formed by the decomposition of carbonates and $LiPF_6$ electrolytes.[47] At 400 °C, $m/z = 85$ and 104 nm are simultaneously detected, showing the presence of POF_3. In contrast, only $m/z = 85$ is present at 200 °C, which indicates the decomposition of silica-fluorinated groups at this temperature. In addition, $m/z = 90$ and 118 are correlated with dimethyl carbonate (DMC) and ethyl carbonate (EC), respectively; both are observed at 380 °C. These two electrolyte species can either be trapped in the porosity of the electrode or strongly bonded to the carbon surface, most likely due to electrolyte decomposition, and are not removed during the washing step. However, the measured intensities for the masses associated with fluorinated compounds, EC, and DMC are very low (3 orders of magnitude) compared to oxygen-based groups, as illustrated by the comparison with Figure 5e, which shows $m/z = 28$ (CO) and $m/z = 44$ (CO_2) for sample 4.6 V. Although the TPD-MS results cannot be strictly compared with the XPS (due to their differences), one might note that XPS also shows low amounts of fluorine and phosphorus groups in the
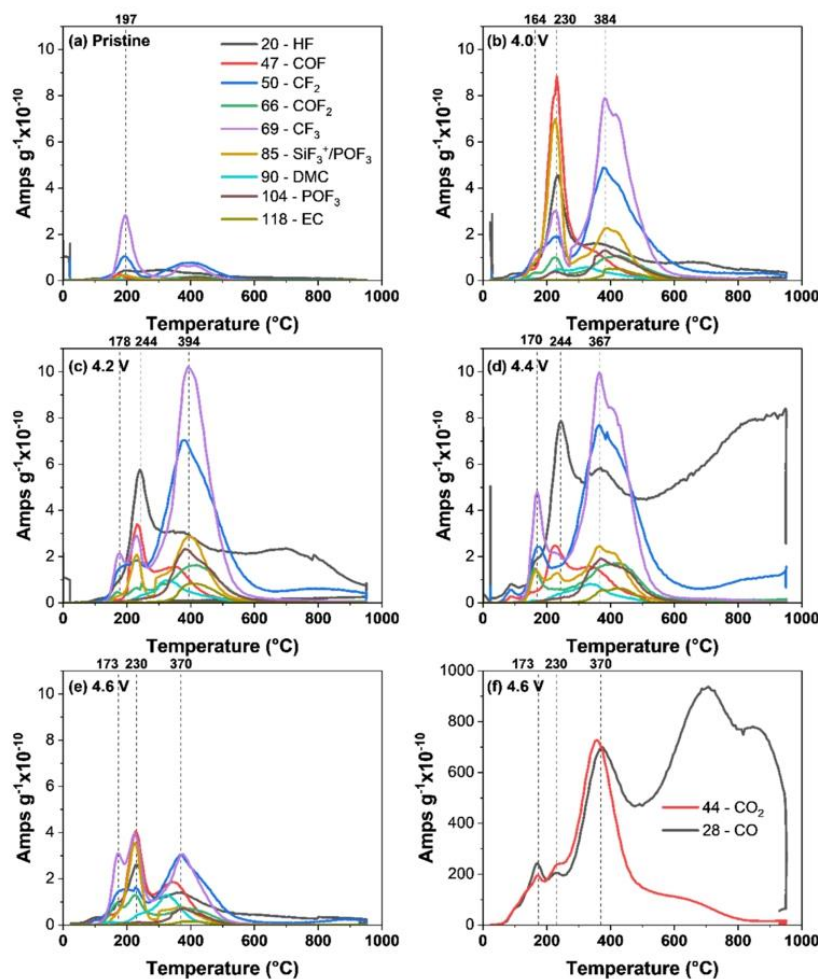
Figure 6. MS profiles for uncalibrated gases from thermal decomposition of (a) pristine material, (b) 4.0 V, (c) 4.2 V, (d) 4.4 V, and (e) 4.6 V. (f) MS profiles for the masses related to CO and CO_2.

materials. Figure 5a,b shows the CO_2 and CO desorption rate profiles of the five samples.

In the low-temperature region, two uncalibrated peaks are observed at 225 and 352 °C; thus, these uncalibrated species also decompose as $m/z = 28$ and 44. The peak of CO_2 at this temperature is potentially due to the decomposition of carbonates, such as Li_2CO_3 and lithium alkyl carbonate species ($ROCO_2Li$). The CO peak is possibly the result of the decomposition of short electrolyte polymer chains, such as the poly(ethylene oxide) polymer (CH_2-CH_2-O) formed on the electrode surface, via the polymerization of EC.[41,42]

Therefore, in this temperature range, the nature of the oxygenated surface groups created during cycling because of the contribution from the uncalibrated compounds is difficult to deduce. However, carboxylic and anhydride groups are susceptible and likely formed, leading to CO_2 and CO groups.[48]

In the high-temperature region (between 650 and 950 °C), only calibrated gases evolve, as demonstrated by the two pressure curves that overlap above 600 °C. In this temperature range, the CO_2 profiles have a low intensity and similar shapes (Figure 5a),

while significant differences are observed in the CO profiles (Figure 5b). For voltages higher than 4.2 V, a new CO peak at ~700 °C is observed and not present in the pristine and 4.0 V electrodes. This peak is attributed to ether and phenol surface groups,[49,50] and its similar intensity for 4.2, 4.4, and 4.6 V electrodes indicate a similar amount. However, the CO peak at 874 °C, showing the presence of oxygenated surface groups, such as carbonyl and quinone, is present in both the pristine and cycled materials, and its intensity increases with voltage. Therefore, these oxygen functionalities continuously form with an increasing voltage. Figure 5c,d shows the total amount of CO_2 and CO that evolved during the TPD-MS analysis, respectively, from room temperature to 950 °C and between 600 and 950 °C. The second temperature range is interesting because it provides accurate amounts of total CO_2 and CO without the contribution of uncalibrated gases. Therefore, between 600 and 950 °C, the amounts of CO_2 and CO are only due to oxygenated surface groups. Figure 5c also shows that the amount of carbonates, short electrolyte polymer chains, and oxygenated surface groups increases significantly and reaches a

peak at 4.4 V. In Figure 5d, above 600 °C, the amount of CO_2 is rather low, while there is an increase in the total amount of CO with voltage, with a peak at 4.4 V also.

These measurements demonstrated an increase in the oxygen-based functional groups with voltage, which is in good agreement with the elemental analysis results. Moreover, these results indicate the presence of by-products coming from the polymerization of solvents, carbonate formation, and, to a lesser degree, the fluorination of carbon. The presence of two strong CO and CO_2 peaks that originated from the decomposition of Li_2CO_3 and polymer chains supports the theory of fast electrolyte decomposition under overcharged conditions. However, several general reasons for the system degradation of LiC can be distinguished.

3.1. Electrolyte Degradation. The interactions between the electrolyte and the electrode can promote the electrolyte decomposition with the formation of SEI and organic/inorganic by-products that will cover the carbon surface or block their porosity porosity and active sites. These undesired reactions can be favored at high voltage.

3.2. Carbon Property Modification.

(i) Porosity (specific surface area and pore volume) changes are caused by pore clogging due to unsolvable species (from electrolyte degradation) and O functional groups, leading to fewer adsorbed species, slower diffusion, and lower capacitance.[9]

(ii) Surface chemistry and oxidation of carbon surface are changed, leading to lower conductivity.[51] The oxygen-based functional groups can disrupt the hexagonal sp^2-bonded carbon network, diminishing the electron mobility and electrical conductivity. They can also participate in undesired reactions with the electrolyte at high voltages.

(iii) Structural changes (defects coming from C sp^3, C−O bonds, polymerized monomers) contribute to the electrolyte decomposition and increase resistance (decreased conductivity).

3.3. Voltage Applied. The increase in voltage might induce faster electrolyte and electrode degradation, as well as gas generation and pressure increase.[52] Also, as the time of the experiment was prolonged, the changes in pore volume in consecutive floating cycles resulted in structure degradation possibly connected with pore clogging. However, at higher voltage, faster oxidation and functionalization of carbon lead to an increase in resistance, resulting in less affected pore structure.

Additionally, one needs to remember that the formation of the SEI layer on the counter electrode might also contribute to the increase in resistance.

Structural changes were monitored also by Raman spectroscopy and the D/G band intensity ratio calculations from spectra deconvolution.[53,54] The experimental data and fitted curves of the pristine Kynol 507−20 carbon are shown in Figure 7a.

The ratio of the intensity of the D/G bands is a measure of the defects present in the graphene structure. The G band is the result of in-plane vibrations of sp^2-bonded carbon atoms, while the D band is due to the out-of-plane vibrations attributed to the presence of structural defects. The D mode is present in all graphite-like carbons and originates from structural defects. A comparison of the I_D/I_G ratio calculated from the integrated area of the deconvoluted peaks presented in Figure 7b shows an insignificant increase in the D/G peak intensity ratio; however, the effect diminished with the increasing voltage.
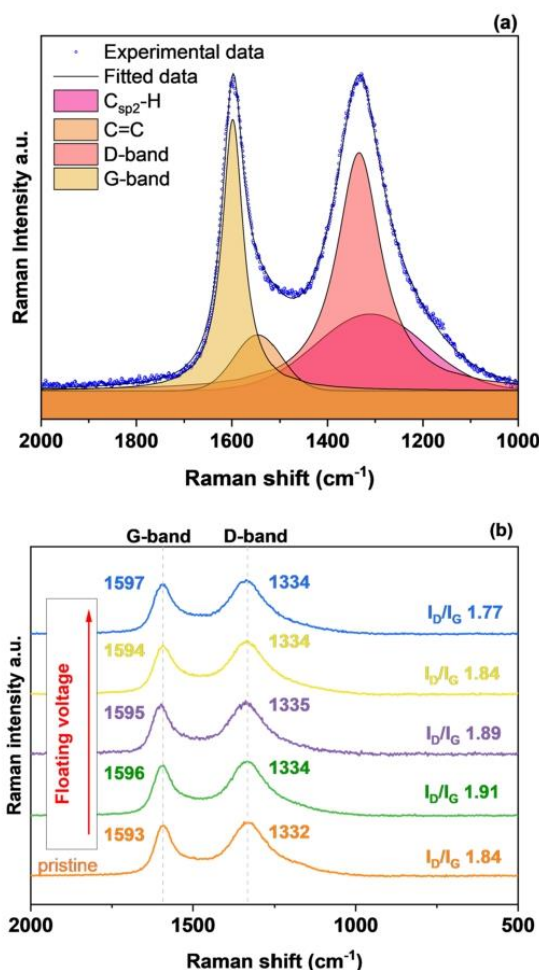

Figure 7. Raman spectroscopy analysis of the positive electrodes after the floating test at various voltages from 4.0 to 4.6 V compared to that of the pristine carbon cloth before aging: (a) deconvoluted spectrum of the pristine Kynol 507-20 electrode and (b) Raman spectrum of the electrodes with the marked positions of the peaks and I_D/I_G ratio.

The lack of significant changes in the I_D/I_G ratio can potentially result from low laser beam penetration. As observed by XPS, much of the oxygen content on the surface of carbon comes from the products of electrolyte decomposition in the form of polymer-like carbonates and Li_2CO_3.[28] However, as observed by TPD-MS and EA, carbon bulk oxidation clearly takes place, which cannot be observed by Raman spectroscopy. Furthermore, the D and G bands remain almost constant for all materials (Figure 7b).

4. CONCLUSIONS

The electrochemical aging of the carbon electrode in LiC, followed by a physiochemical analysis, was presented and discussed. Results from elemental analysis, porosimetry, mass spectrometry, XPS, and Raman spectroscopy provided a complete picture of the capacitance/energy fading during the

accelerated aging test. Therefore, several observations and conclusions could be drawn:

- Depending on the maximum voltage, the systems reached different end-of-life criteria: (i) at 4.0 V: capacitance fades with simultaneous resistance increase; and (ii) between 4.2 and 4.6 V: a similar system failure reason occurred with more pronounced resistance increase;

  aging at 4.0 V: chemical and structural changes of the electrode were observed. Combining the data from N_2 adsorption and TPD-MS enabled the existence of a spatial hindrance in the form of residuals of electrolyte decomposition resulting in pore clogging and specific surface area decrease.

- Aging voltage higher than 4.2 V: The formation of ether and phenol groups was confirmed, resulting in the resistance increase.[42] Further observations via EA, TPD-MS, and XPS confirm the increase in the overall oxygen content. This has two different origins. First, additional sources of oxygen (as identified via XPS) were found at the surface of the electrode coming from electrolyte decomposition in the form of poly(ethylene oxides), polymer-like carbonates, and Li_2CO_3. The amount/nature of these species might vary with voltage and impact their localization in the carbon (micro- or mesopores), with a direct consequence on textural properties. Second, carbon oxidation in the bulk of the material leads to enhanced oxygen content, as recorded via TPD-MS and EA. These results confirm that higher aging voltage induces faster oxidation and carbon functionalization. The formation of new O-functionalities led to a decrease in the conductive C sp^2 content, and their insulating nature contributed to an increase in the resistance and degradation of capacitor performance. Additionally, the potential corrosion of the system caused by the presence of HF needed to be considered and could lead to an increase in cell resistance.[40,55]

Our data show that in the case of LiCs, different aging pathways for the carbon electrode need to be considered during the optimization of the full cell.

■ ASSOCIATED CONTENT

Ⓢ Supporting Information

The Supporting Information is available free of charge at https://pubs.acs.org/doi/10.1021/acsaem.4c01940.

Operando pressure measurement during charge/discharge recorded after the first seven floating sequences at 4 V; charge/discharge cycles before and after floating; pore size distribution for pristine carbon cloth and the positive electrodes after the floating tests; elemental analysis of the pristine and aged positive electrodes; deconvoluted XPS C 1s spectra for pristine and aged carbon electrode after aging at 4.0 and 4.6 V; TPD-MS pressure profiles for pristine and 4.6 V electrodes; theoretical MS spectra from NIST MS search database of dimethyl carbonate; and diethyl carbonate, CF_4, and POF_3 (PDF)

■ AUTHOR INFORMATION

Corresponding Authors

Camélia Matei-Ghimbeu − *Institut de Science des Matériaux de Mulhouse (IS2M), Université de Haute-Alsace, F-68100 Mulhouse, France; Université de Strasbourg, F67081 Strasbourg, France; Réseau sur le Stockage Electrochimique de l'Energie (RS2E), 80039 Amiens Cedex, France;* ⓘ orcid.org/0000-0003-3600-5877; Email: camelia.ghimbeu@uha.fr

Jakub Menzel − *Institute of Chemistry and Technical Electrochemistry, Poznan University of Technology, 60-965 Poznan, Poland;* ⓘ orcid.org/0000-0002-0431-159X; Email: jakub.menzel@put.poznan.pl

Authors

Sylwia Slesinska − *Institute of Chemistry and Technical Electrochemistry, Poznan University of Technology, 60-965 Poznan, Poland;* ⓘ orcid.org/0000-0002-9242-5561

Bénédicte Réty − *Institut de Science des Matériaux de Mulhouse (IS2M), Université de Haute-Alsace, F-68100 Mulhouse, France; Université de Strasbourg, F67081 Strasbourg, France; Réseau sur le Stockage Electrochimique de l'Energie (RS2E), 80039 Amiens Cedex, France*

Krzysztof Fic − *Institute of Chemistry and Technical Electrochemistry, Poznan University of Technology, 60-965 Poznan, Poland;* ⓘ orcid.org/0000-0002-5870-7119

Complete contact information is available at:
https://pubs.acs.org/10.1021/acsaem.4c01940

Author Contributions

S.S. was responsible for the methodology, investigation, and writing of the original draft. B.R. performed the investigation and wrote the original draft. C.M.-G. was responsible for the validation and supervision and reviewed and edited the manuscript. K.F. performed the supervision, funding acquisition, and project administration and reviewed and edited the manuscript. J.M. was responsible for the conceptualization, methodology, funding acquisition, supervision, and project administration and reviewed and edited the manuscript.

Notes

The authors declare no competing financial interest.

■ ACKNOWLEDGMENTS

■ REFERENCES

(1) Yu, S. J.; Ng, V. M. H.; Wang, F. J.; Xiao, Z. H.; Li, C. Y.; Kong, L. B.; Que, W. X.; Zhou, K. Synthesis and application of iron-based nanomaterials as anodes of lithium-ion batteries and supercapacitors. *J. Mater. Chem. A* **2018**, 6 (20), 9332−9367.

(2) Simon, P.; Gogotsi, Y. Materials for electrochemical capacitors. *Nat. Mater.* **2008**, 7 (11), 845−854.

(3) Winter, M.; Brodd, R. J. What are batteries, fuel cells, and supercapacitors? *Chem. Rev.* **2004**, 104 (10), 4245−4269.

(4) Abruña, H. D.; Kiya, Y.; Henderson, J. C. Batteries and electrochemical capacitors. *Phys. Today* **2008**, 61 (12), 43−47.

(5) Chinese Society of Electrochemistry. The Top Ten Scientific Questions in Electrochemistry. *J. Electrochem.* **2024**, 30 (1), No. 2024121.

(6) Simon, P.; Gogotsi, Y. Perspectives for electrochemical capacitors and related devices. *Nat. Mater.* **2020**, 19 (11), 1151−1163.

(7) Lewandowski, A.; Galinski, M. Practical and theoretical limits for electrochemical double-layer capacitors. *J. Power Sources* **2007**, *173* (2), 822−828.

(8) González, A.; Goikolea, E.; Barrena, J. A.; Mysyk, R. Review on supercapacitors: Technologies and materials. *Renewable Sustainable Energy Rev.* **2016**, *58*, 1189−1206.

(9) El Ghossein, N.; Sari, A.; Venet, P.; Genies, S.; Azaïs, P. Post-Mortem Analysis of Lithium-Ion Capacitors after Accelerated Aging Tests. *J. Energy Storage* **2021**, *33*, No. 102039.

(10) Gogotsi, Y.; Simon, P. True performance metrics in electrochemical energy storage. *Science* **2011**, *334* (6058), 917−918.

(11) Sun, X. Z.; Zhang, X.; Liu, W. J.; Wang, K.; Li, C.; Li, Z.; Ma, Y. W. Electrochemical performances and capacity fading behaviors of activated carbon/hard carbon lithium ion capacitor. *Electrochim. Acta* **2017**, *235*, 158−166.

(12) Naoi, K.; Ishimoto, S.; Miyamoto, J.; Naoi, W. Second generation 'nanohybrid supercapacitor': Evolution of capacitive energy storage devices. *Energy Environ. Sci.* **2012**, *5* (11), 9363−9373.

(13) Dsoke, S.; Fuchs, B.; Gucciardi, E.; Wohlfahrt-Mehrens, M. The importance of the electrode mass ratio in a Li-ion capacitor based on activated carbon and $Li_4Ti_5O_{12}$. *J. Power Sources* **2015**, *282*, 385−393.

(14) Cao, W. J.; Shih, J.; Zheng, J. P.; Doung, T. Development and characterization of Li-ion capacitor pouch cells. *J. Power Sources* **2014**, *257*, 388−393.

(15) Zhang, J.; Liu, X. F.; Wang, J.; Shi, J. L.; Shi, Z. Q. Different types of pre-lithiated hard carbon as negative electrode material for lithium-ion capacitors. *Electrochim. Acta* **2016**, *187*, 134−142.

(16) Keil, P.; Schuster, S. F.; Wilhelm, J.; Travi, J.; Hauser, A.; Karl, R. C.; Jossen, A. Calendar Aging of Lithium-Ion Batteries I. Impact of the Graphite Anode on Capacity Fade. *J. Electrochem. Soc.* **2016**, *163* (9), A1872−A1880.

(17) Aida, T.; Murayama, I.; Yamada, K.; Morita, M. Analyses of capacity loss and improvement of cycle performance for a high-voltage hybrid electrochemical capacitor. *J. Electrochem. Soc.* **2007**, *154* (8), A798−A804.

(18) Ruch, P. W.; Cericola, D.; Foelske-Schmitz, A.; Kötz, R.; Wokaun, A. Aging of electrochemical double layer capacitors with acetonitrile-based electrolyte at elevated voltages. *Electrochim. Acta* **2010**, *55* (15), 4412−4420.

(19) Weingarth, D.; Noh, H.; Foelske-Schmitz, A.; Wokaun, A.; Kötz, R. A reliable determination method of stability limits for electrochemical double layer capacitors. *Electrochim. Acta* **2013**, *103*, 119−124.

(20) Oukaour, A.; Tala-Ighil, B.; AlSakka, M.; Gualous, H.; Gallay, R.; Boudart, B. Calendar ageing and health diagnosis of supercapacitor. *Electr. Power Syst. Res.* **2013**, *95*, 330−338.

(21) Liu, Y. H.; Réty, B.; Ghimbeu, C. M.; Soucaze-Guillous, B.; Taberna, P. L.; Simon, P. Understanding ageing mechanisms of porous carbons in non-aqueous electrolytes for supercapacitors applications. *J. Power Sources* **2019**, *434*, No. 226734. ARTN 226734

(22) Bittner, A. M.; Zhu, M.; Yang, Y.; Waibel, H. F.; Konuma, M.; Starke, U.; Weber, C. J. Ageing of electrochemical double layer capacitors. *J. Power Sources* **2012**, *203*, 262−273.

(23) Cao, W. J.; Zheng, J. P. Li-ion capacitors with carbon cathode and hard carbon/stabilized lithium metal powder anode electrodes. *J. Power Sources* **2012**, *213*, 180−185.

(24) Cao, W. J.; Li, Y. X.; Fitch, B.; Shih, J.; Doung, T.; Zheng, J. Strategies to optimize lithium-ion supercapacitors achieving high-performance: Cathode configurations, lithium loadings on anode, and types of separator. *J. Power Sources* **2014**, *268*, 841−847.

(25) Sun, X.; Zhang, X.; Wang, K.; An, Y.; Zhang, X.; Li, C.; Ma, Y. Determination strategy of stable electrochemical operating voltage window for practical lithium-ion capacitors. *Electrochim. Acta* **2022**, *428*, No. 140972.

(26) Song, S.; Zhang, X.; Li, C.; Wang, K.; Sun, X.; Ma, Y. Anomalous diffusion models in frequency-domain characterization of lithium-ion capacitors. *J. Power Sources* **2021**, *490*, No. 229332.

(27) Babu, B.; Neumann, C.; Enke, M.; Lex-Balducci, A.; Turchanin, A.; Schubert, U. S.; Balducci, A. Aging processes in high voltage lithium-ion capacitors containing liquid and gel-polymer electrolytes. *J. Power Sources* **2021**, *496*, No. 229797.

(28) Piwek, J.; Platek, A.; Frackowiak, E.; Fic, K. Mechanisms of the performance fading of carbon-based electrochemical capacitors operating in a LiNO3 electrolyte. *J. Power Sources* **2019**, *438*, No. 227029. ARTN 227029

(29) Platek, A.; Piwek, J.; Fic, K.; Frackowiak, E. Ageing mechanisms in electrochemical capacitors with aqueous redox-active electrolytes. *Electrochim. Acta* **2019**, *311*, 211−220.

(30) Zallouz, S.; Le Meins, J. M.; Ghimbeu, C. M. Alkaline hydrogel electrolyte from biosourced chitosan to enhance the rate capability and energy density of carbon-based supercapacitors. *Energy Adv.* **2022**, *1* (12), 1051−1064.

(31) Balducci, A.; Belanger, D.; Brousse, T.; Long, J. W.; Sugimoto, W. Perspective—A Guideline for Reporting Performance Metrics with Electrochemical Capacitors: From Electrode Materials to Full Devices. *J. Electrochem. Soc.* **2017**, *164* (7), A1487−A1488.

(32) Weingarth, D.; Foelske-Schmitz, A.; Kötz, R. Cycle versus voltage hold − Which is the better stability test for electrochemical double layer capacitors? *J. Power Sources* **2013**, *225*, 84−88.

(33) Zhao, J.; Burke, A. F. Review on supercapacitors: Technologies and performance evaluation. *J. Energy Chem.* **2021**, *59*, 276−291.

(34) Rizoug, N.; Bartholomeus, P.; Moigne, P. L. Study of the Ageing Process of a Supercapacitor Module Using Direct Method of Characterization. *IEEE Trans. Energy Convers.* **2012**, *27* (2), 220−228.

(35) Zhao, L.; Watanabe, I.; Doi, T.; Okada, S.; Yamaki, J.-i. TG-MS analysis of solid electrolyte interphase (SEI) on graphite negative-electrode in lithium-ion batteries. *J. Power Sources* **2006**, *161* (2), 1275−1280.

(36) Jagiello, J.; Olivier, J. P. 2D-NLDFT adsorption models for carbon slit-shaped pores with surface energetical heterogeneity and geometrical corrugation. *Carbon* **2013**, *55*, 70−80.

(37) Jagiello, J.; Olivier, J. P. Carbon slit pore model incorporating surface energetical heterogeneity and geometrical corrugation. *Adsorption* **2013**, *19* (2−4), 777−783.

(38) Ghimbeu, C. M.; Gadiou, R.; Dentzer, J.; Schwartz, D.; Vix-Guterl, C. Influence of surface chemistry on the adsorption of oxygenated hydrocarbons on activated carbons. *Langmuir* **2010**, *26* (24), 18824−18833.

(39) Lou, S.; Liu, Q.; Zhang, F.; Liu, Q.; Yu, Z.; Mu, T.; Zhao, Y.; Borovilas, J.; Chen, Y.; Ge, M.; Xiao, X.; Lee, W.; Yin, G.; Yang, Y.; Sun, X.; Wang, J. Insights into interfacial effect and local lithium-ion transport in polycrystalline cathodes of solid-state batteries. *Nat. Commun.* **2020**, *11* (1), No. 5700.

(40) Bolli, C.; Guéguen, A.; Mendez, M. A.; Berg, E. J. Operando Monitoring of F-Formation in Lithium Ion Batteries. *Chem. Mater.* **2019**, *31* (4), 1258−1267.

(41) Matei Ghimbeu, C.; Vidal, L.; Delmotte, L.; Le Meins, J.-M.; Vix-Guterl, C. Catalyst-free soft-template synthesis of ordered mesoporous carbon tailored using phloroglucinol/glyoxylic acid environmentally friendly precursors. *Green Chem.* **2014**, *16* (6), 3079−3088.

(42) Matei Ghimbeu, C.; Guerin, K.; Dubois, M.; Hajjar-Garreau, S.; Vix-Guterl, C. Insights on the reactivity of ordered porous carbons exposed to different fluorinating agents and conditions. *Carbon* **2015**, *84*, 567−583.

(43) Dedryvère, R.; Gireaud, L.; Grugeon, S.; Laruelle, S.; Tarascon, J. M.; Gonbeau, D. Characterization of lithium alkyl carbonatesby X-ray photoelectron spectroscopy: experimental and theoretical study. *J. Phys. Chem. B* **2005**, *109* (33), 15868−15875.

(44) Peled, E.; Menkin, S. Review—SEI: Past, Present and Future. *J. Electrochem. Soc.* **2017**, *164* (7), A1703.

(45) Adenusi, H.; Chass, G. A.; Passerini, S.; Tian, K. V.; Chen, G. Lithium Batteries and the Solid Electrolyte Interphase (SEI)—Progress and Outlook. *Adv. Energy Mater.* **2023**, *13* (10), No. 2203307.

(46) Li, J.; Ji, Y.; Song, H.; Chen, S.; Ding, S.; Zhang, B.; Yang, L.; Song, Y.; Pan, F. Insights Into the Interfacial Degradation of High-Voltage All-Solid-State Lithium Batteries. *Nano-Micro Lett.* **2022**, *14* (1), 191.

(47) Guéguen, A.; Streich, D.; He, M.; Mendez, M.; Chesneau, F. F.; Novák, P.; Berg, E. J. Decomposition of LiPF6 in High Energy Lithium-Ion Batteries Studied with Online Electrochemical Mass Spectrometry. *J. Electrochem. Soc.* **2016**, *163* (6), A1095−A1100.

(48) Figueiredo, J. L.; Pereira, M. F. R.; Freitas, M. M. A.; Orfao, J. J. M. Modification of the surface chemistry of activated carbons. *Carbon* **1999**, *37* (9), 1379−1389. DOI:

(49) Brender, P.; Gadiou, R.; Rietsch, J. C.; Fioux, P.; Dentzer, J.; Ponche, A.; Vix-Guterl, C. Characterization of carbon surface chemistry by combined temperature programmed desorption with in situ X-ray photoelectron spectrometry and temperature programmed desorption with mass spectrometry analysis. *Anal. Chem.* **2012**, *84* (5), 2147−2153.

(50) Moussa, G.; Ghimbeu, C. M.; Taberna, P. L.; Simon, P.; Vix-Guterl, C. Relationship between the carbon nano-onions (CNOs) surface chemistry/defects and their capacitance in aqueous and organic electrolytes. *Carbon* **2016**, *105*, 628−637.

(51) Eleri, O. E.; Azuatalam, K. U.; Minde, M. W.; Trindade, A. M.; Muthuswamy, N.; Lou, F.; Yu, Z. Towards high-energy-density supercapacitors via less-defects activated carbon from sawdust. *Electrochim. Acta* **2020**, *362*, No. 137152.

(52) Edge, J. S.; O'Kane, S.; Prosser, R.; Kirkaldy, N. D.; Patel, A. N.; Hales, A.; Ghosh, A.; Ai, W.; Chen, J.; Yang, J.; Li, S.; Pang, M.; Diaz, L. B.; Tomaszewska, A.; Marzook, M. W.; Radhakrishnan, K. N.; Wang, H.; Patel, Y.; Wu, B.; Offer, G. J. Lithium ion battery degradation: what you need to know. *Phys. Chem. Chem. Phys.* **2021**, *23* (14), 8200−8221. 10.1039/D1CP00359C

(53) Couzi, M.; Bruneel, J. L.; Talaga, D.; Bokobza, L. A multi wavelength Raman scattering study of defective graphitic carbon materials: The first order Raman spectra revisited. *Carbon* **2016**, *107*, 388−394.

(54) Bokobza, L.; Bruneel, J. L.; Couzi, M. Raman Spectra of Carbon-Based Materials (from Graphite to Carbon Black) and of Some Silicone Composites. *C* **2015**, *1* (1), 77−94.

(55) Lux, S. F.; Lucas, I. T.; Pollak, E.; Passerini, S.; Winter, M.; Kostecki, R. The mechanism of HF formation in LiPF6 based organic carbonate electrolytes. *Electrochem. Commun.* **2012**, *14* (1), 47−50.

Supporting Information

for

Identifying the activated carbon electrode ageing pathways in lithium-ion hybrid capacitors

Sylwia Slesinska[1], Bénédicte Réty[2,3,4], Camélia Matei-Ghimbeu[2,3,4], Krzysztof Fic[1], Jakub Menzel[1*]*

[1] Institute of Chemistry and Technical Electrochemistry, Poznan University of Technology, Berdychowo 4, 60-965 Poznan, Poland
[2] Institut de Science des Matériaux de Mulhouse (IS2M), Université de Haute-Alsace, CNRS UMR 7361, F-68100 Mulhouse, France;
[3] Université de Strasbourg, F67081 Strasbourg, France;
[4] Réseau sur le Stockage Electrochimique de l'Energie (RS2E), CNRS FR3459, 80039 Amiens Cedex, France

*Corresponding authors
jakub.menzel@put.poznan.pl, camelia.ghimbeu@uha.fr
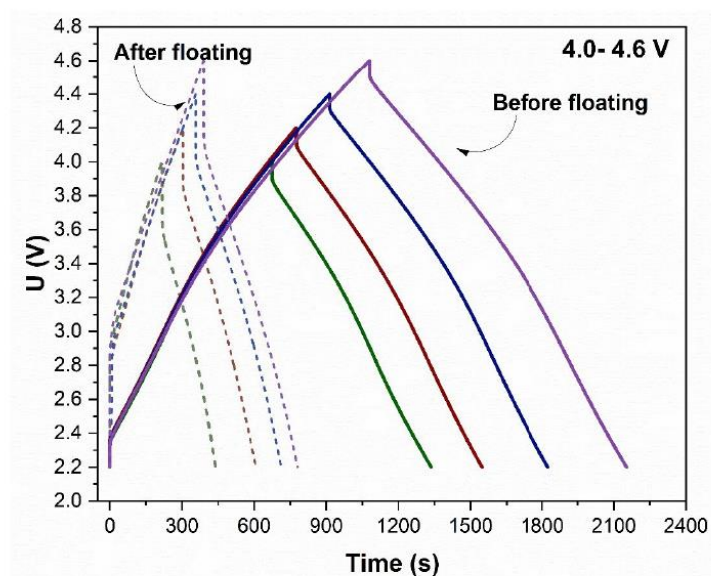
Figure S1 Charge/discharge curves before and after floating for systems 4.0- 4.6 V.
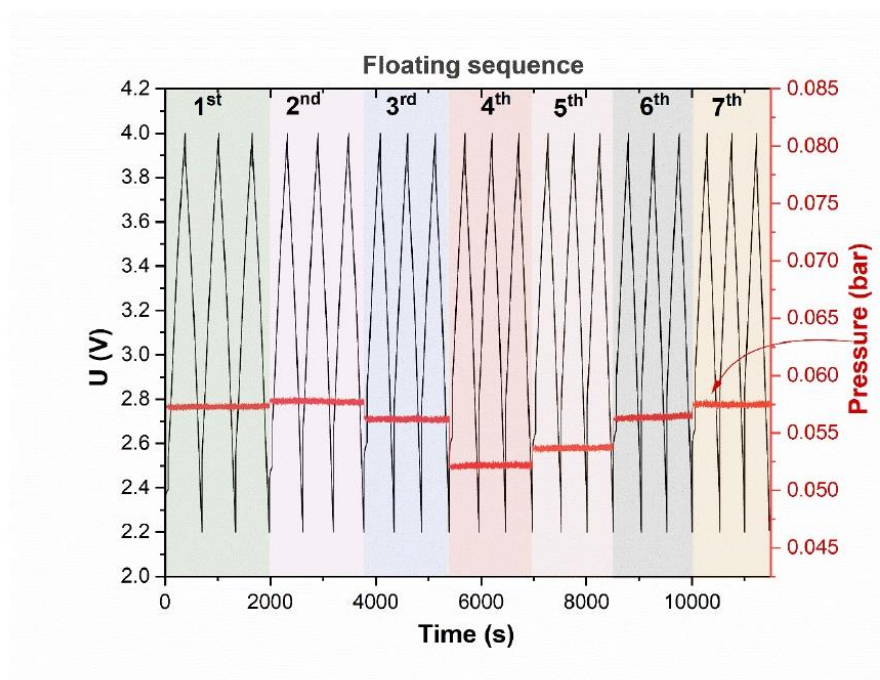
Figure S2 Operando pressure measurement during charge/discharge recorded after the first 7 floating sequences at 4V.
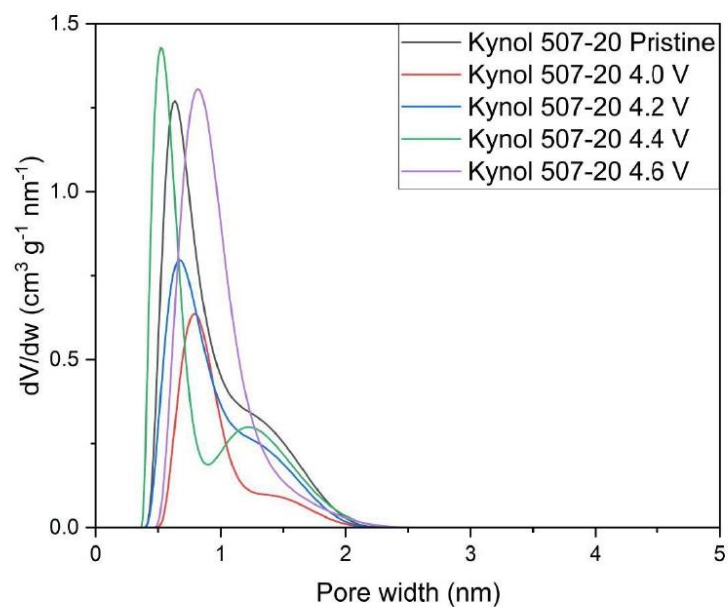
Figure S3 Pore size distribution for pristine carbon cloth and the positive electrodes after the floating test at various voltages (4V – 4.6V)
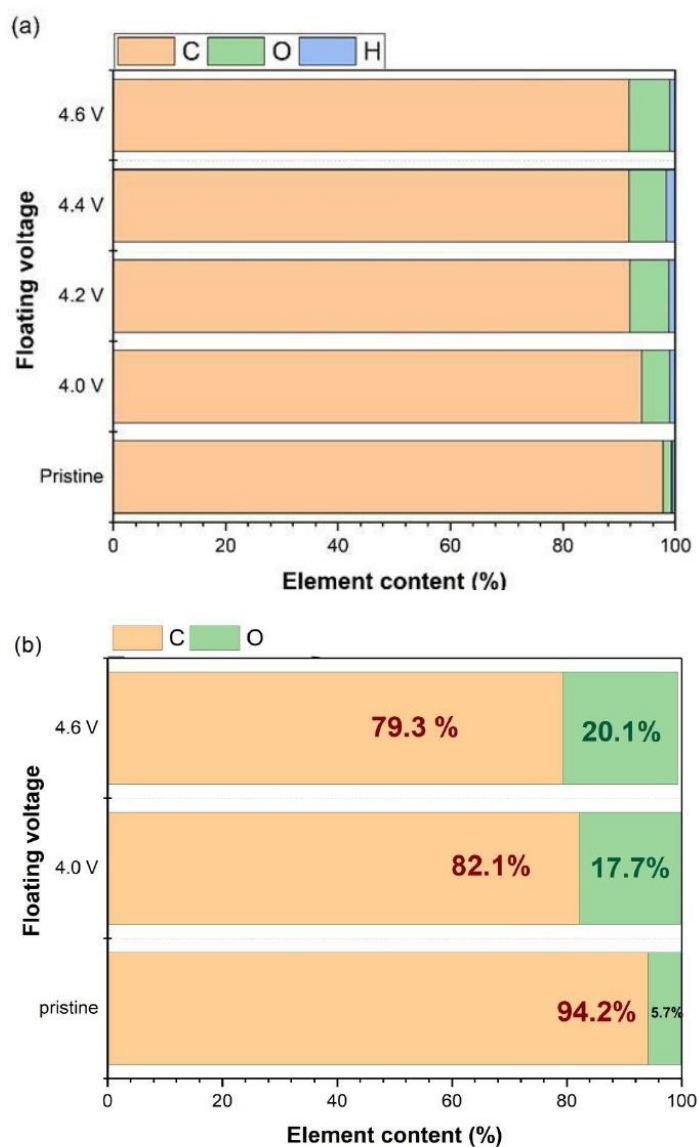
Figure S4 Elemental compositions of the positive electrodes after the floating test at various voltages compared to that of the carbon cloth before ageing, (a) from elemental analysis at 4.0– 4.6 V , (b) from XPS at 4.0 and 4.6 V.
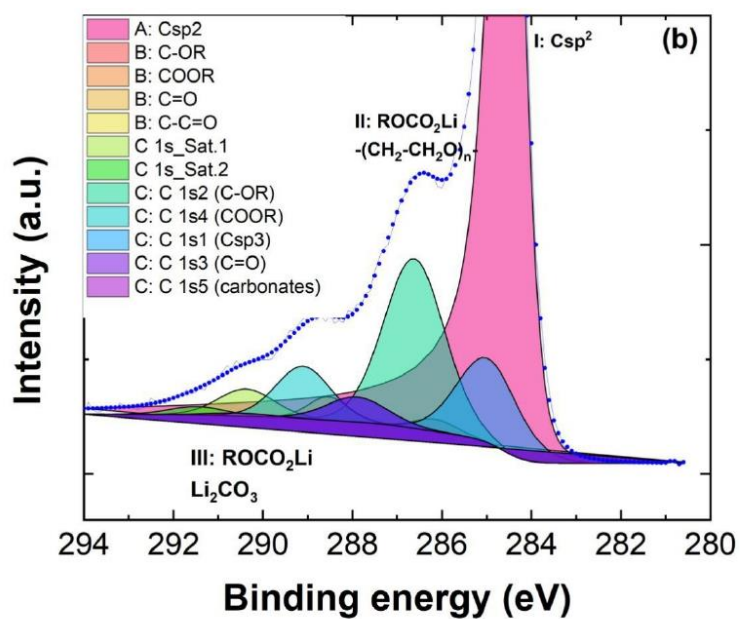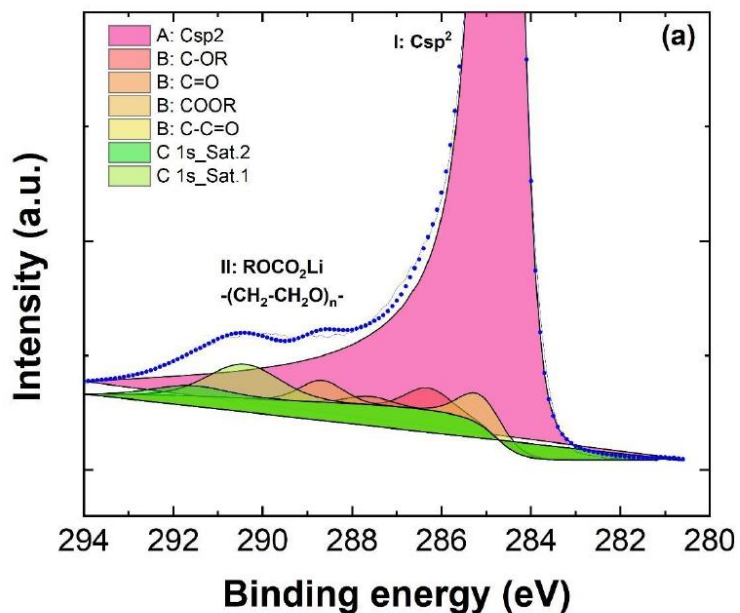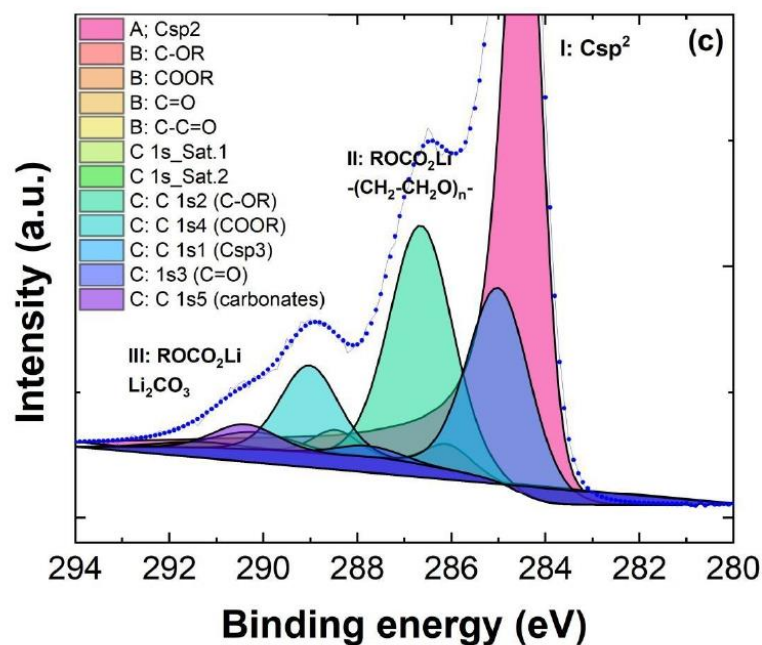
Figure S5 Deconvoluted XPS C1s spectra for a) pristine carbon; b) carbon electrode after aging at 4.0 V; c) carbon electrode after aging at 4.6 V; I corresponds to C sp^2, II corresponds to C-OR, COOR, C=O, and C-C=O bonded to C sp^2, and III corresponds to C-OR, COOR, C=O, C sp^3, and carbonate fractions
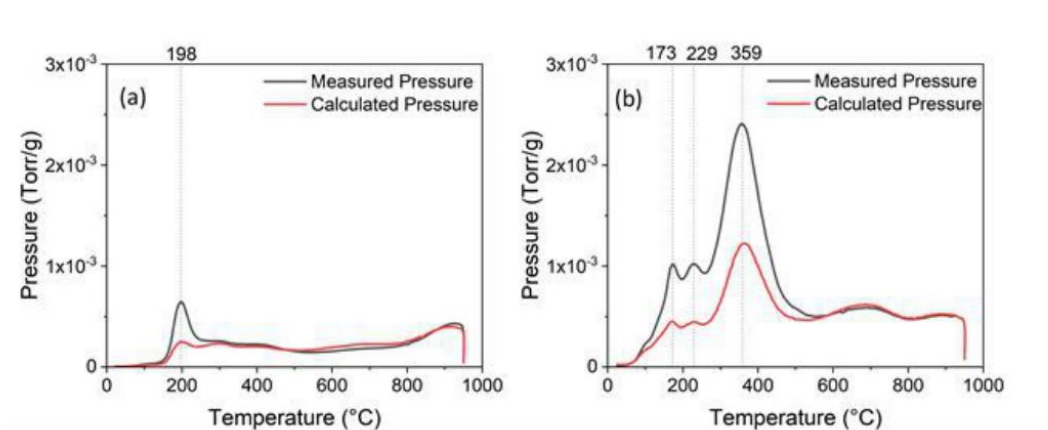
Figure S6 TPD-MS Pressure profiles (a) Pristine and (b) 4.6V electrodes

(a)

(b)

(c)

(d)
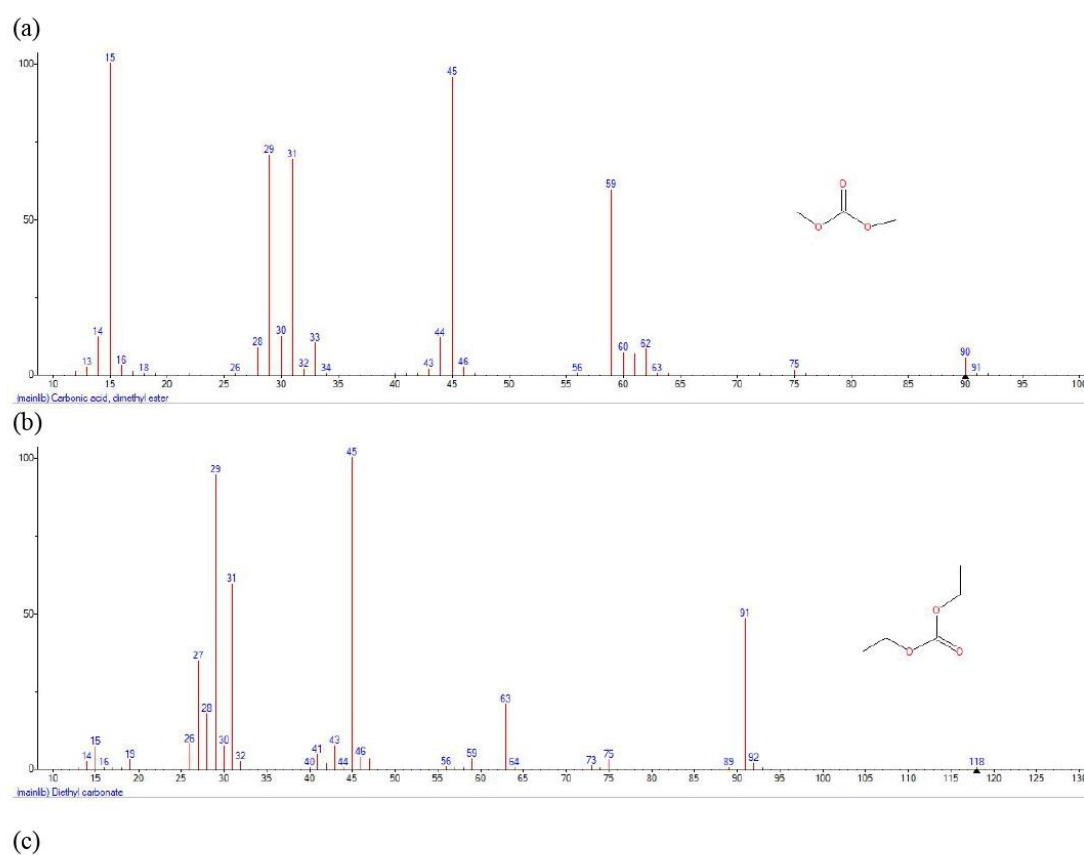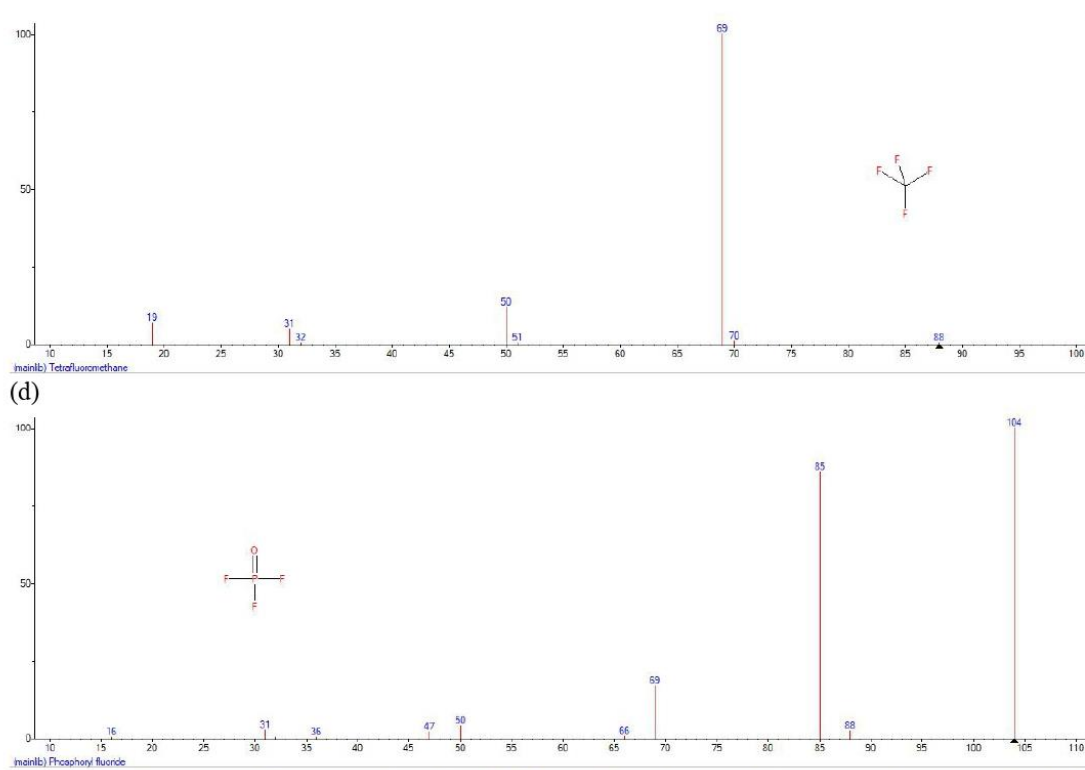
Figure S7 - Theoretical MS spectra from NIST MS Search data base (a) Dimethyl carbonate, (b) Diethyl carbonate, (c) CF_4, (d) POF_3

S8

A1. *The Oxygen Enigma: Deciphering the Role of Carbon Surface Functionalities on Degradation at Electrified Interfaces*

**Authors: Sylwia Slesinska,** Bénédicte Réty, Camélia Matei-Ghimbeu, Samar Hajjar Garreau, Krzysztof Fic, Jakub Menzel

Status: In review

DOI: -

Licence: -

Contribution: Conceptualization, visualization, formal analysis, methodology, investigation: electrochemical analysis, floating measurements, electrode and electrolyte preparation, elemental analysis, operando GC-MS investigation and data collection, TPD-MS and Raman Spectroscopy data measurements, data collection and curation, writing-original draft.

Graphical abstract:
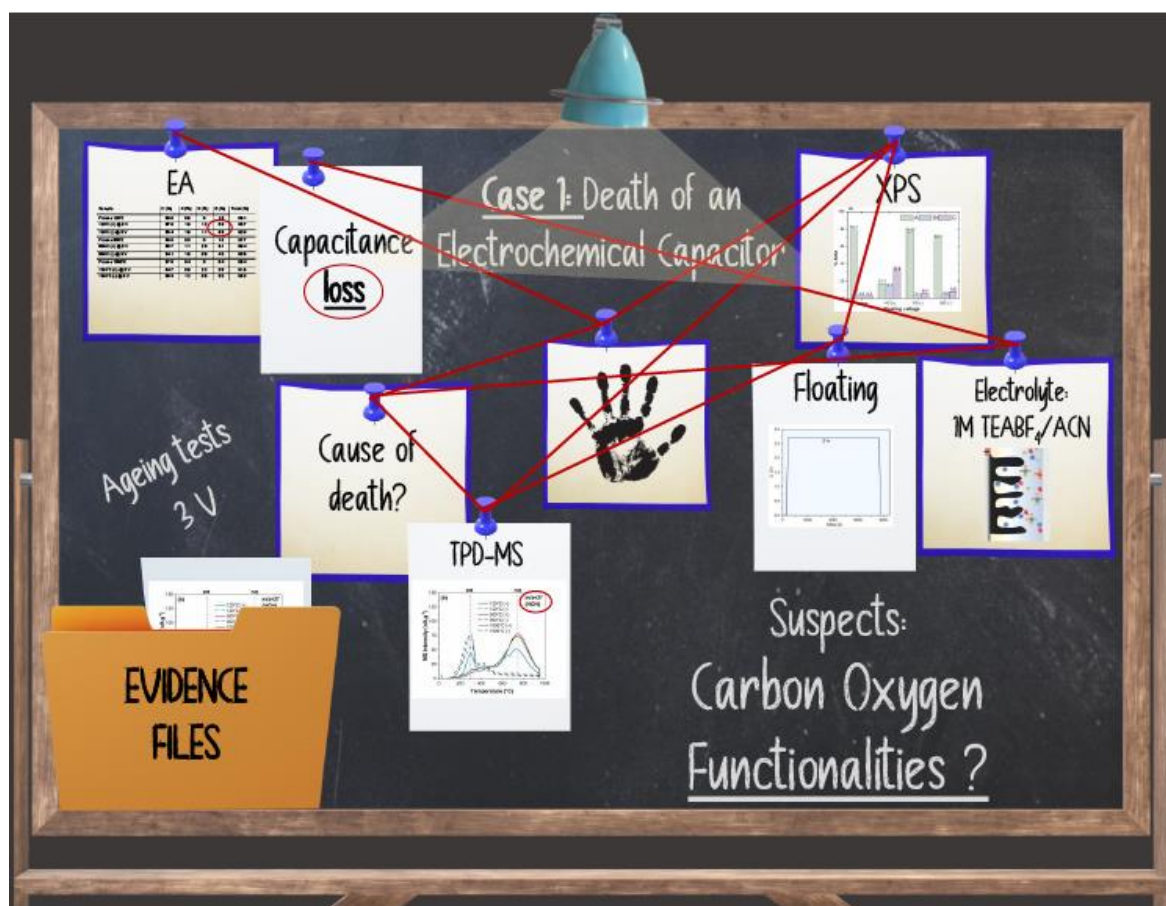
Motivation and Summary

Without systematic ageing studies, the long-term viability and performance limitations of energy storage technologies would remain poorly understood, hindering the development of more durable and reliable devices used for various applications.

EC aging in organic electrolytes, particularly those with AN, has been already shown to be primarily driven by the positive electrode's degradation. This degradation stems from interactions between the AN solvent and oxygen functionalities on the carbon surface, the binder, or/and trace water remains. Therefore, these interactions can lead to the oxidation of surface functionalities on the AC electrode. However, there exists no universal explanation applicable to all electrochemical systems; an individual approach is advised based on the lone complexity of the undergoing chemistries. The following study therefore focuses in more detail, on the specific role of **oxygen functionalities** on the ageing of **binder-free** AC electrodes in an EC under **high voltage** regime (3 V) operating in 1 mol L^{-1} TEABF$_4$/AN electrolyte. Floating protocol was employed to promote faster degradation. This is accompanied by comprehensive *post-mortem* analyses (TPD-MS, Porosity measurements, EA, XPS, Raman Spectroscopy) of both positive and negative electrodes, to elucidate the causes behind the performance fade in the studied systems. The findings suggest that the **type** of oxygenated functionalities on the carbon electrode surface plays a more significant role in dictating accelerated degradation pathways than their overall quantity. Notably, the presence of acidic functionalities appeared to induce the formation of a protective polymer-like layer on the electrode surface, contributing to a longer operational lifespan. It was also evidenced the complete elimination of carbon oxygen functionalities seemed to promote faster degradation. Consequently, increased electrode oxidation, pore blockage, and a reduction in the specific surface area of the carbon electrodes, with the positive electrode showing greater susceptibility to these degradation mechanisms was observed. Based on these findings, the conclusion advocating for "tailored functionalization" is put forward, where specific properties that enhance stability and longevity ultimately leading to more robust and efficient energy storage solutions can be employed.

The Oxygen Enigma: Deciphering the Role of Carbon Surface Functionalities on Degradation at Electrified Interfaces

Sylwia Slesinska[1*], Bénédicte Réty[2,3,4], Camélia Matei Ghimbeu[2,3,4*], Samar Hajjar Garreau[2,3,4], Krzysztof Fic[1], Jakub Menzel[1*]

[1] Institute of Chemistry and Technical Electrochemistry, Poznan University of Technology, Berdychowo 4, 60-965 Poznan, Poland

[2] Institut de Science des Matériaux de Mulhouse (IS2M), Université de Haute-Alsace, CNRS UMR 7361, F-68100 Mulhouse, France;

[3] Université de Strasbourg, F67081 Strasbourg, France;

[4] Réseau sur le Stockage Electrochimique de l'Energie (RS2E), CNRS FR3459, 80039 Amiens Cedex, France

*Corresponding author: sylwia.slesinska@put.poznan.pl, jakub.menzel@put.poznan.pl, camelia.ghimbeu@uha.fr

Abstract

An explanation of ageing failure mechanisms in Electrochemical Capacitors (ECs) under various testing regimes, including high voltage, is an imperative step that can provide long-term operation and future optimization of their performance. Our study elaborates on the ageing mechanisms and the role of oxygen functionalities of three types of binder-free carbon electrode materials, thermally treated at 120℃, 500℃ and 1000℃, operating in 1 mol L^{-1} TEABF$_4$ in acetonitrile (AN). The studied systems followed a floating protocol at 3 V, after which series of post-mortem analyses of positive and negative carbon electrodes were carried out. It seems that the type rather than the total amount of oxygenated functionalities on the carbon electrode directs the accelerated degradation pathways. The presence of acidic functionalities induce the formation of protective polymer-like layer on the surface, whilst complete elimination of carbon oxygen functionalities promotes faster degradation. The system with electrodes thermally treated at 500℃ is characterised by the worst electrochemical performance, withstanding 714h of floating regime (compared to 1086h with electrodes treated at 120℃) and gradual increase in resistance over time. It is assumed that N- selectivity is of key importance here, with CO releasing groups promoting it. Ultimately the decomposition of the electrolyte is more pronounced, as observed via temperature-programmed desorption mass spectrometry (TPD-MS). This leads to oxidation, pore blockage and decrease of specific surface area of the carbon electrodes, where the positive electrode is more affected by the degradation mechanisms.

Keywords: supercapacitor, carbon electrode, oxygen surface functionalities, organic electrolyte, floating ageing

1. Introduction

In the fast-pacing and constantly growing modern global market, especially as a consumer, we demand energy storage devices that will fulfil basic requirements: reliability, inexpensiveness, safety, and eco-consciousness. After all, our dependancy on these devices has increased over the decades, with them "powering" our everyday lives. However, higher dependency generates higher expectations; aimed towards improved performance of such devices, only to become the main focus in the current research and development areas. Amongst those, electrochemical capacitors (ECs) have played an increasing role for high-power applications, owing to their high power density and superior cyclability (>10^6 charge–discharge cycles).[1-3][1-3] However, compared to lithium-ion batteries (LiBs), which without a doubt dominate the actual market, ECs suffer from a low specific energy [4]. Therefore, it is necessary to consider the means of increasing their specific capacitance and/or cell voltage for improved energy,[4,5] according to the equation:

$$E = \frac{1}{2}CU^2 \qquad\qquad (1)$$

with energy (E) proportional to capacitance (C) and squared voltage (U).[6] Thus, electrolytes with wide electrochemical stability window, such as thosed based on organic solutions (2.7 – 3.0 V) are preferred over aqueous electrolytes (0.8- 1.0 V).[7-9]

Regardless of the electrolyte used, all ECs suffer from performance loss over time. Work focused on the application of new materials and establishment of their stability based on various standards and qualitative tests is a key for efficient and improved ECs technologies. However, one cannot neglect the associated aspect of degradation studies. These are equally as important and can shine a better light on the system behaviour under specified conditions for future improvement of such devices.

Because of different charge storage mechanisms, compositions and stability limits of materials used, it is rather difficult to describe a universal ageing proccess for all ECs. Therefore, each system is adviced to be treated individually due to its complex nature. Additionally, the operating conditions need to be considered; such as voltage, temperature and current applied, all of which have a important effect on the rate of

ageing.[10] It is assumed that both temperature and voltage might trigger electrochemical reactions associated with decomposition: the energy necessary to reach the activation energiesof such parasitic reactions is obtained in both cases.[11] The latter is also characterised by much more pronounced electric field,[12,13] causing higher attraction of counter ions towards electrodes during polarisation.

Cell ageing studies in organic electrolytes have been widely investigated in the past, [14-22]. The main causes of ageing in systems containing acetonitrile (AN), have been reported to be due to interactions between the solvent and the oxygen functionalities on the carbon surface, the binder, and/or trace water molecules.[14,16,23,24] In all cases, the positive electrode was found to be more degraded than the negative one, and to be the main driving force of the ageing observed in AN based ECs. [22,25] The issue seems to point towards the content of the surface functionalities on the AC electrode, which can oxidise and form new functionalities.[14,16] However, presence of acidic functionalities was found to aid in protection of carbon surface and further structural changes by formation of a polymer layer on both positive and negative electrodes, as reported by *Liu et al..* This study is an extension to their previous work in which the same systems were analysed by Electrochemical Impedance Spectroscopy (EIS) and diffusion coefficient calculations with some additional anaytical techniques. Two different ageing mechanisms were reported during contstant potential holding at 2.5 V depending on the activated carbon electrode material: commercial microporous carbon (YP-50F) and micro-meso porous carbon used for water purification applications. It was the latter that exhibited a gradual increase in the equivalent series resistance (ESR) and was then linked to formation of ion-conductive protective layer. Additionally, a decrease in porosity, formation of surface defects and pore clogging were reported, which can led to decrease in capacitance and increase in resistance over time. Degradation of the carbon electrodes in aqueous media is characterised by similar phenomena.[26-30]

Most recenty, various operando techniques such as operando temperature dynamic investigations and operando gas chromatography-mass spectrometry (GC-MS) have helped to gain new insights into degradation proccesses of AN based ECs and identification of their optimal operational conditions. [22,31] With the use of the latter, Kreth et al. have shown that the degradation of the solvent is strongly affected by the

surface chemistry of the respective electrode in organic medium, thus it seems to be an important aspect that needs to be considered in subsequent ageing studies and future optimisation of the device.

However, most of the mentioned studies implement a binder, which can inevitably lead to difficult data interpretation and quantification, as previously highlighted by Pourhosseini *et al.* concerning gaseous decomposition by-products of polytetrafluoroethylene (PTFE) during temperature-programmed desorption (TPD) analysis that can overlap with the profiles of those related with decomposition of oxygen functional groups on carbon.[9] Moreover, parasitic reactions at high voltage might differ between binder containing and binder-free electrodes, due to varying amount and types of surface active sites for both.

Herein, we present a study based on ageing phenomena observed for symmetric ECs with binder-free Activated Carbon Cloth (ACC) Kynol® 507-20 electrodes in 1 mol L^{-1} TEABF$_4$ in AN floated at 3.0 V, where the oxygen content for the carbon electrodes was tunned by thermal treatment at 120, 500, and 1000°C. Additionally, the elimination of binder allowed to focus solely on interaction between the electrodes and electrolyte solution from a more fundamental perspective. Ultimately, it allowed for detailed relationship to be established and elaborated, where the effect of oxygen functionalities on ageing at high voltage is discussed.

2. Experimental

2.1. Electrodes and electrochemical cell preparation

Carbon material, namely binder-free Activated Carbon Cloth (ACC Kynol® 507-20 (Germany) was thermally treated in a furnace under a nitrogen atmosphere at different temperatures, namely: 120, 500, and 1000°C. The purpose of this treatment was to investigate the effect of the presence/absence of oxygen functional groups on the surface of carbon. The use of ACC allowed us to exclude the influence of binders on ageing in organic based capacitor. The material was cut into circular self-standing electrodes (Ø = 16 mm) and assembled in a two-electrode ECC-Ref cells (El-Cell®, Germany) separated by a GF-D porous membrane (Whatman®, UK). The systems with

these carbon materials as electrodes are simply referred to as 120°C, 500°C, and 1000°C in the remainder of the article.

TEABF$_4$ (tetraethylammonium tetrafluoroborate) salt (purity ≥99,5% Sigma-Aldrich®; USA) and ACN (acetonitrile) (Sigma-Aldrich®; USA) were used to prepare 1 mol L^{-1} solution of TEABF$_4$/ACN and its water content was determined by the Karl-Fisher method (~50ppm).

After ageing experiments, the positive and negative electrodes were removed and washed in ACN and dried at 100°C in a vacuum overnight to remove physisorbed species.

2.2. Electrochemical Investigation

Electrochemical measurements were performed on a multichannel potentiostat/galvanostat (VMP3, Biologic®, France). Electrochemical analyses can help to determine the electrochemical cell performance before and after accelerated degradation of the electrochemical cell in organic medium.

Firstly, each system was subjected to a series of preliminary electrochemical tests for qualitative assessment by: cyclic voltammetry (CV) at 10 mV s^{-1} and galvanostatic charge/discharge with a current load of 1 A g^{-1}, followed by the floating protocol consisting of, i.e., potentiostatic hold at maximum ECs operation voltage at 3 V for symmetric capacitors for the duration of 2h. According to the international standard (IEC 62391-1), system failure is reported when the initial capacitance drops below 80% of its initial value; thus floating experiments were halted after that value was reached for each system or when the resistance of the cell doubled in value. Other techniques: CV at 10 mV s^{-1} and Current Interrupt (CI) at 1 A g^{-1} were included between each floating, to monitor additional parameters such as cell resistance during accelerated ageing. This allows the systems to be characterized both qualitatively and quantitatively. Specific capacitance values have been calculated from each galvanostatic discharge curve (its integral values) and were expressed per mass of one electrode, whereas specific energy values are expressed per system.

2.3. GC-MS

The evolution of gases during capacitor operation was monitored in a two- electrode PAT-Cell-Gas (El-Cell) in an online mode using gas chromatography-coupled mass spectrometry (GC-MS, Bruker) where positive and negative electrode are analysed separately. The monitored mass was M/z = 44, assigned to carbon dioxide (CO_2). Electrochemical technique consisted of three cycles of CV at $1 \, m \, s^{-1}$ at 2.7 V and 3 V.

2.4. Elemental analysis

The determination of the mass fractions of carbon, hydrogen, nitrogen, and oxygen was carried out with ThermoFisher Scientific® FlashSmart™ (USA) equipment. The amount of oxygen was obtained through direct (separate) elemental analysis. The results presented in this paper are the average value of three separate analyses.

2.5. X-ray photoelectron spectroscopy (XPS)

To analyse and quantify the surface functionalities on carbon surface, high resolution X-ray Photoelectron Spectroscopy (XPS) data were obtained on a VG SCIENTA 2002 spectrometer (Uppsala, Sweden) equipped with a monochromatic Al Kα X-ray source (Al Kα = 1486.6 eV) and a hemispherical analyzer (Uppsala, Sweden). Wide scan (survey) spectra and the high-resolution spectra (C1s, O1s, and N1s) were recorded with a pass energy of 500 eV and 100 eV, respectively. The peaks were fitted by Gaussian-Lorentzian functions using the CASAXPS software (casaXPS software 2.3.18 Ltd., Teignmouth, UK) after having subtracted a Shirley-type background. All the binding energies (BE) are referenced to the C1s peak at Csp2 (284.5 eV).

2.6. Porosity analysis

The nitrogen adsorption/desorption isotherms of the activated carbon electrode before and after aging were recorded using an ASAP 2460 analyzer (Micromeritics®, USA) at 77 K. Prior to analysis, the samples were purged under helium flow for 24 h at 120°C and then placed under high vacuum for 5 h. The specific surface area (SSA) was calculated using the BET equation at relative pressure range (0.01 – 0.05). Micro volume values were determined using 2D nonlocal density functional theory (2D NLDFT) method using Carbon-N2-77, 2D-NLDFT Heterogeneous Surface Model.

2.7. Raman spectroscopy

Raman spectroscopy was performed with LabRAM BX40 (Horiba 300) Raman microspectrometer with a laser emitting at λ = 532nm. Several spectra were measured and the results were analysed by Origin®2021 software. The peak positions and integration of the D/G bands were done by deconvolution of the experimental spectrum.

2.8. TPD-MS

TPD-MS allows for the determination and quantification of carbon electrode oxygenated surface groups,[14,32-34] the identification of species trapped into the sample porosity, or the detection of molecules adsorbed/deposited on the surface of the material. The samples are heated in a quartz tube furnace under secondary vacuum and the evolved gases are continuously analysed by mass spectrometry. Depending on the nature of the gases and the temperature at which they are released, it is possible to determine the carbon material surface functional groups. The measurements were carried out in a home-made set-up with a heating rate of 5°C min^{-1} from room temperature up to 950°C.

The total pressure of the gas released during heat treatment is measured over time. This total pressure is then compared with the sum of the partial pressures of the calibrated gases (CO (m/z=28), CO_2 (m/z=44), H_2O (m/z=18), H_2 (m/z=2), whose calibration is performed prior to the analysis. The pressure profile measured by the gauge and the pressure profile recalculated from the partial pressures overlap if the gases released during the measurement only are calibrated gases. On the contrary, when a difference between the two pressure profiles (measured and calculated) is observed, it indicates the presence of one or several non-calibrated gases. [35]

3.   Results and discussion

3.1. Physicochemical characterization of the pristine materials

After were thermally treated, they were analysed by elemental analysis (EA) to verify their oxygen content; that is, to indicate the successful removal of carbon oxygen functionalities. The oxygen content was determined to be: 1.5%, 1.2%, and 0.4% for

pristine 120, 500, and 1000°C thermally treated ACC Kynol® 507-20 respectively, thus decreasing as desired (Table 1). The carbon content increases, in particular at 1000°C.

Table 1. Chemical composition determined by elemental analysis for pristine electrodes

Sample	C (%)	H (%)	N (%)	O (%)	Total (%)
Pristine 120°C	96.0	0.6	0	1.5	98.1
Pristine 500°C	96.0	0.5	0	1.2	97.7
Pristine 1000°C	97.6	0.4	0	0.4	98.4

The N_2 adsorption/desorption isotherms and pore size distributions (PSD) of the pristine materials are also included (Figure 1). The electrode materials are characterized by a type I isotherm and a microporous texture with some additional contribution coming from the mesopores. The calculated specific surface area (S_{BET}) was similar for all the samples, with values of 1807, 1747 and 1748 $m^2\,g^{-1}$ for 120, 500, and 1000°C thermally treated ACC Kynol® 507-20 respectively, and a comparable V_{micro} of ~ 0.6 $cm^3\,g^{-1}$. The main peak in PSD corresponds to a pore width of 0.7 nm. This allowed to conclude that carbon porosity was not compromised with thermal treatment. The I_D/I_G ratio values are also included in Table 1, and were calculated via integration of the curves from the deconvoluted Raman spectra.[36,37] The Raman spectra fitting parameter = R^2 (to the Gaussian model) was 0.99, which is considered a good fitting value. The ratio of the intensity of D/G bands is a measure of the defects present on the graphene structure. The G band is the result of in-plane vibrations of sp^2 bonded carbon atoms, while the D band is due to out-of-plane vibrations attributed to the presence of structural defects in the sp^2 domains. All three pristine carbons are characterised by disordered structure, where defects are slightly minimised with an increase in treatment temperature, as the I_D/I_G value decreases from 1.45 to 1.20 for 120°C *vs.* 500°C. At 1000°C, defects seem to be re-formed with a value of 1.36, suggesting possible formation of new Csp^2 domains.
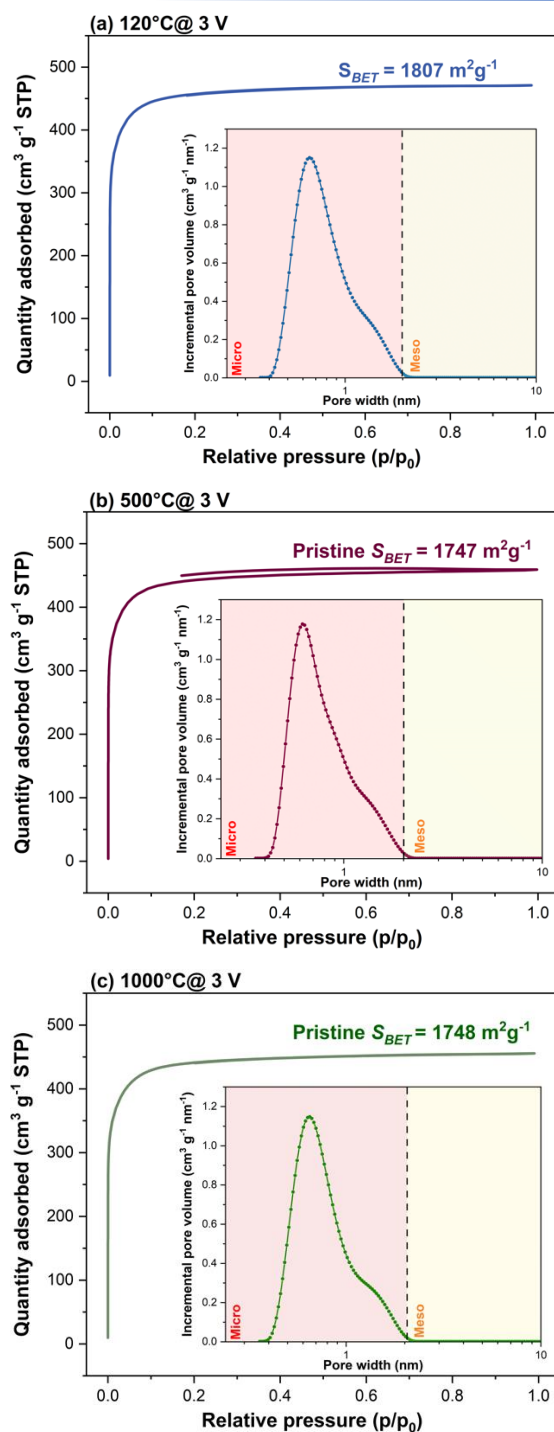
Fig.1. Nitrogen adsorption/desorption isotherms at 77 K and insets of pore size distribution (PSD) of pristine 120°C, 500°C and 1000°C ACC electrode materials

Table 2. S_{BET} values, their corresponding pore volume changes calculated from the 2D NLDFT model and I_D/I_G obtained from deconvolution of Raman spectra for the pristine 120°C 500°C and 1000°C ACC electrode materials

	Surface area	V_{micro} <2 nm	V_{meso} 2-50 nm	I_D/I_G
	$[m^2 \cdot g^{-1}]$	$[cm^3 \cdot g^{-1}]$	$[cm^3 \cdot g^{-1}]$	
Pristine 120°C	1807	0.660	0.004	1.45
Pristine 500°C	1747	0.655	0.002	1.20
Pristine 1000°C	1748	0.652	0.002	1.36

To obtain information about carbon oxygenated functionalities present in the pristine samples, TPD-MS analysis was carried out. The gas desorption rate profiles along with the total amount of each calibrated gases are shown in Figure 2. The desorption of CO_2 below 400°C can be due to the decomposition of carboxylic acid and anhydride surface groups. As expected, these functional groups are almost completely removed by heat treatments at 500°C and 1000°C. The CO profiles show the decomposition of phenol/ether above 600°C and carbonyl groups at higher temperature ≈ 850°C. These oxygenated surface groups are removed to a large extent with the 1000°C thermal treatment. At temperature higher than 800°C, a hydrogen release can be noticed, which can be due to the removal of edge H-terminated groups leading to the reorganization of the materials' structure as well. Figure 2 (d) shows that the amount of functional oxygen groups decreases with the temperature of thermal treatment and that 1000°C sample releases less hydrogen than the other two samples. The water content seems to be similar for all the samples.
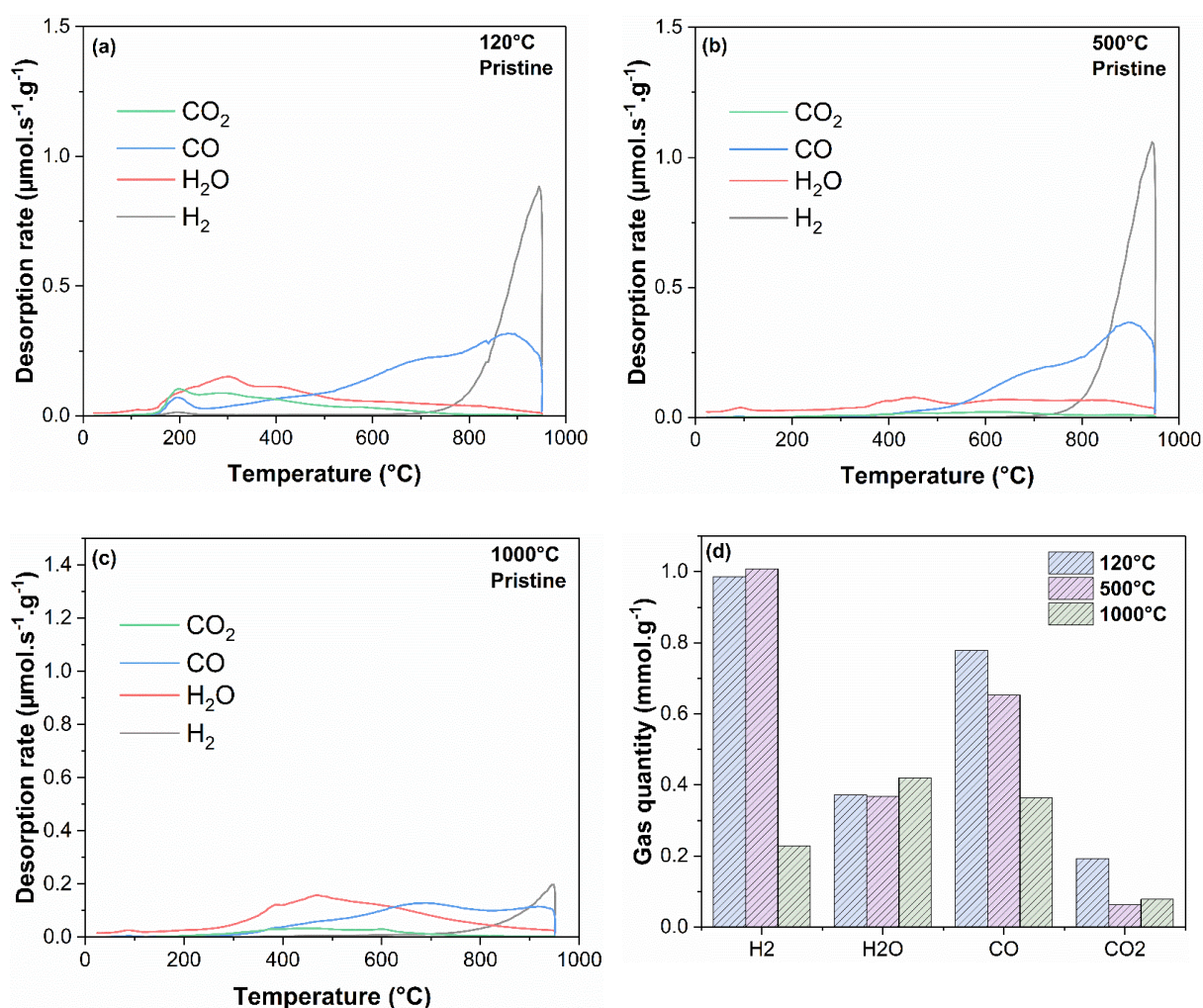
Figure 2. TPD-MS desorption rate profiles of the calibrated gases for the pristine materials thermally treated at (a) 120°C, (b) 500°C and (c) 1000°C and the total quantities of calibrated gases for these three samples

3.2. Electrochemical characterisation and *post-mortem* analyses

The long-term performance of the symmetric capacitors operating in 1 mol L^{-1} TEABF$_4$/ACN electrolyte was tested via potentiostatic hold i.e. *floating*. Each system was floated until the end-of-life criterion was reached (20% of the initial capacitance loss or 100% resistance increase according to the international standard (IEC 62391-1)).[38] Figure 3 (a) and (b) show both changes in relative capacitance with floating time and the corresponding increase in resistance with floating time at 3 V for each system tested, respectively. The highest longevity out of all systems was exhibited by 120°C, reaching

1086 h of floating time, while 500°C and 1000°C operated only for 714 h and 898 h, respectively. To qualitatively compare all systems, CV profiles at 5 mV s^{-1} have been recorded before and after floating (Figure S1). Prior to accelerated ageing, all the systems are characterised by a high degree of rectangularity, denoting a capacitive behaviour associated with EDL formation where most of the pores are accessible to the ions from the electrolyte. Values for specific capacitance and energy prior to *floating* are given in Table S1. After ageing, EDL traits are altered in all the systems, displayed by a loss in specific capacitance values as well as deviation from ideal 'capacitive' response (especially in the case of 500°C and 1000°C, more pronounced in the former). The main reasons for such behaviour are mostly likely pore-clogging, carbon oxidation and/or decomposition of electrolyte.
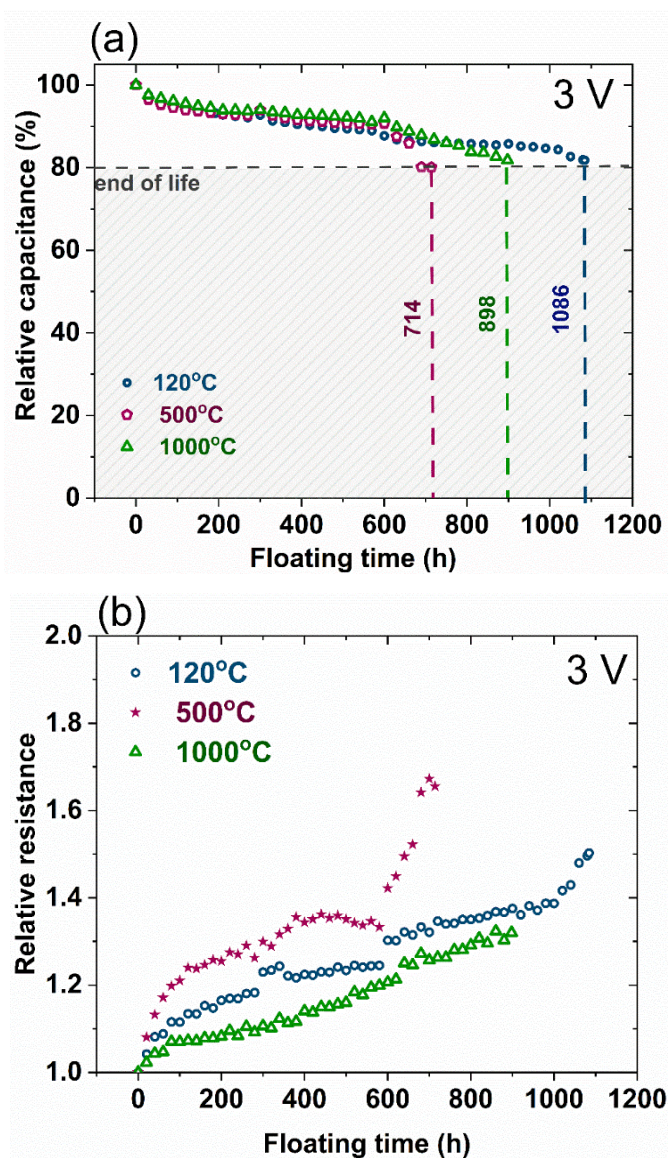
Figure 3. Results of the floating test with 1 mol L^{-1} TEABF$_4$/AN electrolyte at 3 V for (a) Relative capacitance vs. floating time and (b) relative resistance vs. floating time for various ACC electrode materials studied

Unlike previous assumptions, there is no clear trend to the ageing behaviour reported: the decrease in oxygen content of the carbon electrodes does not show a superior electrochemical performance, especially at such high voltage, where especially the electrolyte decomposition is more pronounced. This implies much more complex mechanisms taking place.

Neither of the systems reached their resistance end of life criterion, but a sharp increase in resistance was noted for 500°C after ~600 h of operating time. Also an onset of resistance increase is noted after ~1000h of floating time for 120°C. Evolution of gas can be assumed from the sudden change in linearity in resistance over the course of the floating protocol. This is due to the increase in pressure in the cell caused by the constant evolution and build-up of various gases, which ultimately improve adhesion of the electrodes to the current collectors.

During initial cycles, m/z= 44, most likely corresponding to CO_2 and $CH_3CH_2NH^+$ is detected at both positive and negative electrodes, but in greater extent at positive electrode, as shown in GC-MS profiles (Figure 4). It's important to note that the time of the gas evolution has been recalculated taking into account the gas detection delay during the experiment. The presence of this signal at the negative electrode is most likely a consequence of gas diffusion from positive electrode in the capacitor cell during measurements.[39] It was reported that the self-decomposition of electrolyte salt rather than that of a solvent is what typically contributes to the most gases in the initial state of charge.[40] In particular, decomposition of electrolyte TEA^+ species generates ethylene (m/z=28) and $CH_3CH_2NH^+$ (m/z=44).[14] The absolute amount of gas that is then evolved is strongly correlated with the materials used, that is, the surface functionalities found in AC samples which act as 'catalytic sites' or decompose themselves [41,42] In this context, CO_2 and CO are the by-products of oxidation of the surface functionalities (e.g., carboxyl, phenol, anhydride etc.), as seen when the maxima of the evolved gas peaks are reached upon charge. When the voltage of the cell is increased from 2.7 V to 3 V, the

intensity of the signals corresponding to the evolved gases also increases, proving higher reactivity and/or decomposition rate of the surface functional groups along with electrolyte decomposition. The signal response also changes depending on the electrode material used: for 120°C and 500°C, the m/z= 44 intensity is significantly greater than the one displayed by 1000°C, which seems reasonable since 1000°C contains much less oxygenated functional groups.[39]
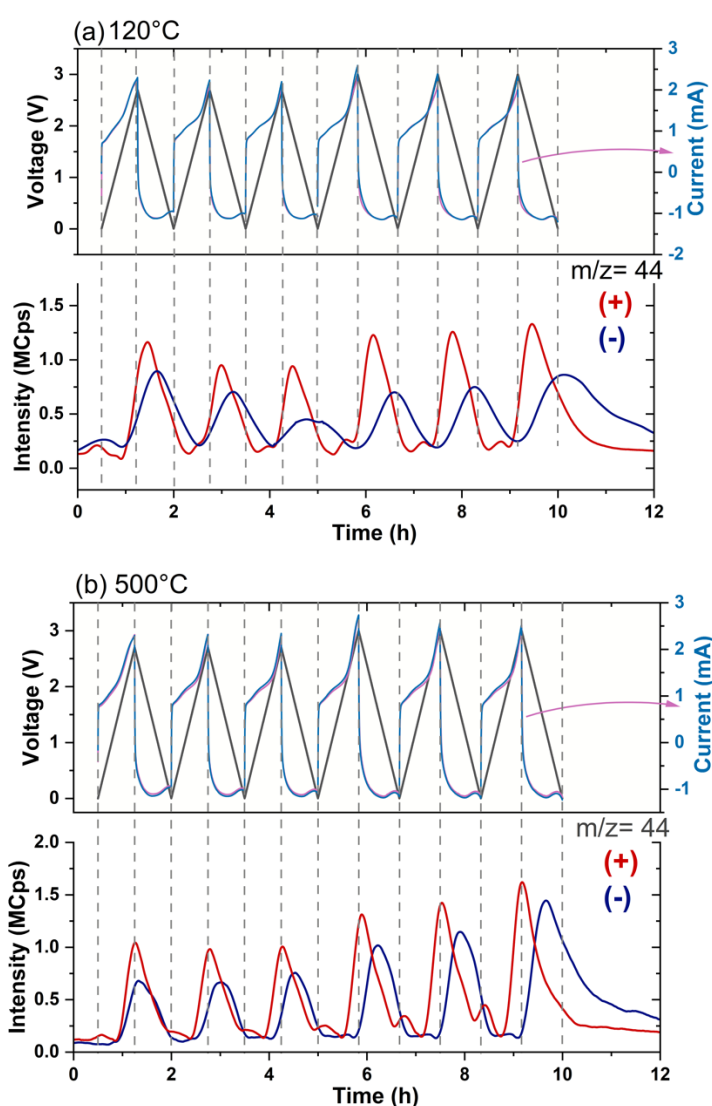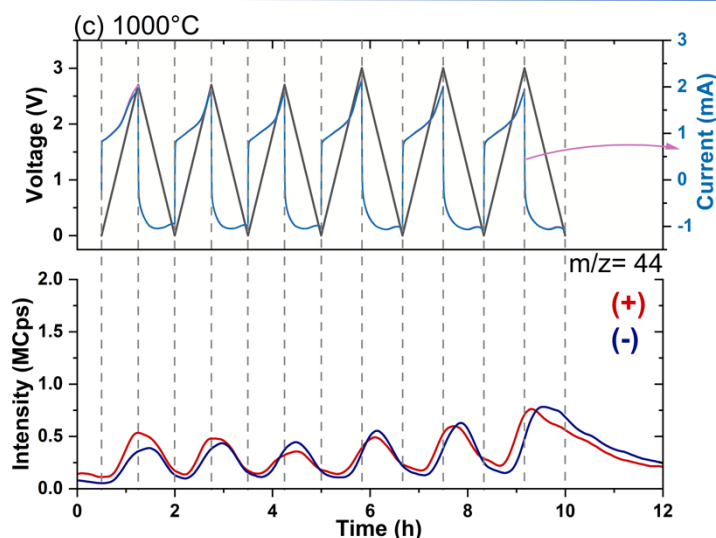
Figure 4. GC-MS profiles (M/z=44) for three different ACC electrode materials studied: a)120°C, b) 500°C and c) 1000°C. The first row represents electrochemical data (CV, 1 mV s^{-1} at 2.7 V for 3 cycles, then at 3 V for the next 3 cycles). The bottom row shows evolution of m/z = 44)

During floating, the gaseous decomposition products especially CO and CO_2 and other species related to the [TEA][BF$_4$] salt as well as ACN solvent decomposition, are expected. Because of the steric effects of quaternary salts, the intermediate product of Et$_4$NBF$_4$ decomposition follows Hofmann elimination, yielding Et$_4$N$^+$ and Et$_3$MeN$^+$. In particular, these two species, are more susceptible to decomposition.[43]

In order to further understand the involved processes, an elemental analysis of pristine and aged electrodes was performed (Table 3). This helped to quantify the elemental composition after floating in the bulk of the electrode.

Sample	C (%)	H (%)	N (%)	O (%)	Total (%)
Pristine 120°C	96.0	0.6	0	1.5	98.1
120°C (+) @ 3 V	87.6	1.0	1.2	5.9	95.7
120°C (-) @ 3 V	83.4	1.6	1.1	5.8	92.0
Pristine 500°C	96.0	0.5	0	1.2	97.7
500°C (+) @ 3 V	80.7	1.1	2.5	5.1	89.4

500°C (-) @ 3 V	84.1	1.6	0.9	4.0	90.6
Pristine 1000°C	97.6	0.4	0	0.4	98.4
1000°C (+) @ 3 V	84.7	0.9	2.2	3.8	91.6
1000°C (-) @ 3 V	90.3	1.2	0.6	3.2	95.3

Table 3. Chemical composition tested by elemental analysis for pristine and aged electrodes

Compared to the pristine electrode, a significant increase in oxygen content was found in both positive and negative electrodes, i.e.,~ 4 times for 120°C and 500°C and almost 10 times for 1000°C. This implies oxidation, slightly more pronounced at the positive electrode. During ageing, oxygen functional groups as well as water trace might cause oxidation of C as well as its consumption.[24] Additional H(%) and N(%) after ageing signify presence of electrolyte decomposition products. Interestingly, nitrogen content is higher in positive electrodes, especially for 500°C and 1000°C systems where it increased ~ 3 times, thus it seems that N compounds have greater affinity/ accumulate to a much larger extent in the positive electrode. In the 120°C system, the amount of nitrogen in the cycled electrodes is comparable. Considering longer floating time compared to the other systems, N% is half in value (1.2% in 120°C) compared to 2.5 and 2.2% for 500°C and 1000°C positive electrodes, respectively. Structural degradation of carbon and formation of defects, especially C-H edge bonds, as will be discussed in more detail in the TPD-MS section, could lead to an increase in H content also. The total % of aged electrodes also decreases, thus suggesting likely presence of other elements, such as boron and fluorine, which are not quantified by this technique.

The trend of the EA results are in accordance with the XPS data analysis (Figure 5), where the surface composition of the electrodes was determined for the pristine and aged 120°C electrodes, as well as a 500°C negative electrode as a comparison. However, much higher oxygen content was noted via XPS, especially for the 120°C positive electrode in comparison to the EA (16.2% and 5.9% respectively). This indicates that most of the ageing occurred on the surface rather than in the bulk of the electrode. An increase in oxygen content along with simultaneous decrease in carbon content can suggest formation of gaseous products from oxidation of surface functionalities. Traces

of nitrogen, as well as fluorine (from the decomposition of the electrolyte) were also found in all electrodes. Compared to EA, the amount of nitrogen determined via XPS is also higher. This means that the adsorption/accumulation of nitrogen compounds from the electrolyte decomposition is greater on the surface rather than in the bulk of the electrodes. The presence of fluorine at the negative electrode contradicts the ion transport during polarisation: BF_4 anion is expected to be adsorbed on the positive electrode. However, it was suggested by Liu et al. that a part of $HF–BF_3$, which is the product of the hydrolysis of BF_4^- can diffuse from the positive electrode to the negative electrode.[44]
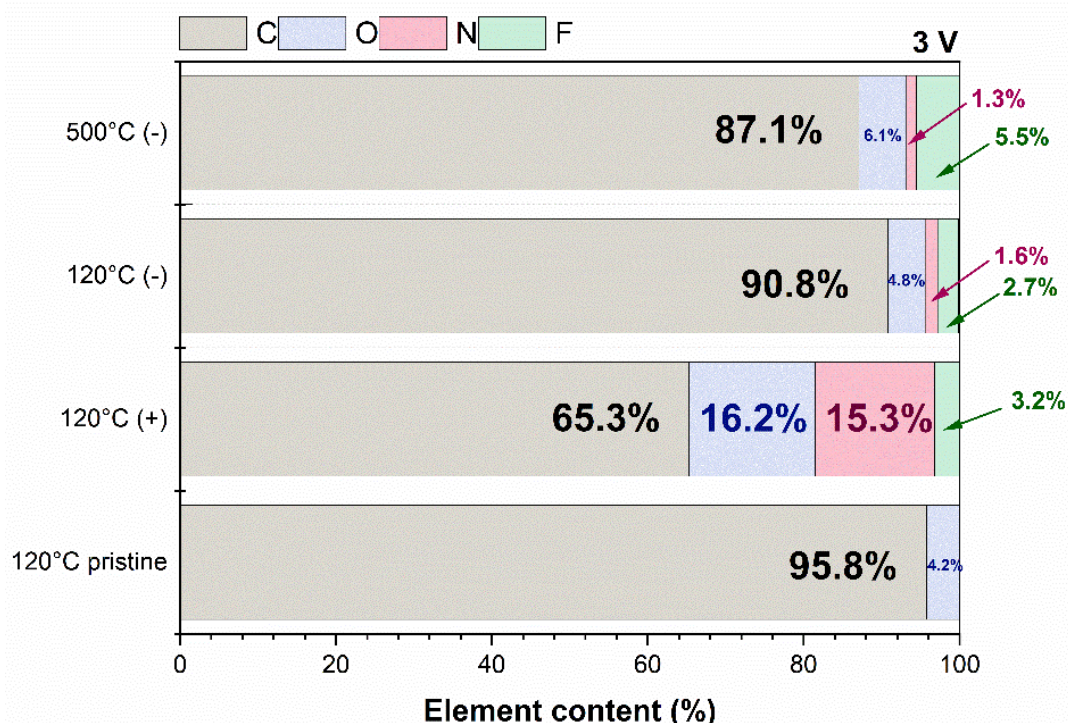
Figure 5. Elemental composition determined from XPS analysis (survey spectra) for aged and pristine ACC electrodes

Moreover, deconvolution of C1s high resolution XPS spectra (Figure 6 (a) - (e)) offers additional information. The fraction of conductive C sp^2 located at 284.4 eV (called group A) decreased from 79.1% in pristine 120 to 17.1% for 120 (+). Oppositely, the O-based functional groups (C-OR, C=O and O-C=O, called group B) increase from 3. 2% (120 pristine) to 12.7 % for 120 (+), therefore, four times increase. For the other

materials, these groups remain stable at around 3.0-3.6 %. The decrease in C amount, along with carbon oxidation (group B), can lead to a notable decrease in conductivity especially at the 120°C positive electrode.

Group C indicate products of salt and solvent decomposition (C=N, C-F, C-N and Csp^3 of the C1s peak). They are found in all electrodes, but with notable dominance of C=N and C-N fractions at the aged positive electrode. In that matter, the N1s spectra (Figure S3) can offer additional information. The peaks obtained give clear indication of covalently bound nitrogen coming from the solvent and the cation. The anodic polymerisation of acetonitrile undergoes following reaction:

$$n\text{CH}_3\text{CN} + (\text{CH}_3)\text{C}^+\text{=NH} \rightarrow \text{H(N=C(CH}_3))_n\text{–N=C}^+(\text{CH}_3) \quad (1)$$
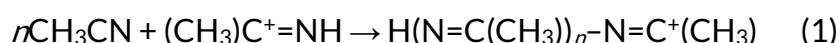
resulting in a polymer which can be covalently bonded to AC or via van der Waals forces.[16,45,46] The polymer is most prominent in the case of 120°C positive electrode, that is in accordance with the previously reported work by Liu *et al.* in which formation of an insoluble polymer film in the presence of a significant number of acidic surface functionalities has been proven.[14] Indeed, 120°C material contains carboxylic groups (O-C=O) which might induce the formation of such polymer layer. When heating the material at 500°C, the carboxylic groups are usually removed due to their low thermal stability.[47] This might explain why this polymer layer is not seen on 500 (+).

The peaks from aged electrodes in Figure S3 can be divided into:

- N1 – pyridine : C=N-C, N=C=N
- N2- Pyridone: OC=N, Pyrrolic: C-N-C, amine: C-N and amide: O=C-N
- N3: Quaternary: C=N
- N4: Pyridine oxide: C=N-O

Corresponding binding energies for all the samples are included in Table S2. Thus, signals at 398 (group N1) and 400 eV (group N2) indicate the presence of polyacetonitrile and amides, respectively. Interestingly, N3 signal for quaternary nitrogen was detected which proves presence of TEA$^+$ in aged electrodes. The percentage area of N3 group in 120°C negative electrode (Figure6 (f)) indicate higher content than in 500°C negative

electrode: 0.42% *vs.* 0.27%, respectively. Because of much longer lifespan of 120℃ system, this comes as no surprise. Upon negative polarisations, TEA^+ cations can be trapped inside the pores due to spatial confinement. Whilst it is plausible for them to come out, it is kinetically unfavoured and can be rather slow. Over time, accumulation of TEA^+ will take place, hence e.g. higher N3 group % content in 120℃ *vs.* 500℃ negative electrodes. Pyridine oxide (group N4) could indicate presence of by-products of electrolyte decomposition, twice as high in the aged 120℃ positive electrode (0.94%) compared to the 120℃ negative electrode (0.4%). Acetylene being one of the fragments formed from elimination reaction of $TEABF_4$ (as confirmed by TPD-MS) can react with acetonitrile through Bönnemann cyclization at high voltage, to form 2-methylpyridine, to be later dealkylated and oxidised to pyridine oxide. Thus, confirmation of additional electrolyte decomposition products on the surface, higher in the positive electrode can be deducted.
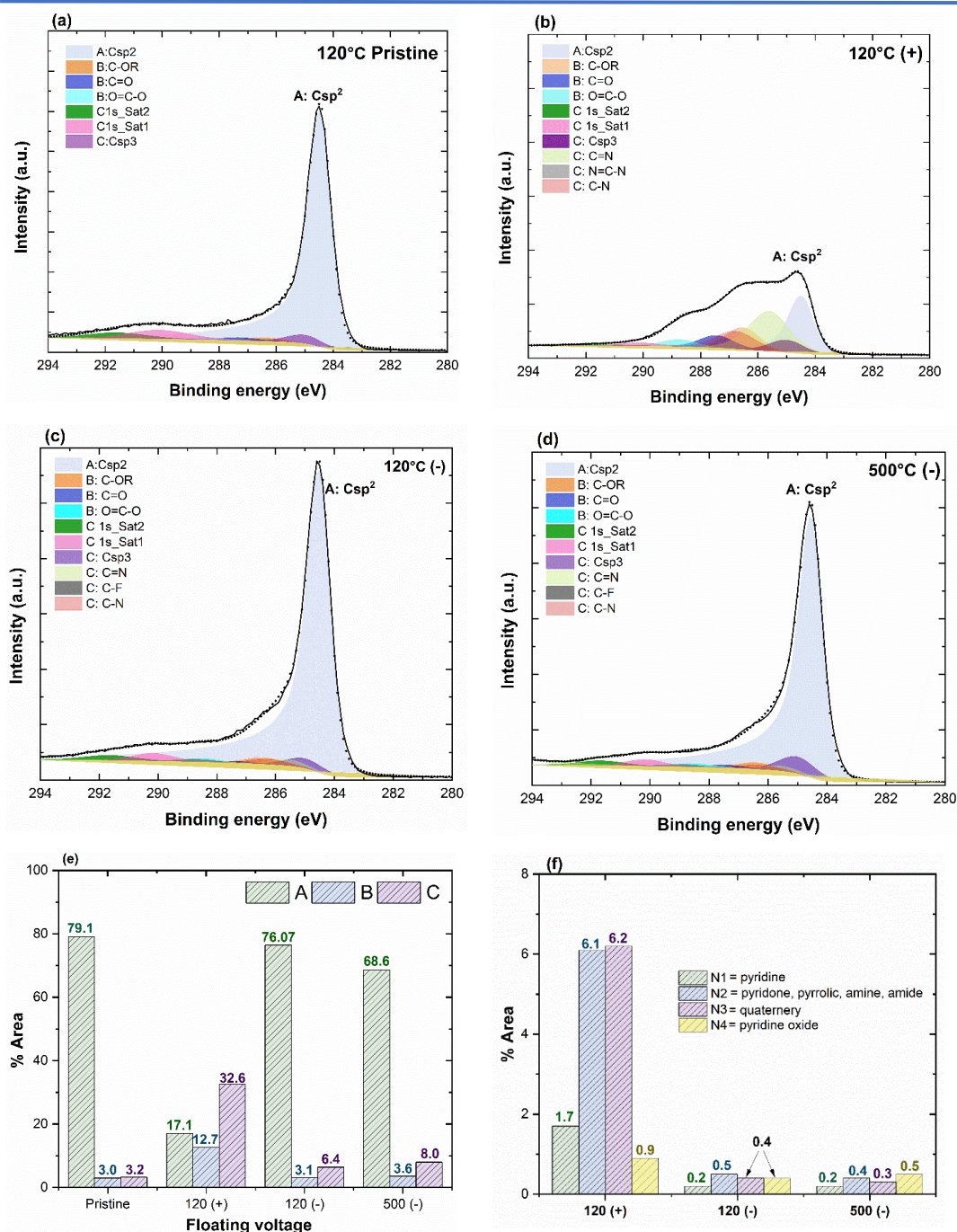
Figure 6. Deconvoluted high-resolution XPS C1s spectra of a) pristine 120°C carbon; b) positive 120°C carbon electrode ; c) negative 120°C carbon electrode; (d) negative 500°C carbon electrode (e) Repartition of surface compositions within the C1s of the carbon electrodes prior to and after the floating test at 3 V from C1s spectra. Group A represents C sp^2, group B corresponds to O-functional groups : C-OR, C=O, and O=C-O bonded to C sp^2, and group C to C sp3, C=N, N=C-N, C-N and C-F in the core level C1s ; (f) Repartition of surface compositions within the N1s spectra of the carbon electrodes after the floating test at 3 V

As discussed in XPS part, the possible blockage of pores with the different salt/solvent fragments or O-functional groups needed to be validated, as those with a size between 1-2nm can ultimately affect the capacitance of EDLCs.[48] Figure 7 represents the isotherms and pore size distributions of pristine and aged electrodes in each system and Table 2 contains information on S_{BET} (Specific Surface Area) and their corresponding pore volume changes calculated from the 2D NLDFT model. After ageing, all systems display a change in textural properties, with decrease in S_{BET} and V_{micro}. For the 500°C system, the changes observed for S_{BET} and V_{micro} are similar in both electrodes, whereas for 1000°C, the positive electrode is slightly more degraded. This decrease on the positive electrode has been previously linked to oxidation which causes pore blockage or pore collapsing. In the case of 120°C system, the negative electrode is characterised by greater S_{BET} and V_{micro} loss. From the XPS and EA data, it can be assumed that most of the oxidation that causes ageing in the 120°C positive electrode takes place at the surface, with formation of polymer like layer. That would explain the small change of S_{BET} of positive electrode compared to the 120°C negative electrode, which more likely oxidises in the bulk. Because of direction of polarisation, TEA$^+$ cations migrate towards the negative electrode and accumulate there over time whilst blocking its porosity, therefore, much pronounced decrease in S_{BET} and V_{micro} is observed, especially when considering its long operating time The mesopores could also be affected by such mechanism, causing possible ionic 'starvation' which would ultimately lead to capacitance loss during EDLC operation, but are not observed in the studied samples. Ultimately, the adsorption data does not give clear explanation of degradation pathways for those two systems, but does confirm changes in porosity of the electrodes after ageing.

Table 2. S_{BET} values and their corresponding pore volume changes calculated from the 2D NLDFT model for the pristine and aged electrodes at 3 V for 120°C 500°C and 1000°C ACC

	Surface area	$V_{micro} < 2$ nm	V_{meso} 2-50 nm
	[m^2·g^{-1}]	[cm^3·g^{-1}]	[cm^3·g^{-1}]
Pristine 120°C	1807	0.660	0.004
Aged 120°C (+)	1514	0.564	0.002
Aged 120°C (-)	1235	0.458	0.002
Pristine 500°C	1747	0.655	0.002
Aged 500°C (+)	1337	0.498	0.009
Aged 500°C (-)	1355	0.507	0.012
Pristine 1000°C	1748	0.652	0.002
Aged 1000°C (+)	1348	0.500	0.001
Aged 1000°C (-)	1457	0.545	0.002
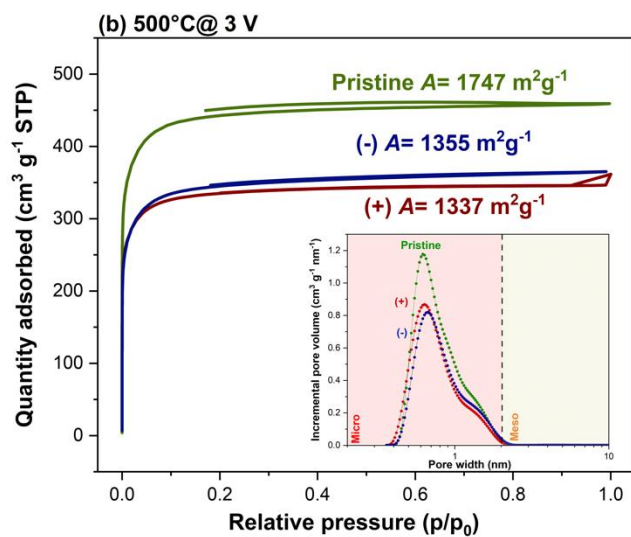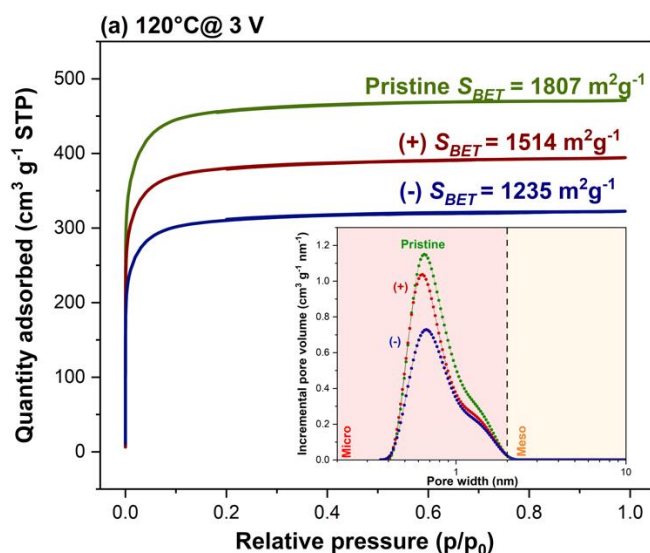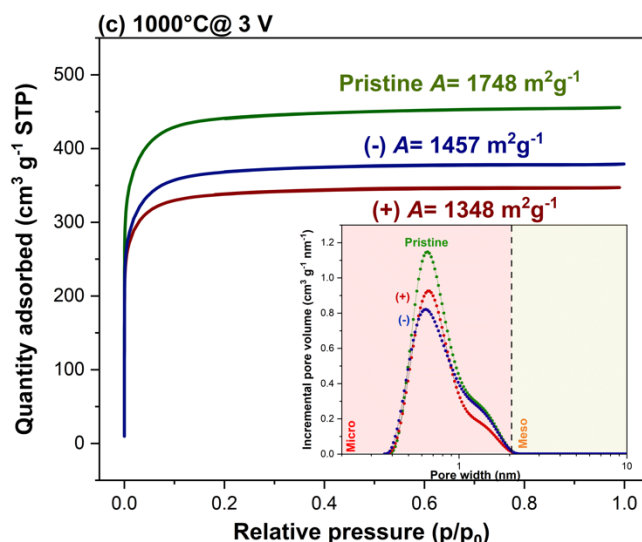
Figure 7. Nitrogen adsorption at 77 K isotherms and insets of pore size distributions of pristine and aged electrodes at 3 V for 120°C 500°C and 1000°C ACC electrode materials

The TPD-MS measured and calculated pressure profiles are shown in Figure 8. The calculated pressures are obtained from the mass spectra and calibration data of the calibrated gases. Therefore, when the calculated pressure profile is lower than the pressure measured by the vacuum gauge, it means that some uncalibrated species are released. Figure 8 (a), (b) and (c), show the comparison between the calibrated and measured pressure profiles, per gram of sample, versus temperature for sample 500°C, pristine material, positive and negative electrodes after cycling at 3V. Since the pressures are divided by the amount of sample, it is possible to relatively compare the amount of gas release between the different samples. The pristine material has overlapping measured and calculated pressure profiles, meaning that only calibrated gases (CO, CO_2, H_2, H_2O) are released from this sample. The same observation can be done for all the pristine materials. On the contrary, one can observe the occurance of an intense measured peak at ≈300°C, indicating that some uncalibrated species are released, for both negative and positive electrodes after cycling (Figures 8c-f). The same observation can be noticed at ≈710°C, but to a lesser extent. Due to the presence of these uncalibrated species, which may contribute to the masses (m/z) of the calibrated gasesmentioned above , it is unfortunately not relevant and accurate to explore the quantitative desorption profiles of those calibrated gases. This prevents also from drawing conclusions on the oxygen-containing surface groups after cycling.Figures 8 (d),

(e) and (f) which display the measured pressure profiles per gram of sample, of respectively 120°C, 500°C and 1000°C samples, positive and negative electrodes, show that there is a huge release of gas at ≈300°C. This might be related to the decomposition of the same molecule and is much more significant in negative electrodes than in positive electrodes. To a lower extent another gas release can be observed at ≈720°C in all the positive electrodes. These two gas release of uncalibrated gases could be due to the decomposition of the electrolyte and solvent.
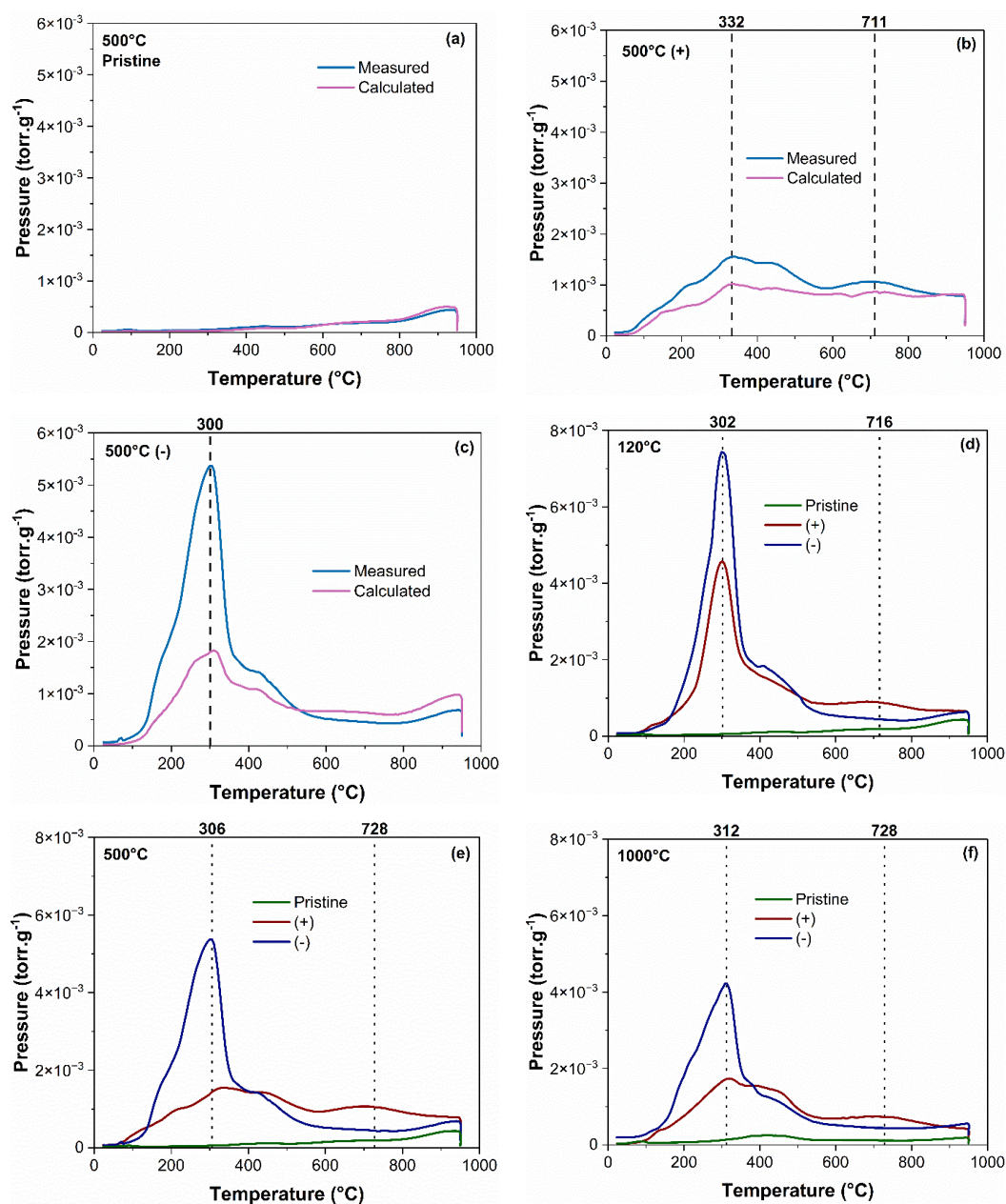
Figure 8. Measured and calculated TPD-MS pressure profiles for sample 500°C (a) Pristine, (b) Positive electrode at 3V, and (c) Negative electrode at 3V; TPD-MS measured pressure profiles for positive and negative electrodes at 3V for sample at (d) 120°C, (e) 500°C and (f) 1000°C.

Figure 9 (a), (b) and (c) show the mass spectrometer intensity profiles of the main masses (M/z) observed at the temperatures at which a significant difference between measured and calculated pressure was noticed on Figure 8. At 300°C, noticeable peaks of masses 20, 27 and 86 are observed. On the contrary, at 745°C, only M/z=86 can be seen. M/z=20 shows the presence of HF, M/z=27 of HCN and M/z=86 of trimethylamine (according to their identification based on Figure S4). Since the MS intensity is divided by the amount of sample it is possible to relatively compare the quantities between the different samples.
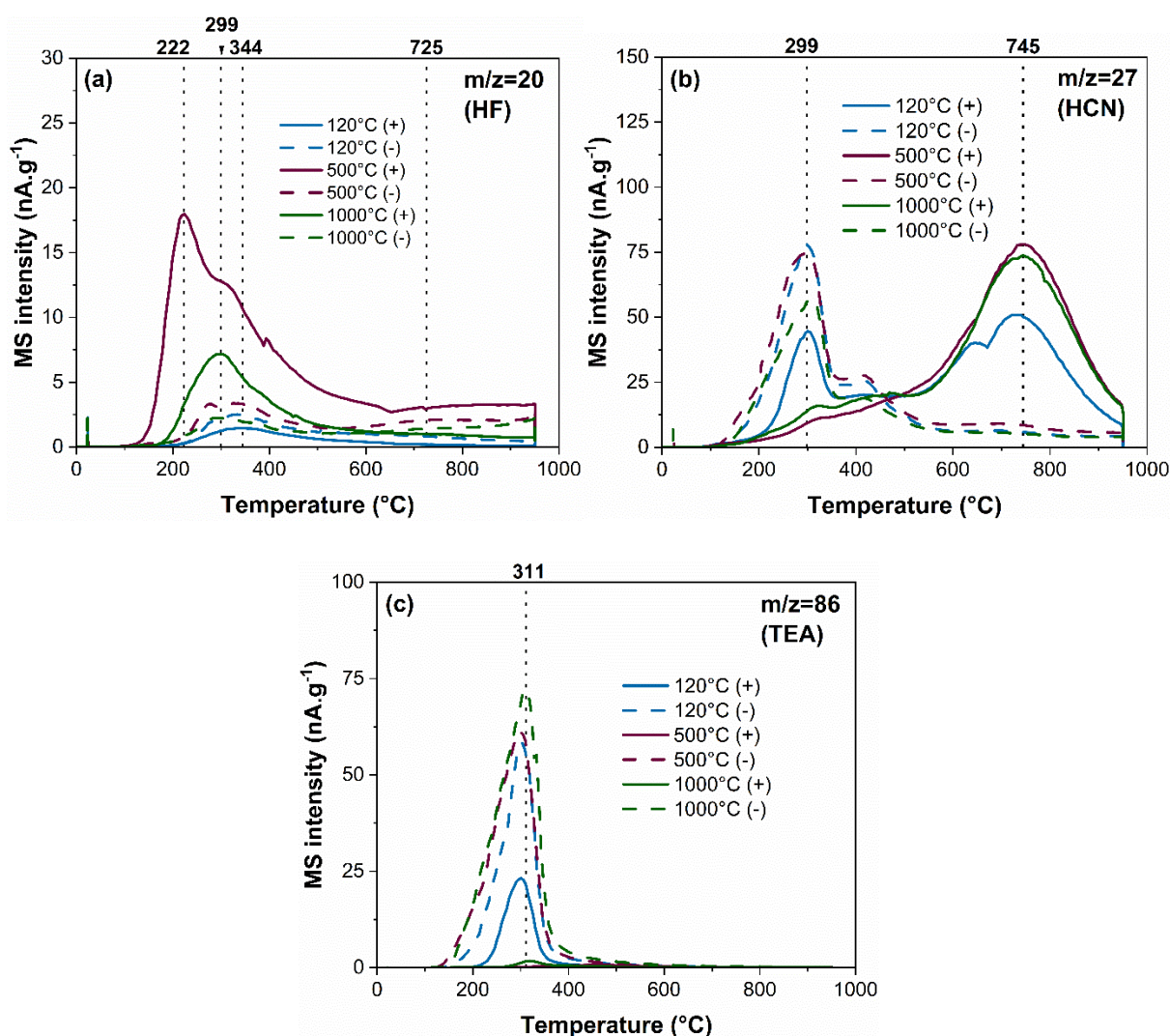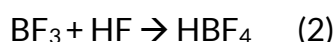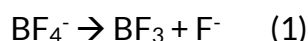
Figure 9.MS profiles of the negative and positive electrodes of all the samples at 3V (a) for M/z=20 (HF), (b) for M/z=27 (HCN) and (c) for M/z=86 (TEA)

In Figure 9 (a), the release of M/z=20 at ≈300°C can be associated to HF coming from the hydrolysis of BF_4 as already described elsewhere:[20]

$$BF_4^- \rightarrow BF_3 + F^- \quad (1)$$

$$BF_3 + HF \rightarrow HBF_4 \quad (2)$$

$$HBF_4 + H_2O \rightarrow HBF_3(OH) + HF \quad (3)$$

$$4\,BF_3 + 3H_2O \rightarrow B(OH)_3 + 3\,HBF_4 \quad (4)$$

The hydrogen and oxygen needed for the reaction can come from various sources, especially when considering long-term operation: water and oxygen permeation and diffusion from air, traces of dissolved oxygen in the electrolyte or water trapped in the porosity of AC or the separator despite thorught drying processes. By means of reactions, ethylene elimination can effectively yield protons, as well as ACN solvent undergoing autoionisation,[16] thus acting as a proton source:

$$2CH_3CN \rightarrow CH_3CNH^+ + CH_2CN^- \quad (5)$$

It is also possible for the oxidation of BF_4^- to BF_4 radical to extract a proton from ACN solvent.

The HF species are most evident in the positive electrodes, with the highest amount found in 500°C, followed by 1000°C. This interaction may explain the higher oxidation observed in the positive electrode.

The decomposition of the acetonitrile solvent can be seen in Figure 9 (b) at 745°C with M/z=27, which is the main mass of HCN as shown from the theoretical MS spectra given in Figure S5. The M/z=27 peak at 300°C may be due to triethylamine decomposition. Indeed, this molecule also decompose as M/z=27 as can be seen in Figure S5. This can be confirmed by the presence of a M/z=86 peak, which is the main MS peak of triethylamine, at that same 300°C temperature on Figure 9 (c). On the M/z=27 graph, HCN is only visible in the positive electrodes and to a higher extent, and in similar

proportions, in 500°C and 1000°C samples. However, considering that 500°C system operated for 184h less compared to 1000°C, the amount of HCN is significant. Previous studies have also shown that acetonitrile can polymerize on the electrode surface and decomposes in the 600-800°C TPD-MS temperature range.[14] On the contrary, the M/z=86 peak related to triethylamine (TEA) decomposition, can be observed in all negative electrodes and only in a lower amount in 120°C positive electrode. Liu *et al.* also pointed out the presence of TEA, in the 300-400°C TPD-MS temperature range in negative electrodes.

In summary, TPD-MS measurements show that BF_4^- and acetonitrile are mainly present at the positive electrodes which agrees with previous studies and with the XPS measurements. The amounts of decomposed BF_4^- and acetonitrile is lower for 120°C sample. At the negative electrodes, TEA decomposition can be observed to similar extent for all the samples. Unfortunately, the contribution of the secondary peaks of these uncalibrated species do not allow accurate determination and quantification of the oxygen surface groups after cycling, using TPD-MS.

Raman spectroscopy analysis of the pristine and aged electrodes and deconvoluted spectrum of the pristine 120°C system is included in Figure S5. For 120°C positive and negative electrodes, I_D/I_G increased by ~5% and 28% respectively, compared to the pristine I_D/I_G = 1.45. The biggest change can be seen for 500°C electrodes, where the ratio has doubled. This might be caused by defects created by the superacid and/or HF oxidising the carbon, as already discussed in the TPD-MS section.

In both cases, an increase in the intensity ratio of the D band to G informs about reduction in the size of the crystal and thus a higher sp^3 content [26-28,49,50] (higher disorder), which is in accorance with the XPS data, where the fraction of C sp^3: 500°C (-) >120°C (-) > 120°C (+). Some sp^3 sites can be formed via the attachment of F, H or O functionalities at different carbon sites, as well as it can stem from a polymer[44] The lack of change to the I_D/I_G ratio and peak position in 1000°C electrodes can suggest that it is less degraded compared to the other studied systems. As observed in the EA and TPD-MS, there is a significant oxidation in the bulk of the electrodes, thus those changes would not be detected via Raman Spectroscopy. Moreover, the D and G band position upshift and downshift can be observed for 120°C and 500°C. As reported, the upshift of

G band (blue shift) can be explained by a compressed lattice, not applicable in this case What is observed in the aged electrodes is the G band downshift (red shift) which indicates tensile strain on the carbon material or an increase in disorder. Additinally, the upshift of the D band can indicate a change in the type of defects present: it can suggest the formation of specific functional groups bonded to the edges of the carbon structure. Ultimately, the results confirm that 500℃ aged electrodes are characterised by higher disorder than 120℃ electrodes after ageing protocol. Moreover, a change in type of defects can be assumed for the pristine 1000℃ carbon, characterised by an upshift in D band compared to pristine 120℃, from 1341 cm^{-1} to 1346 cm^{-1}. Ultimately, the results confirm that 500℃ aged electrodes are characterised by higher disorder than 120℃ electrodes after ageing protocol. Moreover, a change in type of defects can be assumed for the pristine 1000℃ carbon, characterised by an upshift in D band compared to pristine 120℃, from 1341 cm^{-1} to 1346 cm^{-1}.

It can be stated that the presented systems do not undergo the same ageing mechanisms. The type of functional groups, i.e. acidic or basic, seems to play a significant role on the degradation pathway at high voltage:

The 120℃ system is characterised by highest capacitance retention, withstanding 1086h of floating time. At this temperature, both acidic and basic oxygen functionalities are present on the carbon surface as shown via TPD-MS analyses. The abundance of acidic functional groups induced the formation of a protective polymer layer on both positive and negative electrodes, more pronounced in the former. [14] These acidic groups then undergo hydrolysis reactions in the presence of water trace, forming other groups. However, this does not explain the ageing behaviour of the remaining systems studied, namely 500℃ and 1000℃. In that case, nitrogen selectivity presents itself as a possible hypothesis. The CO releasing groups on carbon surface promote nitrogen selectivity, i.e. 'attract' N containing compounds, such as those coming from the electrolyte, whereas CO_2 releasing groups inhibit it.[51] The mechanism of capturing of N-based compounds by oxygen functionalities have been described to undergo H- bond interaction with N-H groups in ammonia or amines and/or acid-base interactions.[52] [53] That is, depending on their structure, some oxygen functionalities can act as Lewis acids or bases: e.g.

carbonyls (C=O) can act as Lewis acids and interact with N-containing functional groups (Lewis base) such as amines (R-NH$_2$) via hydrogen bonding. Physical adsorption of the N-compounds onto the carbon surface is then plausible. After thermal treatment at 500°C, mostly basic functional groups (CO releasing by TPD-MS) are present, thus promoting N containing compound interactions: salt and solvent decomposition by-products. This is most evident in TPD-MS results, where the amount of HCN species from the 500°C positive electrode was the highest. This, along with other decomposition by-products such as HF from hydrolysis of BF$_4$, led to the fastest capacitance loss, affecting both electrodes. 1000°C treated carbon has hardly or any surface oxygen functionalities. Elimination of these groups has led to a slower degradation compared to 500°C as there were no N-selective oxygen groups, but also no acidic groups to form a protective layer that could delay it from further oxidation and degradation. This is evident from the EA and TPD-MS: even with an additional 184h of floating operation, the amount of nitrogen in the bulk was less than in the case of 500°C. The oxygen content from EA compared to the pristine electrode also increased by ~10 times, thus oxidation and subsequent formation of new functionalities is confirmed.

4.Conclusions

In this study, we present the effect of oxygen functionalities on ageing of three types of binder-free AC thermally treated at 120°C, 500°C and 1000°C, in organic medium operating at high voltage. Thermal treatment allowed to remove specific oxygen functionalities from the surface of the carbon material. Based on the vast *post-mortem* analyses, we concluded that the degradation of the electrodes is strongly affected by the type of functionalities on the carbon surface and that other parasitic reactions are involved and need to be considered:

- 120°C system: Its end-of life criterion was reached due to a steady increase in resistance and loss of capacitance. The decrease in conductivity, along with carbon oxidation and pore blockage all contribute to system degradation. However, a protective polymer layer was formed on the electrodes thanks to the acidic functionalities, which allowed the system to reach the longest lifetime (1086 h).

- 500℃ system: Due to the removal of specific acidic oxygen functionalities at the treated temperature, mostly basic ones remain. It is hypothesized that those groups could promote higher affinity of N containing compounds towards the electrode, as shown by EA, XPS and TPD-MS. As a consequence, faster degradation would be favoured, characterized by more pronounced increase in resistance. Pore blockage and loss of specific surface area, together with increased oxidation additionally contributed to system failure, characterised by the shortest lifetime during floating (714 h).

- 1000℃ system: Slower degradation (898 h) was achieved compared to the 500℃ system, where parameters of resistance and capacitance followed through in similar manner. This showed that complete removal of the oxygen functionalities in not favoured for long time operation of ECs. In such case, electrolyte decomposition is the main cause of degradation, especially considering the positive electrode where increased amounts of HF and HCN were found as shown by TPD-MS. Other important contributor was electrode oxidation. These have led to pore blockage, loss of specific surface area and loss of conductivity.

Based on this work, it is suggested for the future studies to focus on 'tailored functionalization' of the carbon material, where methods, specific types and controlled amounts of oxygen functionalities would be achieved to obtain the most optimal system design immune to degradation.

ACKNOWLEDGEMENT

Corresponding Authors

Sylwia Slesinska- Orcid: https://orcid.org/ 0000-0002-9242-5561

Email: sylwia.slesinska@put.poznan.pl

Jakub Menzel- Orcid: https://orcid.org/0000-0002-0431-159X;

Email: jakub.menzel@put.poznan.pl

Camélia Matei-Ghimbeu- Orcid: https://orcid.org/0000-0003-3600-5877;

Email: camelia.ghimbeu@uha.fr

CRediT authorship contribution statement

Sylwia Slesinska: Conceptualization; Methodology; Data curation; Investigation; Formal Analysis; Visualisation; Writing – original draft; **Bénédicte Réty:** Investigation; Formal analysis; Writing-original draft; **Camélia Matei Ghimbeu:** Validation; Supervision; Writing - Review & Editing; **Krzysztof Fic:** Supervision; Funding acquisition; Project administration; Writing - Review & Editing; **Jakub Menzel:** Conceptualization; Funding acquisition; Writing – review & editing; Supervision; Project administration

References

1. Lewandowski, A. & Galinski, M. Practical and theoretical limits for electrochemical double-layer capacitors. Journal of Power Sources 173, 822-828 (2007). https://doi.org/10.1016/j.jpowsour.2007.05.062

2. González, A., Goikolea, E., Barrena, J. A. & Mysyk, R. Review on supercapacitors: Technologies and materials. Renewable and Sustainable Energy Reviews 58, 1189-1206 (2016). https://doi.org/10.1016/j.rser.2015.12.249

3. Simon, P. & Gogotsi, Y. Perspectives for electrochemical capacitors and related devices. Nat Mater 19, 1151-1163 (2020). https://doi.org/10.1038/s41563-020-0747-z

4. Zhao, J. & Burke, A. F. Review on supercapacitors: Technologies and performance evaluation. Journal of energy chemistry 59, 276-291 (2021). https://doi.org/10.1016/j.jechem.2020.11.013

5. Fernão Pires, V., Romero-Cadaval, E., Vinnikov, D., Roasto, I. & Martins, J. F. Power converter interfaces for electrochemical energy storage systems – A review. Energy Conversion and Management 86, 453-475 (2014). https://doi.org/10.1016/j.enconman.2014.05.003

6. Forse, A. C., Merlet, C. l., Griffin, J. M. & Grey, C. P. New Perspectives on the Charging Mechanisms of Supercapacitors. Journal of the American Chemical Society 138, 5731-5744 (2016). https://doi.org/10.1021/jacs.6b02115

7. Ghamouss, F., Brugère, A. & Jacquemin, J. Physicochemical Investigation of Adiponitrile-Based Electrolytes for Electrical Double Layer Capacitor. Journal of physical chemistry. C 118, 14107-14123 (2014). https://doi.org/10.1021/jp5015862

8. Alkire, R. C., Bartlett, P. N. & Lipkowski, J.   285-312 (John Wiley & Sons, Incorporated, 2015).

9. Pourhosseini, S. E. M., Bothe, A., Balducci, A., Beguin, F. & Ratajczak, P. Strategy to assess the carbon electrode modifications associated with the high voltage ageing of electrochemical capacitors in organic electrolyte. ENERGY STORAGE MATERIALS 38, 17-29 (2021). https://doi.org/10.1016/j.ensm.2021.02.028

10. Borenstein, A. et al. A Surprising Failure Mechanism in Symmetric Supercapacitors at High Voltages. ChemElectroChem 4, 2660-2668 (2017). https://doi.org/10.1002/celc.201700421

11. Kops, L., Kreth, F. A., Bothe, A. & Balducci, A. High voltage electrochemical capacitors operating at elevated temperature based on 1,1-dimethylpyrrolidinium tetrafluoroborate. Energy Storage Materials 44, 66-72 (2022).

12. Beguin, F. & Frackowiak, E. Supercapacitors materials, systems, and applications / edited by Francois Beguin and Elzbieta Frackowiak. (Wiley-VCH, 2013).

13. Kar, K. K. Handbook of Nanocomposite Supercapacitor Materials III: Selection. 1st Edition 2021 edn, Vol. 313 (Springer Nature, 2021).

14. Liu, Y. et al. Understanding ageing mechanisms of porous carbons in non-aqueous electrolytes for supercapacitors applications. Journal of power sources 434, 226734 (2019). https://doi.org/10.1016/j.jpowsour.2019.226734

15. Shashurin, A. & Keidar, M. Factors affecting the size and deposition rate of the cathode deposit in an anodic arc used to produce carbon nanotubes. Carbon (New York) 46, 1826-1828 (2008). https://doi.org/10.1016/j.carbon.2008.08.002

16. Bittner, A. M. et al. Ageing of electrochemical double layer capacitors. Journal of Power Sources 203, 262-273 (2012). https://doi.org/10.1016/j.jpowsour.2011.10.083

17. Azaïs, P. et al. Causes of supercapacitors ageing in organic electrolyte. Journal of Power Sources 171, 1046-1053 (2007). https://doi.org/10.1016/j.jpowsour.2007.07.001

18. Ishimoto, S., Asakawa, Y., Shinya, M. & Naoi, K. Degradation Responses of Activated-Carbon-Based EDLCs for Higher Voltage Operation and Their Factors. Journal of the Electrochemical Society 156, A563 (2009). https://doi.org/10.1149/1.3126423

19. Cazorla-Amorós, D. et al. Measuring cycle efficiency and capacitance of chemically activated carbons in propylene carbonate. Carbon (New York) 48, 1451-1456 (2010). https://doi.org/10.1016/j.carbon.2009.12.039

20. Kurzweil, P. & Chwistek, M. Electrochemical stability of organic electrolytes in supercapacitors: Spectroscopy and gas analysis of decomposition products. Journal of Power Sources 176, 555-567 (2008). https://doi.org/10.1016/j.jpowsour.2007.08.070

21. Chiba, K. et al. Electrolyte Systems for High Withstand Voltage and Durability I. Linear Sulfones for Electric Double-Layer Capacitors. Journal of the Electrochemical Society 158, A872 (2011). https://doi.org/10.1149/1.3593001

22. Kreth, F. A., Hess, L. H. & Balducci, A. In-operando GC-MS: A new tool for theunderstanding of degradation processes occurring in electrochemical capacitors. Energy Storage Materials 56, 192-204 (2023).

23. Pameté, E. et al. The Many Deaths of Supercapacitors: Degradation, Aging, and Performance Fading. Advanced Energy Materials 13, n/a (2023). https://doi.org/10.1002/aenm.202301008

24. Huang, Y. et al. Degeneration of Key Structural Components Resulting in Ageing of Supercapacitors and the Related Chemical Ageing Mechanism. ACS applied materials & interfaces 13, 39379-39393 (2021). https://doi.org/10.1021/acsami.1c10369

25. Ruch, P. W., Cericola, D., Foelske, A., Kötz, R. & Wokaun, A. A comparison of the aging of electrochemical double layer capacitors with acetonitrile and propylene carbonate-based electrolytes at elevated voltages. Electrochimica Acta 55, 2352-2357 (2010). https://doi.org/10.1016/j.electacta.2009.11.098

26. Piwek, J., Platek, A., Frackowiak, E. & Fic, K. Mechanisms of the performance fading of carbon-based electrochemical capacitors operating in a LiNO3 electrolyte. Journal of power sources 438, 227029 (2019). https://doi.org/10.1016/j.jpowsour.2019.227029

27. Platek, A., Piwek, J., Fic, K. & Frackowiak, E. Ageing mechanisms in electrochemical capacitors with aqueous redox-active electrolytes. Electrochimica acta 311, 211-220 (2019). https://doi.org/10.1016/j.electacta.2019.04.117

28. Zallouz, S., Le Meins, J.-M. & Matei Ghimbeu, C. Alkaline hydrogel electrolyte from biosourced chitosan to enhance the rate capability and energy density of carbon-based supercapacitors. Energy advances (2022). https://doi.org/10.1039/D2YA00250G

29. Ratajczak, P., Jurewicz, K., Skowron, P., Abbas, Q. & Béguin, F. Effect of accelerated ageing on the performance of high voltage carbon/carbon electrochemical capacitors in salt aqueous electrolyte. Electrochimica acta 130, 344-350 (2014). https://doi.org/10.1016/j.electacta.2014.02.140

30. He, M. et al. Ageing phenomena in high-voltage aqueous supercapacitors investigated by in situ gas analysis. Energy & environmental science 9, 623-633 (2016). https://doi.org/10.1039/c5ee02875b

31. Kreth, F. A., Köps, L., Donne, S. W. & Balducci, A. Operando Temperature Dynamic Investigation of Electric Double-Layer Capacitors Containing Organic Electrolytes. Batteries & supercaps (2024). https://doi.org/10.1002/batt.202300581

32. Moussa, G., Matei Ghimbeu, C., Taberna, P.-L., Simon, P. & Vix-Guterl, C. Relationship between the carbon nano-onions (CNOs) surface chemistry/defects and their capacitance in aqueous and organic electrolytes. Carbon (New York) 105, 628-637 (2016). https://doi.org/10.1016/j.carbon.2016.05.010

33. Peredo-Mancilla, D. et al. Surface-Modified Activated Carbon with a Superior CH4/CO2 Adsorption Selectivity for the Biogas Upgrading Process. Industrial & engineering chemistry research 61, 12710-12727 (2022). https://doi.org/10.1021/acs.iecr.2c01264

34. Brender, P. et al. Characterization of Carbon Surface Chemistry by Combined Temperature Programmed Desorption with in Situ X-ray Photoelectron Spectrometry and Temperature Programmed Desorption with Mass Spectrometry Analysis. Analytical chemistry (Washington) 84, 2147-2153 (2012). https://doi.org/10.1021/ac102244b

35. Peter, A. et al. How to Quantify the Adsorption of Cyanuric Acid on Activated Carbon Used from Swimming Pool Disinfection? Langmuir 39, 12041-12052 (2023). https://doi.org/10.1021/acs.langmuir.3c01127

36. Bokobza, L., Bruneel, J.-L. & Couzi, M. Raman Spectra of Carbon-Based Materials (from Graphite to Carbon Black) and of Some Silicone Composites. C (Basel) 1, 77-94 (2015). https://doi.org/10.3390/c1010077

37. Couzi, M., Bruneel, J.-L., Talaga, D. & Bokobza, L. A multi wavelength Raman scattering study of defective graphitic carbon materials: The first order Raman spectra revisited. Carbon (New York) 107, 388-394 (2016). https://doi.org/10.1016/j.carbon.2016.06.017

38. Oukaour, A. et al. Calendar ageing and health diagnosis of supercapacitor. Electr Pow Syst Res 95, 330-338 (2013). https://doi.org/10.1016/j.epsr.2012.09.005

39. Slesinski, A., Sroka, S., Fic, K., Frackowiak, E. & Menzel, J. Operando Monitoring of Local pH Value Changes at the Carbon Electrode Surface in Neutral Sulfate-Based Aqueous Electrochemical Capacitors. ACS Applied Materials & Interfaces 14, 37782-37792 (2022). https://doi.org/10.1021/acsami.2c09920

40. Liu, P., Verbrugge, M. & Soukiazian, S. Influence of temperature and electrolyte on the performance of activated-carbon supercapacitors. Journal of power sources 156, 712-718 (2006). https://doi.org/10.1016/j.jpowsour.2005.05.055

41. Hahn, M., Würsig, A., Gallay, R., Novák, P. & Kötz, R. Gas evolution in activated carbon/propylene carbonate based double-layer capacitors. Electrochemistry Communications 7, 925-930 (2005). https://doi.org/10.1016/j.elecom.2005.06.015

42. Ruschhaupt, P., Pohlmann, S., Varzi, A. & Passerini, S. Cover Feature: Determining Realistic Electrochemical Stability Windows of Electrolytes for Electrical Double-Layer Capacitors (Batteries & Supercaps 8/2020). Batteries & Supercaps 3, 670-670 (2020). https://doi.org/10.1002/batt.202000156

43. Nikiforidis, G., Phadke, S. & Anouti, M. Comparative Internal Pressure Evolution at Interfaces of Activated Carbon for Supercapacitors Containing Electrolytes Based on Linear and Cyclic Ammonium Tetrafluoroborate Salts in Acetonitrile. Advanced materials interfaces 10, n/a (2023). https://doi.org/10.1002/admi.202202046

44. Liu, Y., Soucaze-Guillous, B., Taberna, P.-L. & Simon, P. Understanding of carbon-based supercapacitors ageing mechanisms by electrochemical and analytical methods. Journal of power sources 366, 123-130 (2017). https://doi.org/10.1016/j.jpowsour.2017.08.104

45. Krtil, P., Kavan, L. & Novak, P. Oxidation of acetonitrile-based electrolyte solutions at high potentials : an in situ Fourier transform infrared spectroscopy study. Journal of the Electrochemical Society 140, 3390-3395 (1993). https://doi.org/10.1149/1.2221100

46. Tourillon, G., Lacaze, P.-C. & Dubois, J.-E. Electrochemical formation of thin polyacetonitrile films on a Pt surface: P.m.t., ir., x.p.s. and s.i.m.s. analyses and study of formation mechanisms. Journal of Electroanalytical Chemistry and Interfacial Electrochemistry 100, 247-262 (1979).

47. Rocha, R. P., Pereira, M. F. R. & Figueiredo, J. L. Characterisation of the surface chemistry of carbon materials by temperature-programmed desorption: An assessment. Catalysis today 418, 114136 (2023). https://doi.org/10.1016/j.cattod.2023.114136

48. Endo, M. et al. Morphology and organic EDLC applications of chemically activated AR-resin-based carbons. Carbon (New York) 40, 2613-2626 (2002). https://doi.org/10.1016/S0008-6223(02)00191-4

49. Knight, D. S. & White, W. B. Characterization of diamond films by Raman spectroscopy. Journal of materials research 4, 385-393 (1989). https://doi.org/10.1557/JMR.1989.0385

50. Beams, R., Gustavo Cançado, L. & Novotny, L. Raman characterization of defects and dopants in graphene. Journal of physics. Condensed matter 27, 083002-083002 (2015). https://doi.org/10.1088/0953-8984/27/8/083002

51. Sano, Y., Choi, K.-H., Korai, Y. & Mochida, I. Selection and Further Activation of Activated Carbons for Removal of Nitrogen Species in Gas Oil as a Pretreatment for Its Deep Hydrodesulfurization. Energy & fuels 18, 644-651 (2004). https://doi.org/10.1021/ef034080e

52. Kim, J. H., Ma, X., Zhou, A. & Song, C. Ultra-deep desulfurization and denitrogenation of diesel fuel by selective adsorption over three different adsorbents: A study on adsorptive selectivity and mechanism. Catalysis today 111, 74-83 (2006). https://doi.org/10.1016/j.cattod.2005.10.017

53. Almarri, M., Ma, X. & Song, C. Role of Surface Oxygen-Containing Functional Groups in Liquid-Phase Adsorption of Nitrogen Compounds on Carbon-Based Adsorbents. Energy & fuels 23, 3940-3947 (2009). https://doi.org/10.1021/ef900051r

Supplementary Information

The Oxygen Enigma: Deciphering the Role of Carbon Surface Functionalities on Degradation at Electrified Interfaces

Sylwia Slesinska[1], Bénédicte Réty[2,3,4], Camélia Matei-Ghimbeu[2,3,4*], Samar Hajjar Garreau[2,3,4], Krzysztof Fic[1], Jakub Menzel[1*]

[1] Institute of Chemistry and Technical Electrochemistry, Poznan University of Technology, Berdychowo 4, 60-965 Poznan, Poland

[2] Institut de Science des Matériaux de Mulhouse (IS2M), Université de Haute-Alsace, CNRS UMR 7361, F-68100 Mulhouse, France;

[3] Université de Strasbourg, F67081 Strasbourg, France;

[4] Réseau sur le Stockage Electrochimique de l'Energie (RS2E), CNRS FR3459, 80039 Amiens Cedex, France

*Corresponding author: sylwia.slesinska@put.poznan.pl, jakub.menzel@put.poznan.pl, camelia.ghimbeu@uha.fr

Fig.S1. Cyclic Voltammograms before and after ageing at 3 V at 10 mV s^{-1} for 120°C, 500°C and 1000°C systems

Table S1. Specific capacitance (F/g) and specific energy (Wh/kg) of the cells with various ACC electrode materials studied prior to floating experiments with 1 mol L^{-1} TEABF$_4$/AN electrolyte at 3 V.

Sample	Specific Capacitance (F/g)	Specific Energy (Wh/kg)
120°C	110	32
500°C	130	39
1000°C	153	45
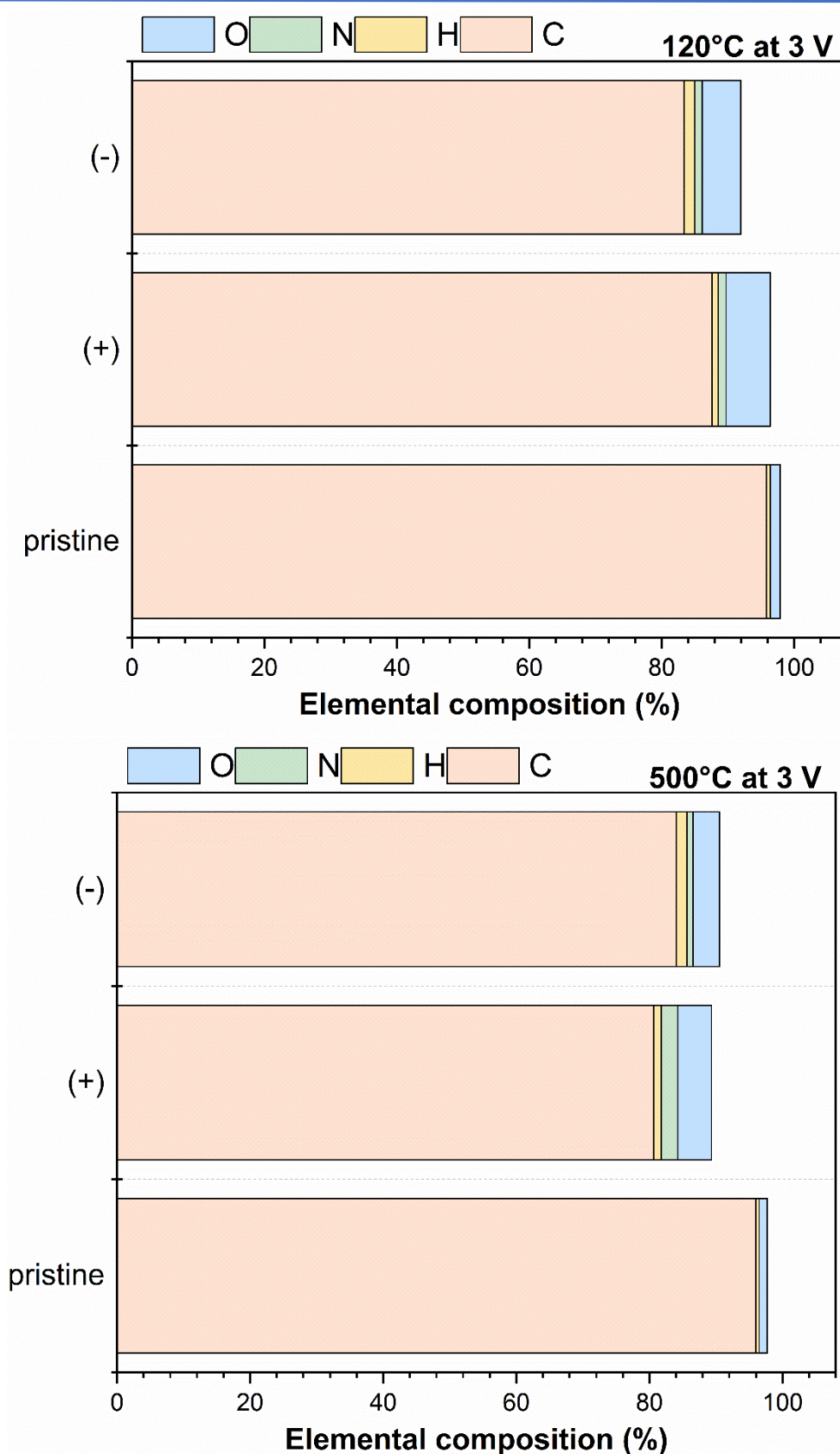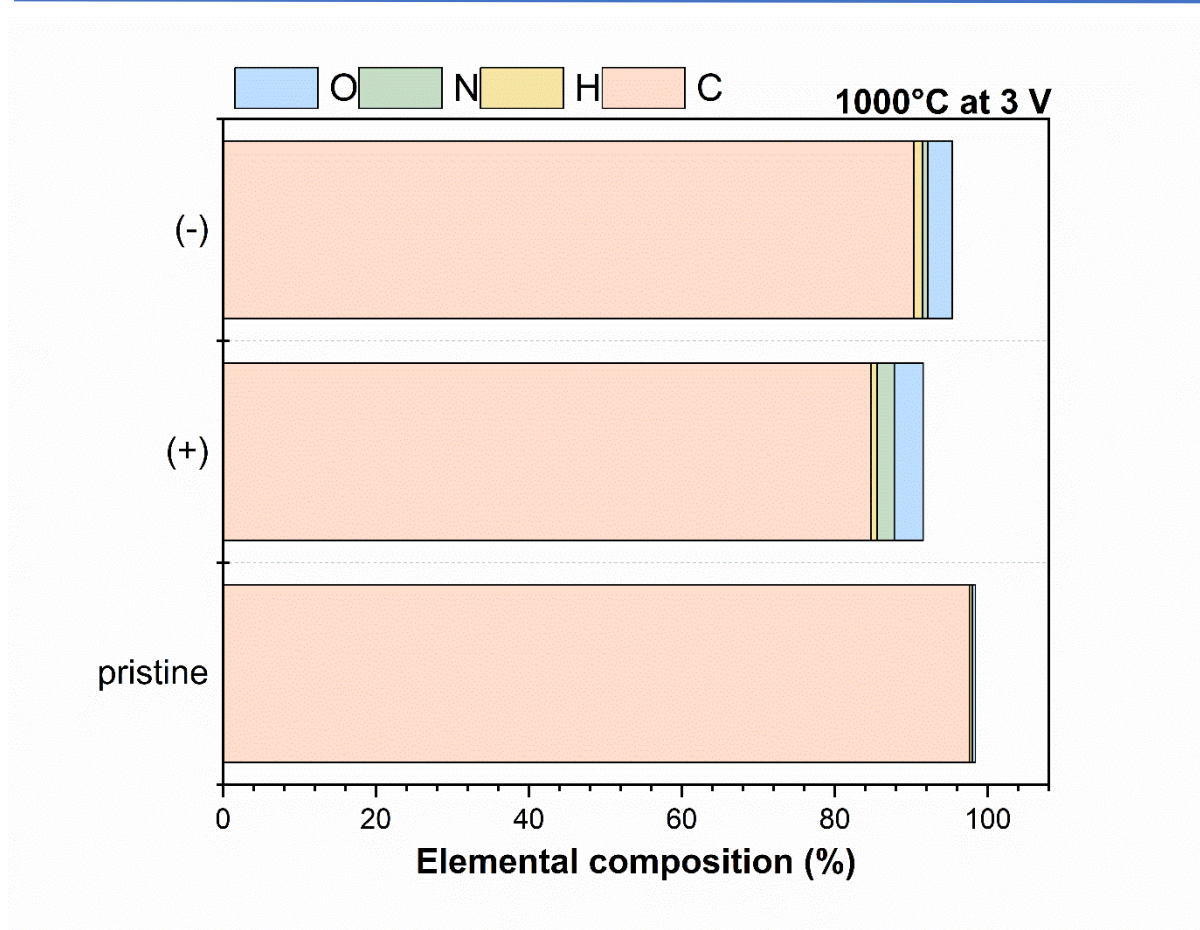
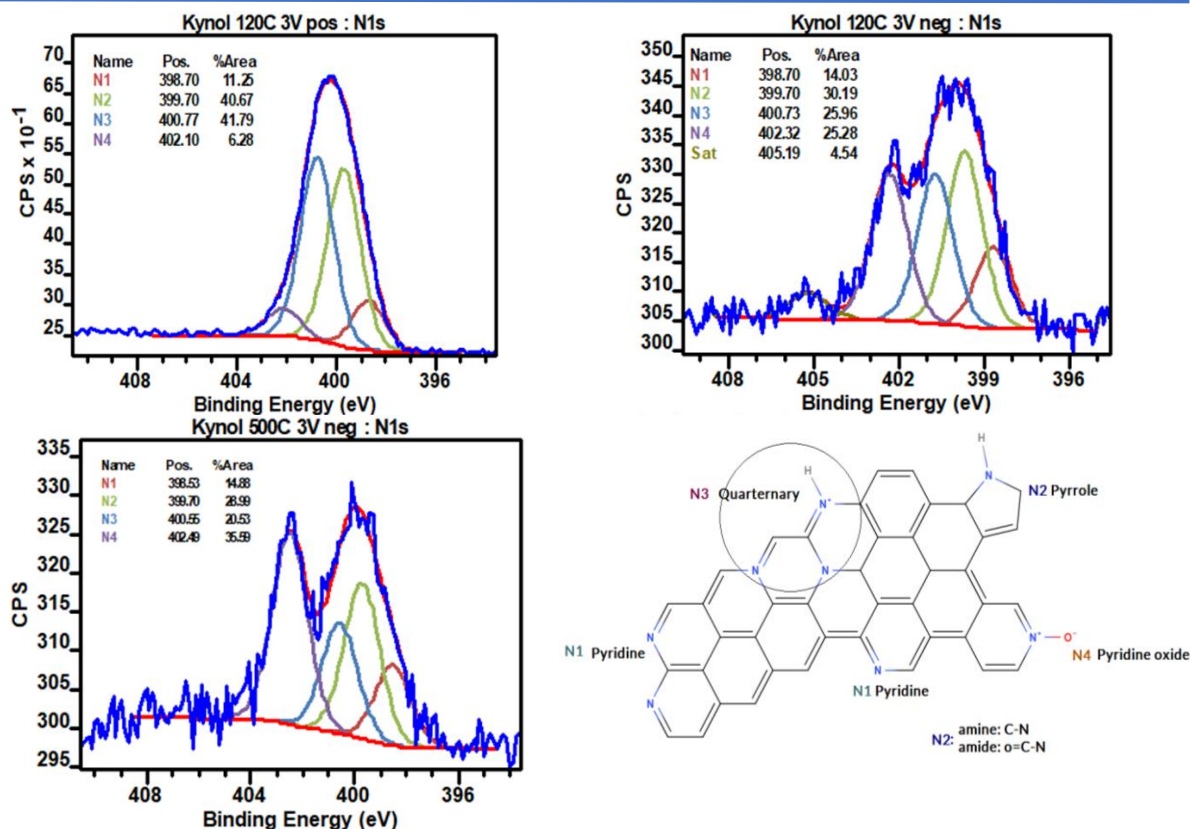**Figure S2.** Chemical composition tested by elemental analysis for pristine and aged 120°C, 500°C and 1000°C ACC electrodes

Figure S3. High resolution deconvoluted XPS N1s spectra for the aged electrodes together with N species and their corresponding groups (N1, N2, N3 and N4)

Table S2. (a) Binding energies from N1s spectra of the aged electrodes and (b) proposed species responsible for the signals for each group

(a)

Sample	N1 (eV)	N2 (eV)	N3 (eV)	N4 (eV)
120°C (+)	398.7	399.7	400.8	402.1
120°C (-)	398.7	399.7	400.7	402.3
500°C(-)	398.5	399.7	400.6	402.5

(b)

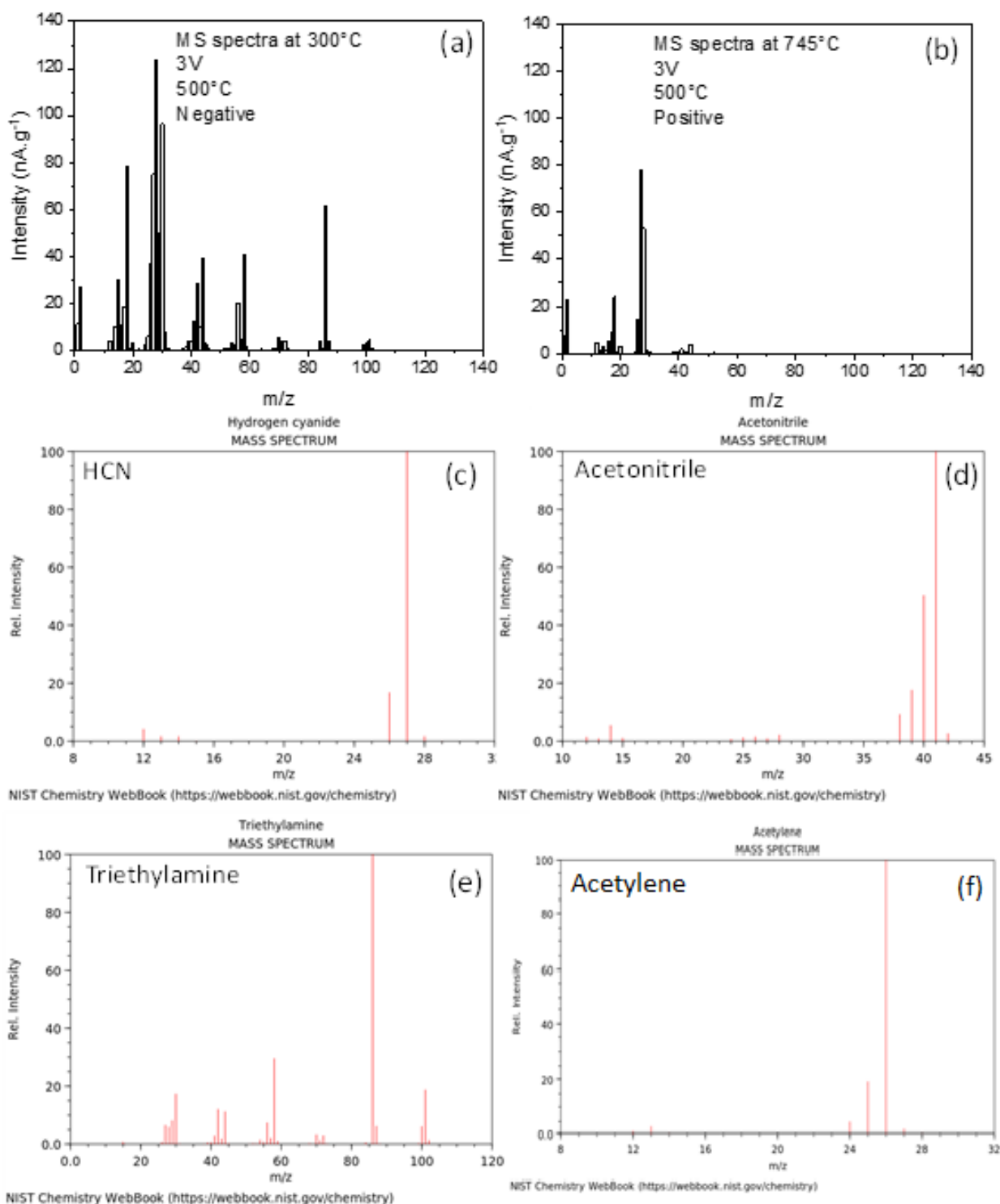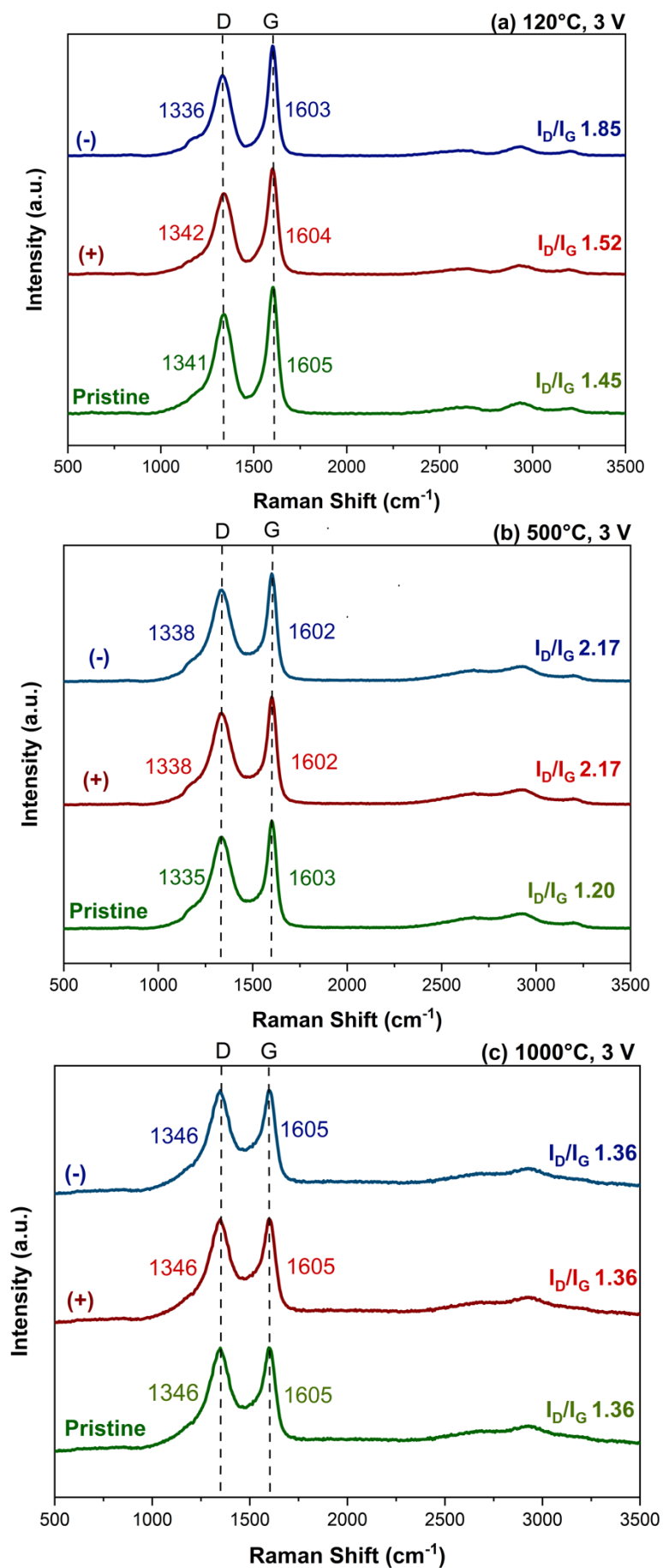| Group	Species
N1	$H(N=C(CH3))_n-N=C^+(CH_3)$
N2	$RCONH_2$
N3	TEA^+
N4	C_5H_5NO

Figure S4. MS spectra of the uncalibrated species for 500°C sample at 3V (a) at 300°C for the negative electrode and (b) at 745°C for the positive electrode -Theoretical MS spectra of (c) HCN, (d) acetonitrile, (e) triethylamine and (f) Acetylene
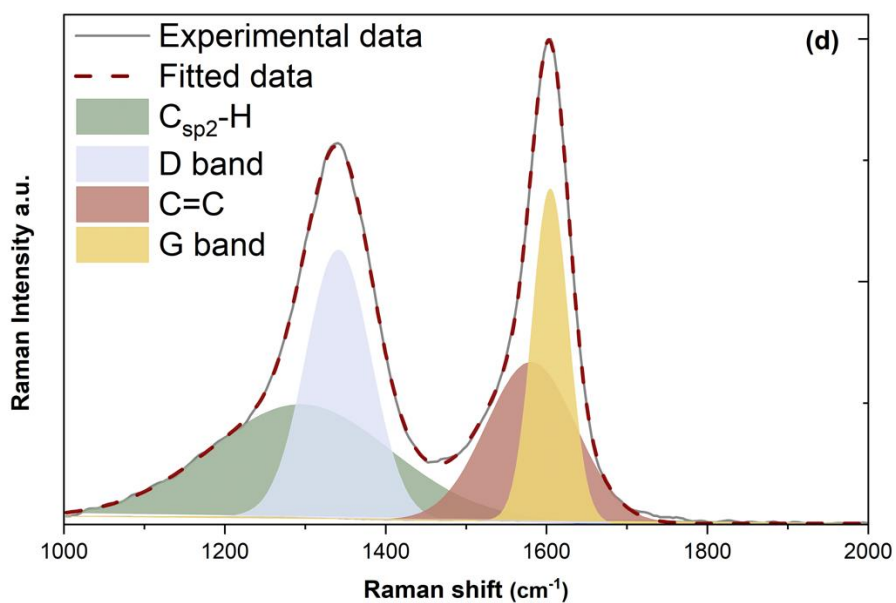
Figure S5. Raman spectroscopy analysis of the pristine and aged electrodes at a floating voltage of 3 V. The I_D/I_G ratio values were calculated from deconvolution of the given spectra (a) 120°C (b) 500°C and (c) 1000°C ACC electrode materials. (d) Deconvoluted spectrum of the pristine Kynol 507-20 thermally treated at 120°C

General Conclusion

The work presented in the dissertation focused on the elucidation of intricate processes taking place at the electrode/electrolyte interface in ECs and LICs, where both aqueous and organic electrolytes coupled with ACs were considered in the case of ECs. This has allowed to paint a more complete picture of AC behavior in both i) various electrochemical systems and ii) with investigation of the influence of various factors (different AC electrode materials, electrolyte compositions, voltage applied, surface chemistries, cell construction etc.). The first part of the work concerned studies based on *operando* (pH, GC-MS) and *in-situ* techniques (EQCM) which offered a glimpse into the dynamic changes within the EC during operation. For aqueous systems, article **P1** evidenced that: pH changes are dynamic, strongly potential dependent and differ at each electrode, therefore, they should not be neglected when considering device optimization. These changes cause a change in theoretical operating voltage; however, it will change due to mixing when the electrodes are in closer proximity. The onset of pH changes starts even at low voltages and so the electrolyte decomposition, evidenced by presence of electrolysis by-products which are produced even below the theoretical decomposition voltage. It was also shown that cycle life can be enhanced by increasing the distance between electrodes, however this causes an increase in resistance. In such case, a thoughtful trade-off and a concept of pH maintenance must be considered for most system optimization. Article **P2** dealt with the PZC determination and ionic fluxes using the EQCM technique in aqueous electrolytes with AC electrodes. Particular attention should be given to the interpretation of the data from this medium since, despite certain similarities, the charge storage mechanism of aqueous-based systems varies greatly. It showed that PZC should be considered as a potential range rather than one value. Moreover, one should consider it as a range of zero charge (RZC) rather than one point (as it covers a potential range of 100-200 mV). An alternative method for PZC determination based on the SPECS technique was also suggested and implemented, and the importance of cell construction (which was somehow ignored until now) was highlighted. It proved the need of direct determination in the EQCM cell to avoid misleading process description, as well as for each system to be considered in an individual manner. The electrolytic solution based on lithium nitrate was also studied

using EQCM for the first time and revealed its capacitive nature. The other half of the research focused on the ageing studies in organic media, which unraveled the mysteries concerning specific causes for accelerated degradation. This was achieved through investigation of degradation mechanisms pathways of carbon electrode after accelerated ageing. The work presented in article **P3** investigated the effect of applied voltage on the ageing of the porous AC electrode. A relationship was established in which an increase in applied voltage resulted in a faster degradation and that depending on the maximum voltage applied, the systems reach different end-of-life criteria. When floated at lower voltage (4 V), an increase in both resistance and decrease in capacitance is observed. This changes once voltage of ≥4.2 is applied. In such cases, a more pronounced increase in resistance is evident. Physicochemical analyses allowed to determine the specific causes of degradation. Overall, it was established that higher voltages induce higher electrolyte decomposition, oxidation levels, and subsequent structure degradation. This also promotes faster electrolyte decomposition under overcharged conditions, with a formation of SEI and organic/inorganic by-products that can ultimately block the porosity of the carbon electrode. Lastly, the effect of oxygen functionalities on ageing in a symmetric organic based EC were established in an article **A1.** Based on this work, it is suggested for the future studies to focus on 'tailored functionalization' of the carbon material as no clear trend in decrease of oxygen functionalities was found. However, it was established for the specific types of those surface oxygenated functionalities to influence system ageing which brings about new insights into the research area. More specifically, complete removal of the oxygen functionalities was found to not be favoured for long time operation of ECs where electrode oxidation and electrolyte decomposition prevail. Conversely, the presence of acidic functionalities was shown to aid in longevity and was attributed to formation of a protective polymer layer on the electrode surface. The study also hypothesizes that specific basic functionalities could promote stronger adsorption of nitrogen-containing compounds, where the system studied was characterised by more pronounced resistance increase, coupled with pore blockage, surface area loss, and increased oxidation. These findings underscore and contribute to new knowledge on the critical role of specific oxygen functionalities in influencing the stability and longevity of AC electrodes in ECs operating in high-voltage organic electrolytes.
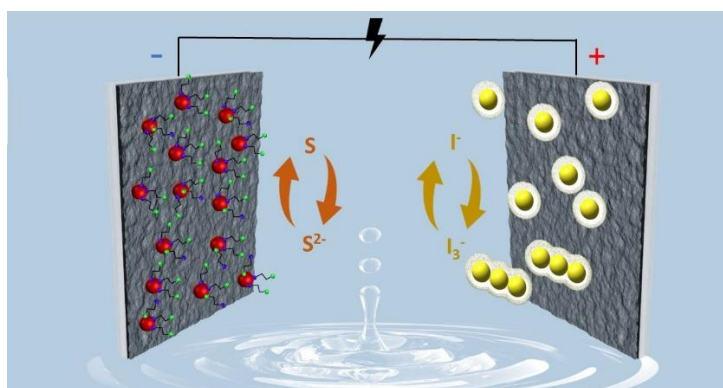
Scientific Articles – not included in the doctoral thesis

Abstract:

The paper puts forward the concept of a double-redox electrochemical capacitor operating in an aqueous electrolyte. The redox activity of sulphur from insoluble Bi_2S_3 nanocrystals embedded in the negative electrode material (up to 10 wt%) operating in 1 mol L^{-1} Li_2SO_4 electrolyte is demonstrated. It is also shown that the performance is significantly boosted using MPA (3-mercaptopropionic acid) as a ligand attached to the surface of the nanocrystals, which allows for more efficient use of Bi_2S_3 redox active species. This redox activity is combined with the reactions of iodides, which occur at the opposite electrode with 1 mol L^{-1} NaI. This enables the formation of a discharge voltage plateau that effectively boosts the capacitance (275 F g^{-1}), and thus specific energy of the device owing to the relatively high cell voltage of 1.5 V. This performance is possible due to the advantageous electrode mass ratio ($m_- : m_+$ = 2 : 1), which helps to balance the charge. The rate capability test of the device demonstrates its capacitance retention of 73% at 10 A g^{-1} of the discharge current. The different states of the redox species ensure their operation at separate electrodes in an immiscible manner without a shuttling effect. The specific interactions of the redox active species with carbon electrodes are supported by *operando* Raman spectroscopy.

Abstract:

Transition metal dichalcogenides (TMDs) with a two-dimensional character are promising electrode materials for an electrochemical capacitor (EC) owing to their unique crystallographic structure, available specific surface area, and large variety of compounds. TMDs combine the capacitive and faradaic contribution in the electrochemical response. However, due to the fact that the TMDs have a strong catalytic effect of promoting hydrogen and oxygen evolution reaction (HER and OER), their usage in aqueous ECs is questioned. Our study shows a hydrothermal l-cysteine–assisted synthesis of two composites based on different carbon materials—multiwalled carbon nanotubes (NTs) and carbon black (Black Pearl-BP2000)—on which MoS$_2$ nanolayers were deposited. The samples were subjected to physicochemical characterization such as X-ray diffraction and Raman spectroscopy which proved that the expected materials were obtained. Scanning electron microscopy coupled with electron dispersive spectroscopy (SEM/EDS) as well as transmission electron microscopy images confirmed vertical position of few-layered MoS$_2$ structures deposited on the carbon supports. The synthetized samples were employed as electrode materials in symmetric ECs, and their electrochemical performance was evaluated and compared to their pure carbon supports. Among the composites, NTs/MoS$_2$ demonstrated the best electrochemical metrics considering the conductivity and capacitance (150 Fg^{-1}), whereas BP2000/MoS$_2$ reached 110 Fg^{-1} at a current load of 0.2 Ag^{-1}. The composites were also employed in a two-electrode cell equipped with an additional reference electrode to monitor the potential range of both electrodes during voltage extension. It has been shown that the active edge sites of MoS$_2$ catalyze the hydrogen evolution, and this limits the EC operational voltage below 1 V. Additional tests with linear sweep voltammetry allowed to determine the operational working voltage for the cells with all materials. It has been proven that the MoS$_2$/carbon composites possess limited operating voltage, that is, comparable to a pure MoS$_2$ material.

List of Figures

Figures

Tables

Scientific Achievements

1. Publications

1. "*Identifying the activated carbon electrode ageing pathways in lithium-ion hybrid capacitors*"

<u>S. Ślesińska</u>, B. Rety, C. Matei-Ghimbeu,[*], K. Fic, J. Menzel [*]

ACS Applied Energy Materials, 2025, 8, 2, 810–820

<div align="right">

I.F= 5.4, MNiSW= 20

</div>

2. "*Fundamentals and Implication of Point of Zero Charge (PZC) Determination for Activated Carbons in Aqueous Electrolytes*"

<u>S. Ślesińska</u>, P. Galek, J. Menzel, S. W. Donne, K. Fic,[*] A. Płatek-Mielczarek[*]

Advanced Science, 2024, 2409162-1 - 2409162-10

<div align="right">

I.F= 14.3, MNiSW= 200

</div>

3. "*A double-redox aqueous capacitor with high energy output*"

A. Ślesiński,[*] <u>S. Sroka,</u> S. Aina, J. Piwek, K. Fic, M. Pilar Lobera, M. Bernechea, E. Frąckowiak[*]

Journal of Materials Chemistry A , 2023, 11, 6258-6273

<div align="right">

I.F= 10.7, MNiSW= 200

</div>

4. "*Operando Monitoring of Local pH Value Changes at the Carbon Electrode Surface in Neutral Sulfate-Based Aqueous Electrochemical Capacitors*"

A. Ślesiński,[*] <u>S. Sroka,</u> K. Fic, E. Frąckowiak, J. Menzel[*]

ACS Applied Materials & Interfaces, 2022, 14, 37782 – 37792

<div align="right">

I.F=9.5, MNiSW= 200

</div>

5. "*Supercapacitor with Carbon/MoS$_2$ Composites*"

M. Tobis, <u>S. Sroka,</u> E. Frąckowiak[*]

Frontiers in Energy Research, 2021, 9, 647878-1 - 647878-11

<div align="right">

I.F= 3.858, MNiSW= 100

</div>

Total IF= 43.76

Total MNiSW= 720

h-index= 3

2. Scientific conferences

Oral presentations at national conferences

*Underlined denotes presenting author

1. <u>**Sylwia Ślesińska**</u>, Przemysław Galek, Anetta Płatek-Mielczarek, Jakub Menzel, Krzysztof Fic, "*Fundamentals and implication of PZC determination for activated carbons in aqueous electrolytes for Electrochemical Quartz Crystal Microbalance (EQCM) applications*", The 11th Torunian Carbon Symposium, Torun, Poland, 15 -18.09.2024

Oral presentations at international conferences

1. <u>Jakub Menzel</u>, **Sylwia Sroka**, "*Ageing of carbon electrodes in li-ion hybrid capacitors*", The World Conference on Carbon – Carbon 2023, Cancun, Mexico, 16-21.07.2023
2. <u>**Sylwia Sroka**</u>, Krzysztof Fic, Jakub Menzel, "*Ageing of Carbon Electrodes in Organic-Based Electrochemical Capacitors: Does Oxygen Content Play a Role?*", 74th Annual Meeting of the International Society of Electrochemistry, Lyon, France, 03- 08.09.2023
3. **Sylwia Sroka**, Benedicte Rety, Camelia Matei-Ghimbeu, Krzysztof Fic, <u>Jakub Menzel</u>, "*Identifying the carbon electrode ageing pathways in lithium-ion hybrid capacitors*", International Conference on Advanced Capacitors (ICAC), Kamakura, Japan, 26.09.2023 – 29.09.2023

Poster presentations at international conferences

1. <u>**Sylwia Sroka**</u>, Przemysław Galek, Anetta Płatek-Mielczarek, Jakub Menzel, Krzysztof Fic, "*Fundamentals and implication of PZC determination for activated carbons in aqueous electrolytes*", 8th Baltic Electrochemistry Conference, Tartu, Estonia, 14 -17.04.2024

2. **Sylwia Sroka**, Przemysław Galek, Krzysztof Fic, Jakub Menzel, *"Step Potential Electrochemical Spectroscopy (SPECS) Technique to Investigate the Ageing of Carbon Electrodes in Organic-Based Electrochemical Capacitors"*, 244th ECS Meeting, Gothenburg, Sweden, 08-12.10.2023

3. **Sylwia Sroka**, Benedicte Rety, Camelia Matei-Ghimbeu, Krzysztof Fic, <u>Jakub Menzel</u>, *"Ageing of Carbon Electrodes in Organic-Based Electrochemical Capacitors: Does Oxygen Content Play a Role?"*, International Conference on Advanced Capacitors (ICAC), Kamakura, Japan, 26.09.2023 – 29.09.2023

4. **Sylwia Sroka,** <u>Krzysztof Fic</u>, Jakub Menzel "Ageing of Carbon Electrodes in Organic-Based Electrochemical Capacitors: Does Oxygen Content Play a Role", The World Conference on Carbon – Carbon 2023, Cancun, Mexico, 16-21.07.2023

5. <u>**Sylwia Sroka**</u>, Krzysztof Fic, Jakub Menzel, *"The Role of Oxygen Content on the Ageing of Electrochemical Capacitors in Organic Medium"*, Regional Meeting of the International Society of Electrochemistry Prague, Czech Republic, 15-19.08.2022

6. <u>**Sylwia Sroka**</u>, Przemysław Galek, Anetta Płatek-Mielczarek, Jakub Menzel, Krzysztof Fic, "*Fundamentals and implication of PZC determination for activated carbons in aqueous electrolytes"*, International Symposium on Enhanced Electrochemical Capacitors Bologne, Italy, 11-15.07.2022

7. <u>**Sylwia Sroka**</u>, Przemysław Galek, Anetta Płatek-Mielczarek, Jakub Menzel, Krzysztof Fic, Point of Zero Charge: Meaning and Determination with the Electrochemical Quartz Crystal Microbalance", 72nd Annual Meeting of the International Society of Electrochemistry (online) Jeju , Korea, 29.08-03.09.2021

3. Specialist courses/trainings

- International Summer School (ISS) on Energy Storage Systems: New Developments and Directions' (Zaragoza, Spain, 18-21.07.2022)
- Safe use of compressed gases, Air Products, Proactive Gas Safety Ltd, (online) 19.10.2023

4. Participation in research projects

- IMMOSTORE ERC Proof on Concept Grants (GA 101138710), European Research Council (ERC)

  Project title: "It yet remains to see."-Hybrid electrochemical energy storage system of high power and improved cycle life

  Principal investigator: Dr. Krzysztof Fic

  Role: Research assistant

- SONATA 15 (2019/35/D/ST4/02582), National Science Centre

  Project title: How does activated carbon age? Research on the influence of oxygen functional groups on the degradation of carbon electrodes in an organic medium

  Principal investigator: Dr. Jakub Menzel

  Role: Young scientist

- OPUS 16 (2018/31/B/ST4/01852), National Science Centre

  Project title: Study of electrode/electrolyte interface of high stability and quick charge response

  Principal investigator: Prof. Elżbieta Frąckowiak

  Role: Young scientist

5. Scientific Internship and Scholarships

Host institution: Carbon and Hybrid Materials" group from Institute of Materials Science of Mulhouse (IS2M), Mixed research Unit, CNRS-University of Haute Alsace (UMR 7361)

Funding body (scholarship awarded): 2023 French Government Scholarship – High level scientific stay (France Excellence scholarship SSHN)

Project Title: "Ageing mechanisms of carbon electrodes in organic based electrochemical capacitors"

Scientific supervisor abroad: Dr. Camélia Matei- Ghimbeu

Length of stay: 01/04/2023 to 31/05/2023 (2 months)

References

[1] K.F. Kuh, The Law of Climate Change Mitigation: An Overview, Elsevier Inc2018, pp. 505-510.

[2] C. Acen, O. Bamisile, D. Cai, C.C. Ukwuoma, S. Obiora, Q. Huang, D. Uzun Ozsahin, H. Adun, The complementary role of carbon dioxide removal: A catalyst for advancing the COP28 pledges towards the 1.5 °C Paris Agreement target, The Science of the total environment 947 (2024) 174302.

[3] Y. Liu, 2024 the 8th International Conference on Energy and Environmental Science (ICEES 2024) : ICEES 2024, 1st 2024. ed., Springer Nature Switzerland, Cham, 2024.

[4] Energy Storage Systems Market - Global Industry Analysis, Size, Share, Growth, Trends, and Forecast, 2021-2031: Energy Storage Systems Market – Scope of Report The latest study collated and published analyses the historical and present-day scenario of the global energy storage systems market in order to accurately gauge its future growth, NASDAQ OMX's News Release Distribution Channel (2022).

[5] Energy Storage Systems Market Size to Worth USD 535.53 Bn By 2033: The global energy storage systems market size is calculated at USD 266.82 billion in 2024 and is expected to be worth around USD 535.53 billion by 2033, growing at a CAGR of 8.05% between 2024 and 2033, NASDAQ OMX's News Release Distribution Channel (2024).

[6] M. Amir, R.G. Deshmukh, H.M. Khalid, Z. Said, A. Raza, S.M. Muyeen, A.-S. Nizami, R.M. Elavarasan, R. Saidur, K. Sopian, Energy storage technologies: An integrated survey of developments, global economical/environmental effects, optimal scheduling model, and sustainable adaption policies, Journal of energy storage 72 (2023) 108694.

[7] Ayesha, M. Numan, M.F. Baig, M. Yousif, Reliability evaluation of energy storage systems combined with other grid flexibility options: A review, Journal of energy storage 63 (2023) 107022.

[8] F. Nadeem, S.M.S. Hussain, P.K. Tiwari, A.K. Goswami, T.S. Ustun, Comparative Review of Energy Storage Systems, Their Roles, and Impacts on Future Power Systems, IEEE access 7 (2019) 4555-4585.

[9] P. Simon, Y. Gogotsi, Perspectives for electrochemical capacitors and related devices, Nature materials 19(11) (2020) 1151-1163.

[10] K.V.G. Raghavendra, R. Vinoth, K. Zeb, C.V.V. Muralee Gopi, S. Sambasivam, M.R. Kummara, I.M. Obaidat, H.J. Kim, An intuitive review of supercapacitors with recent progress and novel device applications, Journal of energy storage 31 (2020) 101652.

[11] Y. Parvini, J.B. Siegel, A.G. Stefanopoulou, A. Vahidi, Supercapacitor Electrical and Thermal Modeling, Identification, and Validation for a Wide Range of Temperature and Power Applications, IEEE transactions on industrial electronics (1982) 63(3) (2016) 1574-1585.

[12] J. Ajuria, E. Redondo, M. Arnaiz, R. Mysyk, T. Rojo, E. Goikolea, Lithium and sodium ion capacitors with high energy and power densities based on carbons from recycled olive pits, Journal of power sources 359 (2017) 17-26.

[13] R. Kötz, M. Carlen, Principles and applications of electrochemical capacitors, Electrochimica acta 45(15) (2000) 2483-2498.

[14] F. Beguin, E. Frackowiak, Supercapacitors materials, systems, and applications / edited by Francois Beguin and Elzbieta Frackowiak, Wiley-VCH, Weinheim, 2013.

[15] J.R. Miller, A. Burke, Electrochemical Capacitors: Challenges and Opportunities for Real-World Applications, The Electrochemical Society interface 17(1) (2008) 53-57.

[16] A. Zulkifli, Polymers in electronics : optoelectronic properties, design, fabrication, and applications, Elsevier, Amsterdam, 2023.

[17] A. Nguyen Tuan, K. Gupta Ram, Smart Multifunctional Polymeric Inks for Supercapacitor Applications, Elsevier2023, pp. 2-2.

[18] M.S. Guney, Y. Tepe, Classification and assessment of energy storage systems, Renewable & sustainable energy reviews 75 (2017) 1187-1197.

[19] L.W. McKeen, FILM PROPERTIES OF PLASTICS AND ELASTOMERS, Elsevier Science & Technology Books, United States, 2017.

[20] A.L. Schulz, Capacitors theory, types and applications, 1st ed., Nova Science Publishers, Inc., New York, 2011.

[21] F. Béguin, V. Presser, A. Balducci, E. Frackowiak, Carbons and Electrolytes for Advanced Supercapacitors, Advanced materials (Weinheim) 26(14) (2014) 2219-2251.

[22] J. Ho, T.R. Jow, S. Boggs, Historical introduction to capacitor technology, IEEE electrical insulation magazine 26(1) (2010) 20-25.

[23] A. González, E. Goikolea, J.A. Barrena, R. Mysyk, Review on supercapacitors: Technologies and materials, Renewable & sustainable energy reviews 58 (2016) 1189-1206.

[24] A. Lewandowski, M. Galinski, Practical and theoretical limits for electrochemical double-layer capacitors, Journal of power sources 173(2) (2007) 822-828.

[25] L. Yang, L. Zhang, X. Jiao, Y. Qiu, W. Xu, The electrochemical performance of reduced graphene oxide prepared from different types of natural graphites, RSC advances 11(7) (2021) 442-452.

[26] A. Farooq, K. Muhammad Ahmed, W. Umer, S.M. Ramay, S. Atiq, Elucidating an efficient super-capacitive response of a Sr2Ni2O5/rGO composite as an electrode material in supercapacitors, RSC advances 13(36) (2023) 25316-25326.

[27] A. Qayyum, M.O.u. Rehman, F. Ahmad, M.A. Khan, S.M. Ramay, S. Atiq, Performance optimization of Nd-doped LaNiO3 as an electrode material in supercapacitors, Solid state ionics 395 (2023) 116227.

[28] M.A. Tahir, N. Arshad, M. Akram, Recent advances in metal organic framework (MOF) as electrode material for super capacitor: A mini review, Journal of energy storage 47 (2022) 103530.

[29] K. Fic, E. Frackowiak, P. Galek, P. Bujewska, Redox Mediated Electrolytes in Electrochemical Capacitors, 2018.

[30] P. Simon, Y. Gogotsi, Materials for electrochemical capacitors, Nature materials 7(11) (2008) 845-854.

[31] G. Jeanmairet, B. Rotenberg, M. Salanne, Microscopic Simulations of Electrochemical Double-Layer Capacitors, Chemical reviews 122(12) (2022) 10860-10898.

[32] C. Zhao, W. Zheng, A Review for Aqueous Electrochemical Supercapacitors, Frontiers in energy research 3 (2015).

[33] Y. Zhang, H. Feng, X. Wu, L. Wang, A. Zhang, T. Xia, H. Dong, X. Li, L. Zhang, Progress of electrochemical capacitor electrode materials: A review, International journal of hydrogen energy 34(11) (2009) 4889-4899.

[34] B.E. Conway, W.G. Pell, Double-layer and pseudocapacitance types of electrochemical capacitors and their applications to the development of hybrid devices, Journal of solid state electrochemistry 7(9) (2003) 637-644.

[35] Z. Wei, J.D. Elliott, A.A. Papaderakis, R.A.W. Dryfe, P. Carbone, Relation between Double Layer Structure, Capacitance, and Surface Tension in Electrowetting of Graphene and Aqueous Electrolytes, Journal of the American Chemical Society 146(1) (2024) 760-772.

[36] Q. Liang, Y. Wang, Y. Yang, T. Xu, Y. Xu, Q. Zhao, S.-H. Heo, M.-S. Kim, Y.-H. Jeong, S. Yao, X. Song, S.-E. Choi, C. Si, Nanocellulose/two dimensional nanomaterials composites for advanced supercapacitor electrodes, Frontiers in bioengineering and biotechnology 10 (2022) 1024453-1024453.

[37] F. Béguin, V. Presser, A. Balducci, E. Frackowiak, Supercapacitors: Carbons and Electrolytes for Advanced Supercapacitors (Adv. Mater. 14/2014), Advanced materials (Weinheim) 26(14) (2014) 2283-2283.

[38] B.E. Conway, Electrochemical Supercapacitors : Scientific Fundamentals and Technological Applications, 1st 1999. ed., Springer US, New York, NY, 1999.

[39] G. Wang, L. Zhang, J. Zhang, A review of electrode materials for electrochemical supercapacitors, Chemical Society reviews 41(2) (2012) 797-828.

[40] H. Helmholtz, Ueber einige Gesetze der Vertheilung elektrischer Ströme in körperlichen Leitern mit Anwendung auf die thierisch-elektrischen Versuche, Annalen der Physik 165 (1853) 211-233.

[41] H. Helmholtz, Studien über electrische Grenzschichten, Annalen der Physik (243) (1879) 337-382.

[42] M. Gouy, Constitution of electric charge at the surface of an electrolyte, Comptes Rendus Hebdomadaires des Seances de l'Academie des Sciences (149) (1909) 654-657.

[43] D.L. Chapman, A Contribution to the Theory of Electrocapillarity, Philosophical Magazine (25) (1913) 475-481.

[44] O. Stern, The theory of the electrolytic double-layer, Zeitschrift fuer Elektrochemie und Angewandte Physikalische Chemie (30) (1924) 508-516.

[45] D.C. Grahame, The electrical double layer and the theory of electro-capillarity, Chemical Reviews (1947) 441-501.

[46] J. Huang, Zooming into the Inner Helmholtz Plane of Pt(111)–Aqueous Solution Interfaces: Chemisorbed Water and Partially Charged Ions, JACS Au 3(2) (2023) 550-564.

[47] J. Zhou, G. Jing, J. Xie, W. Tang, X. Xu, S. Zhao, Pore-Size Effect on Capacitive Energy Extraction from the Salinity Gradient with Porous Electrodes, ACS applied energy materials 7(23) (2024) 11011-11019.

[48] B. Suthar, J. Landesfeind, A. Eldiven, H.A. Gasteiger, Method to Determine the In-Plane Tortuosity of Porous Electrodes, Journal of the Electrochemical Society 165(10) (2018) A2008-A2018.

[49] D. Henderson, D. Boda, Insights from theory and simulation on the electrical double layer, Physical chemistry chemical physics : PCCP 11(20) (2009) 3822-3830.

[50] D.A. Welch, B.L. Mehdi, H.J. Hatchell, R. Faller, J.E. Evans, N.D. Browning, Using molecular dynamics to quantify the electrical double layer and examine the potential for its direct observation in the in-situ TEM, Advanced structural and chemical imaging 1(1) (2015) 1-11.

[51] D. Kalderis, S. Bethanis, P. Paraskeva, E. Diamadopoulos, Production of activated carbon from bagasse and rice husk by a single-stage chemical activation method at low retention times, Bioresource technology 99(15) (2008) 6809-6816.

[52] C.-S. Yang, Y.S. Jang, H.K. Jeong, Bamboo-based activated carbon for supercapacitor applications, Current applied physics 14(12) (2014) 1616-1620.

[53] E.H. Sujiono, D. Zabrian, Zurnansyah, Mulyati, V. Zharvan, Samnur, N.A. Humairah, Fabrication and characterization of coconut shell activated carbon using variation chemical activation for wastewater treatment application, Results in Chemistry 4 (2022) 100291.

[54] S. Yu, D. Liu, S. Zhao, B. Bao, C. Jin, W. Huang, H. Chen, Z. Shen, Synthesis of wood derived nitrogen-doped porous carbon-polyaniline composites for supercapacitor electrode materials, RSC advances 5(39) (2015) 3943-3949.

[55] S. Cheng, X. Cheng, M.H. Tahir, Z. Wang, J. Zhang, Synthesis of rice husk activated carbon by fermentation osmotic activation method for hydrogen storage at room temperature, International journal of hydrogen energy 62 (2024) 443-450.

[56] J. Cheng, C. Bi, X. Zhou, D. Wu, D. Wang, C. Liu, Z. Cao, Preparation of Bamboo-Based Activated Carbon via Steam Activation for Efficient Methylene Blue Dye Adsorption: Modeling and Mechanism Studies, Langmuir 39(39) (2023) 14119-14129.

[57] M. Mirzaeian, Q. Abbas, A. Ogwu, P. Hall, M. Goldin, M. Mirzaeian, H.F. Jirandehi, Electrode and electrolyte materials for electrochemical capacitors, International journal of hydrogen energy 42(40) (2017) 25565-25587.

[58] I. Yang, M. Jung, M.-S. Kim, D. Choi, J.C. Jung, Physical and chemical activation mechanisms of carbon materials based on the microdomain model, Journal of materials chemistry. A, Materials for energy and sustainability 9(15) (2021) 9815-9825.

[59] H. Marsh, E.A. Heintz, F. Rodríguez-Reinoso, Introduction to carbon technologies, Universidad de Alicante, Alicante, 1997.

[60] W. Tian, H. Zhang, X. Duan, H. Sun, G. Shao, S. Wang, Porous Carbons: Structure-Oriented Design and Versatile Applications, Advanced functional materials 30(17) (2020) n/a.

[61] M. Jung, I. Yang, J. Yoo, M.-S. Kim, J.C. Jung, Low-Cost Activated Carbon Electrodes from Waste Maple Leaves for Organic Electric Double-Layer Capacitors, Journal of the Electrochemical Society 168(8) (2021) 80532.

[62] F. Rodríguez-reinoso, The role of carbon materials in heterogeneous catalysis, Carbon (New York) 36(3) (1998) 159-175.

[63] D. Lennon, D.T. Lundie, S.D. Jackson, G.J. Kelly, S.F. Parker, Characterization of Activated Carbon Using X-ray Photoelectron Spectroscopy and Inelastic Neutron Scattering Spectroscopy, Langmuir 18(12) (2002) 4667-4673.

[64] J.L. Figueiredo, M.F.R. Pereira, M.M.A. Freitas, J.J.M. Órfão, Modification of the surface chemistry of activated carbons, Carbon (New York) 37(9) (1999) 1379-1389.

[65] P. Ratajczak, M.E. Suss, F. Kaasik, F. Béguin   Carbon electrodes for capacitive technologies, Energy Storage Materials 16 (2019) 126-145.

[66] H. Shao, Y.-C. Wu, Z. Lin, P.-L. Taberna, P. Simon, Nanoporous carbon for electrochemical capacitive energy storage, Chemical Society reviews 49(1) (2020) 35-339.

[67] J. Chmiola, G. Yushin, Y. Gogotsi, C. Portet, P. Simon, P.L. Taberna, Anomalous Increase in Carbon Capacitance at Pore Sizes Less Than 1 Nanometer, Science (American Association for the Advancement of Science) 313(5794) (2006) 1760-1763.

[68] V. Jiménez, P. Sánchez, A. Romero, 2 - Materials for activated carbon fiber synthesis, Elsevier Ltd2017, pp. 21-38.

[69] A.G. Pandolfo, A.F. Hollenkamp, Carbon properties and their role in supercapacitors, Journal of power sources 157(1) (2006) 11-27.

[70] V. Presser, M. Heon, Y. Gogotsi, Carbide-Derived Carbons - From Porous Networks to Nanotubes and Graphene, Advanced functional materials 21(5) (2011) 810-833.

[71] S.-W. Hwang, S.-H. Hyun, Capacitance control of carbon aerogel electrodes, Journal of non-crystalline solids 347(1-3) (2004) 238-245.

[72] Y. Wang, A. Du Pasquier, D. Li, P. Atanassova, S. Sawrey, M. Oljaca, Electrochemical double layer capacitors containing carbon black additives for improved capacitance and cycle life, Carbon (New York) 133 (2018) 1-5.

[73] W. Zhang, R.-r. Cheng, H.-h. Bi, Y.-h. Lu, L.-b. Ma, X.-j. He, A review of porous carbons produced by template methods for supercapacitor applications, New carbon materials 36(1) (2021) 69-81.

[74] A.K. Geim, K.S. Novoselov, The rise of graphene, Nature materials 6(3) (2007) 183-191.

[75] C.N.R. Rao, A.K. Sood, K.S. Subrahmanyam, A. Govindaraj, Graphene: The New Two-Dimensional Nanomaterial, Angewandte Chemie (International ed.) 48(42) (2009) 7752-7777.

[76] R.R. Salunkhe, Y.-H. Lee, K.-H. Chang, J.-M. Li, P. Simon, J. Tang, N.L. Torad, C.-C. Hu, Y. Yamauchi, Nanoarchitectured Graphene-Based Supercapacitors for Next-Generation Energy-Storage Applications, Chemistry : a European journal 20(43) (2014) 13838-13852.

[77] C. Liu, Z. Yu, D. Neff, A. Zhamu, B.Z. Jang, Graphene-Based Supercapacitor with an Ultrahigh Energy Density, Nano letters 10(12) (2010) 4863-4868.

[78] Z. Li, P. Qin, L. Wang, C. Yang, Y. Li, Z. Chen, D. Pan, M. Wu, Amine-enriched Graphene Quantum Dots for High-pseudocapacitance Supercapacitors, Electrochimica acta 208 (2016) 260-266.

[79] J. Chen, C. Li, G. Shi, Graphene Materials for Electrochemical Capacitors, The journal of physical chemistry letters 4(8) (2013) 1244-1253.

[80] N.N. Joshi, J. Narayan, R. Narayan, Multifunctional carbon-based nanostructures (CBNs) for advanced biomedical applications - a perspective and review, Materials advances 5(23) (2024) 916-9174.

[81] B. De, S. Banerjee, K.D. Verma, T. Pal, P.K. Manna, K.K. Kar, Carbon Nanotube as Electrode Materials for Supercapacitors, Springer International Publishing AG, Switzerland, 2020, pp. 229-243.

[82] H. Wu, C. Liu, Z. Jiang, Z. Yang, X. Mao, L. Wei, R. Sun, Electrospun flexible lignin/polyacrylonitrile-based carbon nanofiber and its application in electrode materials for supercapacitors, Textile research journal 92(3-4) (2022) 456-466.

[83] M.E. Plonska-Brzezinska, L. Echegoyen, Carbon nano-onions for supercapacitor electrodes: recent developments and applications, Journal of materials chemistry. A, Materials for energy and sustainability 1(44) (2013) 13703-13714.

[84] N. Sano, Y. Kimura, T. Suzuki, Synthesis of carbon nanohorns by a gas-injected arc-in-water method and application to catalyst-support for polymer electrolyte fuel cell electrodes: Carbon nanostructures, Journal of materials chemistry 18(13) (2008) 1555-1560.

[85] A.M. Grumezescu, V. Grumezescu, Carbon nanotube-based matrices for tissue engineering, Elsevier, United States, 2019.

[86] J.P. John, A comprehensive review on the environmental applications of graphene-carbon nanotube hybrids: recent progress, challenges and prospects, Materials advances 2(21) (2021) 6816-6838.

[87] C. Zheng, W. Qian, F. Wei, Integrating carbon nanotube into activated carbon matrix for improving the performance of supercapacitor, Materials science & engineering. B, Solid-state materials for advanced technology 177(13) (2012) 1138-1143.

[88] M. Tobis, S. Sroka, E.B. FrÄckowiak, Supercapacitor with Carbon/MoS2 Composites, Frontiers in energy research 9 (2021).

[89] E. Frąckowiak, M. Foroutan Koudahi, M. Tobis, Electrochemical Capacitor Performance of Nanotextured Carbon/Transition Metal Dichalcogenides Composites, Small (Weinheim an der Bergstrasse, Germany) 17(48) (2021) e2006821-n/a.

[90] Q. Meng, K. Cai, Y. Chen, L. Chen, Research progress on conducting polymer based supercapacitor electrode materials, Nano energy 36 (2017) 268-285.

[91] C. An, Y. Zhang, H. Guo, Y. Wang, Metal oxide-based supercapacitors: progress and prospectives, Nanoscale advances 1(12) (2019) 4644-4658.

[92] R. Adalati, M. Sharma, S. Sharma, A. Kumar, G. Malik, R. Boukherroub, R. Chandra, Metal nitrides as efficient electrode material for supercapacitors: A review, Journal of energy storage 56(part B) (2022) 105912.

[93] X. Chen, Q. Su, J. Yu, M. Wei, G. Guo, Y. Wang, Experimental study on the degradation mechanism of LaCoO3-based symmetric supercapacitors, RSC advances 11(41) (2021) 25170-25178.

[94] B. Arumugam, G. Mayakrishnan, S.K. Subburayan Manickavasagam, S.C. Kim, R. Vanaraj, An Overview of Active Electrode Materials for the Efficient High-Performance Supercapacitor Application, Crystals (Basel) 13(7) (2023) 1118.

[95] C. Zhong, Y. Deng, W. Hu, J. Qiao, L. Zhang, J. Zhang, A review of electrolyte materials and compositions for electrochemical supercapacitors, Chemical Society reviews 44(21) (2015) 7484-7539.

[96] K. Fic, G. Lota, M. Meller, E. Frackowiak, Novel insight into neutral medium as electrolyte for high-voltage supercapacitors, Energy & environmental science 5(2) (2012) 5842-585.

[97] J. Krummacher, C. Schütter, L.H. Hess, A. Balducci, Non-aqueous electrolytes for electrochemical capacitors, Current opinion in electrochemistry 9 (2018) 64-69.

[98] S.-E. Chun, B. Evanko, X. Wang, D. Vonlanthen, X. Ji, G.D. Stucky, S.W. Boettcher, Design of aqueous redox-enhanced electrochemical capacitors with high specific energies and slow self-discharge, Nature communications 6(1) (2015) 7818-7818.

[99] J. Menzel, E. Frąckowiak, K. Fic, Agar-based aqueous electrolytes for electrochemical capacitors with reduced self-discharge, Electrochimica acta 332 (2020) 135435.

[100] B. Akinwolemiwa, C. Peng, G.Z. Chen, Redox Electrolytes in Supercapacitors, Journal of the Electrochemical Society 162(5) (2015) A5054-A5059.

[101] B. Pal, S. Yang, S. Ramesh, V. Thangadurai, R. Jose, Electrolyte selection for supercapacitive devices: a critical review, Nanoscale advances 1(1) (2019) 387-3835.

[102] A. Platek-Mielczarek, E. Frackowiak, K. Fic, Specific carbon/iodide interactions in electrochemical capacitors monitored by EQCM technique, Energy & environmental science 14(4) (2021) 2381-2393.

[103] M. Tobis, J. Piwek, A. Płatek-Mielczarek, Ł. Przypis, D. Janas, E. Frąckowiak, Probing iodide/iodonium salt interactions with single-walled carbon nanotubes for resilient electrochemical capacitor, Electrochimica acta 492 (2024).

[104] Q. Abbas, H. Fitzek, V. Pavlenko, B. Gollas, Towards an optimized hybrid electrochemical capacitor in iodide based aqueous redox-electrolyte: Shift of equilibrium potential by electrodes mass-balancing, Electrochimica acta 337 (2020) 135785.

[105] B. Gorska, P. Bujewska, K. Fic, Thiocyanates as attractive redox-active electrolytes for high-energy and environmentally-friendly electrochemical capacitors, Physical chemistry chemical physics : PCCP 19(11) (2017) 7923-7935.

[106] P. Bujewska, B. Gorska, K. Fic, Redox activity of selenocyanate anion in electrochemical capacitor application, Synthetic metals 253 (2019) 62-72.

[107] J. Piwek, A. Platek, E. Frackowiak, K. Fic, Mechanisms of the performance fading of carbon-based electrochemical capacitors operating in a LiNO3 electrolyte, Journal of power sources 438 (2019) 227029.

[108] J. Piwek, A. Platek-Mielczarek, E. Frackowiak, K. Fic, Enhancing capacitor lifetime by alternate constant polarization, Journal of power sources 506 (2021) 230131.

[109] P. Galek, P. Bujewska, S. Donne, K. Fic, J. Menzel, New insight into ion dynamics in nanoporous carbon materials: An application of the step potential electrochemical spectroscopy (SPECS) technique and electrochemical dilatometry, Electrochimica acta 377 (2021) 138115.

[110] K. Fic, M. Meller, J. Menzel, E. Frackowiak, Around the thermodynamic limitations of supercapacitors operating in aqueous electrolytes, Electrochimica acta 206 (2016) 496-503.

[111] K. Fic, M. He, E.J. Berg, P. Novák, E. Frackowiak, Comparative operando study of degradation mechanisms in carbon-based electrochemical capacitors with Li2SO4 and LiNO3 electrolytes, Carbon (New York) 120 (2017) 281-293.

[112] V. Khomenko, E. Raymundo-Piñero, E. Frackowiak, F. Béguin, High-voltage asymmetric supercapacitors operating in aqueous electrolyte, Applied Physics A 82(4) (2006) 567-573.

[113] A. Klimek, M. Tobis, E. Frackowiak, Effect of a buffer/iodide electrolyte on the performance of electrochemical capacitors, Green chemistry : an international journal and green chemistry resource : GC 26(11) (2024) 6684-6695.

[114] A. Slesinski, C. Matei-Ghimbeu, K. Fic, F. Béguin, E. Frackowiak, Self-buffered pH at carbon surfaces in aqueous supercapacitors, Carbon (New York) 129 (2018) 758-765.

[115] M. He, K. Fic, P. Novák, E.J. Berg, E. Frackowiak, (Invited) In Situ Gas Analysis of Carbon Based Supercapacitor Operating in Aqueous Electrolyte, Meeting abstracts (Electrochemical Society) MA2016-02(7) (2016) 1018-1018.

[116] J.Y. Hwang, M.F. El-Kady, M. Li, C.-W. Lin, M. Kowal, X. Han, R.B. Kaner, Boosting the capacitance and voltage of aqueous supercapacitors via redox charge contribution from both electrode and electrolyte, Nano today 15 (2017) 15-25.

[117] S. Zallouz, J.-M. Le Meins, C. Matei Ghimbeu, Alkaline hydrogel electrolyte from biosourced chitosan to enhance the rate capability and energy density of carbon-based supercapacitors, Energy advances 1(12) (2022) 1051-1064.

[118] A. Mendhe, H.S. Panda, A review on electrolytes for supercapacitor device, Discover materials 3(1) (2023) 29-27.

[119] E.G. Calvo, N. Ferrera-Lorenzo, J.A. Menéndez, A. Arenillas, Microwave synthesis of micro-mesoporous activated carbon xerogels for high performance supercapacitors, Microporous and mesoporous materials 168 (2013) 206-212.

[120] Y. Zhao, M. Liu, L. Gan, X. Ma, D. Zhu, Z. Xu, L. Chen, Ultramicroporous Carbon Nanoparticles for the High-Performance Electrical Double-Layer Capacitor Electrode, Energy & fuels 28(2) (2014) 1561-1568.

[121] K. Fic, A. Płatek, J. Piwek, J. Menzel, A. Ślesiński, P. Bujewska, P. Galek, E. Frąckowiak, Revisited insights into charge storage mechanisms in electrochemical capacitors with Li4-based electrolyte, 2019, pp. 1-14.

[122] B. Karamanova, A. Stoyanova, M. Shipochka, S. Veleva, R. Stoyanova, Effect of Alkaline-Basic Electrolytes on the Capacitance Performance of Biomass-Derived Carbonaceous Materials, Materials 13(13) (2020) 2941.

[123] P. Ratajczak, K. Jurewicz, F. Béguin, Factors contributing to ageing of high voltage carbon/carbon supercapacitors in salt aqueous electrolyte, Journal of applied electrochemistry 44(4) (2014) 475-480.

[124] E. Frackowiak, M. Meller, J. Menzel, D. Gastol, K. Fic, Redox-active electrolyte for supercapacitor application, Faraday discussions 172 (2014) 179-198.

[125] S.T. Senthilkumar, R.K. Selvan, J.S. Melo, Redox additive/active electrolytes: a novel approach to enhance the performance of supercapacitors, Journal of materials chemistry. A, Materials for energy and sustainability 1(40) (2013) 12386-12394.

[126] S. Roldán, C. Blanco, M. Granda, R. Menéndez, R. Santamaría, Towards a Further Generation of High-Energy Carbon-Based Capacitors by Using Redox-Active Electrolytes, Angewandte Chemie (International ed.) 50(7) (2011) 1699-1701.

[127] L. Chen, H. Bai, Z. Huang, L. Li, Mechanism investigation and suppression of self-discharge in active electrolyte enhanced supercapacitors, Energy & environmental science 7(5) (2014) 1750-1759.

[128] G. Lota, K. Fic, E. Frackowiak, Alkali metal iodide/carbon interface as a source of pseudocapacitance, Electrochemistry communications 13(1) (2011) 38-41.

[129] M. Pourbaix, Atlas of electrochemical equilibria in aqueous solutions / by Marcel Pourbaix ; translated from the French by James A. Franklin (except sections I, III 5, and III 6, which were originally written in English), 2d English edition ed., National Association of Corrosion Engineers, Houston, Tex, 1974.

[130] P. Przygocki, Q. Abbas, P. Babuchowska, F. Béguin, Confinement of iodides in carbon porosity to prevent from positive electrode oxidation in high voltage aqueous hybrid electrochemical capacitors, Carbon (New York) 125 (2017) 391-400.

[131] H. Schranger, F. Barzegar, Q. Abbas, Hybrid electrochemical capacitors in aqueous electrolytes: Challenges and prospects, Current opinion in electrochemistry 21 (2020) 167-174.

[132] P. Bujewska, P. Galek, K. Fic, Monitoring the ion population at a carbon electrode/aqueous electrolyte interface at various pHs using electrochemical dilatometry, Energy Storage Materials 63 (2023) 103003.

[133] M. Ue, K. Ida, S. Mori, Electrochemical properties of organic liquid electrolytes based on quaternary onium salts for electrical double-layer capacitors, Journal of the Electrochemical Society 141(11) (1994) 2989-2996.

[134] S. Vaquero, R. Díaz, M. Anderson, J. Palma, R. Marcilla, Insights into the influence of pore size distribution and surface functionalities in the behaviour of carbon supercapacitors, Electrochimica acta 86 (2012) 241-247.

[135] A.M. Bittner, M. Zhu, Y. Yang, H.F. Waibel, M. Konuma, U. Starke, C.J. Weber, Ageing of electrochemical double layer capacitors, Journal of power sources 203 (2012) 262-273.

[136] B.W. Ricketts, C. Ton-That, Self-discharge of carbon-based supercapacitors with organic electrolytes, Journal of power sources 89(1) (2000) 64-69.

[137] L. Köps, F.A. Kreth, D. Leistenschneider, K. Schutjajew, R. Gläßner, M. Oschatz, A. Balducci, Improving the Stability of Supercapacitors at High Voltages and High Temperatures by the Implementation of Ethyl Isopropyl Sulfone as Electrolyte Solvent, Advanced energy materials 13(5) (2023) n/a.

[138] J. Wang, X. Li, J. Yang, W. Sun, Q. Ban, L. Gai, Y. Gong, Z. Xu, L. Liu, Flame-Retardant, Highly Conductive, and Low-Temperature-Resistant Organic Gel Electrolyte for High-Performance All-Solid Supercapacitors, ChemSusChem 14(9) (2021) 2056-2066.

[139] A.A. Mroziewicz, K. Solska, G.Z. Żukowska, M. Skunik-Nuckowska, Water/N,N-Dimethylacetamide-Based Hybrid Electrolyte and Its Application to Enhanced Voltage Electrochemical Capacitors, Batteries (Basel) 10(6) (2024) 213.

[140] M.S. Ding, K. Xu, J.P. Zheng, T.R. Jow, γ-Butyrolactone-acetonitrile solution of triethylmethylammonium tetrafluoroborate as an electrolyte for double-layer capacitors, Journal of power sources 138(1) (2004) 340-350.

[141] S. Ai, X. Wu, J. Wang, X. Li, X. Hao, Y. Meng, Research Progress on Solid-State Electrolytes in Solid-State Lithium Batteries: Classification, Ionic Conductive Mechanism, Interfacial Challenges, Nanomaterials (Basel, Switzerland) 14(22) (2024) 1773.

[142] J.K. McDonough, A.I. Frolov, V. Presser, J. Niu, C.H. Miller, T. Ubieto, M.V. Fedorov, Y. Gogotsi, Influence of the structure of carbon onions on their electrochemical performance in supercapacitor electrodes, Carbon (New York) 50(9) (2012) 3298-3309.

[143] A.R. Koh, B. Hwang, K.C. Roh, K. Kim, The effect of the ionic size of small quaternary ammonium BF_4 salts on electrochemical double layer capacitors, Physical chemistry chemical physics : PCCP 16(29) (2014) 15146-15151.

[144] D. Aurbach, M.D. Levi, G. Salitra, N. Levy, J. Maier, Application of a quartz-crystal microbalance to measure ionic fluxes in microporous carbons for energy storage, Nature materials 8(11) (2009) 872-875.

[145] D.-e. Jiang, Z. Jin, D. Henderson, J. Wu, Solvent Effect on the Pore-Size Dependence of an Organic Electrolyte Supercapacitor, The journal of physical chemistry letters 3(13) (2012) 1727-1731.

[146] A. Tanaka, T. Iiyama, T. Ohba, S. Ozeki, K. Urita, T. Fujimori, H. Kanoh, K. Kaneko, Effect of a Quaternary Ammonium Salt on Propylene Carbonate Structure in Slit-Shape Carbon Nanopores, Journal of the American Chemical Society 132(7) (2010) 2112-2113.

[147] C.-W. Liew, K.H. Arifin, J. Kawamura, Y. Iwai, S. Ramesh, A.K. Arof, Effect of halide anions in ionic liquid added poly(vinyl alcohol)-based ion conductors for electrical double layer capacitors, Journal of non-crystalline solids 458 (2017) 97-106.

[148] B. Wu, K. Kuroda, K. Takahashi, E.W. Castner, Structural analysis of zwitterionic liquids vs. homologous ionic liquids, The Journal of chemical physics 148(19) (2018) 193807-193807.

[149] L. Timperman, P. Skowron, A. Boisset, H. Galiano, D. Lemordant, E. Frackowiak, F. Beguin, M. Anouti, Triethylammonium bis(tetrafluoromethylsulfonyl)amide protic ionic liquid as an electrolyte for electrical double-layer capacitors, Physical chemistry chemical physics : PCCP 14(22) (2012) 8199-8207.

[150] L. Demarconnay, E.G. Calvo, L. Timperman, M. Anouti, D. Lemordant, E. Raymundo-Piñero, A. Arenillas, J.A. Menéndez, F. Béguin, Optimizing the performance of supercapacitors based on carbon electrodes and protic ionic liquids as electrolytes, Electrochimica acta 108 (2013) 361-368.

[151] L. Timperman, F. Béguin, E. Frackowiak, M. Anouti, Comparative Study of Two Protic Ionic Liquids as Electrolyte for Electrical Double-Layer Capacitors, Journal of the Electrochemical Society 161(3) (2014) A228-A238.

[152] X. Zhang, D. Zhao, Y. Zhao, P. Tang, Y. Shen, C. Xu, H. Li, Y. Xiao, High performance asymmetric supercapacitor based on MnO2 electrode in ionic liquid electrolyte, Journal of materials chemistry. A, Materials for energy and sustainability 1(11) (2013) 3706.

[153] X. Liu, S. Chen, Z. Xiong, K. Li, Y. Zhang, Tungsten oxide-based nanomaterials for supercapacitors: Mechanism, fabrication, characterization, multifunctionality, and electrochemical performance, Progress in materials science 130 (2022) 100978.

[154] D.P. Dubal, O. Ayyad, V. Ruiz, P. Gómez-Romero, Hybrid energy storage: the merging of battery and supercapacitor chemistries, Chemical Society reviews 44(7) (2015) 1777-179.

[155] B. Babu, P. Simon, A. Balducci, Fast Charging Materials for High Power Applications, Advanced energy materials 10(29) (2020) n/a.

[156] W.J. Cao, J. Shih, J.P. Zheng, T. Doung, Development and characterization of Li-ion capacitor pouch cells, Journal of power sources 257 (2014) 388-393.

[157] J. Zhang, X. Liu, J. Wang, J. Shi, Z. Shi, Different types of pre-lithiated hard carbon as negative electrode material for lithium-ion capacitors, Electrochimica acta 187 (2016) 134-142.

[158] R. Kang, W.-Q. Zhu, S. Li, B.-B. Zou, L.-L. Wang, G.-C. Li, X.-H. Liu, D.H.L. Ng, J.-X. Qiu, Y. Zhao, F. Qiao, J.-B. Lian, Fe2TiO5 nanochains as anode for high-performance lithium-ion capacitor, Rare metals 40(9) (2021) 2424-2431.

[159] Y.-Q. Dai, G.-C. Li, X.-H. Li, H.-J. Guo, Z.-X. Wang, G.-C. Yan, J.-X. Wang, Ultrathin porous graphitic carbon nanosheets activated by alkali metal salts for high power density lithium-ion capacitors, Rare metals 39(12) (2020) 1364-1373.

[160] D. Sui, M. Wu, Y. Liu, Y. Yang, H. Zhang, Y. Ma, L. Zhang, Y. Chen, High performance Li-ion capacitor fabricated with dual graphene-based materials, Nanotechnology 32(1) (2021) 015403-015403.

[161] J. Ding, W. Hu, E. Paek, D. Mitlin, Review of Hybrid Ion Capacitors: From Aqueous to Lithium to Sodium, Chemical reviews 118(14) (2018) 6457-6498.

[162] K. Naoi, S. Ishimoto, J.-i. Miyamoto, W. Naoi, Second generation 'nanohybrid supercapacitor': Evolution of capacitive energy storage devices, Energy & environmental science 5(11) (2012) 9363-9373.

[163] G.G. Amatucci, F. Badway, A. Du Pasquier, Z. Tao, An asymmetric hybrid nonaqueous energy storage cell, Journal of the Electrochemical Society 148(8) (2001) A930-A939.

[164] C. Cementon, T. Ramireddy, D. Dewar, M. Brennan, A.M. Glushenkov, We may be underestimating the power capabilities of lithium-ion capacitors, Journal of power sources 591 (2024) 233857.

[165] F. Zhang, T. Zhang, X. Yang, L. Zhang, K. Leng, Y. Huang, Y. Chen, A high-performance supercapacitor-battery hybrid energy storage device based on graphene-enhanced electrode materials with ultrahigh energy density, Energy & environmental science 6(5) (2013) 1623.

[166] S.R. Sivakkumar, J.Y. Nerkar, A.G. Pandolfo, Rate capability of graphite materials as negative electrodes in lithium-ion capacitors, Electrochimica acta 55(9) (2010) 3330-3335.

[167] S.W. Bokhari, A.H. Siddique, H. Pan, Y. Li, M. Imtiaz, Z. Chen, S.M. Zhu, D. Zhang, Nitrogen doping in the carbon matrix for Li-ion hybrid supercapacitors: state of the art, challenges and future prospective, RSC advances 7(31) (2017) 18926-18936.

[168] J.H. Lee, W.H. Shin, M.-H. Ryou, J.K. Jin, J. Kim, J.W. Choi, Functionalized Graphene for High Performance Lithium Ion Capacitors, ChemSusChem 5(12) (2012) 2328-2333.

[169] G. Xu, P. Han, S. Dong, H. Liu, G. Cui, L. Chen, Li4Ti5O12-based energy conversion and storage systems: Status and prospects, Coordination chemistry reviews 343 (2017) 139-184.

[170] H. Du, D. Cao, H. Zhang, High-Power Energy Storage: Ultracapacitors, Elsevier Science & Technology, United States, 2017.

[171] M. Soltani, S.H. Beheshti, A comprehensive review of lithium ion capacitor: development, modelling, thermal management and applications, Journal of energy storage 34 (2021) 102019.

[172] N. Omar, J. Ronsmans, Y. Firozu, M. Monem, A. Samba, H. Gualous, O. Hegazy, J. Smekens, T. Coosemans, P. Van den Bossche, J. Van Mierlo, Lithium-Ion Capacitor - Advanced Technology for Rechargeable Energy Storage Systems, World electric vehicle journal 6(3) (2014) 484-494.

[173] S. Zhao, X. Sun, N. Wang, C. Li, Y. An, Y. Xu, K. Wang, X. Zhang, Y. Ma, Recent Advances in Hybrid Lithium-Ion Capacitors: Materials and Processes, ACS applied energy materials 7(24) (2024) 11553-11570.

[174] J.S. Edge, S. O'Kane, R. Prosser, N.D. Kirkaldy, A.N. Patel, A. Hales, A. Ghosh, W. Ai, J. Chen, J. Yang, S. Li, M.-C. Pang, L. Bravo Diaz, A. Tomaszewska, M.W. Marzook, K.N. Radhakrishnan, H. Wang, Y. Patel, B. Wu, G.J. Offer, Lithium ion battery degradation: what you need to know, Physical chemistry chemical physics : PCCP 23(14) (2021) 82-8221.

[175] L. Yue, M. Yu, X. Li, Y. Shen, Y. Wu, C. Fa, N. Li, J. Xu, Wide Temperature Electrolytes for Lithium Batteries: Solvation Chemistry and Interfacial Reactions, Small methods 8(11) (2024) e2400183-n/a.

[176] Y. Itou, N. Ogihara, S. Kawauchi, Role of Conductive Carbon in Porous Li-Ion Battery Electrodes Revealed by Electrochemical Impedance Spectroscopy Using a Symmetric Cell, Journal of physical chemistry. C 124(10) (2020) 5559-5564.

[177] J. Choi, C. Lee, S. Park, T.J. Embleton, K. Ko, M. Jo, K. Saleem Saqib, J. Yun, M. Jo, Y. Son, P. Oh, Analysis of Electrochemical Performance with Dispersion Degree of CNTs in Electrode According to Ultrasonication Process and Slurry Viscosity for Lithium-Ion Battery, Nanomaterials (Basel, Switzerland) 12(23) (2022) 4271.

[178] J.-M. Jiang, Z.-W. Li, Z.-T. Zhang, S.-J. Wang, H. Xu, X.-R. Zheng, Y.-X. Chen, Z.-C. Ju, H. Dou, X.-G. Zhang, Recent advances and perspectives on prelithiation strategies for lithium-ion capacitors, Rare metals 41(10) (2022) 3322-3335.

[179] M. Arnaiz, J. Ajuria, Pre-Lithiation Strategies for Lithium Ion Capacitors: Past, Present, and Future, Batteries & supercaps 4(5) (2021) 733-748.

[180] L. Kolzenberg, A. Latz, B. Horstmann, Solid–Electrolyte Interphase During Battery Cycling: Theory of Growth Regimes, ChemSusChem 13(15) (2020) 3901-3910.

[181] Z. Huang, Z. Deng, Y. Zhong, M. Xu, S. Li, X. Liu, Y. Zhou, K. Huang, Y. Shen, Y. Huang, Progress and challenges of prelithiation technology for lithium-ion battery, Carbon energy 4(6) (2022) 1107-1132.

[182] A.K. Samantara, S. Ratha, Metal-ion hybrid capacitors for energy storage : a balancing strategy toward energy-power density, 1st 2020. ed., Springer, Cham, Switzerland, 2020.

[183] G. Li, Z. Yang, Z. Yin, H. Guo, Z. Wang, G. Yan, Y. Liu, L. Li, J. Wang, Non-aqueous dual-carbon lithium-ion capacitors: a review, Journal of materials chemistry. A, Materials for energy and sustainability 7(26) (2019) 15541-15563.

[184] T. Aida, K. Yamada, M. Morita, An Advanced Hybrid Electrochemical Capacitor That Uses a Wide Potential Range at the Positive Electrode, Electrochemical and solid-state letters 9(12) (2006) A534-A536.

[185] F. Baskoro, C.-M. Ngue, K.B. Labasan, H.Q. Wong, M.-K. Leung, H.-J. Yen, Dual-Ligand Zn-Based Metal–Organic Framework as Reversible and Stable Anode Material for Next Generation Lithium-Ion Batteries, Energy technology (Weinheim, Germany) 9(11) (2021) n/a.

[186] S. Tian, Z. Chen, Z. Li, W. He, Y. An, H. Xie, L. Shen, H. Dou, X. Zhang, NaV1.25Ti0.75O4 Engineered by an Element Regulation Strategy as a Low-Potential and Pseudocapacitive Anode for Li-Ion Capacitors, ACS sustainable chemistry & engineering 11(36) (2023) 13342-13352.

[187] B. Li, J. Zheng, H. Zhang, L. Jin, D. Yang, H. Lv, C. Shen, A. Shellikeri, Y. Zheng, R. Gong, J.P. Zheng, C. Zhang, Electrode Materials, Electrolytes, and Challenges in Nonaqueous Lithium-Ion Capacitors, Advanced materials (Weinheim) 30(17) (2018) e1705670-n/a.

[188] H. Ma, H. Geng, B. Yao, M. Wu, C. Li, M. Zhang, F. Chi, L. Qu, Highly Ordered Graphene Solid: An Efficient Platform for Capacitive Sodium-Ion Storage with Ultrahigh Volumetric Capacity and Superior Rate Capability, ACS nano 13(8) (2019) 9161-9170.

[189] J. Lin, Y.-H. Shi, Y.-F. Li, Y.-H. Song, X.-L. Wu, H.-Z. Sun, B/N/O-Codoped 2D Porous Carbon Nanosheets for High-Performance Dual-Carbon Lithium-Ion Capacitors, ACS applied energy materials 6(17) (2023) 8867-8874.

[190] H. Shi, M. Du, W. Wu, Q. Zheng, B. Hao, Application of microdiverse carbon materials and loaded binary metals in lithium-ion capacitors, Journal of energy storage 60 (2023) 106550.

[191] X. Sun, X. Zhang, B. Huang, H. Zhang, D. Zhang, Y. Ma, (LiNi0.5Co0.2Mn0.3O2 + AC)/graphite hybrid energy storage device with high specific energy and high rate capability, Journal of power sources 243 (2013) 361-368.

[192] N.N. Sinha, N. Munichandraiah, Synthesis and Characterization of Carbon-Coated LiNi1/3Co1/3Mn1/3O2 in a Single Step by an Inverse Microemulsion Route, ACS applied materials & interfaces 1(6) (2009) 1241-1249.

[193] S.-T. Myung, S. Komaba, K. Hosoya, N. Hirosaki, Y. Miura, N. Kumagai, Synthesis of LiNi0.5Mn0.5-xTixO2 by an Emulsion Drying Method and Effect of Ti on Structure and Electrochemical Properties, Chemistry of materials 17(9) (2005) 2427-2435.

[194] O.E. Eleri, F. Lou, Z. Yu, Lithium-Ion Capacitors: A Review of Strategies toward Enhancing the Performance of the Activated Carbon Cathode, Batteries (Basel) 9(11) (2023) 533.

[195] X. Peng, L. Zhang, Z. Chen, L. Zhong, D. Zhao, X. Chi, X. Zhao, L. Li, X. Lu, K. Leng, C. Liu, W. Liu, W. Tang, K.P. Loh, Hierarchically Porous Carbon Plates Derived from Wood as Bifunctional ORR/OER Electrodes, Advanced materials (Weinheim) 31(16) (2019) e1900341-n/a.

[196] Y. Tong, J. Yang, J. Li, Z. Cong, L. Wei, M. Liu, S. Zhai, K. Wang, Q. An, Lignin-derived electrode materials for supercapacitor applications: progress and perspectives, Journal of materials chemistry. A, Materials for energy and sustainability 11(3) (2023) 161-182.

[197] B. Zhu, B. Liu, C. Qu, H. Zhang, W. Guo, Z. Liang, F. Chen, R. Zou, Tailoring biomass-derived carbon for high-performance supercapacitors from controllably cultivated algae microspheres, Journal of materials chemistry. A, Materials for energy and sustainability 6(4) (2018) 1523-153.

[198] P. Kleszyk, P. Ratajczak, P. Skowron, J. Jagiello, Q. Abbas, E. Frąckowiak, F. Béguin, Carbons with narrow pore size distribution prepared by simultaneous carbonization and self-activation of tobacco stems and their application to supercapacitors, Carbon (New York) 81 (2015) 148-157.

[199] T. Akintola, A. Shellikeri, T. Akintola, J.P. Zheng, The Influence of Li4Ti5O12 Preparation Method on Lithium-Ion Capacitor Performance, Batteries (Basel) 7(2) (2021) 33.

[200] G. Yang, B. Zhang, J. Feng, Y. Lu, Z. Wang, V. Aravindan, A. Muthiah, J. Liu, M. Srinivasan, Z. Shen, Y. Huang, Morphology controlled lithium storage in Li3VO4 anodes, Journal of materials chemistry. A, Materials for energy and sustainability 6(2) (2018) 456-463.

[201] W. Liu, X. Zhang, C. Li, K. Wang, X. Sun, Y. Ma, Carbon-coated Li3VO4 with optimized structure as high capacity anode material for lithium-ion capacitors, Chinese chemical letters 31(9) (2020) 2225-2229.

[202] L. Wang, X. Zhang, C. Li, X.-Z. Sun, K. Wang, F.-Y. Su, F.-Y. Liu, Y.-W. Ma, Recent advances in transition metal chalcogenides for lithium-ion capacitors, Rare metals 41(9) (2022) 2971-2984.

[203] T. Yan, F. Wen, J. Duan, C. Zhu, J. Wen, Y. Wang, J. Tong, Z. Chen, Fabricating tunable metal sulfides embedded with honeycomb-structured N-doped carbon matrices for high-performance lithium-ion capacitors, Chemical engineering journal (Lausanne, Switzerland : 1996) 474 (2023) 145839.

[204] L. Su, Z. Zhou, M. Ren, Core double-shell Si@SiO2@C nanocomposites as anode materials for Li-ion batteries, Chemical communications (Cambridge, England) 46(15) (2010) 2590-2592.

[205] P. Wuamprakhon, R. Songthan, T. Sangsanit, K. Santiyuk, J. Phojaroen, K. Homlamai, W. Tejangkura, M. Sawangphruk, Designing electrolytes for enhancing stability and performance of lithium-ion capacitors at large-scale cylindrical cells, Journal of power sources 622 (2024) 235331.

[206] P. Yu, G. Cao, S. Yi, X. Zhang, C. Li, X. Sun, K. Wang, Y. Ma, Binder-free 2D titanium carbide (MXene)/carbon nanotube composites for high-performance lithium-ion capacitors, Nanoscale 1(13) (2018) 596-5913.

[207] M. Ghidiu, M.R. Lukatskaya, M.-Q. Zhao, Y. Gogotsi, M.W. Barsoum, Conductive two-dimensional titanium carbide 'clay' with high volumetric capacitance, Nature (London) 516(7529) (2014) 78-81.

[208] L. Wang, X. Zhang, C. Li, Y. Xu, Y. An, W. Liu, T. Hu, S. Yi, K. Wang, X. Sun, Y. Gong, Z.-S. Wu, Y. Ma, Cation-deficient T-Nb2O5/graphene Hybrids synthesized via chemical oxidative etching of MXene for advanced lithium-ion capacitors, Chemical engineering journal (Lausanne, Switzerland : 1996) 468 (2023) 143507.

[209] F.A. Kreth, L. Köps, C. Leibing, S. Darlami Magar, M. Hermesdorf, K. Schutjajew, C. Neumann, D. Leistenschneider, A. Turchanin, M. Oschatz, J.L. Gómez Urbano, A. Balducci, Enabling Fluorine-Free Lithium-Ion Capacitors and Lithium-Ion Batteries for High-Temperature Applications by the Implementation of Lithium Bis(oxalato)Borate and Ethyl Isopropyl Sulfone as Electrolyte, Advanced energy materials 14(13) (2024) n/a.

[210] K.G. Khatmullina, O.V. Yarmolenko, L.M. Bogdanova, Network polymer electrolytes based on poly(ester diacrylate), ethylene carbonate, and LiClO4, Polymer science. Series A, Chemistry, physics 52(12) (2010) 1327-1333.

[211] T. Abe, N. Kawabata, Y. Mizutani, M. Inaba, Z. Ogumi, Correlation between cointercalation of solvents and electrochemical intercalation of lithium into graphite in propylene carbonate solution, Journal of the Electrochemical Society 150(3) (2003) A257-A261.

[212] J.S. Gnanaraj, R.W. Thompson, J.F. DiCarlo, K.M. Abraham, The Role of Carbonate Solvents on Lithium Intercalation into Graphite, Journal of the Electrochemical Society 154(3) (2007) A185.

[213] M. Winter, G.H. Wrodnigg, J.O. Besenhard, W. Biberacher, P. Novak, Dilatometric investigations of graphite electrodes in nonaqueous lithium battery electrolytes, Journal of the Electrochemical Society 147(7) (2000) 2427-2431.

[214] P.-L. Wang, X.-Z. Sun, Y.-B. An, X. Zhang, C.-Z. Yuan, S.-H. Zheng, K. Wang, Y.-W. Ma, Additives to propylene carbonate-based electrolytes for lithium-ion capacitors, Rare metals 41(4) (2022) 1304-1313.

[215] M. Barawi, C.A. Mesa, L. Collado, I.J. Villar-García, F. Oropeza, V.A. de la Peña O'Shea, M. García-Tecedor, Latest advances in in situ and operando X-ray-based techniques for the characterisation of photoelectrocatalytic systems, Journal of materials chemistry. A, Materials for energy and sustainability 12(35) (2024) 23125-23146.

[216] R. Venancio, R. Vincentini, M.J. Pinzon C., D.A. Correa, A.N. Miranda, A.C. Queiroz, F.T. Degasperi, L.J.A. Siqueira, L.M. Da Silva, H. Zanin, Combining electrochemical, molecular simulation and operando techniques to investigate the stability of electrodes and organic electrolytes used in EDLCs, Energy Storage Materials 62 (2023) 1029943.

[217] A. Parejo-Tovar, C. Merlet, P. Ratajczak, F. Beguin, O*perando* tracking of ion population changes in the EDL electrode of a lithium-ion capacitor during its charge/discharge, Energy Storage Materials 73 (2024) 103810.

[218] J.W. Gittins, K. Ge, C.J. Balhatchet, P.-L. Taberna, P. Simon, A.C. Forse, Understanding Electrolyte Ion Size Effects on the Performance of Conducting Metal–Organic Framework Supercapacitors, Journal of the American Chemical Society 146(18) (2024) 12473-12484.

[219] N. Shpigel, M.D. Levi, S. Sigalov, O. Girshevitz, D. Aurbach, L. Daikhin, P. Pikma, M. Marandi, A. Jänes, E. Lust, N. Jäckel, V. Presser, In situ hydrodynamic spectroscopy for structure characterization of porous energy storage electrodes, Nature materials 15(5) (2016) 570-575.

[220] S. Boyd, K. Ganeshan, W.-Y. Tsai, T. Wu, S. Saeed, D.-e. Jiang, N. Balke, A.C.T. van Duin, V. Augustyn, Effects of interlayer confinement and hydration on capacitive charge storage in birnessite, Nature materials 20(12) (2021) 1689-1694.

[221] W.-Y. Tsai, P.-L. Taberna, P. Simon, Electrochemical Quartz Crystal Microbalance (EQCM) Study of Ion Dynamics in Nanoporous Carbons, Journal of the American Chemical Society 136(24) (2014) 8722-8728.

[222] S. Sigalov, M.D. Levi, L. Daikhin, G. Salitra, D. Aurbach, Electrochemical quartz crystal admittance studies of ion adsorption on nanoporous composite carbon electrodes in aprotic solutions, Journal of solid state electrochemistry 18(5) (2014) 1335-1344.

[223] S. Slesinska, P. Galek, J. Menzel, S.W. Donne, K. Fic, A. Płatek-Mielczarek, Fundamentals and Implication of Point of Zero Charge (PZC) Determination for Activated Carbons in Aqueous Electrolytes, Advanced science (2024) e2409162.

[224] Y.-C. Wu, P.-L. Taberna, P. Simon, Tracking ionic fluxes in porous carbon electrodes from aqueous electrolyte mixture at various pH, Electrochemistry communications 93 (2018) 119-122.

[225] M.D. Levi, S. Sigalov, D. Aurbach, L. Daikhin, In Situ Electrochemical Quartz Crystal Admittance Methodology for Tracking Compositional and Mechanical Changes in Porous Carbon Electrodes, Journal of physical chemistry. C 117(29) (2013) 14876-14889.

[226] M.D. Levi, N. Levy, S. Sigalov, G. Salitra, D. Aurbach, J. Maier, Electrochemical Quartz Crystal Microbalance (EQCM) Studies of Ions and Solvents Insertion into Highly Porous Activated Carbons, Journal of the American Chemical Society 132(38) (2010) 13220-13222.

[227] J. Ye, Y.-C. Wu, K. Xu, K. Ni, N. Shu, P.-L. Taberna, Y. Zhu, P. Simon, Charge Storage Mechanisms of Single-Layer Graphene in Ionic Liquid, Journal of the American Chemical Society 141(42) (2019) 16559-16563.

[228] R. Yan, M. Antonietti, M. Oschatz, Toward the Experimental Understanding of the Energy Storage Mechanism and Ion Dynamics in Ionic Liquid Based Supercapacitors, Advanced energy materials 8(18) (2018) 1800026-n/a.

[229] Q. Dou, L. Liu, B. Yang, J. Lang, X. Yan, Silica-grafted ionic liquids for revealing the respective charging behaviors of cations and anions in supercapacitors, Nature communications 8(1) (2017) 2188-9.

[230] L. Zhang, X. Hu, Z. Wang, F. Sun, D.G. Dorrell, A review of supercapacitor modeling, estimation, and applications: A control/management perspective, Renewable & sustainable energy reviews 81 (2018) 1868-1878.

[231] E. Pameté, L. Köps, F.A. Kreth, S. Pohlmann, A. Varzi, T. Brousse, A. Balducci, V. Presser, The Many Deaths of Supercapacitors: Degradation, Aging, and Performance Fading, Advanced energy materials 13(29) (2023) n/a.

[232] P. Simon, Y. Gogotsi, Capacitive Energy Storage in Nanostructured Carbon–Electrolyte Systems, Accounts of chemical research 46(5) (2013) 1094-1103.

[233] A. Oukaour, B. Tala-Ighil, M. AlSakka, H. Gualous, R. Gallay, B. Boudart, Calendar ageing and health diagnosis of supercapacitor, Electric power systems research 95 (2013) 330-338.

[234] A. Platek, J. Piwek, K. Fic, E. Frackowiak, Ageing mechanisms in electrochemical capacitors with aqueous redox-active electrolytes, Electrochimica acta 311 (2019) 211-220.

[235] P. Azaïs, L. Duclaux, P. Florian, D. Massiot, M.-A. Lillo-Rodenas, A. Linares-Solano, J.-P. Peres, C. Jehoulet, F. Béguin, Causes of supercapacitors ageing in organic electrolyte, Journal of power sources 171(2) (2007) 1046-1053.

[236] Y. Liu, B. Réty, C. Matei Ghimbeu, B. Soucaze-Guillous, P.-L. Taberna, P. Simon, Understanding ageing mechanisms of porous carbons in non-aqueous electrolytes for supercapacitors applications, Journal of power sources 434 (2019) 226734.

[237] S.E.M. Pourhosseini, A. Bothe, A. Balducci, F. Beguin, P. Ratajczak, Strategy to assess the carbon electrode modifications associated with the high voltage ageing of electrochemical capacitors in organic electrolyte, ENERGY STORAGE MATERIALS 38 (2021) 17-29.

[238] P. Ratajczak, K. Jurewicz, P. Skowron, Q. Abbas, F. Béguin, Effect of accelerated ageing on the performance of high voltage carbon/carbon electrochemical capacitors in salt aqueous electrolyte, Electrochimica acta 130 (2014) 344-350.

[239] Q. Abbas, D. Pajak, E. Frąckowiak, F. Béguin, Effect of binder on the performance of carbon/carbon symmetric capacitors in salt aqueous electrolyte, Electrochimica acta 140 (2014) 132-138.

[240] R. German, P. Venet, A. Sari, O. Briat, J.-M. Vinassa, Improved Supercapacitor Floating Ageing Interpretation Through Multipore Impedance Model Parameters Evolution, IEEE transactions on power electronics 29(7) (2014) 3669-3678.

[241] Y. Liu, B. Soucaze-Guillous, P.-L. Taberna, P. Simon, Understanding of carbon-based supercapacitors ageing mechanisms by electrochemical and analytical methods, Journal of power sources 366 (2017) 123-130.

[242] F.A. Kreth, L.H. Hess, A. Balducci, In-operando GC-MS: A new tool for the

understanding of degradation processes occurring in electrochemical capacitors, Energy Storage Materials 56 (2023) 192-204.

[243] F.A. Kreth, L. Köps, S.W. Donne, A. Balducci, Operando Temperature Dynamic Investigation of Electric Double-Layer Capacitors Containing Organic Electrolytes, Batteries & supercaps (2024).

[244] O. Bohlen, J. Kowal, D.U. Sauer, Ageing behaviour of electrochemical double layer capacitors Part II. Lifetime simulation model for dynamic applications, Journal of power sources 173(1) (2007) 626-632.

[245] R. Venâncio, R. Vicentini, L.H. Costa, R. Teófilo, L.M. Da Silva, H. Zanin, In-situ electrochemical and operando Raman techniques to investigate the effect of porosity in different carbon electrodes in organic electrolyte supercapacitors, Journal of energy storage 50 (2022).

[246] H. Cao, X. Peng, M. Zhao, P. Liu, B. Xu, J. Guo, Oxygen functional groups improve the energy storage performances of graphene electrochemical supercapacitors, RSC advances 8(6) (2018) 2858-2865.

[247] N. Noor, T. Baker, H. Lee, E. Evans, S. Angizi, J.D. Henderson, A. Rakhsha, D. Higgins, Redox-Active Phenanthrenequinone Molecules and Nitrogen-Doped Reduced Graphene Oxide as Active Material Composites for Supercapacitor Applications, ACS omega 9(9) (2024) 10080-10089.

[248] X.-r. Li, Y.-h. Jiang, P.-z. Wang, Y. Mo, W.-d. Lai, Z.-j. Li, R.-j. Yu, Y.-t. Du, X.-r. Zhang, Y. Chen, Effect of the oxygen functional groups of activated carbon on its electrochemical performance for supercapacitors, New carbon materials 35(3) (2020) 232-243.

[249] K. Kierzek, E. Frackowiak, G. Lota, G. Gryglewicz, J. Machnikowski, Electrochemical capacitors based on highly porous carbons prepared by KOH activation, Electrochimica acta 49(4) (2004) 515-523.

[250] M. He, K. Fic, E. Frackowiak, P. Novák, E.J. Berg, Ageing phenomena in high-voltage aqueous supercapacitors investigated by in situ gas analysis, Energy & environmental science 9(2) (2016) 623-633.

[251] T. Morimoto, K. Hiratsuka, Y. Sanada, K. Kurihara, Electric double-layer capacitor using organic electrolyte, Journal of power sources 60(2) (1996) 239-247.

[252] C.-H. Yang, Q.D. Nguyen, T.-H. Chen, A.S. Helal, J. Li, J.-K. Chang, Functional Group-Dependent Supercapacitive and Aging Properties of Activated Carbon Electrodes in Organic Electrolyte, ACS sustainable chemistry & engineering 6(1) (2018) 1208-1214.

[253] W. Pholauyphon, P. Charoen-amornkitt, T. Suzuki, S. Tsushima, Perspectives on accurately analyzing cyclic voltammograms for surface- and diffusion-controlled contributions, Electrochemistry communications 159 (2024) 107654.

[254] F. Licht, M.A. Davis, H.A. Andreas, Charge redistribution and electrode history impact galvanostatic charging/discharging and associated figures of merit, Journal of power sources 446 (2020) 227354.

[255] T. Krenz, T. Gottschalk, L. Helmers, P. Trinke, B. Bensmann, R. Hanke-Rauschenbach, Current Interrupt Technique to Fully Characterize PEMWE Cells, Journal of the Electrochemical Society 171(3) (2024) 34509.

[256] W. Zheng, iR Compensation for Electrocatalysis Studies: Considerations and Recommendations, ACS energy letters 8(4) (2023) 1952-1958.

[257] A. Lasia, Impedance of porous electrodes, Journal of electroanalytical chemistry (Lausanne, Switzerland) 397(1) (1995) 27-33.

[258] A. Lasia, Electrochemical impedance spectroscopy and its applications, Springer, New York, 2014.

[259] O.E. Barcia, E. D'Elia, I. Frateur, O.R. Mattos, N. Pébère, B. Tribollet, Application of the impedance model of de Levie for the characterization of porous electrodes, Electrochimica acta 47(13) (2002) 2109-2116.

[260] S. Wang, J. Zhang, O. Gharbi, V. Vivier, M. Gao, M.E. Orazem, Electrochemical impedance spectroscopy, Nature Reviews Methods Primers 1(1) (2021).

[261] M. Libber, N. Gariya, M. Kumar, A comprehensive analysis of supercapacitors with current limitations and emerging trends in research, Journal of solid state electrochemistry 29(2) (2025) 513-527.

[262] M.F. Dupont, S.W. Donne, A Step Potential Electrochemical Spectroscopy Analysis of Electrochemical Capacitor Electrode Performance, Electrochimica acta 167 (2015) 268-277.

[263] M.F. Dupont, S.W. Donne, Separating Faradaic and Non-Faradaic Charge Storage Contributions in Activated Carbon Electrochemical Capacitors Using Electrochemical Methods: I. Step Potential Electrochemical Spectroscopy, Journal of the Electrochemical Society 162(7) (2015) A1246-A1254.

[264] M. Forghani, S.W. Donne, Modification of the Step Potential Electrochemical Spectroscopy Analysis Protocol to Improve Outcomes, Journal of the Electrochemical Society 166(13) (2019) A2727-A2735.

[265] A. Maćkowiak, P. Galek, P. Jeżowski, K. Fic, Impact of lithium bis(fluorosulfonyl)imide (LiFSI) concentration on lithium intercalation into graphite monitored with Step Potential ElectroChemical Spectroscopy (SPECS), Electrochimica acta 463 (2023) 142796.
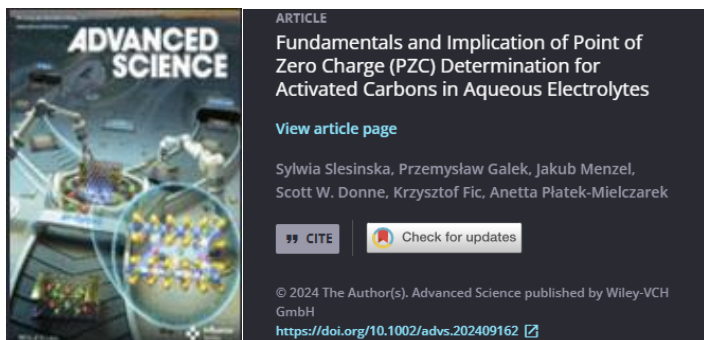
Copyrights

Fundamentals and Implication of Point of Zero Charge (PZC) Determination for Activated Carbons in Aqueous Electrolytes

Sylwia Slesinska, Przemysław Galek, Jakub Menzel, Scott W. Donne, Krzysztof Fic ✉, Anetta Płatek-Mielczarek ✉

ADVANCED SCIENCE

ARTICLE
Fundamentals and Implication of Point of Zero Charge (PZC) Determination for Activated Carbons in Aqueous Electrolytes

View article page

Sylwia Slesinska, Przemysław Galek, Jakub Menzel, Scott W. Donne, Krzysztof Fic, Anetta Płatek-Mielczarek

99 CITE | (R) Check for updates

---

99 🔗 ☰ ⤢
Cite Share Jump to Expand

Operando Monitoring of Local pH Value Changes at the Carbon Electrode Surface in Neutral Sulfate-Based Aqueous Electrochemical Capacitors 📋 Click to copy article link

Adam Slesinski*, Sylwia Sroka, Krzysztof Fic, Elzbieta Frackowiak, and Jakub Menzel*
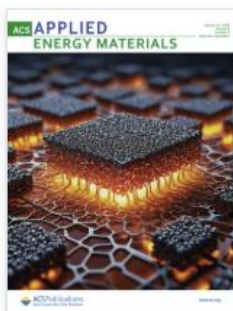
ACS APPLIED MATERIALS & INTERFACES

---

99 🔗 ☰ ⤢
Cite Share Jump to Expand

Identifying the Activated Carbon Electrode Aging Pathways in Lithium-Ion Hybrid Capacitors

Sylwia Slesinska, Bénédicte Réty, Camélia Matei-Ghimbeu*, Krzysztof Fic, and Jakub Menzel*

ACS APPLIED ENERGY MATERIALS

Co-authorship statements

POZNAN UNIVERSITY OF TECHNOLOGY

mgr inż. Sylwia Ślesińska
Institute of Chemistry and Technical Electrochemistry
Poznan University of Technology, Berdychowo 4
61-131 Poznań, tel: +48 61 665 32 38
e-mail: sylwia.slesinska@put.poznan.pl

Poznan, 07.02.2025

Declaration of individual contribution in publications

As the co-author of the following article:

Article: Operando Monitoring of Local pH Value Changes at the Carbon Electrode Surface in Neutral Sulfate-Based Aqueous Electrochemical Capacitors

Authors: Adam Slesinski, **Sylwia Sroka**, Krzysztof Fic, Elzbieta Frackowiak, Jakub Menzel

Journal: ACS Applied Materials & Interfaces

DOI: 10.1021/acsami.2c09920

I hereby declare that my contribution to this work was:

Contribution: Investigation: *operando* pH measurements, floating measurements, EQCM measurements and data curation, writing—original draft and formal analysis.

Signature

POZNAN UNIVERSITY OF TECHNOLOGY

mgr inż. Sylwia Ślesińska
Institute of Chemistry and Technical Electrochemistry
Poznan University of Technology, Berdychowo 4
61-131 Poznań, tel: +48 61 665 32 38
e-mail: sylwia.slesinska@put.poznan.pl

Poznan, 07.02.2025

Declaration of individual contribution in publications

As the co-author of the following article:

Article: Fundamentals and Implication of Point of Zero Charge (PZC) Determination for
                Activated Carbons in Aqueous Electrolytes

Authors: **Sylwia Slesinska,** Przemysław Galek, Jakub Menzel, Scott W. Donne, Krzysztof Fic,
                Anetta Płatek-Mielczarek

Journal: Advanced Science

DOI: 10.1002/advs.202409162

I hereby declare that my contribution to this work was:

Contribution: Conceptualization, methodology, investigation: EQCM measurements, resonator
                and coating preparation, electrodes and electrolyte preparation, electrochemical
                measurements in Swagelok, EQCM and volume cells, elemental analysis, data
                collection, writing-original draft.

Signature

POZNAN UNIVERSITY OF TECHNOLOGY

dr hab. inż. Krzysztof Fic, prof. PP
Institute of Chemistry and Technical Electrochemistry
Poznan University of Technology, Berdychowo 4
61-131 Poznań, tel: +48 (61) 665-3303
e-mail: krzysztof.fic@put.poznan.pl

Poznan, 07.02.2025

Declaration of individual contribution in publications

As the co-author of the following article:

Article: Identifying the Activated Carbon Electrode Aging Pathways in Lithium-Ion Hybrid Capacitors

Authors: **Sylwia Slesinska**, Bénédicte Réty, Camélia Matei-Ghimbeu, Krzysztof Fic, Jakub Menzel

Journal: ACS Applied Energy Materials

DOI: 10.1021/acsaem.4c01940

I hereby declare that my contribution to this work was:

Contribution: Methodology planning, investigation: electrochemical analysis, physicochemical analysis and corresponding data curation, visualization and writing of the original draft.

_____
Signature

POZNAN UNIVERSITY OF TECHNOLOGY

mgr inż. Sylwia Ślesińska
Institute of Chemistry and Technical Electrochemistry
Poznan University of Technology, Berdychowo 4
61-131 Poznań, tel: +48 61 665 32 38
e-mail: sylwia.slesinska@put.poznan.pl

Poznan, 20.03.2025

Declaration of individual contribution in publications

As the co-author of the following article:

Article: Oxygen Enigma: Deciphering the Role of Carbon Surface Functionalities on Degradation at Electrified Interfaces

Authors: **Sylwia Slesinska**, Bénédicte Réty, Camélia Matei-Ghimbeu, Samar Hajjar Garreau, Krzysztof Fic, Jakub Menzel

Journal: Submitted

DOI: -

I hereby declare that my contribution to this work was:

Contribution: Conceptualization, visualization, formal analysis, methodology, investigation: electrochemical analysis, floating measurements, electrode and electrolyte preparation, elemental analysis, operando GC-MS investigation and data collection, TPD-MS and Raman Spectroscopy data measurements, data collection and curation, writing-original draft.

Signature

umicore

Jakub Menzel
Umicore Battery Materials Poland Sp. z o.o.
Radzikowice 1c
48-300 Nysa
Poland
Jakub.Menzel@eu.umicore.com
Poznań, 27.03.2025

Declaration of individual contribution in publications

As the co-author of the following article:

Article:	Operando Monitoring of Local pH Value Changes at the Carbon Electrode Surface in Neutral Sulfate-Based Aqueous Electrochemical Capacitors
Authors:	Adam Slesinski, Sylwia Sroka, Krzysztof Fic, Elzbieta Frackowiak, **Jakub Menzel**
Journal:	ACS Applied Materials & Interfaces
DOI:	10.1021/acsami.2c09920

I hereby declare that my contribution to this work was:
Contribution: Methodology, investigation, resources, funding acquisition, and writing-original draft .

Signature

umicore

Jakub Menzel
Umicore Battery Materials Poland Sp. z o.o.
Radzikowice 1c
48-300 Nysa
Poland
Jakub.Menzel@eu.umicore.com
Poznań, 27.03.2025

Declaration of individual contribution in publications

As the co-author of the following article:

Article:	Fundamentals and Implication of Point of Zero Charge (PZC) Determination for Activated Carbons in Aqueous Electrolytes
Authors:	Sylwia Slesinska, Przemysław Galek, **Jakub Menzel**, Scott W. Donne, Krzysztof Fic, Anetta Płatek-Mielczarek
Journal:	Advanced Science
DOI:	10.1002/advs.202409162

I hereby declare that my contribution to this work was:
Contribution: Funding acquisition, supervision, writing- review and editing the manuscript.

Signature

Jakub Menzel
Umicore Battery Materials Poland Sp. z o.o.
Radzikowice 1c
48-300 Nysa
Poland
Jakub.Menzel@eu.umicore.com
Poznań, 27.03.2025

Declaration of individual contribution in publications

As the co-author of the following article:

Article:	Identifying the Activated Carbon Electrode Aging Pathways in Lithium-Ion Hybrid Capacitors
Authors:	Sylwia Slesinska, Bénédicte Réty, Camélia Matei-Ghimbeu, Krzysztof Fic, **Jakub Menzel**
Journal:	ACS Applied Energy and Materials
DOI:	10.1021/acsaem.4c01940

I hereby declare that my contribution to this work was:

Contribution:	Conceptualization, methodology, funding acquisition, supervision, project administration, review and editing the manuscript.

Signature

Jakub Menzel
Umicore Battery Materials Poland Sp. z o.o.
Radzikowice 1c
48-300 Nysa
Poland
Jakub.Menzel@eu.umicore.com
Poznań, 27.03.2025

Declaration of individual contribution in publications

As the co-author of the following article:

Article:	Oxygen Enigma: Deciphering the Role of Carbon Surface Functionalities on Degradation at Electrified Interfaces
Authors:	Sylwia Slesinska, Bénédicte Réty, Camélia Matei-Ghimbeu, Samar Hajjar Garreau, Krzysztof Fic, **Jakub Menzel**
Journal:	Submitted
DOI:	-

I hereby declare that my contribution to this work was:

Contribution: Conceptualization, funding acquisition, writing – review and editing, supervision, project administration.

Signature

POZNAN UNIVERSITY OF TECHNOLOGY

dr inż. Adam Ślesiński
Institute of Chemistry and Technical Electrochemistry
Poznan University of Technology, Berdychowo 4
61-131 Poznań, tel: +48 61 665 32 38
e-mail: adam.slesinski@put.poznan.pl

Poznan, 07.02.2025

Declaration of individual contribution in publications

As the co-author of the following article:

Article: Operando Monitoring of Local pH Value Changes at the Carbon Electrode Surface in Neutral Sulfate-Based Aqueous Electrochemical Capacitors

Authors: **Adam Slesinski,** Sylwia Sroka, Krzysztof Fic, Elzbieta Frackowiak, Jakub Menzel

Journal: ACS Applied Materials & Interfaces

DOI: 10.1021/acsami.2c09920

I hereby declare that my contribution to this work was:

Contribution: Conceptualization, methodology, investigation, and writing-original draft.

Ślesiński

Signature

POZNAN UNIVERSITY OF TECHNOLOGY

prof. dr hab. Elżbieta Frąckowiak
Institute of Chemistry and Technical Electrochemistry
Poznan University of Technology, Berdychowo 4
61-131 Poznań, tel: +48 61 665 3632
e-mail: elzbieta.frackowiak@put.poznan.pl

Poznan, 07.02.2025

Declaration of individual contribution in publications

As the co-author of the following article:

Article: Operando Monitoring of Local pH Value Changes at the Carbon Electrode Surface in Neutral Sulfate-Based Aqueous Electrochemical Capacitors

Authors: Adam Slesinski, Sylwia Sroka, Krzysztof Fic, **Elzbieta Frackowiak,** Jakub Menzel

Journal: ACS Applied Materials & Interfaces

DOI: 10.1021/acsami.2c09920

I hereby declare that my contribution to this work was:

Contribution: Supervision, resources, funding acquisition, and project administration.

E. Frąckowiak

Signature

POZNAN UNIVERSITY OF TECHNOLOGY

dr hab. inż. Krzysztof Fic, prof. PP
Institute of Chemistry and Technical Electrochemistry
Poznan University of Technology, Berdychowo 4
61-131 Poznań, tel: +48 61 665 3632
e-mail: krzysztof.fic@put.poznan.pl

Poznan, 07.02.2025

Declaration of individual contribution in publications

As the co-author of the following article:

Article: Operando Monitoring of Local pH Value Changes at the Carbon Electrode Surface
            in Neutral Sulfate-Based Aqueous Electrochemical Capacitors
Authors: Adam Slesinski, Sylwia Sroka, **Krzysztof Fic**, Elzbieta Frackowiak, Jakub Menzel

Journal: ACS Applied Materials & Interfaces

DOI: 10.1021/acsami.2c09920

I hereby declare that my contribution to this work was:

Contribution: Supervision, funding acquisition, project administration, writing— review and
               editing

Signature

POZNAN UNIVERSITY OF TECHNOLOGY

dr hab. inż. Krzysztof Fic, prof. PP
Institute of Chemistry and Technical Electrochemistry
Poznan University of Technology, Berdychowo 4
61-131 Poznań, tel: +48 (61) 665-3303
e-mail: krzysztof.fic@put.poznan.pl

Poznan, 07.02.2025

Declaration of individual contribution in publications

As the co-author of the following article:

Article: Fundamentals and Implication of Point of Zero Charge (PZC) Determination for Activated Carbons in Aqueous Electrolytes

Authors: Sylwia Slesinska, Przemysław Galek, Jakub Menzel, Scott W. Donne, **Krzysztof Fic**, Anetta Płatek-Mielczarek

Journal: Advanced Science

DOI: 10.1002/advs.202409162

I hereby declare that my contribution to this work was:

Contribution: Funding acquisition, supervision, writing- review and editing.

Signature

POZNAN UNIVERSITY OF TECHNOLOGY

dr hab. inż. Krzysztof Fic, prof. PP
Institute of Chemistry and Technical Electrochemistry
Poznan University of Technology, Berdychowo 4
61-131 Poznań, tel: +48 (61) 665-3303
e-mail: krzysztof.fic@put.poznan.pl

Poznan, 07.02.2025

Declaration of individual contribution in publications

As the co-author of the following article:

Article: Identifying the Activated Carbon Electrode Aging Pathways in Lithium-Ion Hybrid Capacitors

Authors: Sylwia Slesinska, Bénédicte Réty, Camélia Matei-Ghimbeu, **Krzysztof Fic**, Jakub Menzel

Journal: ACS Applied Energy Materials

DOI: 10.1021/acsaem.4c01940

I hereby declare that my contribution to this work was:

Contribution: Supervision, funding acquisition, project administration, writing- review and editing

Signature

POZNAN UNIVERSITY OF TECHNOLOGY

dr hab. inż. Krzysztof Fic, prof. PP
Institute of Chemistry and Technical Electrochemistry
Poznan University of Technology, Berdychowo 4
61-131 Poznań, tel: +48 (61) 665-3303
e-mail: krzysztof.fic@put.poznan.pl

Poznan, 20.03.2025

Declaration of individual contribution in publications

As the co-author of the following article:

Article: Oxygen Enigma: Deciphering the Role of Carbon Surface Functionalities on Degradation at Electrified Interfaces

Authors: Sylwia Slesinska, Bénédicte Réty, Camélia Matei-Ghimbeu, Samar Hajjar Garreau, **Krzysztof Fic**, Jakub Menzel

Journal: Submitted

DOI: -

I hereby declare that my contribution to this work was:

Contribution: Supervision, funding acquisition, project administration, writing - review and editing.

Signature

Dresden, 18.02.2025

Declaration of individual contribution in publications

As the co-author of the following article:

Article:	Fundamentals and Implication of Point of Zero Charge (PZC) Determination for Activated Carbons in Aqueous Electrolytes
Authors:	Sylwia Slesinska, **Przemysław Galek**, Jakub Menzel, Scott W. Donne, Krzysztof Fic, Anetta Płatek-Mielczarek
Journal:	Advanced Science
DOI:	10.1002/advs.202409162

I hereby declare that my contribution to this work was:

Contribution: conceptualization, investigation, methodology, SPECS data processing, visualization, electrochemical investigation, EQCM measurements, writing - original draft.

_____
Signature

Basel, 18.02.2025

Declaration of individual contribution in publications

As the co-author of the following article:

Article: Fundamentals and Implication of Point of Zero Charge (PZC) Determination for Activated Carbons in Aqueous Electrolytes

Authors: Sylwia Slesinska, Przemysław Galek, Jakub Menzel, Scott W. Donne, Krzysztof Fic, **Anetta Płatek-Mielczarek**

Journal: Advanced Science

DOI: 10.1002/advs.202409162

I hereby declare that my contribution to this work was:

Contribution: Conceptualization, methodology, supervision, visualization, data curation, writing- original draft

Signature

THE UNIVERSITY OF NEWCASTLE AUSTRALIA

Professor Scott Donne
Discipline of Chemistry
Ph: +61 2 4921 5477
Email: Scott.Donne@newcastle.edu.au

22 April 2025

Declaration of individual contribution in publications

As the co-author of the following article:

Article:	Fundamentals and Implication of Point of Zero Charge (PZC) Determination for Activated Carbons in Aqueous Electrolytes
Authors:	Sylwia Slesinska, Przemysław Galek, Jakub Menzel, **Scott W. Donne**, Krzysztof Fic, Anetta Płatek-Mielczarek
Journal:	Advanced Science
DOI:	10.1002/advs.202409162

I hereby declare that my contribution to this work was:
Contribution: Validation, supervision, writing- review and editing

Scott Donne

Mulhouse, 25.03.2025

Declaration of individual contribution in publications

As the co-author of the following article:

Article:	Identifying the Activated Carbon Electrode Aging Pathways in Lithium-Ion Hybrid Capacitors
Authors:	Sylwia Slesinska, **Bénédicte Réty**, Camélia Matei-Ghimbeu, Krzysztof Fic, Jakub Menzel
Journal:	ACS Applied Energy and Materials
DOI:	10.1021/acsaem.4c01940

I hereby declare that my contribution to this work was:

Contribution: Investigation: TPD-MS measurements, writing- original draft.

Réty

_____
Signature

Mulhouse, 25.03.2025

Declaration of individual contribution in publications

As the co-author of the following article:

Article:	Oxygen Enigma: Deciphering the Role of Carbon Surface Functionalities on Degradation at Electrified Interfaces
Authors:	Sylwia Slesinska, **Bénédicte Réty**, Camélia Matei-Ghimbeu, Samar Hajjar Garreau, Krzysztof Fic, Jakub Menzel
Journal:	Submitted
DOI:	-

I hereby declare that my contribution to this work was:

Contribution: Investigation, Formal analysis, Writing-original draft.

Ré⟋

_____
Signature

Mulhouse, 21.03.2025

Declaration of individual contribution in publications

As the co-author of the following article:

Article:	Oxygen Enigma: Deciphering the Role of Carbon Surface Functionalities on Degradation at Electrified Interfaces
Authors:	Sylwia Slesinska, Bénédicte Réty, Camélia Matei-Ghimbeu, **Samar Hajjar Garreau**, Krzysztof Fic, Jakub Menzel
Journal:	Submitted
DOI:	-

I hereby declare that my contribution to this work was:

Contribution: Investigation: XPS analysis

_____
Signature

Mulhouse, 20/03/2025

Declaration of individual contribution in publications

As the co-author of the following article:

Article: Identifying the Activated Carbon Electrode Aging Pathways in Lithium-Ion Hybrid Capacitors

Authors: Sylwia Slesinska, Bénédicte Réty, **Camélia Matei-Ghimbeu**, Krzysztof Fic, Jakub Menzel

Journal: ACS Applied Energy and Materials

DOI: 10.1021/acsaem.4c01940

I hereby declare that my contribution to this work was:

Contribution: Validation, supervision, review and editing the manuscript.

_____

Signature

Mulhouse, 20/03/2025

Declaration of individual contribution in publications

As the co-author of the following article:

Article: Oxygen Enigma: Deciphering the Role of Carbon Surface Functionalities on Degradation at Electrified Interfaces

Authors: Sylwia Slesinska, Bénédicte Réty, **Camélia Matei-Ghimbeu**, Samar Hajjar Garreau, Krzysztof Fic, Jakub Menzel

Journal: Submitted

DOI: -

I hereby declare that my contribution to this work was:

Contribution: Validation, supervision, writing - review and editing.

_____

Signature